Tesi di Dottorato di FRANCESCO MAESTRI
Matricola D01601

POLITECNICO DI MILANO

**DIPARTIMENTO
DI
CHIMICA,
MATERIALI
E
INGEGNERIA CHIMICA
"Giulio Natta"**

SAFE AND PRODUCTIVE OPERATION OF SEMIBATCH REACTORS: DEVELOPMENT AND VALIDATION OF A GENERAL PROCEDURE

**Dottorato di Ricerca in
Chimica Industriale e
Ingegneria Chimica (CII)**

XVIII ciclo
2003 - 2006

Coordinatore: prof. RENATO ROTA
Tutore: prof. RENATO ROTA
Relatore: prof. RENATO ROTA

“Complicare è facile, semplificare è difficile”

Bruno Munari

A mia moglie Cristiana e mio figlio Pierfrancesco,
senza la cui pazienza mai avrei potuto
portare a termine questa avventura.

Ringraziamenti

Desidero ringraziare il Prof. Renato Rota per avermi dato la possibilità di intraprendere questa esperienza, per me di particolarissimo valore non soltanto scientifico e per la serietà che da sempre caratterizza la nostra collaborazione.
Desidero inoltre ringraziare il Dr. Paolo Cardillo, Direttore della Stazione Sperimentale per i Combustibili, e i suoi collaboratori, il Dr. Angelo Lunghi e la Dr.ssa Lucia Gigante per il supporto sperimentale fornitoci e per i preziosi suggerimenti che ci hanno permesso di orientare la nostra attività di ricerca verso problematiche di rilevante interesse nello studio e nella valutazione delle reazioni fuggitive.

Bergamo-Milano, Marzo 2006
Francesco Maestri

List of publications

1. Maestri, F.; Rota, R. Thermally safe operation of liquid-liquid semibatch reactors. Part I: single kinetically controlled reactions with arbitrary reaction order. *Chem. Eng. Sci.* 2005, *60*, 3309-3322.

2. Maestri, F.; Rota, R. Thermally safe operation of liquid-liquid semibatch reactors. Part II: single diffusion controlled reactions with arbitrary reaction order. *Chem. Eng. Sci.* 2005, *60*, 5590-5602.

3. Maestri, F.; Rota, R. Temperature diagrams for preventing decomposition or side reactions in liquid-liquid semibatch reactors. *Chem. Eng. Sci.* 2006, *61*, 3068-3078.

4. Maestri, F.; Rota, R. Safe and productive operation of homogeneous semibatch reactors with arbitrary reaction kinetics. Part I: development of a procedure. *Ind. Eng. Chem. Res.* 2006, *submitted for publication.*

5. Maestri, F.; Rota, R. Safe and productive operation of homogeneous semibatch reactors with arbitrary reaction kinetics. Part II: the nitration of N-(2-phenoxyphenyl) methane sulphonamide. *Ind. Eng. Chem. Res.* 2006, *submitted for publication.*

Contents

List of figures

SUMMARY

2. THERMALLY SAFE OPERATION OF LIQUID-LIQUID SEMIBATCH REACTORS. PART II: SINGLE DIFFUSION CONTROLLED REACTIONS WITH ARBITRARY REACTION ORDER

Legend and other parameters as in Figure 11.

3. TEMPERATURE DIAGRAMS FOR PREVENTING DECOMPOSITION OR SIDE REACTIONS IN LIQUID-LIQUID SEMIBATCH REACTORS

Figure 1 *A) temperature and B) boundary diagram.*

Figure 2 *Slow reaction regime. Reaction in the dispersed phase.*
Co=10, R_H=1, n=1, m=1.
0.025< ν_A Da RE<14, 0.3<ε<0.55, 32<γ<42, 0.29<$\Delta\tau_{ad,0}$<0.7.
A) temperature diagram; B) boundary diagram.

Figure 3 *Slow reaction regime. Reaction in the dispersed phase.*
Co=20, R_H=1, n=1, m=1.
0.025< ν_A Da RE<14, 0.3<ε<0.55, 32<γ<42, 0.29<$\Delta\tau_{ad,0}$<0.7.
A) temperature diagram; B) boundary diagram.

Figure 4 *Slow reaction regime. Reaction in the dispersed phase.*
Co=5, R_H=1, n=1, m=1.
0.025< ν_A Da RE<14, 0.3<ε<0.55, 32<γ<42, 0.29<$\Delta\tau_{ad,0}$<0.7.
A) temperature diagram; B) boundary diagram.

Figure 5 *Slow reaction regime. Reaction in the dispersed phase.*
Co=10, R_H=2.5, n=1, m=1.
0.025< ν_A Da RE<14, 0.3<ε<0.55, 32<γ<42, 0.29<$\Delta\tau_{ad,0}$<0.7.
A) temperature diagram; B) boundary diagram.

Figure 6 *Slow reaction regime. Reaction in the dispersed phase.*
Co=10, R_H=0.4, n=1, m=1.
0.025< ν_A Da RE<14, 0.3<ε<0.55, 32<γ<42, 0.29<$\Delta\tau_{ad,0}$<0.7.
A) temperature diagram; B) boundary diagram.

Figure 7 *Slow reaction regime. Reaction in the dispersed phase.*
Co=10, R_H=1, n=2, m=1.
0.025< ν_A Da RE<14, 0.3<ε<0.55, 32<γ<42, 0.29<$\Delta\tau_{ad,0}$<0.7.
A) temperature diagram; B) boundary diagram.

Figure 8 *Slow reaction regime. Reaction in the dispersed phase.*

5. SAFE AND PRODUCTIVE OPERATION OF HOMOGENEOUS SEMIBATCH REACTORS WITH ARBITRARY REACTION KINETICS. PART II: THE NITRATION OF N-(2-PHENOXYPHENYL) METHANE SULPHONAMIDE

List of tables

Table 3 *Displacement of the $E_{x,MIN}$ and $R_{y,QFS}$ values for single fast reactions occurring in the dispersed and continuous phase, respectively, for some couples of boundary diagrams.*

$$\Delta R_{y,QFS} = \left| \left(R_{y,QFS} \right)_d - \left(R_{y,QFS} \right)_c \right|$$

$$\Delta E_{x,MIN} = \left| \left(E_{x,MIN} \right)_d - \left(E_{x,MIN} \right)_c \right|$$

Fast reaction regime with Co=10, m=1, R_H=1.

0.025< ν_A Da RE<14, 0.3<ε<0.55, 32<γ<42, 0.29<$\Delta\tau_{ad,0}$<0.7.

3. TEMPERATURE DIAGRAMS FOR PREVENTING DECOMPOSITION OR SIDE REACTIONS IN LIQUID-LIQUID SEMIBATCH REACTORS

Table 1 *Expressions of the reactivity enhancement factor, RE, and of the function, f, for slow and fast reactions taking place in the dispersed or continuous phase. [10,11].*

4. SAFE AND PRODUCTIVE OPERATION OF HOMOGENEOUS SEMIBATCH REACTORS WITH ARBITRARY REACTION KINETICS. PART I: DEVELOPMENT OF A PROCEDURE

Table 1 *Normalized sensitivity coefficients of $R_{y,QFS}$ and $E_{x,MIN}$ computed from the data shown in Figure 3.*

Table 2 *Functional dependences of the relative coreactant amount, M_A, and of the relative coreactant concentration, Γ_A on ϑ and ζ_B. Expressions valid up to ϑ=1. For ϑ>1, the (ϑ-ζ_B)/ϑ and the (ϑ-ζ_B) terms must be replaced with (1-ζ_B), and the $\varepsilon\vartheta$ terms with ε.*

5. SAFE AND PRODUCTIVE OPERATION OF HOMOGENEOUS SEMIBATCH REACTORS WITH ARBITRARY REACTION KINETICS. PART II: THE NITRATION OF N-(2-PHENOXYPHENYL) METHANE SULPHONAMIDE

Table 1 *Process and equipment parameters for reaction (1) carried out in a 2.5 lt RC1 calorimeter.*

Table 2 *Exothermicity and reactivity parameters for the operating conditions tested, according to the kinetic expression (2) and estimated values of the peak reaction temperature according to the temperature diagrams.*

Table 3 *Exothermicity and reactivity parameters for the operating conditions tested, according to the kinetic expression (12).*

Summary

The thermal loss of control of batch (BR) and semibatch (SBR) reactors in which exothermic reactions are performed occurs more frequently than one could believe: in the early 90's and in the single EU country more than 100 events of this typology per year had been estimated to occur, a little number of which, fortunately, had serious consequences on the environment or in terms of human lives. However, the consequences of the single industrial accident can be so severe that the risk factor associated with such events remains very high. For these reasons the huge amount of work that in the last thirty years (from the accident of 1976 in Seveso, Italy) has been done in order to study and prevent the aforementioned phenomena is well justified. In particular, a number of criteria for the safe scale up of a process from the laboratory or pilot to the industrial scale has been developed. However, for a practical application of such criteria it must be taken into account that typically in the fine chemical and pharmaceutical industries it is often not possible to perform detailed kinetic investigations and mathematical modelling of the single process, because of the huge variety of products involved and the relatively small amount of the single productions. Such a constraint requires to the single safety criterion that wants to achieve a practical diffusion to be at the same time reliable, general and easy to use.

It is well known that relatively fast and exothermic reactions cannot be carried out safely in batch reactors [1]: in such cases, the heat effects associated with a chemical reaction of the form $\nu_A A+\nu_B B\rightarrow C+\nu_D D$ can be better controlled by adding (at a rate dependent on the heat removal efficiency) the reactant A (usually called coreactant) to the reactant B previously charged in the reactor, that is performing the reaction in an indirectly cooled SBR operating with a sufficiently low coreactant accumulation. The mass and energy balance equations for such reaction systems can be written in dimensionless form as:

$$\frac{d\zeta_B}{d\vartheta} = \nu_A \, Da \, RE \, f \exp\left[\gamma_{app}\left(1-\frac{1}{\tau}\right)\right] \qquad (1)$$

$$\left(1+\alpha R_H \varepsilon \vartheta\right)\frac{d\tau}{d\vartheta} = \Delta\tau_{ad,0}\frac{d\zeta_B}{d\vartheta} - \varepsilon\left[Co\left(1+\varepsilon\vartheta\right)+R_H\right]\left(\tau-\tau_{cool}^{eff}\right) \quad (2)$$

where: ζ_B is the molar conversion of the reactant initially charged in the reactor, ϑ is the dimensionless time variable (defined assuming as a reference value the supply period), Da is the Damköhler number, related to the dosing time, RE is the reactivity enhancement factor, whose expression depends on the typology of reaction system (that is, homogeneous or heterogeneous SBRs with reaction occurring in the dispersed or in the continuous phase), f is the only factor containing the functional dependence of the conversion rate on ϑ and ζ_B, γ_{app} is an apparent activation energy in dimensionless form, R_H is the ratio between the volumetric heat capacities of the dosing stream and the reacting mixture, ε is the relative volume increase at the end of the supply period, $\Delta T_{ad,0}$ is the adiabatic temperature rise at ϑ=0, Co is the cooling number, which is related to the volumetric feed rate and to the heat transfer efficiency, and τ_{cool}^{eff} is an effective cooling temperature, which takes into account the effects of both the heat removal by the coolant and the sensible heat of the dosing stream (see Chapter 1). Moreover, α is a flag parameter equal to 1 or $1/R_H$ for heterogeneous (liquid-liquid) or homogeneous SBRs respectively. The initial conditions for the numerical integration of eqs. (1) and (2) are: ζ_B=0 and $\tau=\tau_0$ at ϑ=0.

In the literature a number of criteria for the safe scale up of a chemical process carried out in a SBR can be found [2,3], that are based on the mathematical behaviour of the temperature and conversion time profiles. Such criteria are independent on any arbitrary definition of what an excessive coreactant accumulation is but are not always easy to use in practice, since they require the knowledge of mathematical properties of the aforementioned profiles that are often not straightforward to estimate for end users. Other criteria through an on line analysis of the reactor temperature evolution allow for an early warning detection of a runaway event [4,5] and can therefore be implemented in the control system of the reactor. The first studies for selecting safe and productive operating conditions of homogeneous SBRs in which an exothermic reaction is carried out were performed by Hugo and Steinbach [6,7] who introduced a semiempirical quantitative criterion based on the concept of coreactant accumulation in the system: in particular, as the aforementioned accumulation increases (which is the consequence of a not negligible characteristic time of the chemical reaction compared with that of the coreactant dosing) the reaction system switches from semibatch to batch like operating conditions. In such a situation, the heat removal contribution from the system can be insufficient to counteract effectively the enthalpic contribution associated with too fast and exothermic chemical reactions. For this reason, accumulation phenomena in exothermic SBRs must be limited below a threshold value, in order to keep the thermal control of the process. Few years later, Steensma and Westerterp [8-10] extended

the criterion of Hugo and Steinbach to the case of heterogeneous (liquid-liquid) SBRs, introducing the concept of target temperature. Such a target thermal profile is the consequence of both a negligible characteristic time of the chemical reaction with respect to that of the coreactant dosing and of a negligible characteristic time of the heat removal from the system compared with that of the enthalpic contribution associated with the conversion rate. Such assumptions lead to the following expression of the target temperature during the supply period, that can be easily derived from the energy balance (2) for the reactor:

$$T_{ta} = T_0 + 1.05\frac{\Delta T_{ad,0}}{\varepsilon\left[Co\left(1+\varepsilon\vartheta\right)+R_H\right]} \tag{3}$$

The 5% overestimation of the T_{ta}-T_0 difference in expression (3) has been firstly introduced by Steensma and Westerterp [8] in order to account for the deviation of the operating conditions of a real SBR from the ideal situation of no coreactant accumulation. Through a comparison between the target and the actual temperature time profiles it is possible to classify the reactor thermal behaviour from the safety point of view and to generate on this basis boundary diagrams which, in a suitable dimensionless space that can be derived from the energy balance (2) of the reactor, separate inherently safe and excessive accumulation operating conditions. Such a dimensionless space is given by an exothermicity number, E_x, that contains the information about the reaction enthalpy and a reactivity number, R_y, which is related to the initial dependence of the conversion rate on temperature. These parameters can be computed through the following generalized expressions:

$$E_x = \frac{\gamma_{app}}{\tau_{cool}^2}\frac{\Delta\tau_{ad,0}}{\varepsilon\left(Co+R_H\right)} \tag{4}$$

$$R_y = \frac{\nu_A Da\, RE \exp\left[\gamma_{app}\left(1-1/\tau_{cool}\right)\right]}{\varepsilon\left(Co+R_H\right)} \tag{5}$$

In Figure 1, an example of boundary diagram is reported, from which the following operating regions of an indirectly cooled SBR can be recognized increasing the value of the initial reaction temperature (which is assumed to be equal to the coolant temperature and to the dosing stream temperature under isoperibolic conditions):

1) for sufficiently low values of the coolant temperature, the peak reaction temperature attained is lower than the local target value: this means that the reaction is not ignited. In such a situation the accumulation of the coreactant in the system reaches obviously high values but the characteristic time of the reaction is never low enough to cause the thermal loss of control of the system;

2) as the coolant temperature increases, the maximum temperature “pinches” locally the target line: this situation is referred to as a marginal ignition;
3) increasing further the coolant temperature, the characteristic time of the reaction is at the same time not so low to limit the accumulation of the coreactant and not so high to avoid -when the reaction itself ignites- the loss of control of the system from the thermal point of view. This situation implies maximum reaction temperatures higher than the local target value and corresponds to excessive accumulation operating conditions;
4) as the coolant temperature still increases, the characteristic time of the reaction becomes low enough to limit the accumulation of the coreactant A in the system, so that no exceeding of the target temperature can occur. The minimum coolant temperature for which the exceeding of the local target value by the maximum reaction temperature disappears is referred to as a QFS (Quick onset, Fair conversion, Smooth temperature profile) situation [8], because it is characterized by a temperature evolution which quickly approaches the target line and remains close to it throughout the dosing period, at the end of which the conversion ζ_B is almost complete.

The boundary line represented in Figure 1 separates the excessive accumulation region (inside the line itself), the no ignition region (for low R_y values), the QFS region (for high R_y values) and the inherently safe region (for either E_x values lower than $E_{x,MIN}$ or R_y values higher than $R_{y,QFS}$).

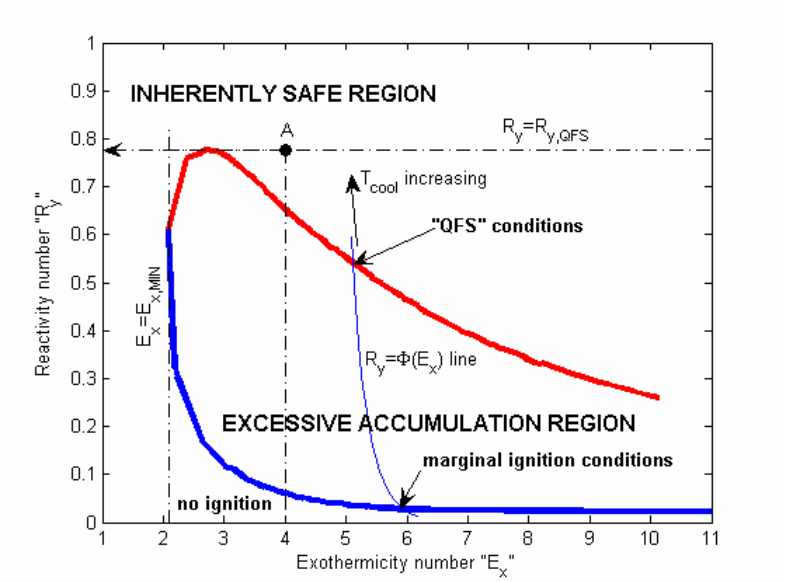

Figure 1 *Different thermal behavior regions for an indirectly cooled SBR represented through the boundary diagram.*

The boundary diagrams can be employed to solve two typologies of problems:

1) identify for an existing SBR thermally safe operating conditions, that is operating conditions characterized by a sufficiently low coreactant accumulation;
2) scale up a given set of safe operating conditions for a SBR from the laboratory or pilot to the industrial scale, without solving the mathematical model of the reactor.

The method introduced by Steensma and Westerterp has been then experimentally validated by van Woezik and Westerterp [11,12] who analyzed the nitric acid oxidation of 2-octanol to 2-octanone, followed by a much more exothermic oxidation of the reaction product to unwanted carboxylic acids. Recently Westeterp and Molga [13,14] improved the application of the original works of Steensma and Westerterp, providing useful correlations for the estimation in the industrial practice of the parameters involved and generating new boundary diagrams for (1,1) order reactions and wider Co and R_H ranges.

On the basis of this state of the art, the aim of the present work has been firstly to investigate the influence of the whole set of kinetic parameters (in particular of the estimated reaction orders) on the boundary diagrams and hence on the conclusions drawn from the method in question. Moreover, since the boundary diagrams do not provide quantitative information about the peak reaction temperature to be expected for a given set of operating conditions, a new typology of diagrams (called temperature diagrams) has been developed, which, on the basis of the same dimensionless parameters involved in the use of the boundary diagrams, provide such an information to be compared with a maximum allowable temperature (in the following referred to as MAT) for the process under examination. Such a threshold temperature value is typically related to chemical factors (e.g. when strongly exothermic decomposition or unwanted side reactions can be triggered) or to plant factors (e.g. when solvent boiling must be prevented). In particular, the model developed by Steensma and Westerterp [8-10] for heterogeneous (liquid-liquid) reactions of (1,1) orders carried out in indirectly cooled semibatch reactors has been extended to the (n,m) case and then to the homogeneous case and a general procedure for calculating the boundary diagrams has been also developed. It has been proved that the parameter with respect to which the boundary diagrams are most sensitive is the estimated reaction order of the dosed coreactant, so that for a reliable application of the method no uncontrolled approximations on this parameter can be accepted. Moreover, the temperature diagrams method has been introduced, providing a general procedure for the calculation of such diagrams for homogeneous as well as for heterogeneous (liquid-liquid) reaction systems. A general criterion based on the combined use of boundary and temperature diagrams has been developed, through which safe and productive operating conditions

of indirectly cooled SBRs can be easily predicted without solving the mathematical model of the reactor. Such an approach allows for a significant reduction of the experimental effort in the identification of the aforementioned operating conditions, with a significant saving of time and money. Finally, since the most critical step in the application of the method by end users is the calculation of the boundary and temperature diagrams (when not available) for the exact values of the estimated parameters, a number of rules of thumb has been provided for the safe use of diagrams with approximated values of the parameters involved. Such rules of thumb have been finally experimentally verified analyzing through the boundary and temperature diagrams an industrial nitration process for the production of a pharmaceutical active ingredient, that is the nitration of N-(2-phenoxyphenyl) methane sulfonamide (in the following referred to as FAM) to N-(4-nitro, 2-phenoxyphenyl) methane sulfonamide (in the following referred to as NIM), carried out in homogeneous phase in indirectly cooled SBRs.

1. Prevention of coreactant accumulation in heterogeneous (liquid-liquid) semibatch reactors: development of a general procedure

When analyzing exothermic reaction processes carried out in indirectly cooled SBRs, after a preliminary characterization of the thermal stability of each species involved as well as of the reacting mixture, the experimental data obtained from calorimetric experiments are often fitted through a power law type rate of reaction: $r=k_{n,m}C_A^{n}C_B^{m}$. In this expression the reaction order of the dosed coreactant, n, and of the reactant initially charged in the reactor, m, usually differ from (1,1). However, the criteria available in the literature for the prediction of safe and productive operating conditions of indirectly cooled SBRs have been developed only for reactions of (1,1) orders. In Chapter 1 the boundary diagrams method for heterogeneous (liquid-liquid) semibatch reaction systems of (1,1) order kinetics operating in the kinetically controlled (or slow reaction) regime has been extended to the general (n,m) case. The slow reaction regime corresponds to characteristic times of the chemical reaction much higher than those of the mass transfer phenomena between the two liquid phases and is characterized by values of the Hatta number, Ha, and of the Hinterland ratio, Al, such that $Ha<0.2$ and $Al\cdot Ha^2>>1$ [15]; experimentally the slow regime can be easily recognized since it is characterized by a negligible influence of the interfacial area (and hence of the stirring rate) on the reactor operation. Such a behavior is useful when performing calorimetric experiments (e.g. in a RC1 equipment) for the determination of the *microkinetic* rate of reaction expression, that is of a rate expression that must not be affected by interphase mass transfer phenomena.

The aim of the work presented in Chapter 1 is therefore to verify the influence of the microkinetic rate expression (and in particular of the estimated reaction orders, n and m) on the

conclusions drawn trough the boundary diagrams method for heterogeneous (liquid-liquid) SBRs operating in the slow regime.

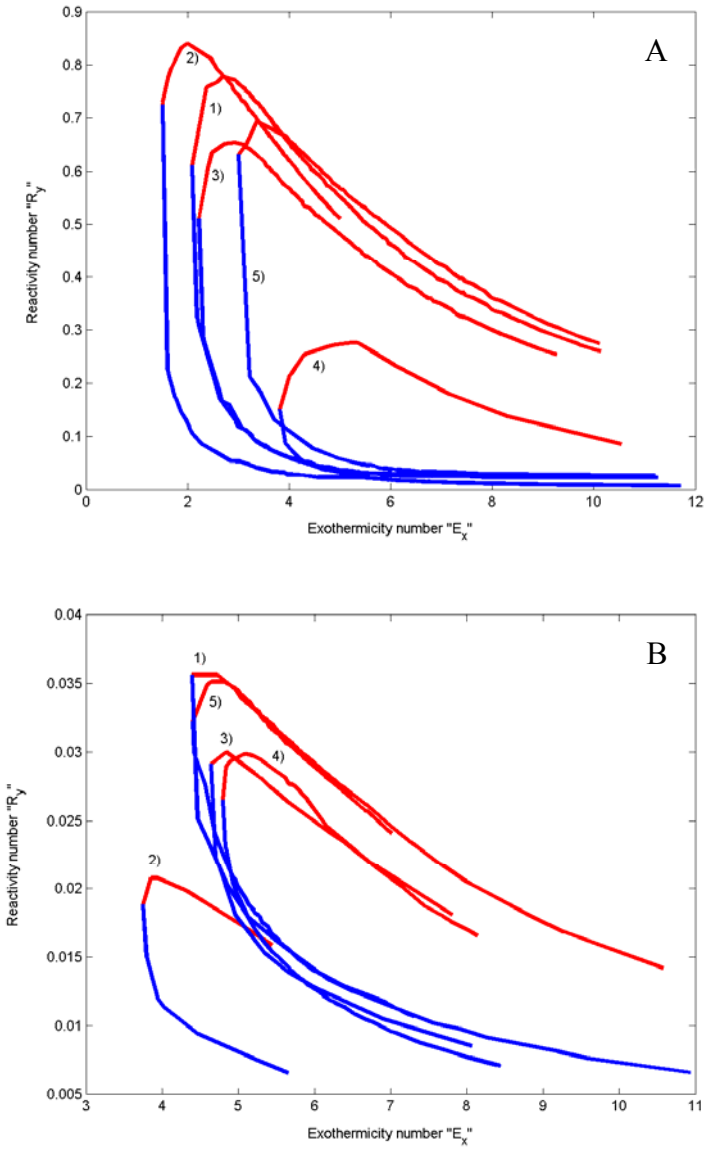

Figure 2 *Sensitivity of the boundary diagrams with respect to the model parameters. Slow reaction regime. 0.025< ν_A Da RE<14, 0.3<ε<0.55, 32<γ<42, 0.29<$\Delta\tau_{ad,0}$<0.7. 1) Co=10, R_H=1, n=1, m=1; 2) Co=20, R_H=1, n=1, m=1; 3) Co=10, R_H=2, n=1, m=1; 4) Co=10, R_H=1, n=2 (A) and n=1.25 (B), m=1; 5) Co=10, R_H=1, n=1, m=2 (A) and m=1.25 (B). A) reaction in the dispersed phase; B) reaction in the continuous phase.*

The mathematical model presented by Steensma and Westererp [8] has been generalized to arbitrary reaction orders, developing the corresponding expressions of the parameters involved as well as of the dimensionless space in which the boundary diagrams are represented (that is of the E_x and R_y parameters). A general procedure for calculating the boundary diagrams (never provided before in the literature, at least in my knowledge) has been developed and several boundary diagrams have been calculated for slow semibatch reactions occurring in the continuous and in the dispersed phase, and for values of the parameters involved (that is: Co, R_H, n and m) normally encountered in the practice.

As it can be observed from Figures 2.A and 2.B, the parameter with respect to which the boundary diagrams shape and location (identified through the $E_{x,MIN}$ and $R_{y,QFS}$ values) are most sensitive is the reaction order of the dosed coreactant, n. The same results can be better summarized in terms of normalized objective sensitivity coefficients of $E_{x,MIN}$ and $R_{y,QFS}$ with respect to the considered parameters. Such sensitivity coefficients can be defined as [2]:

$$S_{i,j} = \frac{\alpha_j}{\beta_i}\frac{\partial \beta_i}{\partial \alpha_j} \approx \frac{\alpha_j}{\beta_i}\frac{\Delta \beta_i}{\Delta \alpha_j} \tag{6}$$

where β_i is either $R_{y,QFS}$ or $E_{x,MIN}$, and α_j is one of the investigated parameters. The computed values of such sensitivity coefficients are summarized in Table 1, clearly showing the influence of the various parameters considered.

Table 1 *Normalized sensitivity coefficients of $R_{y,QFS}$ and $E_{x,MIN}$ computed from the data shown in Figure 2.*

	Slow reaction in the *dispersed* phase, d				**Slow reaction in the *continuous* phase, c**			
	Co	**R_H**	**n**	**m**	**Co**	**R_H**	**n**	**m**
$R_{y,QFS}$	0.08	0.16	0.64	0.11	0.43	0.18	0.72	0.14
$E_{x,MIN}$	0.28	0.07	0.82	0.44	0.17	0.03	0.27	0.08

We can see that the influence of the reaction orders on the values of $R_{y,QFS}$ or $E_{x,MIN}$ can be higher than that of both Co and R_H. This conclusion is only partially tempered by noting that the range of variation of Co in practical conditions is much larger than that of both n and m [1,13,14]: it is quite evident that the influence of n and m on the shape and location of the boundary diagrams cannot be disregarded as had previously been proposed in the literature [13,14]. Moreover, it has been verified that the E_x and R_y values are much less sensitive than $E_{x,MIN}$ and $R_{y,QFS}$ with respect to uncontrolled constraints on the reaction orders in fitting the experimental data. Such a result is of crucial importance for a reliable application of the method since the classification of a selected set of operating conditions arises from a comparison between the E_x and $E_{x,MIN}$, and the R_y and $R_{y,QFS}$ values. These conclusions have been summarized in a number of rules of thumb, never underlined

before in the literature (at least in my knowledge), in order to allow end users to safely analyze through an available boundary diagram the operating conditions of a liquid-liquid SBR which operation is better described by slightly different values of the aforementioned parameters. In particular, uncontrolled approximations on the reaction order of the dosed coreactant, n, cannot be accepted since they can lead to unsafe (or low production) operating conditions if the real n value is lower (or higher) than that of the diagram. The influence of the reaction order of the reactant initially charged in the reactor, m, is much lower. For this reason, the global reaction order (n+m) cannot be used as a discriminating parameter for establishing whether a given diagram can be safely employed for the analysis of the operating conditions of a SBR whose behavior is described by different n and m values.

The analysis performed in Chapter 1 for heterogeneous (liquid-liquid) SBRs operating in the slow regime has been extended to the case of diffusion controlled (or fast reaction) systems, as discussed in Chapter 2. Such a kinetic regime implies a characteristic time of the interphase mass transfer phenomena much higher than that of the chemical reaction and is characterized by Ha>3; moreover, no diffusion limitations for the component already present in the reaction phase from the bulk to the film are assumed to occur [15]. The mathematical model for fast reaction systems of (1,1) reaction orders has been extended to the general (n,m) case, developing the corresponding expressions of the parameters involved as well as of the dimensionless space where the boundary diagrams are represented (that is, the new expressions of E_x and R_y). For the sake of example, a comparison between the mass balance eqs. (1) for slow and fast reaction systems shows that in the fast reaction regime the apparent activation energy is halved with respect to its microkinetic value; this is the reason why a runaway in the fast reaction regime is normally accompanied by a lower exceeding of the target temperature, which in practice means that it usually exerts a more moderate effect.

On the basis of a procedure similar to that developed for slow reaction systems, a number of boundary diagrams for liquid-liquid SBRs operating in the fast regime has been calculated for reactions occurring in the dispersed as well as in the continuous phase and for several values of the parameters involved (that is: Co, R_H, n and m).

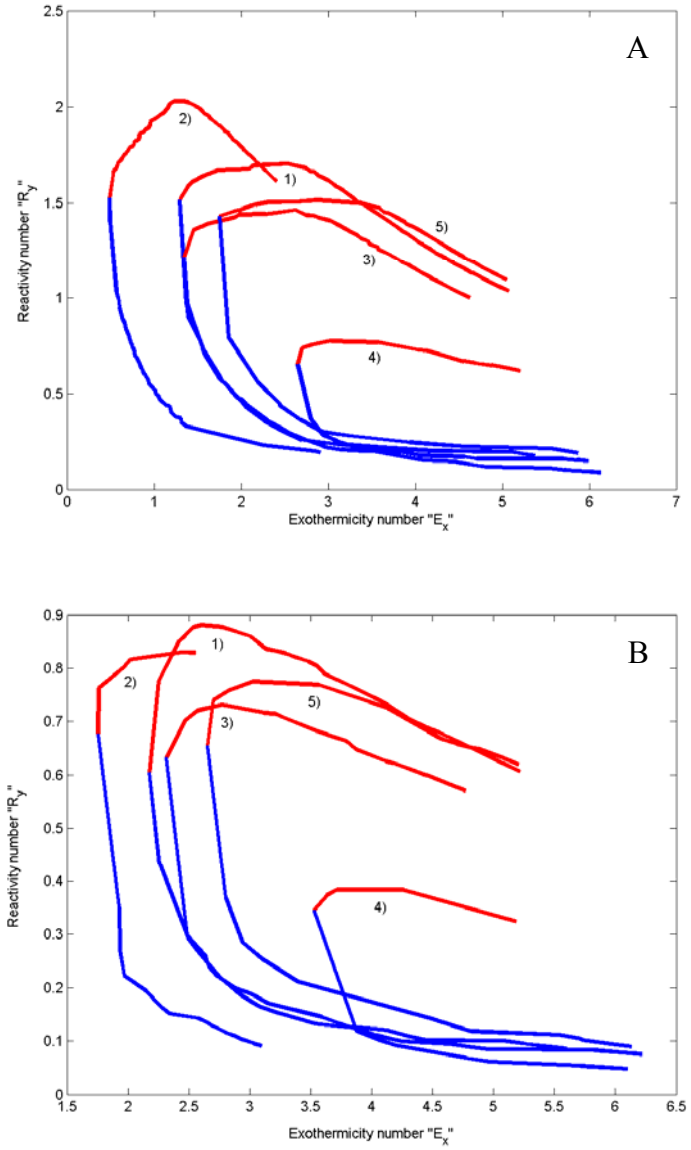

Figure 3 *Sensitivity of the boundary diagrams with respect to the model parameters.*

Fast reaction regime. $0.025<\nu_A\,Da\,RE<14$, $0.3<\varepsilon<0.55$, $32<\gamma<42$, $0.29<\Delta\tau_{ad,0}<0.7$.

1) $Co=10$, $R_H=1$, $n=1$, $m=1$; *2)* $Co=20$, $R_H=1$, $n=1$, $m=1$;

3) $Co=10$, $R_H=2$, $n=1$, $m=1$; *4)* $Co=10$, $R_H=1$, $n=2$, $m=1$;

5) $Co=10$, $R_H=1$, $n=1$, $m=2$.

A) reaction in the dispersed phase; B) reaction in the continuous phase.

As it can be observed from Figures 3.A and 3.B as well as from the results reported in Table 2, that summarizes the values of the parametric sensitivity coefficients for fast reaction systems, also in the fast regime the parameter with respect to which the boundary diagrams shape and extension are most sensitive is the reaction order of the dosed coreactant, n.

Table 2 *Normalized sensitivity coefficients of $R_{y,QFS}$ and $E_{x,MIN}$ computed from the data shown in Figure 3.*

	Fast reaction in the *dispersed* phase, d				**Fast reaction in the *continuous* phase, c**			
	Co	**R_H**	**n**	**m**	**Co**	**R_H**	**n**	**m**
$R_{y,QFS}$	0.19	0.14	0.54	0.11	0.06	0.17	0.56	0.12
$E_{x,MIN}$	0.62	0.04	1.04	0.35	0.19	0.06	0.62	0.22

Moreover, a weaker dependence of the thermal behavior of the reactor on the reaction phase (resulting in a significantly different extension of the corresponding excessive accumulation regions) has been found, due to the relatively low degree of utilization of the reaction phase in the fast than in the slow regime [15].

Also in this case, the results obtained have been summarized in some rules of thumb, according to which when using a boundary diagram calculated for a different kinetic expression than the real one, no uncontrolled approximations on the reaction order of the dosed coreactant must be accepted. The requirements about the reaction order of the reactant initially charged in the reactor are much less stringent.

2. Prevention of decomposition and side reactions in heterogeneous (liquid-liquid) semibatch reactors: development of a general procedure

Limiting coreactant accumulation phenomena in indirectly cooled semibatch reactors can be a necessary, but not a sufficient condition in order to classify as thermally safe a given set of operating conditions. For many reacting systems, if the reaction temperature exceeds a threshold value, dangerous decomposition reactions can be triggered, leading to a thermal runaway. Such events, that can be detected through proper calorimetric techniques, are normally characterized by a much higher exothermicity than that of the desired reaction and by the evolution of huge gas amounts, which imply dangerous increases of the reactor pressure. For these reasons, a less exothermic reaction system characterized by a relatively low MAT value can be much more critical than a more exothermic one with a very high MAT value. On the basis of a number of process information (e.g. the reaction enthalpy and the heat capacity of the reacting mixture, the adiabatic temperature rise under the process conditions, the boiling point of the reacting mixture, the temperature range in which dangerous decomposition reactions can be triggered and their reaction enthalpy, the amount and rate of gas evolution, the effect of operational errors and impurities) Stoessel [16] classified the exothermic reaction processes into five categories, arising from a comparison among the reaction temperature increase with respect to the initial temperature, the maximum temperature reached by the synthesis reaction under adiabatic conditions ($MTSR_{ad}$), the

solvent boiling point and the maximum allowable temperature for the triggering of unwanted consecutive events (MAT).

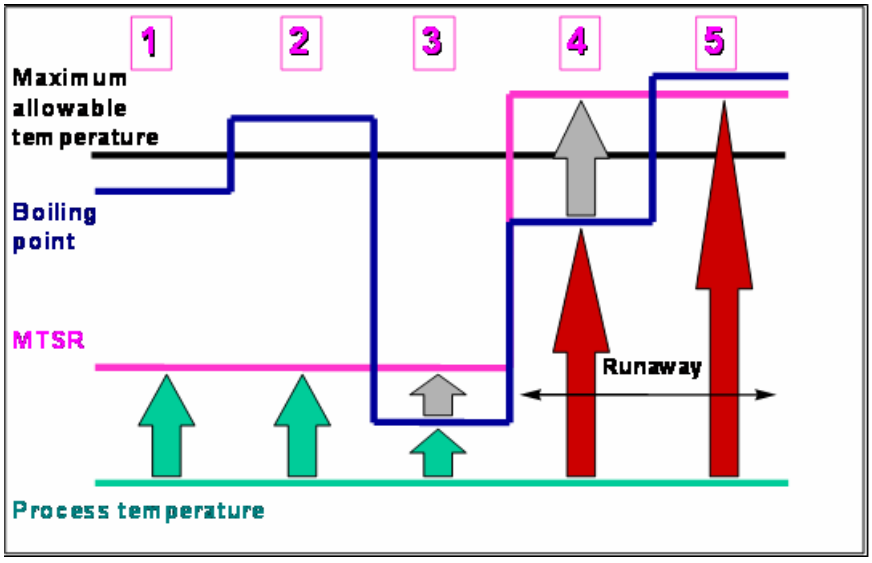

Figure 4 *Classification of exothermic reaction processes according to Stoessel [16].*

Such classes (represented in Figure 4) correspond to the following scenarios:

1) after the thermal loss of control of the desired reaction, neither the solvent boiling point, nor the MAT are normally reached. In any case, the solvent evaporation would occur at a temperature lower than the MAT, thus counteracting further temperature increases;
2) after the thermal loss of control of the desired reaction, neither the solvent boiling point, nor the MAT are normally reached. However, the solvent evaporation would occur at a temperature value higher than the MAT: this means that in case of a long time cooling system failure an exothermic decomposition reaction could be triggered, followed by the solvent evaporation at rates that could be dangerous;
3) after the thermal loss of control of the desired reaction, the solvent boiling point is reached. In such a situation the process safety depends on the heat removal efficiency from the system, that must balance the net enthalpic contribution associated with the exothermic desired reaction and the endothermic solvent evaporation;
4) after the thermal loss of control of the desired reaction, both the solvent boiling and the decomposition event take place. In such a situation the process safety depends on the heat removal efficiency from the system, that must balance the net enthalpic contribution associated with both the desired and the decomposition reactions, and the solvent evaporation.

5) after the thermal loss of control of the desired reaction, the MAT is firstly reached and then the solvent boiling point. In such situations the endothermic contribution associated with the solvent evaporation is often negligible compared with the exothermic one associated with the decomposition reaction, so that a properly sized quenching system is required. Such a situation is the most critical one and should therefore be avoided.

It is important to notice that the conclusions above do not apply only to process safety problems (typically related to the triggering of strongly exothermic decomposition reactions) but to every process situation in which a threshold temperature must not be exceeded: such situations are very frequent in the fine chemical and pharmaceutical industries, where a number of processes can be affected by unwanted side reactions above a threshold temperature that can compromise the reactor productivity or the product quality. In other words, regardless the typology of problem we are dealing with, the condition to fulfill in the conduction of an exothermic semibatch reaction process is often summarized through a threshold temperature value that must not be exceeded neither during the normal reactor operation, nor during upset conditions, such as those arising from a cooling system failure.

As detailed in Chapters 1 and 2, performing an exothermic semibatch reaction in an indirectly cooled SBR, too low initial temperature values can imply an excessive coreactant accumulation, that can lead to the thermal loss of control of the system as the reaction itself ignites. For these reasons, operating conditions characterized by a higher initial temperature are often safer, since they imply a lower coreactant accumulation. However, when a threshold reaction temperature must not be exceeded, a too high initial temperature can lead to the exceeding of the MAT. In such cases, the only use of the boundary diagrams does not allow to establish whether a given set of operating conditions can be adopted.

For these reasons, as discussed in detail in Chapter 3, the boundary diagrams for the prevention of excessive coreactant accumulation in indirectly cooled SBRs in which liquid-liquid reactions are performed have been coupled with another typology of diagrams that had never been previously proposed in the literature, called temperature diagrams, an example of which is provided in Figure 5. Such diagrams, in the same dimensionless space in which the boundary diagrams are represented, allow to estimate the maximum temperature increase with respect to the initial temperature to be expected for a given set of operating conditions.

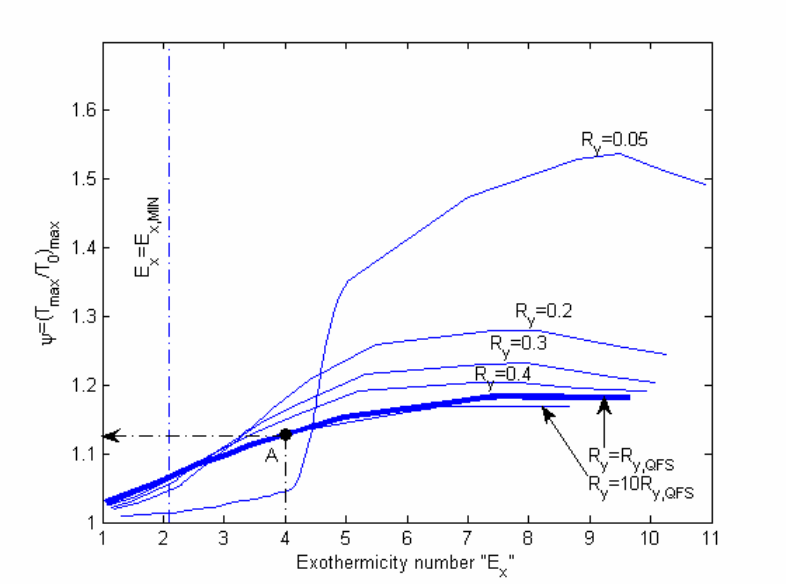

Figure 5 *Temperature diagram for the determination of the peak reaction temperature in a heterogeneous (liquid-liquid) SBR with reaction occurring in the dispersed phase.*

When analyzing a set of operating conditions for a SBR (to which an E_x and R_y value corresponds, according to eqs. (4) and (5)) the temperature diagrams must be firstly used, in order to verify the fulfillment of the condition:

$$\psi \cdot T_0 < MAT \tag{7}$$

If check (7) is satisfied, two situations may be possible:

a) the calculated (E_x,R_y) point belongs to the $E_x \leq E_{x,MIN}$ zone of the temperature diagram (see Figure 5) or to the $E_x > E_{x,MIN}$ zone with $R_y \geq R_{y,QFS}$. In this case the selected operating conditions can be accepted since they cannot lead to the triggering of unwanted reactions and they belong to the inherently safe region of the boundary diagram, where no excessive coreactant accumulation can occur;

b) the calculated (E_x,R_y) point belongs to the $E_x > E_{x,MIN}$ zone of the temperature diagram (see Figure 5) with $R_y < R_{y,QFS}$. In this case, it is necessary to refer to the related boundary diagram, to check whether the aforementioned point belongs to the safe region, to the excessive accumulation region or to the no ignition region. It must in fact be noticed that even operating conditions which satisfy the check (7) cannot be considered thermally safe if they imply an excessive coreactant accumulation since such operating conditions are typically characterized by sudden temperature and conversion jumps which are responsible for a bad control of the reactor. Moreover, it must be taken into account that a given set of operating conditions must be safe not only during the normal reactor operation, but also

during upset conditions, such as those arising from a cooling system failure: in such situations, operating with a minimum coreactant accumulation allows to keep the process safe by stopping immediately the coreactant feed. Finally, no ignition operating conditions must be obviously avoided since they imply a low reactor productivity.

In Chapter 3 a general procedure for calculating a temperature diagram is also discussed in detail. The combination of the boundary and temperature diagrams method in the generalized form provided in Chapters 1, 2, and 3 is therefore a simple, reliable and general tool for the selection of operating conditions of indirectly cooled liquid-liquid SBRs, characterized by both a sufficiently low coreactant accumulation and by peak reaction temperatures lower than a threshold value.

3. Identification of safe and productive operating conditions in homogeneous semibatch reactors: development and validation of a general procedure

For homogeneous SBRs a number of safety criteria developed for (1,1) order reactions can be found in the literature [6,7,17]. However, the calorimetric experimental data are usually fitted through power law type rate expressions with reaction orders different from (1,1). Consequently, the model discussed in Chapters 1 and 2 for heterogeneous (liquid-liquid) SBRs has been extended to the homogeneous reaction case, developing the corresponding expressions of the parameters involved as well as of the dimensionless space for the representation of the diagrams (that is, the E_x and R_y parameters).

On the basis of a procedure similar to that discussed in Chapter 1, a number of boundary diagrams has been generated for several sets of the parameters involved (that is: Co, R_H, n and m).

It has been found that, as required by the criteria reported in the literature, when dealing with homogeneous semibatch reactions of (1,1) orders a given set of operating conditions can be considered safe if it implies R_y values higher than one. However, for other values of the reaction orders, this safety criterion does not hold anymore.

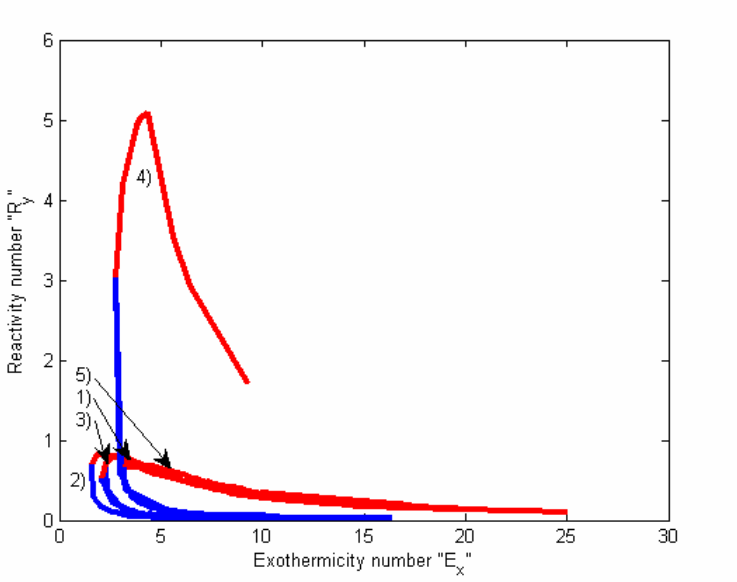

Figure 6 *Sensitivity of the boundary diagrams for homogeneous semibatch reactions with respect to the model parameters. 0.02< ν_A Da RE<20, 0.05<ε<0.6, 30<γ<45, 0.1<$\Delta\tau_{ad,0}$<0.7. 1) Co=10, R_H=1, n=1, m=1; 2) Co=20, R_H=1, n=1, m=1; 3) Co=10, R_H=2, n=1, m=1; 4) Co=10, R_H=1, n=2, m=1; 5) Co=10, R_H=1, n=1, m=2.*

As can be deduced from Figure 6, where boundary diagrams for various operating parameters are represented, and from the results reported in Table 3, that summarizes the values of the sensitivity coefficients with respect to the main operating parameters, also in the homogeneous case using boundary diagrams calculated for different (n,m) values than the real ones can lead to strongly unsafe or low production operating conditions.

Table 3 *Normalized sensitivity coefficients of $R_{y,QFS}$ and $E_{x,MIN}$ computed from the data shown in Figure 6.*

	Co	**R_H**	**n**	**m**
$R_{y,QFS}$	0.032	$9.7\cdot10^{-4}$	5.376	0.154
$E_{x,MIN}$	0.295	0.075	0.232	0.401

However, as a significant difference with respect to the heterogeneous (liquid-liquid) case, it has been found that if the n value according to which the diagram has been calculated is lower than the real value, the conclusions drawn can be unsafe. Such an opposite behavior between homogeneous and heterogeneous (liquid-liquid) SBRs can be explained analyzing the time evolution of the coreactant accumulation in the two cases (as discussed in Chapter 4).

Moreover, also in the homogeneous case if the reaction order of the reactant initially loaded in the reactor, m, changes the approximated boundary diagram or safety criterion can in general be used, since the sensitivity of the $E_{x,MIN}$ and $R_{y,QFS}$ values with respect to the parameter m

is relatively low. Finally, because of the significantly different sensitivities of $E_{x,MIN}$ and $R_{y,QFS}$ to n and m, the global reaction order cannot be used as a discriminating parameter in order to establish whether a boundary diagram or safety criterion developed for given reaction orders can be used for the safety analysis of a system involving different values of these parameters.

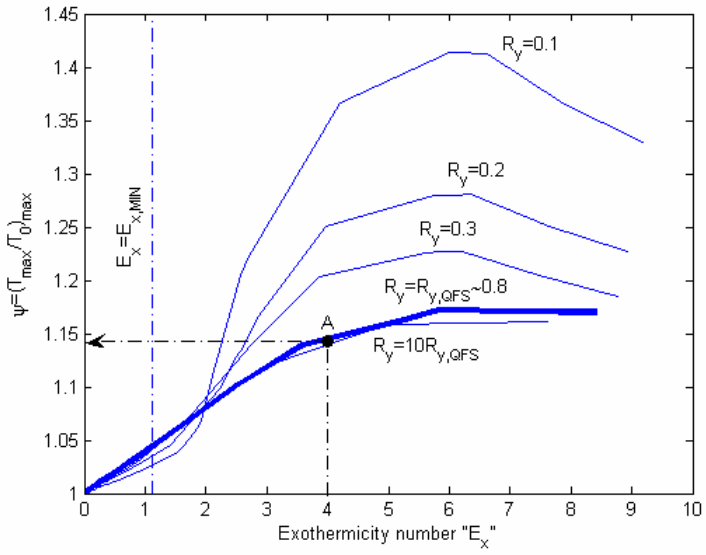

Figure 7 *Temperature diagram for the determination of the peak reaction temperature in a homogeneous SBR.*

Also the temperature diagrams method, discussed in Chapter 3 for heterogeneous (liquid-liquid) SBRs, has been extended to homogeneous reaction systems. A number of temperature diagrams for several Co, R_H, n and m values has been computed, an example of which is presented in Figure 7. As described in the previous section for heterogeneous (liquid-liquid) SBRs, when selecting a set of operating conditions for a homogeneous SBR, the corresponding temperature diagrams can firstly be used to verify that during the normal reactor operation no exceeding of the MAT can occur. Subsequently, the related boundary diagrams can be used to prevent excessive coreactant accumulation, that can become dangerous during upset conditions.

The method developed for the prediction of safe and productive operating conditions of homogeneous SBRs has been validated using, as a test case, the final reaction step for the production of a pharmaceutical active ingredient, that is the nitration of N-(2-phenoxyphenyl) methane sulfonamide (FAM) to N-(4-nitro, 2-phenoxyphenyl) methane sulfonamide (NIM). Such a reaction is performed in homogeneous phase in indirectly cooled SBRs, in which nitric acid is added to an acetic acid solution of the reactant to be nitrated, as discussed in detail in Chapter 5.

It is well known that nitration reactions can be critical from the safety point of view, since an excessive nitric acid accumulation in the system can trigger consecutive oxidations of the

reaction products and, as a final consequence, strongly exothermic decompositions of the reacting mixture.

A preliminary characterization of the thermal stability of the species involved as well as of the reaction mixture has been performed through the software CHETAH of ASTM [18] and experimentally verified through DSC measurements, leading to the conclusion that the most critical situation involves a strongly exothermic decomposition event of the final reacting mixture at 210°C. However, since the reaction is carried out at the industrial scale at atmospheric pressure, the solvent boiling point (equal to 120°C) represents the maximum allowable temperature for the process in question.

A kinetic characterization of the production reaction performed through adiabatic (Phi-TEC II) and further verified through isoperibolic (RC1) experiments [19], results in values of the reaction orders of the dosed coreactant (that is, nitric acid) and of the reactant initially charged in the reactor (that is, FAM) equal to 2 and 0.2, respectively.

To select safe and productive operating conditions for the process the boundary and temperature diagrams have been used and their predictions have been validated through a number of RC1 experiments.

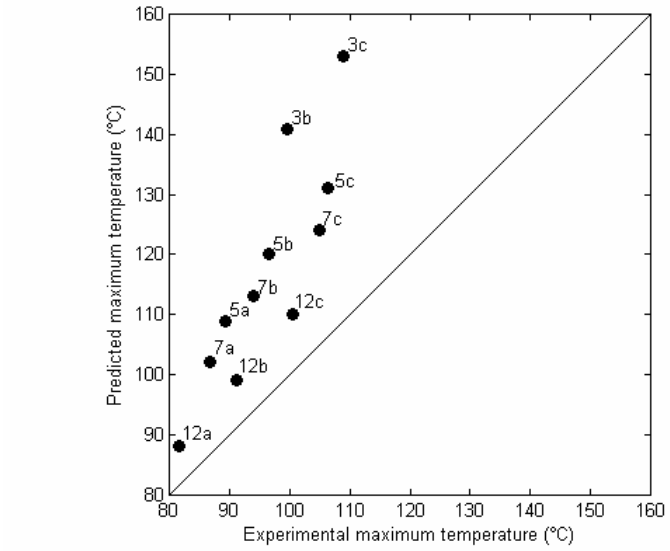

Figure 8 *Parity plot for the comparison of the experimental maximum temperatures reached and the corresponding values predicted through the temperature diagrams.*

In Figure 8, the predictions of the temperature diagrams have been compared with the corresponding experimental values: as it is evident, the temperature diagrams always overestimate the maximum temperature. This is not only a welcome feature since it provides conservative estimations but it follows from the procedure used to build the diagrams. As discussed in detail in Chapter 3 and 4, for a given couple of E_x and R_y values, the temperature diagrams provide the

maximum achievable value of the peak temperature among all the possible combinations of the dimensionless parameters characterizing the SBR dynamics. This means that the particular combination of such parameters representing the system under examination can be the one providing the maximum peak temperature, but most probably it is not. In this case, the experimental temperature will be lower than that predicted through the temperature diagrams. In any case, the experimental maximum temperature can never be higher than the value predicted through the temperature diagrams, coherently with the findings summarized in Figure 8. Moreover, it should be noticed that predicted temperature values higher than the reaction mixture boiling point means only that the MAT is exceeded, since the mathematical model does not account for solvent evaporation. However, this is not a problem since disregarding solvent evaporation leads to conservative results in terms of maximum achievable temperature. We can also note from Figure 8 that all the main experimental trends are correctly predicted by the temperature diagrams. For instance, the values of the maximum temperature for the experiments performed at the same initial temperature decrease with increasing the dosing time (runs 3→5→7→12 with the same letter in Figure 8) as well as it decreases by decreasing the initial temperature at the same dosing time (runs c→b→a with the same number in Figure 8). The predictions of the boundary diagrams have been analogously validated with respect to the experimental values of the relative coreactant amount at the end of the dosing time: operating conditions characterized by (E_x,R_y) values located inside the excessive accumulation region imply higher values of the aforementioned quantity.

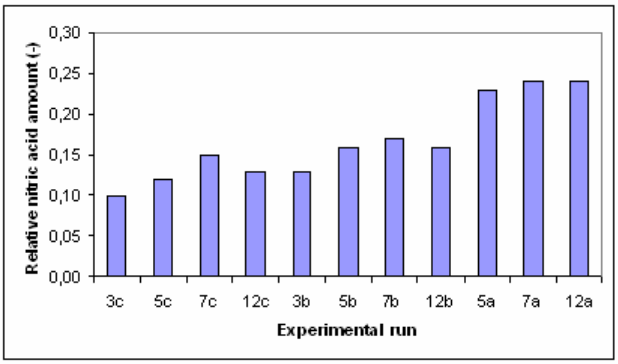

Figure 9 *Experimental values of the relative coreactant amount at the end of the dosing period.*

Coherently, we can see from Figure 9 that all the experimental runs belonging to the inherently safe region imply values of the relative coreactant amount in the range 10÷15%, whereas the three runs characterized by operating parameters located inside the excessive accumulation region imply relative coreactant amounts close to 25% (see Figures 5 to 7 in Chapter 5).

According to the rules of thumb presented in Chapter 4 for the safe use of diagrams calculated for approximated values of the parameters involved, the same conclusions have been

drawn using boundary and temperature diagrams calculated for R_H=1 and m=1, because of the relatively low sensitivity of the location and extension of the diagrams themselves on the R_H and m values. On the contrary, it has been verified that uncontrolled approximations on the reaction order of the dosed coreactant lead to unreliable conclusions. Forcing n=m=1 in the fitting procedure of the Phi-TEC II data the difference between the R_y values calculated according to the two sets of reaction orders (that is n=2, m=0.2 and n=m=1 respectively) is much lower than the corresponding difference between the $R_{y,QFS}$ values: in particular, for the experiments performed at 68°C R_y varies approximately between 6 (for n=2, m=0.2) and 7 (for n=m=1), whereas $R_{y,QFS}$ undergoes an order of magnitude variation, ranging from 9 (for n=2, m=0.2) to 0.9 (for n=m=1). In other words, a-priori constraints on the reaction orders followed by a correspondent adjustment of the remaining kinetic parameters (that is the pre-exponential factor and the activation energy) in order to fit the experimental data, typically lead to minor changes in the R_y values, but to significant variations in the $R_{y,QFS}$ values: however, since the classification of a given set of operating conditions from the safety point of view arises from a comparison between the R_y and $R_{y,QFS}$ values, it is clear that the aforementioned assumptions can lead to unreliable results. For the sake of example, in Figure 10 the (E_x,R_y) points for the experiment performed at T_0=68°C and t_D=12' (that is, for the maximum tested value of the dosing time) have been represented together with the related boundary diagrams, according to the two aforementioned sets of kinetic parameters. As can be observed, the constraint n=m=1 in the fitting of the calorimetric data results in a (E_x,R_y) point belonging to the inherently safe region of the corresponding diagram, representing operating conditions characterized by a low nitric acid accumulation in the system. The same results can also be obtained through the safety criterion of Hugo et al. [6,7,17] for homogeneous (1,1) order reactions, according to which operating conditions implying R_y values higher than one can be considered safe. However, such conclusions do not agree with the experimental results and with the predictions of the method in question without uncontrolled constraints on the reaction order of the dosed coreactant, thus confirming that when using boundary and temperature diagrams such approximations can lead to unsafe conclusions.

It can be finally noticed that the method of boundary and temperature diagrams is a very useful tool for selecting with a minimum experimental effort safe and productive operating conditions of SBRs in which exothermic reactions are performed, since they allow for a planning of the experimental activity (that is, of the RC1 experiments) through a rapid a priori screening of the operating conditions.

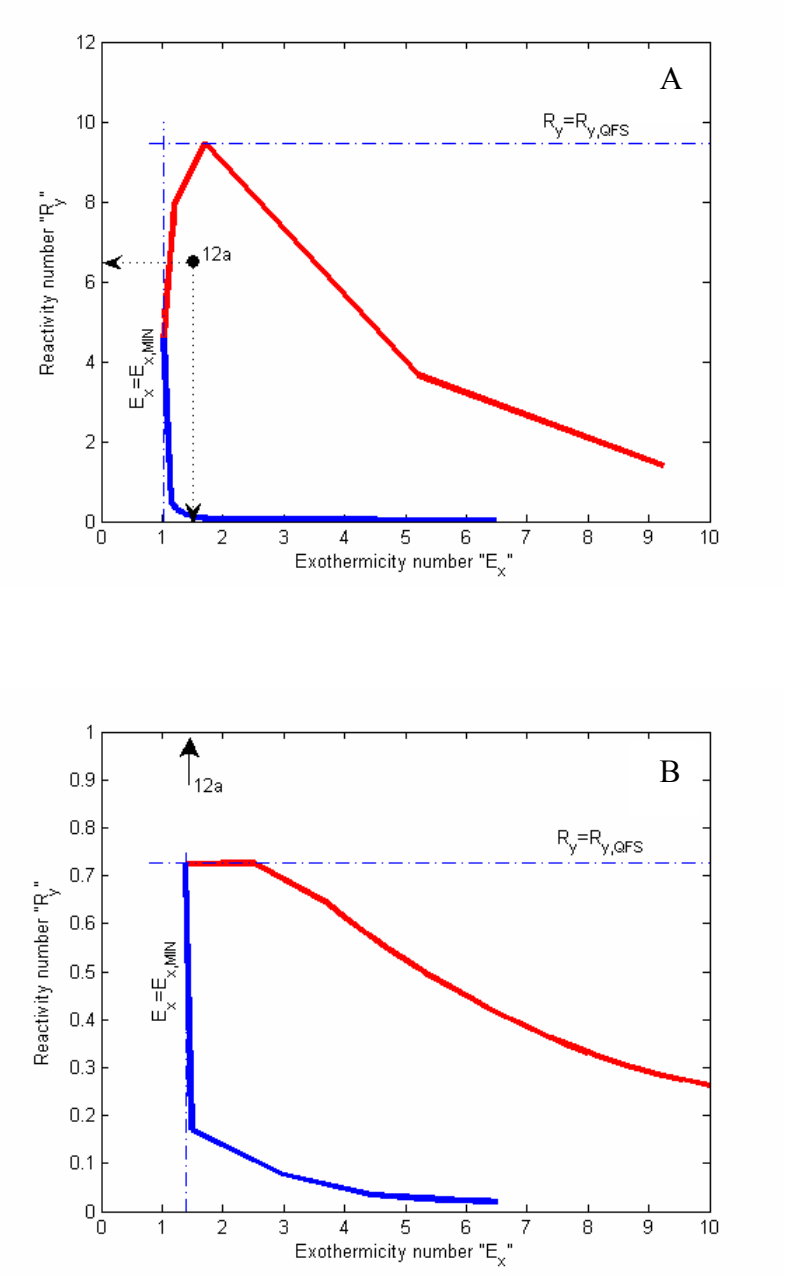

Figure 10 *Safety characterization of the operating conditions with t_D=12min and T_0=68°C through the boundary diagrams. A) Co=50, R_H=1.4, n=2, m=0.2. B) Co=50, R_H=1.4, n=1, m=1. 0.02<Da<20, 0.05<ε<0.6, 30<γ<45, 0.1<$\Delta\tau_{ad,0}$<0.7 (T_R=303K).*

4. Conclusions

The boundary and temperature diagrams method in the generalized form developed in this thesis is a reliable and easy tool for identifying operating conditions of indirectly cooled SBRs characterized by both a low coreactant accumulation and peak reaction temperatures not exceeding a threshold value. The method has been developed for both homogeneous and heterogeneous (liquid-liquid) reaction systems whose behavior can be described by a general power law rate of reaction.

Contrary to what previously proposed in the literature, it has been proved that a detailed kinetic investigation on the reaction system is of crucial importance for a reliable application of the method. Moreover, taking into account that the calculation of the diagrams for the real values of the parameters involved (when not available) is normally not straightforward for end users, a number of rules of thumb for the safe use of approximated diagrams has been provided as for homogeneous as for heterogeneous (liquid-liquid) SBRs.

Nomenclature

Symbols	
A	heat transfer area of the reactor (associated to the jacket and/or the coil), m^2
Al	Hinterland ratio, -
C	molar concentration, $kmol/m^3$
Co	$=U^*Da/\varepsilon$, cooling number, -
$\tilde{C}_P$	molar heat capacity, kJ/(kmol·K)
Da	$=k_{n,m,R}t_D C_{B,0}^{n+m-1}$, Damköhler number for (n,m) order reactions, -
E	activation energy, kJ/kmol
E_x	exothermicity number, -
f	function of the dimensionless time and conversion of B in eq. (1), -
Ha	Hatta number, -
$\Delta\tilde{H}$	reaction enthalpy, kJ/kmol
$k_{n,m}$	reaction rate constant, $m^{3(n+m-1)}/(kmol^{n+m-1}\cdot s)$
MAT	maximum allowable temperature, K
MTSR	maximum temperature reached due to the synthesis reaction, K
r	reaction rate, $kmol/(m^3\cdot s)$
R	gas constant = 8.314, kJ/(kmol·K)
RE	reactivity enhancement factor in eq. (1), -
R_H	heat capacity ratio, -
R_y	reactivity number, -
S	normalized objective sensitivity coefficient, -
t	time or characteristic time, s
T	temperature, K
$\Delta T_{ad,0}$	$= \dfrac{\left(-\Delta\tilde{H}_r\right)C_{B,0}}{\nu_B\tilde{\rho}_m\tilde{C}_{P,m}}$, adiabatic temperature rise, K
U	overall heat transfer coefficient, $kW/(m^2\cdot K)$
U^*Da	$=(UA)_0 t_D/\left(\tilde{\rho}_m\tilde{C}_{P,m}V_{r,0}\right)$, modified Stanton number, -
V	liquid volume, m^3
Greek symbols	
α	flag parameter, eq. (2), -
α, β	generic symbols, eq. (6), -
γ	$=E/(RT_R)$, dimensionless activation energy, -

ε	relative volume increase at the end of the semibatch period, -
ζ	molar conversion, -
ϑ	$=t/t_D$, dimensionless time, -
κ	$=k/k_R$, dimensionless reaction rate constant, -
ν	stoichiometric coefficient, -
$\tilde{\rho}$	molar density, $kmol/m^3$
τ	$=T/T_R$, dimensionless temperature, -
ψ	$=(T_{max}/T_0)_{max}$, maximum dimensionless temperature rise, -

Subscripts and superscripts

A,B,C,D	components A, B, C and D
ad	adiabatic
app	apparent
cool	coolant
D	dosing stream or dosing time
eff	effective
FAM	N-(2-phenoxyphenyl) methane sulphonamide
H	in the heat capacity ratio R_H
m	order of reaction respect to component B
max	maximum value of a quantity or at the maximum value of a quantity
n	order of reaction respect to component A
NIM	N-(4-nitro, 2-phenoxyphenyl) methane sulphonamide
MIN	in $E_{x,MIN}$
QFS	in $R_{y,QFS}$
r	reaction
R	reference
ta	target
x	in the exothermicity number E_x
y	in the reactivity number R_y
0	start of the semibatch period

Literature cited

1. Steinbach, J. Safety assessment for chemical processes. *Wiley-WCH* 1999.

2. Varma, A.; Morbidelli, M.; Wu, H. Parametric Sensitivity in Chemical Systems. *Cambridge University Press*. 1999.

3. Alòs, M.A.; Nomen, R.; Sempere, J.M.; Strozzi, F.; Zaldìvar, J.M. Generalized criteria for boundary safe conditions in semibatch processes: simulated analysis and experimental results. *Chem. Eng. Process.* 1998, *37,* 405-421.

4. Zaldìvar, J.M.; Cano, J.; Alos, M.A.; Sempere, J.; Nomen, R.; Lister, D.G.; Maschio G.; Obertopp, T.; Gilles E.D.; Bosch, J.; Strozzi, F. A General criterion to define runaway limits in chemical reactors. *J. Loss Prev. Process Ind.* 2003, *16 (3),* 187-200.

5. Bosch, J.; Strozzi, F.; Lister, D.G.; Maschio, G.; Zaldìvar, J.M. Sensitivity analysis in polymerization reactions using the divergence criterion. *Process Safety and Environmental Protection* 2004, *82 (B1),* 18-25.

6. Hugo, P.; Steinbach, J. Praxisorientierte Darstellung der thermischen Sicherheitsgrenzen für den indirekt gekühlten Semibatch-Reaktor. *Chem. Ing. Tech.* 1985, *57, Nr. 9,* 780-782.

7. Hugo, P.; Steinbach, J. A comparison of the limits of safe operation of a SBR and a CSTR. *Chem. Eng. Sci.* 1986, *41*, 1081-1087.

8. Steensma, M.; Westerterp, K.R. Thermally safe operation of a cooled semibatch reactor. Slow liquid-liquid reactions. *Chem. Eng. Sci.* 1988, *43, Nr.8,* 2125-2132.

9. Steensma, M.; Westerterp, K.R. Thermally safe operation of a semibatch reactor for liquid-liquid reactions. Slow reactions. *Ind. Eng. Chem. Res.* 1990, *29,* 1259-1270.

10. Steensma, M.; Westerterp, K.R. Thermally safe operation of a semibatch reactor for liquid-liquid reactions. Fast reactions. *Chem. Eng. Technol.* 1991, *14,* 367-375.

11. van Woezik, B.A.A.; Westerterp K.R. The nitric acid oxidation of 2-octanol. A model reaction for multiple heterogeneous liquid-liquid reactions. *Chem. Eng. Process.* 2000, *39,*

521-537.

12. van Woezik, B.A.A.; Westerterp K.R. Runaway behaviour and thermally safe operation of multiple liquid-liquid reactions in the semibatch reactor. The nitric acid oxidation of 2-octanol. *Chem. Eng. Process.* 2001, *41,* 59-77.

13. Westerterp, K.R.; Molga, E.J. No more runaways in fine chemical reactors. *Ind. Eng. Chem. Res.* 2004, *43 (16),* 4585-4594.

14. Westerterp, K.R.; Molga, E.J. Runaway prevention in liquid-liquid semibatch reactors. *Inzynieria Chemiczna i Procesowa* 2004, *25(3/4)*, 2041-2050.

15. Westerterp, K.R., van Swaaij, W.P.M., Beenackers, A.A.C.M. Chemical reactor design and operation. *2nd ed.* 1984, *John Wiley & Sons, Chichester, U.K.*.

16. Stoessel, F., What is your thermal risk? *Chem. Eng. Prog.* 1975, 68-75.

17. Hugo, P.; Steinbach, J.; Stoessel, F. Calculation of the maximum temperature in stirred tank reactors in case of a breakdown of cooling. *Chem. Eng. Sci.* 1988, *43, 8*, 2147-2152.

18. Seaton, W.H.; Freedman, E.; Treweek, D.N. CHETAH – The ASTM Chemical Thermodynamics and Energy Release Potential Evaluation Program, ASTM DS 51, Philadelphia, 1974.

19. Ampelli, C.; Di Bella, D.; Lister D.G.; Maschio G. Fitting isoperibolic calorimeter data for reactions with pseudo-first order chemical kinetics. *J. Therm. Anal.* 2005, *79 (1),* 89-94.

1. Thermally safe operation of liquid-liquid semibatch reactors. Part I: single kinetically controlled reactions with arbitrary reaction order

Francesco Maestri, Renato Rota*

Politecnico di Milano

Dip. di Chimica, Materiali e Ingegneria Chimica "G. Natta"

via Mancinelli 7 - 20131 Milano – Italy

fax: +39 0223993180; e-mail: renato.rota@polimi.it

Abstract

The thermally safe operation of an indirectly cooled semibatch reactor in which an exothermic reaction occurs corresponds to conditions of potentially very high effective reaction rate compared to the dosing rate of the coreactant, which accumulation in the reaction system is consequently small. On this basis it is possible to build boundary diagrams in terms of suitable dimensionless parameters, which summarize all the possible thermal behaviors of the reactor and can be used for safe scale-up purposes.

In this work the influence of the reaction kinetics on the shape and location of boundary diagrams for a single liquid-liquid reaction in the slow regime is discussed. First of all, the theory of boundary diagrams, originally developed for (1,1) reaction order, is extended to a generic (n,m) rate of reaction expression. Then it is shown that in many practical systems, using boundary diagrams based on (1,1) reaction order can lead to both unsafe and not necessary (from a safety point of view) low-production operating conditions. New boundary diagrams for a few (n,m) reaction orders are presented. Some rules-of-thumb are also discussed to identify in which cases a boundary diagram developed for a given (n,m) reaction order can be reasonably used to approximate the real kinetic behavior of the system of interest. Moreover, since building a boundary diagram for the specific kinetics considered can be necessary, a simple and general

* to whom correspondence should be addressed

procedure for building such diagrams that can be easily implemented in a computer code is also presented.

Keywords: Semibatch reactors; Boundary diagrams; Kinetics; Runaway; Safety; Scale-up.

1.1 Introduction

Runaway in chemical batch and semibatch reactors involving exothermic reactions are very frequent; for instance, in a typical EU country more than 100 runaways are expected to occur annually [1]. Fortunately, a little quantity of these accidents leads to serious consequences to either the workers or the inhabitants of the neighborhood of the factory. However, when strong runaways occur, the consequences can be really serious, as happened, for instance, in 1976 in Seveso, Italy. This motivates the huge amount of work that have been done on runaway phenomena in chemical batch and semibatch reactors, for developing simple and reliable procedures to scale up chemical processes from laboratory to industrial scale. The main problem to face in practice is that in fine chemical industries, which produce very different amounts of a wide range of chemical compounds, it is usually not possible, because of time and money constraints, to investigate in detail the kinetics of all the reactions involved. This calls for a procedure that must be not only reliable but also simple, and explains why, in spite of the progress that has been made in understanding runaway phenomena, the problem has not been solved yet for practice, so that runaways still occur [2]. It should be mentioned that the incorrect scale up of the process is not the only responsible for runaways. Other events can initiate a runaway, such as those related to human factors, maintance, failure of the control system, agitator breakdown, etc. However, these events can be easily identified through standard techniques used for hazard identification processes, such as the hazard and operability (HAZOP) analysis. Moreover, they can be handled enforcing suitable design, working and maintance procedure. Consequently, a correct scale-up is the key point for runaway prevention.

When the heat effects associated to a chemical reaction are high, the process cannot be carried out safely in a batch reactor [3]. The rate of heat evolution can be controlled by adding one of the reactants slowly to the other component already present in the reactor, that is, by using an indirectly cooled semibatch reactor (SBR). The dosing rate of one of the reactants (usually called coreactant) must be slow enough so that the cooling system can remove all the heat released.

The first studies about the thermally safe operation of SBRs were conducted by Hugo and Steinbach [4,5]. Their work, based on *homogeneous* reaction systems, introduced the accumulation criterion for the analysis of the thermal behavior of SBRs: accumulation of the coreactant in the system arises from a not negligible characteristic time of the chemical reaction, compared with that of the coreactant supply and must be kept at sufficiently low values to avoid the thermal loss of control of the reactor (runaway). If the coreactant accumulates in the reactor, the system switches from semibatch to batch like conditions and the cooling system cannot control anymore the heat evolution.

Steensma and Westerterp [6-8] extended the results obtained by Hugo and Steinbach to

heterogeneous (liquid-liquid) SBRs, introducing the concept of target temperature and producing the so-called boundary diagrams for single reactions (both in the slow or fast regime) of (1,1) reaction order kinetics, that is of the type: $r=kC_AC_B$. Boundary diagrams define, in a suitable dimensionless space, the regions where different reactor behaviors are expected. In particular, runaway and inherently safe regions are defined, allowing for identifying safe and dangerous operating conditions.

Van Woezik and Westerterp [9,10] extended the concepts introduced by Steensma and Westerterp to the case of *multiple (consecutive) reactions*, studying both theoretically and experimentally the nitric acid oxidation of 2-octanol to 2-octanone with further oxidation of the desired reaction product to carboxylic acids.

Recently, the work of Steensma and Westerterp on slow liquid-liquid reaction systems was improved by Westerterp and Molga [2], with particular emphasis on how to use in practice the boundary diagrams and on how to define inherently safe operating conditions.

As previously mentioned, detailed information on the reaction mechanism and kinetics are seldom available in practice. However, modeling the behavior of a liquid-liquid SBR requires the knowledge of the *reaction kinetics*, at least in terms of a lumped overall reaction. Such an information can be obtained through calorimetric (e.g., RC1) experiments carried out in the slow reaction (microkinetic) regime. This means that some laboratory experimental work cannot be avoided [2]. The main aim of developing simple scale-up procedures is to keep such an experimental effort as low as possible. Boundary diagrams are a suitable tool to achieve this goal. Experimental data are usually interpreted through power law rate of reaction expressions with (n,m) reaction orders: $r=kC_A^nC_B^m$. In spite of (n,m) usually differ from (1,1), boundary diagrams have been developed till now only for the (1,1) case, and some rules-of-thumb have been proposed to use the (1,1) boundary diagrams for a generic (n,m) reaction order [2]. Consequently, the main aim of this work is to analyze in detail the influence of the reaction orders on the boundary diagrams, providing runaway and inherently safe regions for some (n,m) couples. These boundary diagrams can be used as a guide for a preliminary analysis of any reaction order. Moreover, to allow for a more rigorous analysis of a generic (n,m) reaction order, also a practical procedure for building boundary diagrams for generic (n,m) reaction orders is presented, with particular attention to the physical meaning of the various dimensionless parameters required.

1.2 Mathematical model

Developing a boundary diagram for a generic (n,m) reaction order and discussing the physical meaning of the dimensionless parameters introduced to define the space where runaway or inherently safe regions are defined requires a preliminary discussion on how the investigated process can be modeled. We assume that at time equal to zero the feed of the coreactant A to a SBR filled with a given amount of component B is started at a constant rate, until the stoichiometric ratio between the two species is reached, according to the overall stoichiometry:

$$\nu_A A + \nu_B B \rightarrow C + \nu_D D \tag{1}$$

The process involves two liquid phases: a continuous phase and a dispersed phase (in the following referred to respectively as the “c” phase and the “d” phase). We further assume that the microkinetic rate expression of the reaction (1) can be described by a generic power law expression:

$$r = k_{n,m} C_A^n C_B^m \tag{2}$$

A simple mathematical model can be formulated assuming that:

1) the reaction mass is perfectly macromixed;
2) the influence of the chemical reaction on the volume of the single phase is negligible;
3) no phase inversions occur;
4) the solubility of the species A and C in the continuous phase, c, and of components B and D in the dispersed phase, d, is small (in other words, species A and C are almost all in phase d, whereas species B and D are present almost only in phase c);
5) the chemical reaction takes place only in one of the two liquid phases: this situation is very common in many industrial processes (such as nitrations and oxidations), in which the catalyst (typically a strong acid) is present only in one phase;
6) the heat effects are associated to the chemical reaction only;
7) at the beginning, the reaction mass is at the mean coolant temperature, T_{cool}, which is assumed to remain constant for the whole duration of the process (that is, the reactor operates in isoperibolic conditions).

The mass balance equation for the i-th chemical species is:

$$\frac{dn_i}{dt} = F_{i,D} + \nu_i r^{eff} V_r \tag{3}$$

The molar feed rate, $F_{i,D}$, differs from zero only for the species A during the supply period

and, as usual, the stoichiometric coefficient, ν_i, is negative for reactants and positive for products. Moreover, the number of moles in the reactor at t=0, $n_{i,0}$, is different from zero only for species B. The effective reaction rate, r^{eff}, depends on the microkinetic rate expression, the phase in which the reaction takes place and the controlling step among the chemical reaction, the interphase mass transfer and the supply of the coreactant.

In this work we investigate the slow reaction regime, which means that the interphase mass transfer phenomena never control the effective rate of the process, resulting in nearly uniform concentration profiles in both the phases. Since we assume to feed a stoichiometric amount of coreactant, the quantity of species A supplied to the reactor throughout the dosing period, t_D, (or, equivalently, from the beginning to the dimensionless time $\vartheta=t/t_D=1$) can be computed as: $n_{A,1}=F_{A,D}t_D=(\nu_A/\nu_B)n_{B,0}$. Moreover, since we are considering a single reaction, one scalar, such as the conversion of species B, $\zeta_B=1-n_B/n_{B,0}$, suffices to define the extent of the reaction. Performing suitable combinations of the mass balance eqs. (3) and integrating the resulting differential equations, it is possible -using the assumptions 2) and 4) stated before- to derive the following equations, relating the concentrations of A in the dispersed phase, $C_{A,d}$, and of B in the continuous phase, $C_{B,c}$, to ϑ and ζ_B:

$$C_{A,d} = \frac{n_{B,0}\left(\vartheta - \zeta_B\right)\nu_A/\nu_B}{V_D\vartheta} \tag{4}$$

$$C_{B,c} = \frac{n_{B,0}\left(1-\zeta_B\right)}{V_c} \tag{5}$$

Moreover, the mass balance equation for the reactant B can be rewritten as:

$$\frac{d\zeta_B}{d\vartheta} = \frac{\nu_B t_D}{n_{B,0}} r^{eff} V_r \tag{6}$$

Along the line discussed by Steensma and Westerterp [6-8], this equation can be rewritten in the following form:

$$\frac{d\zeta_B}{d\vartheta} = \nu_A \, Da \, RE_{slow,c/d} \; f_{slow,c/d} \; \kappa_{n,m} \tag{7}$$

where $Da=k_{n,m,R}t_D C_{B,0}^{n+m-1}$ is the Damköhler number for (n,m) order kinetics, which contains the physical information about the dosing time, and $\kappa_{n,m}=\exp[\gamma(1-1/\tau)]$ is the dimensionless reaction rate constant, that is the ratio of the reaction rate to the reaction rate evaluated at a reference temperature, T_R, with $\gamma=E/(RT_R)$ and $\tau=T/T_R$. Introducing eq. (2) in eq. (7) and using relations (4), (5) and (6), the expressions of the reactivity enhancement factor, RE, and of the function, f, can be easily derived for the cases of slow reaction taking place respectively in the dispersed ($RE_{slow,d}$ and

$f_{slow,d}$) or in the continuous ($RE_{slow,c}$ and $f_{slow,c}$) phase. These expressions, which are summarized in Table 1, also involve the relative volume increase throughout the dosing period, $\varepsilon=V_D/V_c$, as well as the distribution coefficient, m_i, which is defined as the ratio between the equilibrium concentrations of component i in the two phases (more precisely, it is the ratio of the concentration of component i in the phase in which its solubility is small to that in the other phase). The main difference with respect to the case n=m=1 is that now the function $f_{slow,c/d}$ does not depend only on ε but also on the values of n and m. This dependence will reflect, as discussed in the following, on the shape and location of the boundary diagrams.

The energy balance equation for the reactor is:

$$\left(n_d\tilde{C}_{P,d}+n_c\tilde{C}_{P,c}\right)\frac{dT}{dt}=F_D\tilde{C}_{P,D}\left(T_D-T\right)+V_r r^{eff}\left(-\Delta\tilde{H}_r\right)-UA\left(T-T_{cool}\right) \tag{8}$$

showing that the reactor temperature variations are the result of three enthalpic contributions, associated to the dosing stream, the chemical reaction and the heat removal by the coolant, respectively. As done previously for the mass balance equation, using eq. (7), the energy balance can be rewritten in the following dimensionless form:

$$\left(1+R_H\varepsilon\vartheta\right)\frac{d\tau}{d\vartheta}=\Delta\tau_{ad,0}\frac{d\zeta_B}{d\vartheta}-\left[U^*Da\left(1+\varepsilon\vartheta\right)+\varepsilon R_H\right]\left(\tau-\tau_{cool}^{eff}\right) \tag{9}$$

where: $R_H=\dfrac{\tilde{\rho}_d\tilde{C}_{P,d}}{\tilde{\rho}_c\tilde{C}_{P,c}}\approx\dfrac{\tilde{\rho}_D\tilde{C}_{P,D}}{\tilde{\rho}_0\tilde{C}_{P,0}}$ is the ratio between the volumetric thermal capacities of the dispersed and the continuous phase respectively. Moreover, the reaction enthalpy has been expressed in the form of an adiabatic temperature rise, $\Delta T_{ad,0}=\dfrac{\left(-\Delta\tilde{H}_r\right)n_{B,0}}{\nu_B\tilde{\rho}_c\tilde{C}_{P,c}V_c}$, and a modified Stanton number for the system has been defined as: $U^*Da=\dfrac{\left(UA\right)_0 t_D}{\tilde{\rho}_c\tilde{C}_{P,c}V_c}$. Finally, an effective coolant temperature has been introduced, which takes into account the enthalpic contributions of both the heat removal by the coolant and the dosing stream, $T_{cool}^{eff}=\dfrac{U^*Da\left(1+\varepsilon\vartheta\right)T_{cool}+\varepsilon R_H T_D}{U^*Da\left(1+\varepsilon\vartheta\right)+\varepsilon R_H}$.

The numerical integration (carried out using the MATLAB suite of programs) of the eqs. (7) and (9) with their initial conditions generates the time evolutions of conversion and temperature in the reactor. Figures 1 and 2 show, for the sake of example, the temperature-time profiles for different reaction orders. We can see that the influence of the order of reaction with respect to the dosed component, n, on the thermal behavior of the system is much greater than that of the order of reaction with respect to the reactant initially charged in the reactor, m. For the same set of

parameters and the same initial conditions, a runaway situation can disappear for greater values of n but not of m. This is correct, since the reaction order with respect to the coreactant has a direct influence on the accumulation of the coreactant itself in the reactor: the higher the value of n is, the higher the reaction rates normally become, for a given increase of the hold-up of unreacted coreactant in the system. This fact counteracts obviously the accumulation phenomenon and results in a safer operation of the reactor, as discussed in detail in the following paragraphs.

1.3 Thermally safe operating conditions

The thermally safe operation of a SBR in which an exothermic reaction occurs corresponds to conditions in which the overall kinetics of the process is largely determined by the dosing rate of the coreactant, which accumulation in the system is consequently confined below a critical value. This implies that the characteristic time of the chemical reaction (eventually affected by the influence of interphase mass transfer) is much smaller than the characteristic time of the coreactant supply. This can be quantified by introducing the concept of target temperature, T_{ta} [6]. If we assume that the overall kinetics of the process is completely determined by the dosing rate of the coreactant, the mass balance eq. (7) simplifies to:

$$\frac{d\zeta_B}{d\vartheta} = 1 \tag{10}$$

If we further assume that the reaction temperature evolution is completely dominated by the heat removal contribution, we can introduce a quasi-steady-state assumption for the temperature itself, which yields:

$$\frac{d\tau}{d\vartheta} = 0 \tag{11}$$

Looking at the right side of the energy balance eq. (9), this physically means that the characteristic time of the heat removal contribution from the system (related to both the cooling efficiency and the sensible heat of the dosing stream) is much lower than that of the enthalpic contribution associated to the chemical reaction: these operating conditions minimize the time variations of the reactor temperature, which can be theoretically equal to zero, as stated in eq. (11). Substituting these expressions into the energy balance eq. (9), we obtain the following temperature-time relation, corresponding to the assumptions stated above:

$$\tau - \tau_{cool}^{eff} = \frac{\Delta\tau_{ad,0}}{U^* Da\left(1+\varepsilon\vartheta\right)+\varepsilon R_H} \tag{12}$$

Even if it is natural to associate a “safe” operation of the reactor to the absence of

temperature jumps above a “target temperature”, it is basically arbitrary to give a quantitative definition of what an acceptable accumulation of the dosed coreactant in the system is. Eq. (12) refers to a theoretically negligible ratio between the characteristic times of the chemical reaction and the coreactant supply. To take into account the unavoidable accumulation of the coreactant which occurs in every real system, Steensma and Westerterp [6] suggest -on the basis of the analysis of a number of industrial cases- a 5% overestimation of this temperature difference and call the resulting temperature-time relation target temperature, T_{ta}:

$$\tau_{ta} = \tau_{cool}^{eff} + 1.05 \frac{\Delta \tau_{ad,0}}{U^* Da\left(1+\varepsilon\vartheta\right)+\varepsilon R_H} \tag{13}$$

In the literature it is also possible to find a number of “intrinsic” criteria, based for the sake of example on parametric sensitivity arguments [11]. However, we feel that the “target temperature” method, despite some degree of arbitrariness, arises from arguments (involved in the definition of the target temperature itself) which are more evidently related to the physics of the system to be analyzed.

Comparing now the real temperature evolution of a SBR with the corresponding target temperature, it is possible to classify the thermal behavior of the system from the safety point of view: the exceeding of the target temperature line is regarded as a runaway and provides the starting point for building boundary diagrams on a suitable dimensionless space. The corresponding dimensionless groups can be identified looking at the right side of the energy balance eq. (9). We can recognize an enthalpic contribution associated to the chemical reaction:

$$\dot{Q}_r = \Delta \tau_{ad,0} \frac{d\zeta_B}{d\vartheta} \tag{14}$$

and a combined enthalpic contribution which takes into account the heat removal from the reactor by both the coolant and the dosing stream:

$$\dot{Q}_{cool} = \left[U^* Da\left(1+\varepsilon\vartheta\right)+\varepsilon R_H\right]\left(\tau - \tau_{cool}^{eff}\right) \tag{15}$$

Following the same approach as in the classical explosion theory of Semenov [12], we can quantify the entity of the temperature dependence of the two contributions (14) and (15) by evaluating the corresponding temperature derivatives:

$$\frac{d\dot{Q}_r}{d\tau} = \Delta \tau_{ad,0}\, \nu_A\, Da\, RE\, f \cdot \kappa \frac{\gamma}{\tau^2} \tag{16}$$

$$\frac{d\dot{Q}_{cool}}{d\tau} = U^* Da\left(1+\varepsilon\vartheta\right)+\varepsilon R_H \tag{17}$$

The use of these derivatives can be simplified by introducing some dimensionless

quantities, that is a reactivity factor, F_R, which is mainly related to the reaction rate, an exothermicity factor, F_E, which is mainly related to the adiabatic temperature rise, and a cooling factor, F_{cool}, related to the cooling potential:

$$F_R = \nu_A \, Da \, RE \, \kappa = \frac{1}{f} \frac{d\zeta_B}{d\vartheta} \tag{18}$$

$$F_E = \Delta\tau_{ad,0} \frac{\gamma}{\tau^2} \tag{19}$$

$$F_{cool} = U^* Da \left(1 + \varepsilon\vartheta\right) + \varepsilon R_H \tag{20}$$

leading to a more compact expression of eqs. (16) and (17):

$$\frac{d\dot{Q}_r}{d\tau} = f F_R F_E \tag{21}$$

$$\frac{d\dot{Q}_{cool}}{d\tau} = F_{cool} \tag{22}$$

It is easy to observe that, at the current value of f, for different sets of the parameters which appear in eqs. (7) and (9), the same value of the expression (21) can correspond to two asymptotic situations and precisely:

a) to a very high (theoretically infinite) value of F_R and a very low (theoretically approaching zero) value of F_E;
b) to a very low (theoretically approaching zero) value of F_R and a very high (theoretically infinite) value of F_E.

The situations a) and b), which generate the same instantaneous value of $d\dot{Q}_r / d\tau$, are on opposite sides from the safety point of view. Situation a) corresponds to a very high reaction rate (which counteracts the accumulation of the coreactant in the system) and very low values of the activation energy and/or the adiabatic temperature rise: regardless of the cooling potential this situation is always safe. Situation b) implies the opposite and, regardless of the cooling potential, certainly results in a runaway. Intermediate cases, characterized by finite values of F_R and F_E, cannot be classified (in terms of runaway or safe conditions) without relating them to the heat removal contribution from the system, $d\dot{Q}_{cool} / d\tau$. The ratios of the reactivity and the exothermicity factor to the cooling factor, evaluated at the coolant temperature are the two suitable dimensionless parameters to define the space where boundary diagrams can be reported. These ratios, called reactivity, R_y, and exothermicity, E_x, numbers were introduced by Steensma and

Westerterp [6] and assume the following expressions:

$$R_y = \left.\frac{F_R}{F_{cool}}\right|_{\vartheta=0} = \frac{\nu_A\, Da\, RE\, \kappa\left(\tau_{cool}\right)}{U^* Da + \varepsilon R_H} = \frac{\nu_A\, Da\, RE\, \kappa\left(\tau_{cool}\right)}{\varepsilon\left(Co + R_H\right)} \tag{23}$$

$$E_x = \left.\frac{F_E}{F_{cool}}\right|_{\vartheta=0} = \frac{\gamma}{\tau_{cool}^2}\frac{\Delta\tau_{ad,0}}{U^* Da + \varepsilon R_H} = \frac{\gamma}{\tau_{cool}^2}\frac{\Delta\tau_{ad,0}}{\varepsilon\left(Co + R_H\right)} \tag{24}$$

where the cooling number $Co=U^*Da/\varepsilon$ has been also introduced. The aforementioned asymptotic situations a) and b), reported in the R_y vs E_x space, imply that the left-upper region of the diagram always corresponds to safe conditions and that the right-bottom region always corresponds to runaway conditions.

The comparison between the temperature-time profile and the corresponding target temperature line represents a useful way for classifying the thermal behavior of the system [6]. Given a set of values for the parameters which appear in eqs. (7) and (9), and solving such equations for increasingly values of the coolant temperature, it is possible to identify four typologies of thermal behaviors of the reactor:

1) for sufficiently low values of the coolant temperature, the maximum reaction temperature attained is lower than the local target value: this means that the reaction is not ignited. In such a situation the accumulation of the coreactant in the system reaches obviously high values but the reaction is never fast enough to cause the loss of control of the system from the thermal point of view;
2) as the coolant temperature increases, the maximum temperature “pinches” locally the target line: this situation is referred to as a marginal ignition;
3) increasing further the coolant temperature, the reaction rate is at the same time not so high to keep the accumulation of the coreactant sufficiently low and not so low to avoid -when the reaction itself ignites- the loss of control of the system from the thermal point of view. This situation implies maximum reaction temperatures larger than the local target value and it is referred to as a runaway;
4) as the coolant temperature still increases, the reaction rate becomes fast enough to keep the accumulation of the coreactant A in the system sufficiently low that no runaways can occur. The minimum coolant temperature for which the exceeding of the local target value by the maximum reaction temperature disappears is referred to as a QFS (Quick onset, Fair conversion, Smooth temperature profile) situation [6], because it is characterized by a temperature evolution which quickly approaches the target line and remains close to it throughout the dosing period, at

the end of which the conversion ζ_B is almost complete.

These regions can be reported on a boundary diagram as shown, for the sake of example, in Figure 3. The runaway region is enclosed inside the continuous line and is surrounded by the no ignition region (for low R_y values), the QFS region (for high R_y values) and by an inherently safe region. The letter is characterized by either E_x values lower than the minimum E_x value of the runaway boundary, $E_{x,MIN}$, or by R_y values larger than the maximum R_y value of the runaway boundary, $R_{y,QFS}$. The aforementioned asymptotic behaviors a) and b) are also shown in the figure, the former always resulting in a safe operation of the reactor, the latter in a runaway situation: this is for instance the reason why the runaway regions are not close in the positive "E_x" direction and extended in the diagrams reported until realistic values of the exothermicity number [2]. These diagrams can be easily used to solve two typologies of problems:

1. for an existing reactor, operating at known values of the fixed parameters Co, R_H, n and m, and in the slow reaction regime, the corresponding boundary diagram can be used to identify thermally safe operating conditions without solving the mathematical model of the reactor;
2. the conclusions drawn for a given reactor from the use of the corresponding boundary diagram can be extended to scaled up systems, provided that both the reactors are characterized by the same Co, R_H, n and m values and operate in the same kinetic regime (in this case, the slow reaction regime).

As previously mentioned, to carry out a model simulation it is necessary to give a fixed value for all the dimensionless groups involved in the model, i.e. in eqs. (7) and (9). Such dimensionless groups are: ν_A Da RE, ε, γ, R_H, $\Delta\tau_{ad,0}$, Co, n, and m. As will be discussed in detail in the section "Procedure for building the boundary diagrams", each boundary diagram involves a given range of the parameters: ν_A Da RE, ε, γ and $\Delta\tau_{ad,0}$, but a fixed value of the parameters Co, R_H, n and m. In particular, it is well known that both Co and R_H can strongly influence the shape and location of the boundary diagram [2], as shown for the sake of example in Figure 4. The same results can be better summarized in terms of normalized objective sensitivity coefficients of $E_{x,MIN}$ and $R_{y,QFS}$ with respect to the considered parameters. Such sensitivity coefficients can be defined as [13]:

$$S_{i,j} = \frac{\alpha_j}{\beta_i}\frac{\partial \beta_i}{\partial \alpha_j} \approx \frac{\alpha_j}{\beta_i}\frac{\Delta \beta_i}{\Delta \alpha_j} \tag{25}$$

where β_i is either $R_{y,QFS}$ or $E_{x,MIN}$, and α_j is one of the investigated parameters. The computed

values of such sensitivity coefficients are summarized in Table 2, clearly showing the influence of the various parameters considered. From these data, we can see that the influence of the reaction order on the values of $R_{y,QFS}$ or $E_{x,MIN}$ can be larger than that of both Co and R_H. This conclusion is only partially tempered by noting that the range of variation of Co in practical conditions is much larger than that of both n and m [2,3]: it is quite evident that the influence of n and m on the shape and location of the boundary diagrams can be disregarded only as a first approximation. However, the available boundary diagrams refer to reaction orders equal to (1,1) [2]. This is obviously a limitation since reaction orders are not always equal to one. The influence of the reaction order values on the shape and location of the boundary diagrams is shown in Figures 5 and 6, referring to reactions in the dispersed and in the continuous phase respectively. These diagrams are the results of a series of simulations extended to the following ranges of parameters: $0.025<\nu_A$ Da RE<14, $0.3<\varepsilon<0.55$, $32<\gamma<42$, $0.29<\Delta\tau_{ad,0}<0.7$, Co=10, R_H=1. From these data we can observe that, when the order of only one component (that is, either n or m) changes, the use of a boundary diagram obtained for a certain reaction order is safe for reactions of larger order. Moreover, for both the cases (reaction taking place in the dispersed or in the continuous phase), variations in the order of the dosed coreactant, n, imply much larger differences in the extension of the correspondent runaway regions than variations of the reaction order of the reactant initially charged in the reactor, m. This is obvious because the higher the reaction order of the dosed coreactant is, the faster the reaction rates become for a given increase (due to accumulation phenomena) of the hold-up of unreacted coreactant in the system: this counteracts directly the accumulation of the coreactant itself in the reactor and consequently can result in a narrower runaway region, even for relatively small increases of n. Consequently, if between the kinetic expression to which a boundary diagram refers to and that of the investigated system the order of the dosed component changes, the conclusions drawn from the use of the diagram, even when safe, can be too conservative and hence unrealistic. For these reasons, the use of the correct boundary diagram is always advisable. Finally it is quite evident that, for the same reaction order, the boundary diagram for the reaction taking place in the dispersed phase shows always a larger runaway region than the analogous diagram for the reaction occurring in the continuous phase. This is correct because for reactions taking place in the dispersed phase, the reaction volume starts from zero and increases throughout the dosing period: this implies that the net production rates (i.e., the $r^{eff}V_r$ term in eq. (6)) during the semibatch period are lower and the accumulation of the coreactant is consequently higher. It must be emphasized that the conclusions drawn above about the safe use of an available boundary diagram for the analysis of a system of different kinetics are true if between the kinetic expression to which the boundary diagram refers to and that of the real system, only the reaction order of one component (that is, either n or m) changes, as is the case of Figures 5 and 6. If between the two kinetic expressions both n and m change, the overall reaction order (that is, n+m) is not a suitable

parameter for establishing if the use of the boundary diagram is safe: this comes from the different dependence of the shape and location of a boundary diagram on n and m respectively, the former being much stronger. For the sake of example, in Figure 7, the boundary diagram for a reaction occurring in the dispersed phase with n=0.7 and m=1.4 are compared with that for n=m=1. This figure clearly shows that the runaway region for (0.7,1.4) is larger than that for (1,1) reaction order, even if the overall reaction order for the former case is higher (that is, 0.7+1.4=2.1 vs. 1+1=2).

As previously discussed, while the influence of the reaction order of the reactant initially charged in the reactor can be disregarded as a first approximation, the opposite is true for the reaction order of the coreactant. At a given m value, increasing n leads to a significant narrowing of the runaway region, until, above a certain n, it is no more possible to find a runaway region at the current values of Co, R_H, n, m in the investigated ranges of the parameters ν_A Da RE, ε, γ, $\Delta\tau_{ad,0}$. This is correct, since, as previously shown, the higher n is, the more the reaction rates potentially increase as the hold-up of unreacted A in the system tends to grow. The aforementioned critical value of n is lower for slow reactions occurring in the continuous phase: this is also correct since in this case the reaction volume is maximum at the beginning of the supply period and the $r^{eff}V_r$ term in eq. (6) is consequently higher than for reactions occurring in the dispersed phase.

For a practical use, boundary diagrams for different values of are reported in Figures 8 to 11. In these figures, the influence of the cooling number and of the heat capacity ratio on the location and extension of a boundary diagram is shown for n=0.5 and 2, for reactions taking place in the dispersed phase, and for n=0.5 and 1.25, for reactions taking place in the continuous phase. Boundary diagrams for the basic case of n=m=1 have been already reported in the literature [2].

1.4 Procedure for building the boundary diagrams

As shown in the previous section, the use of a boundary diagram built for a given reaction order can be unsafe for the analysis of a system characterized by a different kinetics, and the comparison between the overall reaction orders is not a suitable way for establishing that. Besides, even when the use of a boundary diagram for a different kinetics is safe, the conclusions drawn can be too conservative. Consequently, the boundary diagrams reported in this work can be used as a first approximation, according to the rules-of-thumb given in the previous section and following the procedure discussed in detail elsewhere [2]. On the other hand, there are several systems for which it could be useful to refer to the correct boundary diagram. Once built, the boundary diagram for the real rate of reaction expression can be used for the a-priori analysis of several changes in operating conditions of an existing reactor and for scale-up problems, provided that the remaining fixed parameters of the diagram (Co and R_H) and the kinetic regime (slow or fast reaction) are the same. In the following, a simple and general procedure for building the boundary diagrams for

liquid-liquid SBR, in which a single slow reaction of general power law kinetics occurs, is presented. This procedure is not straightforward, since it involves the combination of many dimensionless parameters in several ways.

As previously mentioned, eight dimensionless parameters appear in the mass and energy balance eqs. (7) and (9) or, analogously, in the expression (23) and (24) of the reactivity and exothermicity numbers: ν_A Da RE, ε, γ, R_H, $\Delta\tau_{ad,0}$, Co, n, and m. Assigning a value to each of these parameters in compliance with its accepted range and letting the coolant temperature as a variable parameter, the functional dependence between the exothermicity and reactivity numbers, $R_y=\Phi(E_x)$, is univocally identified. Eqs. (23) and (24) are the parametric form of this functional dependence since they provide, for each value of the coolant temperature, a couple of related values of R_y and E_x, as shown, for the sake of example, in Figure 3. From eqs. (23) and (24), it is evident that the *single* $R_y=\Phi(E_x)$ line (that is, a line representing the functional dependence between R_y and E_x) on the *single* boundary diagram (that is, for Co, R_H, n, m values assigned and constant) is identified through the values of the following three dimensionless groups:

$$\begin{cases} \dfrac{\gamma\Delta\tau_{ad,0}}{\varepsilon\left(Co+R_H\right)}=const \\ \dfrac{\nu_A\, Da\, RE}{\varepsilon\left(Co+R_H\right)}=const \\ \gamma=const \end{cases} \tag{26}$$

that must be also constant along the single $R_y=\Phi(E_x)$ line. The number of parameters that must be assigned to solve the mathematical model of the reactor at the current coolant temperature, as previously mentioned, is equal to eight. Since four of them must be constant when a single boundary diagram is considered, the number of independent parameters is equal to four. These must also fulfill the three constraints (26). It follows that the number of sets of parameters which generate the same line $R_y=\Phi(E_x)$ on a given boundary diagram is equal to ∞^1. These sets of parameters can be generated from each member of the single family multiplying by the same factor K the parameters ν_A Da RE, ε, $\Delta\tau_{ad,0}$ and U^*Da, while keeping the remaining four (R_H, γ, n, m) constant. It should be noticed that this allows to keep $Co=U^*Da/\varepsilon$ constant as well as to fulfill the constraints (26). The problem consists now in finding, on the single line $R_y=\Phi(E_x)$, two particular values of the multiplying factor K: the first one corresponds to the set of parameters which generates the *minimum coolant temperature for which we have marginal ignition*; the second one corresponds to the set of parameters which generates the *maximum coolant temperature for which we have QFS*, as shown in Figure 3. This procedure, which involves a cumbersome minimization or maximization procedure, cannot be avoided because it allows obtaining the maximum extension

of the runaway region. In fact, among all the sets of parameters that originate the same $R_y=\Phi(E_x)$ line, we chose the ones related to the minimum cooling temperature, for marginal ignition, and the maximum cooling temperature, for QFS. Since the runaway boundary corresponds to a situation in which the maximum reactor temperature is just equal to the local target temperature, we must look for conditions fulfilling the constraint:

$$FF\left(\tau_{cool}\right)=\tau_{\max}\left(\tau_{cool}\right)-\tau_{ta}\left(\tau_{cool}\right)\Big|_{g(\tau_{\max})}=0 \tag{27}$$

The numerical search for the roots of this equation requires the solution of the system of ordinary differential eqs. (7) and (9) for different values of the coolant temperature. The function $FF(\tau_{cool})$, to which we are searching the roots, is shown in Figure 12 for a single slow reaction taking place in the dispersed phase and for the following set of parameters: ν_A Da RE=1.8, ε=0.4, γ=38, $\Delta\tau_{ad,0}$=0.6, Co=10, R_H=1, n=1, m=1. In general, this function can have, in the considered range of τ_{cool}, zero, one or two roots. In this last case, the first root corresponds to a marginal ignition, while the second one to a QFS situation. In fact, for initial coolant temperatures immediately *below* the *first* root, the function FF is *negative*, which means that the reaction is not ignited; for initial temperatures immediately *above* the same root instead, the function FF is *positive*, which means that a runaway occurs. Analogously, for initial temperatures immediately *below* the *second* root, the function FF is *positive*, which again corresponds to a runaway; for initial temperatures immediately *above* the same root the function FF is *negative*, corresponding to QFS conditions. These criteria permit to distinguish between the nature (marginal ignition or QFS) of the single root of the function FF. The same procedure is repeated for several sets of parameters fulfilling two constraints: sharing the same $R_y=\Phi(E_x)$ line (that is, they are obtained from a basic set of parameters by multiplying ν_A Da RE, ε, $\Delta\tau_{ad,0}$, U^*Da for the same factor, K) and lying inside the given ranges of interest. We obtain then several values of cooling temperatures for both marginal ignition and QFS: choosing the minimum (for marginal ignition) and the maximum (for QFS), defines the boundary of the runaway region. Repeating the same procedure for several $R_y=\Phi(E_x)$ lines on the same diagram (that is, choosing different basic sets for the values of the parameters ν_A Da RE, ε, $\Delta\tau_{ad,0}$, γ), two curves can be generated: the first one results from joining the marginal ignition points, previously determined on the several $R_y=\Phi(E_x)$ lines; the second one results from joining the QFS points on the same lines. The union of the two curves identifies the runaway region and consequently the boundary diagram. This procedure can be easily implemented in a computer code to provide any boundary diagram.

1.5 Conclusions

The boundary diagrams are a powerful tool to perform simple and fast safety analyses of any change in the operating conditions of a liquid-liquid SBR without solving the correspondent mathematical model, as well as to scale up a process from the laboratory or pilot to the industrial scale. Practical procedures for using boundary diagrams in order to identify inherently safe conditions have been thoroughly discussed elsewhere [2], where also rules-of-thumb for estimating the values of the dimensionless parameters involved in the use of these diagrams are reported.

However, it has been shown that the conclusions drawn from the use of boundary diagrams developed assuming a (1,1) reaction order are not always safe for the analysis of systems characterized by different kinetics. Moreover the comparison between the overall reaction orders is not a suitable way for establishing if an available boundary diagram can be safely used when the orders of both the reactants change. Even when the use of a (1,1) boundary diagram is safe, if the order of the dosed coreactant changes the conclusions drawn can be too conservative. In the paper a number of boundary diagrams are provided for reaction orders different from one, which can be used -according to the rules-of-thumb reported- for better approximating the real conditions. Requirements related to the reaction order of the reactant initially charged in the reactor are less stringent. When just this parameter changes, a boundary diagram obtained for a given reaction order can be used also for the preliminary analysis of higher reaction order systems. However, the best and more reliable results are obtained using the proper boundary diagram for the case of interest. The required boundary diagram can be built following the procedure presented in this work. Once built, the diagram can be used with a minimal calculation effort.

Nomenclature

Symbols	
A	heat transfer area of the reactor (associated to the jacket and/or the coil), m^2
C	molar concentration, $kmol/m^3$
Co	$=U^{*}Da/\varepsilon$, cooling number, -
$\tilde{C}_P$	molar heat capacity, kJ/(kmol·K)
D	diffusivity, m^2/s
Da	$=k_{n,m,R}t_D C_{B,0}^{n+m-1}$, Damköhler number for (n,m) order reactions, -
E	activation energy, kJ/kmol
E_x	exothermicity number, eq. (24), -
f	function of the dimensionless time and conversion of B in eq. (7), -
F	molar feed rate, kmol/s
F_E	exothermicity factor, eq. (19), -
F_R	reactivity factor, eq. (18), -
F_{cool}	cooling factor, eq. (20), -
FF	difference between the maximum temperature and the local target value, eq. (27), -
$\Delta\tilde{H}$	reaction enthalpy, kJ/kmol
Ha	Hatta number, -
$k_{n,m}$	reaction rate constant, $m^{3(n+m-1)}/(kmol^{n+m-1}\cdot s)$
k_L	mass transfer coefficient, m/s
m	equilibrium distribution coefficient ($m_A=C_{A,c}/C_{A,d}$; $m_B=C_{B,d}/C_{B,c}$), -
n	number of moles, kmol
$\dot{Q}_r$	enthalpic contribution due to reaction, eq. (14), -
$\dot{Q}_{cool}$	enthalpic contribution due to heat removal, eq. (15), -
r	reaction rate referred to the total liquid volume, $kmol/(m^3\cdot s)$
R	gas constant = 8.314, kJ/(kmol·K)
RE	reactivity enhancement factor in eq. (7), -
R_H	heat capacity ratio, -
R_y	reactivity number, eq. (23), -
S	normalized objective sensitivity coefficient, eq. (25), -
t	time, s
T	temperature, K
$\Delta T_{ad,0}$	adiabatic temperature rise, K
U	overall heat transfer coefficient, $kW/(m^2\cdot K)$

U^*Da	modified Stanton number, -
V	liquid volume, m^3

Greek symbols

α, β	generic symbols, eq. (25), -
γ	$=E/(RT_R)$, dimensionless activation energy, -
ε	relative volume increase at the end of the semibatch period, -
ζ	molar conversion, -
ϑ	$=t/t_D$, dimensionless time, -
κ	$=k/k_R$, dimensionless reaction rate constant, -
ν	stoichiometric coefficient, -
$\tilde{\rho}$	molar density, $kmol/m^3$
τ	$=T/T_R$, dimensionless temperature, -
Φ	functional dependence between R_y and E_x

Subscripts and superscripts

A,B,C,D	components A, B, C and D
ad	adiabatic
c	continuous phase
cool	coolant
d	dispersed phase
D	dosing stream or dosing time
E	in the cooling factor F_E
eff	effective
H	in the heat capacity ratio R_H
i	"i-th" component
I	interface
L	in the liquid phase
m	order of reaction respect to component B
n	order of reaction respect to component A
max	maximum value of a quantity or at the maximum value of a quantity
MIN	in $E_{x,MIN}$
QFS	in $R_{y,QFS}$
r	reaction
R	reference
R	in the reactivity factor F_R
slow	slow reaction regime

ta	target
x	in the exothermicity number E_x
y	in the reactivity number R_y
0	start of the semibatch period
1	end of the semibatch period

Literature cited

1. Benuzzi, A., Zaldìvar, J.M. Eds. Safety of Chemical Reactors and Storage Tanks. 1998, *Kluwer Academic Publishers: Dordrecht, The Netherlands*.

2. Westerterp, K.R., Molga, E.J. No more runaways in fine chemical reactors. *Ind. Eng. Chem. Res.* 2004, *43 (16),* 4585-4594.

3. Steinbach, J. Safety assessment for chemical processes. 1999, *Wiley-vch, Weinheim.*

4. Hugo, P., Steinbach, J. Praxisorientierte Darstellung der thermischen Sicherheitsgrenzen für den indirekt gekühlten Semibatch-Reaktor. *Chem. Ing. Tech.* 1985, *57, Nr. 9,* 780-782.

5. Hugo, P., Steinbach, J. A comparison of the limits of safe operation of a SBR and a CSTR. *Chem. Eng. Sci.* 1986, *41*, 1081-1087.

6. Steensma, M., Westerterp, K.R. Thermally safe operation of a cooled semi-batch reactor. Slow liquid-liquid reactions. *Chem. Eng. Sci.* 1988, *43, Nr.8,* 2125-2132.

7. Steensma, M., Westerterp, K.R. Thermally safe operation of a semibatch reactor for liquid-liquid reactions. Slow reactions. *Ind. Eng. Chem. Res.* 1990, *29,* 1259-1270.

8. Steensma, M., Westerterp, K.R. Thermally safe operation of a semibatch reactor for liquid-liquid reactions. Fast reactions. *Chem. Eng. Technol.* 1991, *14,* 367-375.

9. van Woezik, B.A.A., Westerterp K.R. The nitric acid oxidation of 2-octanol. A model reaction for multiple heterogeneous liquid-liquid reactions. *Chem. Eng. Process.* 2000, *39,* 521-537.

10. van Woezik, B.A.A., Westerterp K.R. Runaway behaviour and thermally safe operation of multiple liquid-liquid reactions in the semibatch reactor. The nitric acid oxidation of 2-octanol. *Chem. Eng. Process.* 2001, *41,* 59-77.

11. Morbidelli, M., Varma, A. Generalized criterion for parametric sensitivity to thermal explosion theory. *Chem. Eng. Sci.* 1988, *43, 91.*

12. Semenov, N.N. Thermal theory of combustion and explosion. Progress of physical science. 1940, *23*, 251-292.

13. Varma, A., Morbidelli, M., Wu, H. Parametric Sensitivity in Chemical Systems. 1999, *Cambridge University Press*.

14. Westerterp, K.R., van Swaaij, W.P.M., Beenackers, A.A.C.M. Chemical reactor design and operation. *2nd ed.* 1984, *John Wiley & Sons, Chichester, U.K.*.

Table 1 *Expressions of the reactivity enhancement factor, RE, and of the function, f, for slow reactions taking place in the dispersed or continuous phase. Requirements for slow regime are also reported [14].*

	Slow reaction in the *dispersed* phase, d	**Slow reaction in the *continuous* phase, c**
$\mathbf{RE_{slow,c/d}}$	$\left(\frac{\nu_B}{\nu_A}\right)^{1-n} m_B^m$	$\left(\frac{\nu_B}{\nu_A}\right)^{1-n} m_A^n$
$\mathbf{f_{slow,c/d}}$	$\frac{\left(\vartheta-\zeta_B\right)^n\left(1-\zeta_B\right)^m}{\left(\varepsilon\vartheta\right)^{n-1}}$	$\frac{\left(\vartheta-\zeta_B\right)^n\left(1-\zeta_B\right)^m}{\left(\varepsilon\vartheta\right)^{n}}$
check for *slow reactions*	$Ha_d = \frac{1}{k_{L,B}}\sqrt{\frac{2}{m+1}k_{n,m}D_{L,B}C_{B,I_d}^{m-1}C_{A,d}^n} < 0.3$ $C_{B,d}/C_{B,I_d} > 0.95$	$Ha_c = \frac{1}{k_{L,A}}\sqrt{\frac{2}{n+1}k_{n,m}D_{L,A}C_{A,I_c}^{n-1}C_{B,c}^m} < 0.3$ $C_{A,c}/C_{A,I_c} > 0.95$

Table 2 *Normalized sensitivity coefficients of $R_{y,QFS}$ and $E_{x,MIN}$ computed from the data shown in Figure 4.*

	Slow reaction in the *dispersed* phase, d				**Slow reaction in the *continuous* phase, c**			
	Co	$\mathbf{R_H}$	**n**	**m**	**Co**	$\mathbf{R_H}$	**n**	**m**
$\mathbf{R_{y,QFS}}$	0.08	0.16	0.64	0.11	0.43	0.18	0.72	0.14
$\mathbf{E_{x,MIN}}$	0.28	0.07	0.82	0.44	0.17	0.03	0.27	0.08

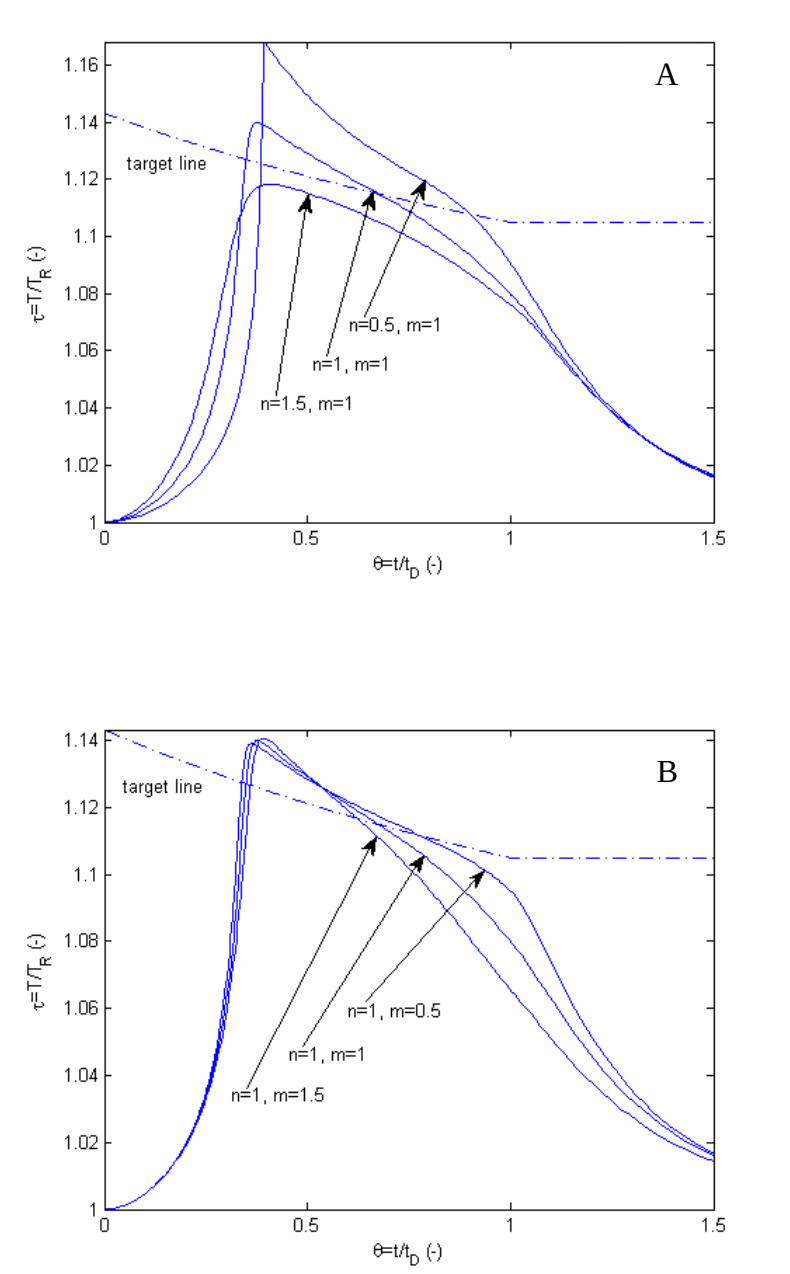

Figure 1 *Temperature-time profiles in a SBR for a slow reaction in the dispersed phase.* ν_A *Da RE=1.8,* ε*=0.4,* γ*=38,* R_H*=1,* $\Delta\tau_{ad,0}$*=0.6, Co=10. Coolant and dosing stream temperature values equal to the initial reactor temperature. A) influence of the reaction order of the coreactant, n; B) influence of the reaction order of the reactant initially charged in the reactor, m.*

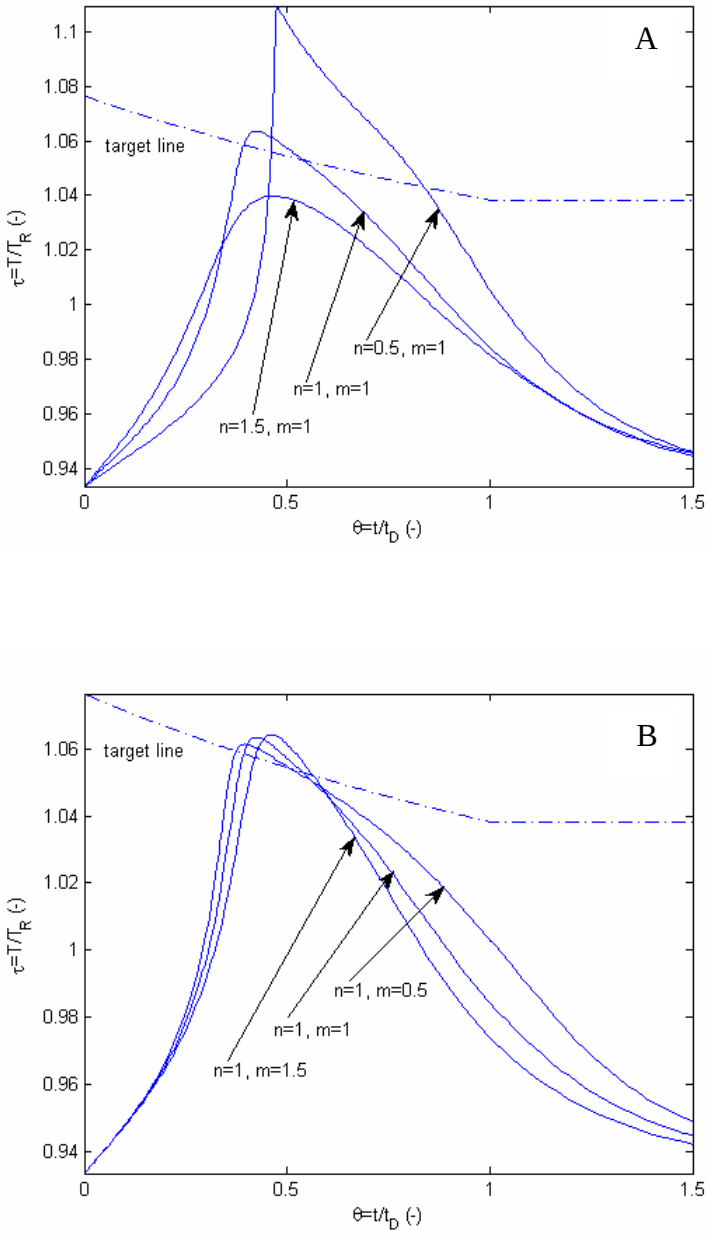

Figure 2 *Temperature-time profiles for a slow reaction in the continuous phase. Legend and other parameters as in Figure 1.*

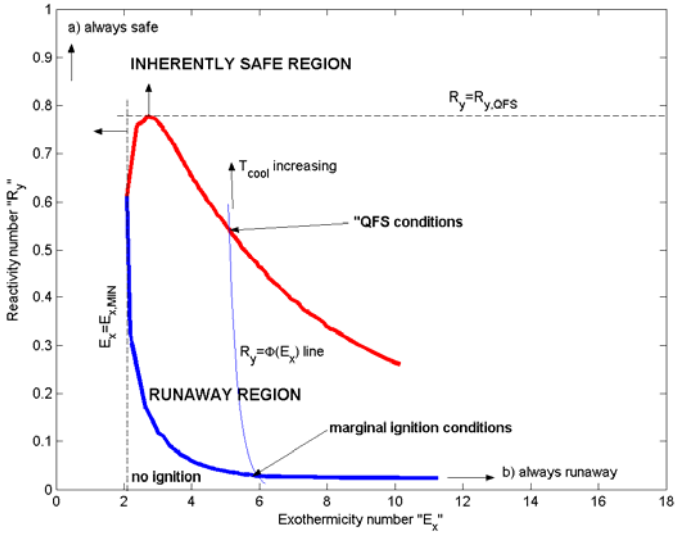

Figure 3 *Different SBR behavior regions and relation between R_y and E_x with T_{cool} as a parameter.*

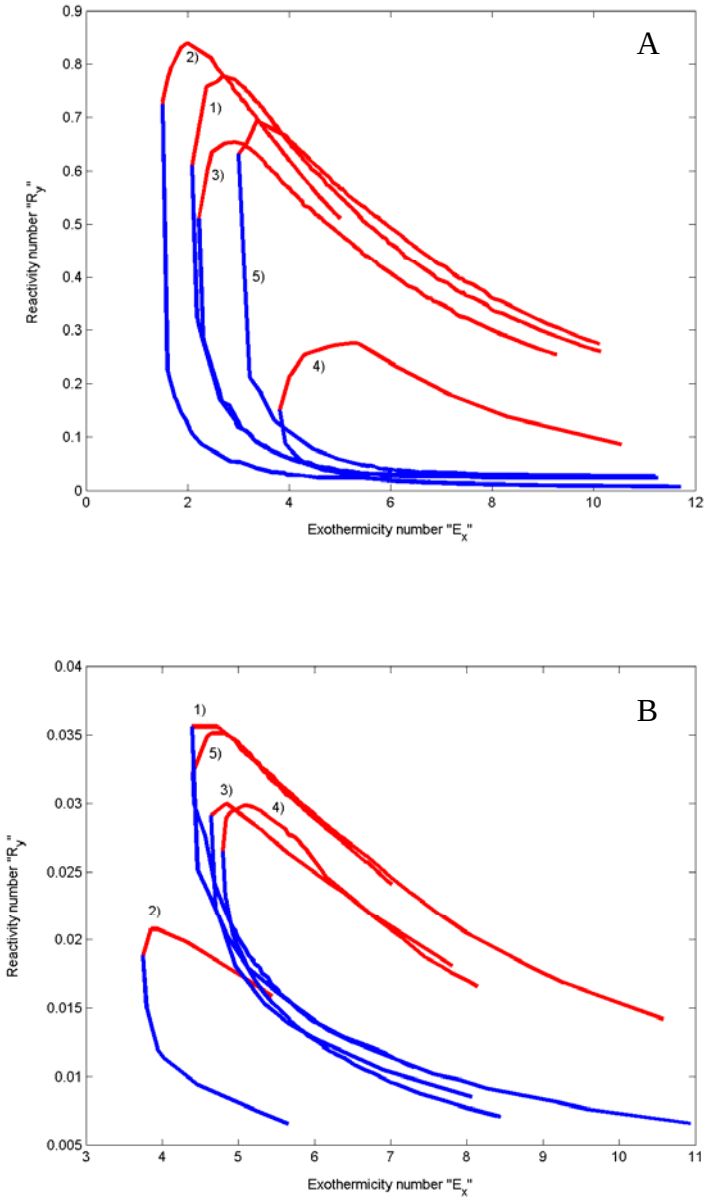

Figure 4 *Sensitivity of the boundary diagrams with respect to the model parameters. Slow reaction regime. 0.025< ν_A Da RE<14, 0.3<ε<0.55, 32<γ<42, 0.29<$\Delta\tau_{ad,0}$<0.7. 1) Co=10, R_H=1, n=1, m=1; 2) Co=20, R_H=1, n=1, m=1; 3) Co=10, R_H=2, n=1, m=1; 4) Co=10, R_H=1, n=2 (A) and n=1.25 (B), m=1; 5) Co=10, R_H=1, n=1, m=2 (A) and m=1.25 (B). A) reaction in the dispersed phase; B) reaction in the continuous phase.*

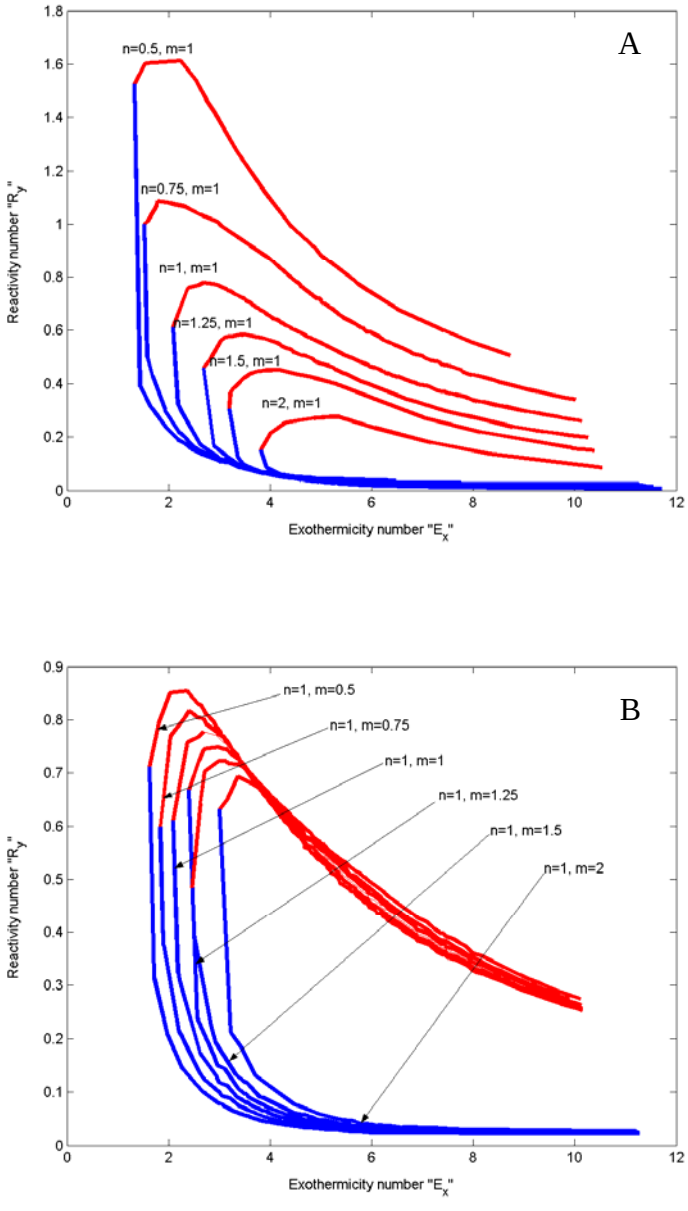

Figure 5 *Boundary diagrams for slow (n,m) order reactions in the dispersed phase. 0.025< ν_A Da RE<14, 0.3<ε<0.55, 32<γ<42, 0.29<$\Delta\tau_{ad,0}$<0.7, Co=10, R_H=1. A) influence of the reaction order of the coreactant, n; B) influence of the reaction order of the reactant initially charged in the reactor, m.*

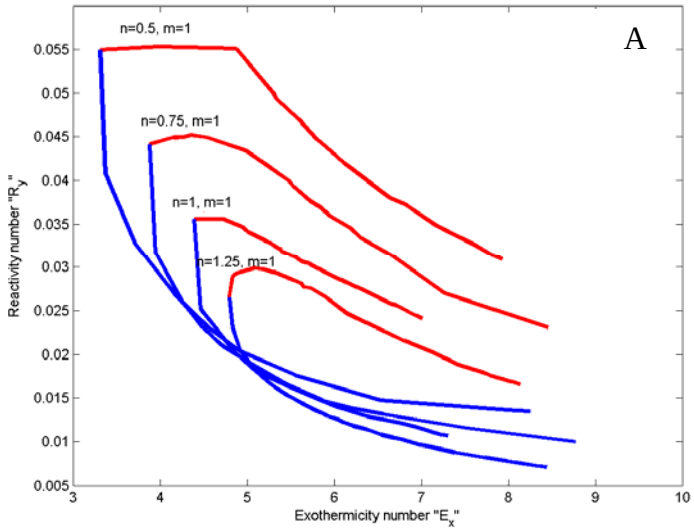

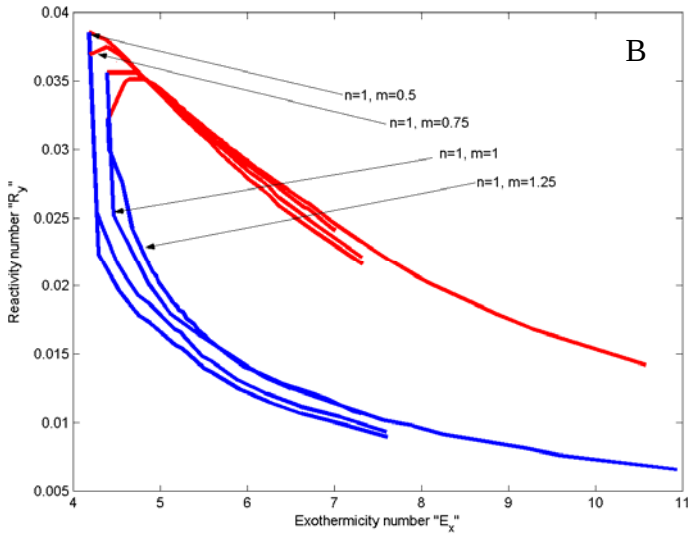

Figure 6 *Boundary diagrams for slow (n,m) order reactions in the continuous phase. Legend and other parameters as in Figure 5.*

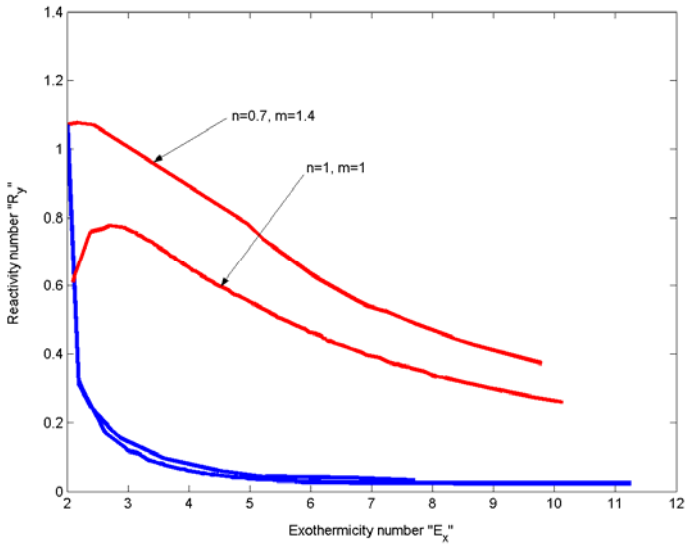

Figure 7 *Boundary diagrams for slow (n,m) order reactions in the dispersed phase. Legend and other parameters as in Figure 5.*

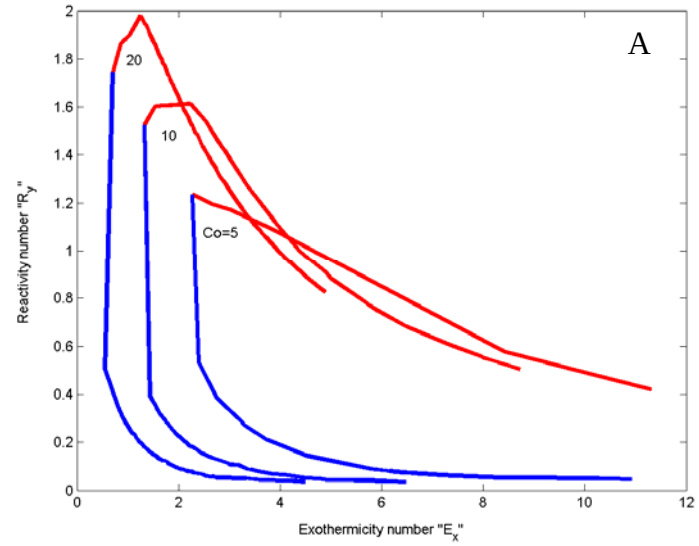

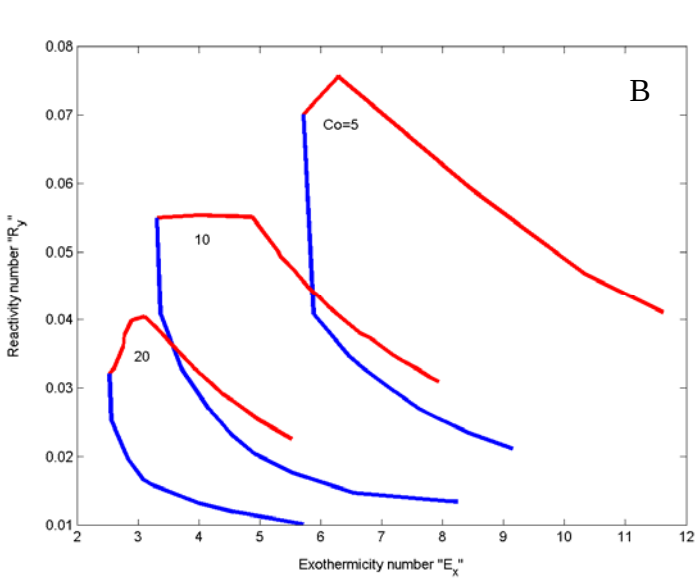

Figure 8 *Influence of the cooling number on the boundary diagrams shape and location. Slow reaction regime with n=0.5, m=1, R_H=1. 0.025< ν_A Da RE<14, 0.3<ε<0.55, 32<γ<42, 0.29<$\Delta\tau_{ad,0}$<0.7. A) reaction in the dispersed phase; B) reaction in the continuous phase.*

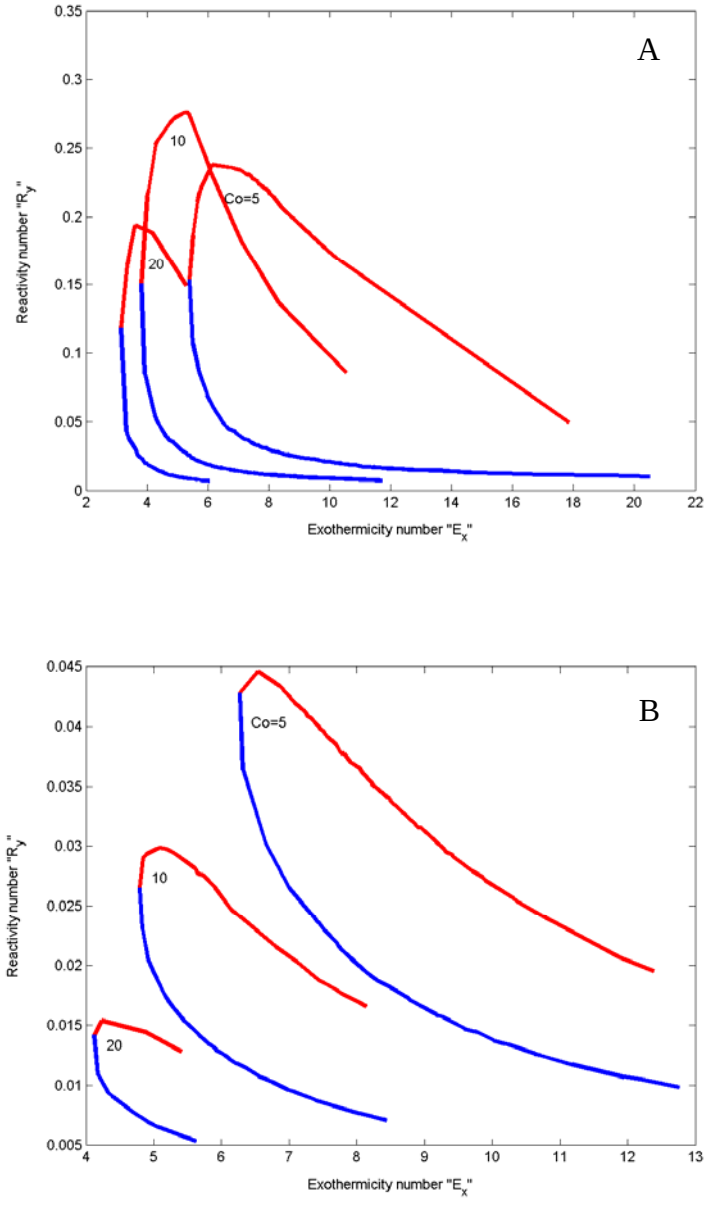

Figure 9 *Influence of the cooling number on the boundary diagrams shape and location. Slow reaction regime with n=2 (A) and n=1.25 (B), m=1, R_H=1. Legend and other parameters as in Figure 7.*

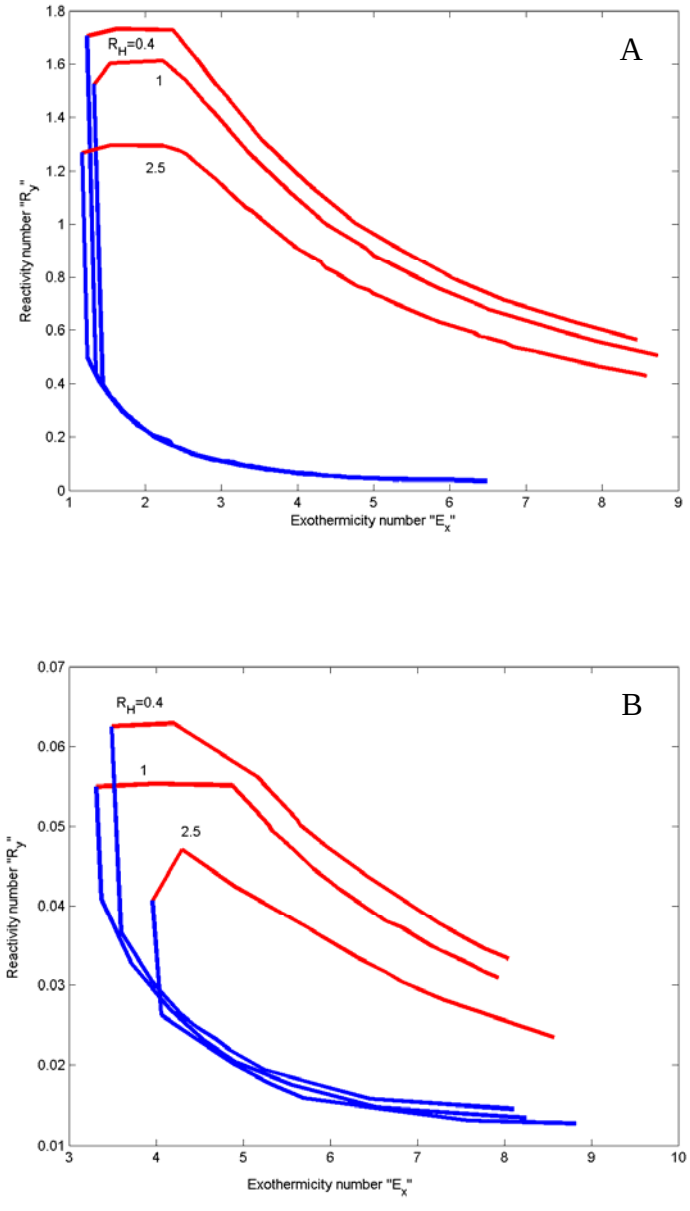

Figure 10 *Influence of the heat capacity ratio on the boundary diagrams shape and location. Slow reaction regime with n=0.5, m=1, Co=10. 0.025< ν_A Da RE<14, 0.3<ε<0.55, 32<γ<42, 0.29<$\Delta\tau_{ad,0}$<0.7. A) reaction in the dispersed phase; B) reaction in the continuous phase.*

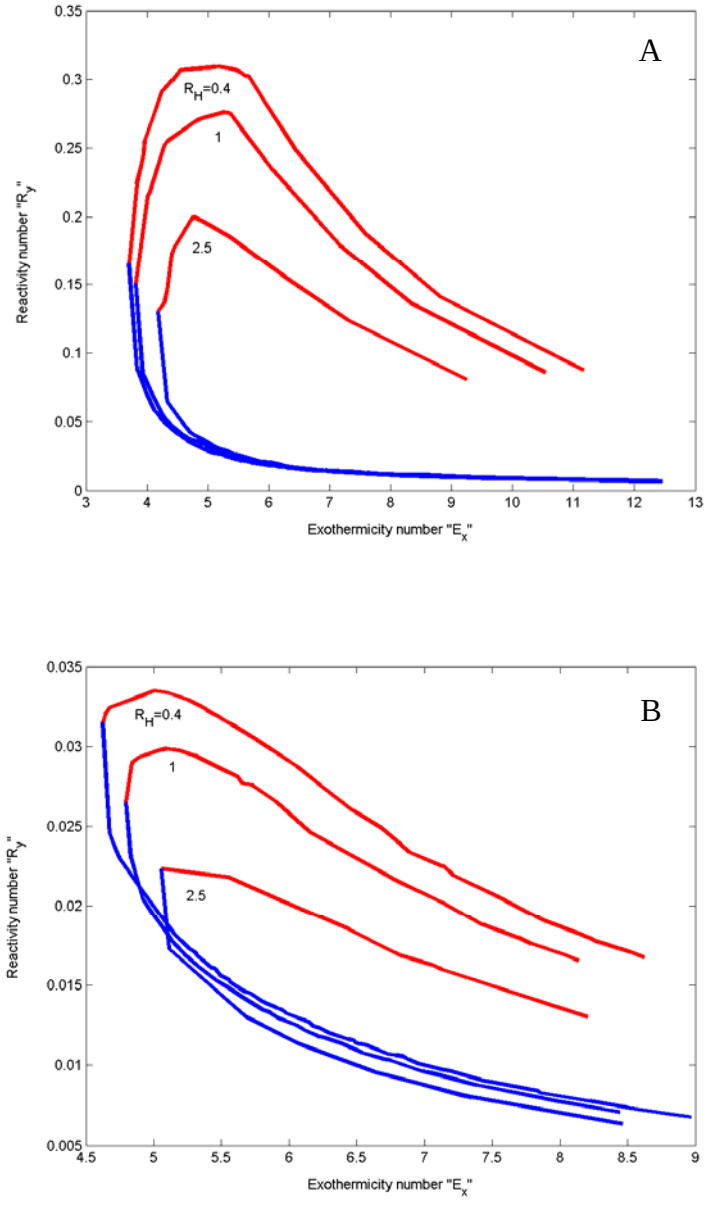

Figure 11 *Influence of the heat capacity ratio on the boundary diagrams shape and location. Slow reaction regime with n=2 (A) and n=1.25 (B), m=1, Co=10. Legend and other parameters as in Figure 9.*

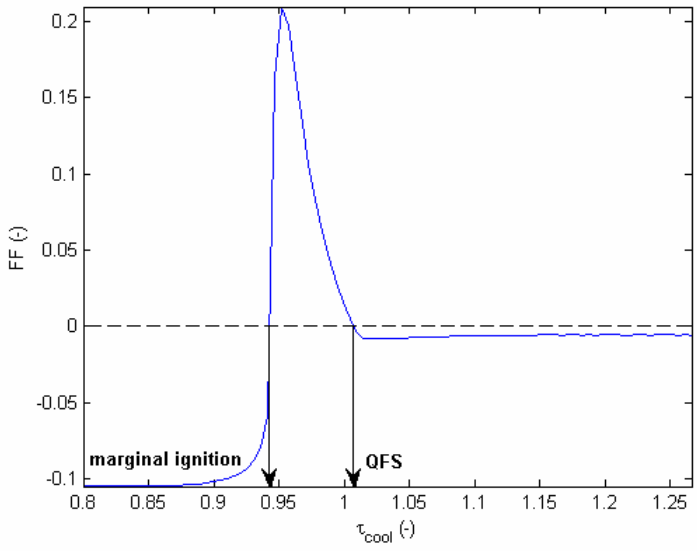

Figure 12 *"FF" function behavior in a SBR for a slow reaction in the dispersed phase.* ν_A *Da RE=1.8,* ε*=0.4,* γ*=38,* R_H*=1,* $\Delta\tau_{ad,0}$*=0.6, Co=10, n=1, m=1. Coolant and dosing stream temperature values equal to the initial reactor temperature.*

2. Thermally safe operation of liquid-liquid semibatch reactors. Part II: single diffusion controlled reactions with arbitrary reaction order

Francesco Maestri, Renato Rota*

Politecnico di Milano

Dip. di Chimica, Materiali e Ingegneria Chimica "G. Natta"

via Mancinelli 7 - 20131 Milano – Italy

fax: +39 0223993180; e-mail: renato.rota@polimi.it

Abstract

The thermally safe operation of an indirectly cooled semibatch reactor in which an exothermic liquid-liquid reaction occurs corresponds to conditions of potentially very high *macrokinetic* conversion rates compared with the supply rate of the coreactant, which accumulation in the system remains consequently low. This leads to the definition of a target temperature that can be compared with the real temperature-time profile, in order to develop boundary diagrams which summarize all the possible thermal behaviors of the reactor and can be used for safe scale-up purposes. The variable parameters which appear in such diagrams are an exothermicity and a reactivity number derived from the expressions of the conversion rates in the kinetically or diffusion controlled regime, respectively.

In this work the influence of the *microkinetic* rate of reaction on the shape and location of the boundary diagrams for single liquid-liquid diffusion controlled reaction systems is discussed, extending to this regime the results previously obtained for kinetically controlled reactions. Also in the case of diffusion controlled reactions, it is shown that for many practical systems, using boundary diagrams based on (1,1) reaction orders can lead to both unsafe or not necessary low production operating conditions. Consequently, a number of new boundary diagrams for arbitrary reaction orders is presented and some rules-of-thumb useful to their application are discussed.

* to whom correspondence should be addressed

Keywords: Semibatch reactors; Boundary diagrams; Macrokinetiks; Runaway; Safety; Scale-up.

2.1 Introduction

Runaway in chemical batch and semibatch reactors involving exothermic reactions is a very common problem in the chemical industry. For instance, in a typical EU country more than 100 runaways are expected to occur annually [1]. However, despite only a little amount of these accidents leads to serious consequences to either the workers or the inhabitants of the neighborhood of the factory, when strong runaways occur the consequences can be really serious. This motivates the huge amount of work that has been done on runaway phenomena in chemical batch and semibatch reactors, in order to develop procedures to scale up chemical processes from laboratory to industrial scale. Such procedures must be not only reliable but also simple, since the main problem to face in practice is that in fine chemical industries, which produce very different amounts of a wide range of chemical compounds, it is usually not possible, because of time and money constraints, to investigate in detail the kinetics of all the reactions involved. As a consequence, in spite of the progress that has been made in understanding runaway phenomena, the problem has not been solved yet for practice, so that runaways still occur [2].

The thermally safe operation of an indirectly cooled semibatch reactor (SBR) requires the dosing rate of one of the reactants (usually called coreactant) to be slow enough so that the cooling system can remove all the heat released. This naturally leads to the basic concept of minimizing the accumulation of the coreactant in the system, which is the result of a not negligible characteristic time of the chemical reaction, compared with that of the coreactant supply [3,4]: if the coreactant accumulates in the reactor, the system switches from semibatch to batch like conditions and the cooling system cannot control anymore the heat evolution.

The thermally safe operating conditions for *heterogeneous* (liquid-liquid) SBRs have been defined along the same line by introducing the concept of target temperature, that leads to the so-called boundary diagrams: such diagrams define, in a suitable dimensionless space, the regions where different reactor behaviors are expected. In particular, runaway and inherently safe regions are defined, allowing for identifying safe and dangerous operating conditions [5].

As previously mentioned, detailed information on the reaction mechanism and kinetics are seldom available in practice. However, modeling the behavior of a liquid-liquid SBR requires the knowledge of the *reaction kinetics*, at least in terms of a lumped overall reaction. Such an information can be obtained through calorimetric experiments carried out in the kinetically controlled regime. This means that some laboratory experimental work cannot be avoided [2]. The main aim of developing simple scale-up procedures is to keep such an experimental effort as low as possible. Boundary diagrams are a suitable tool to achieve this goal.

As previously mentioned, the thermally safe operation of a SBR corresponds to conditions of potentially very high conversion rates compared with the supply rate of the coreactant, which

accumulation in the system is consequently confined below a critical value. However, in a multiphase reaction system, the conversion rate can be controlled by either the chemical reaction (microkinetic or kinetically controlled regime, in the following referred to as “slow” reaction regime) or by the mass transfer phenomena (macrokinetic or diffusion controlled regime, in the following referred to as “fast” reaction regime). In both the cases, the chemical kinetics, which is represented through power law rate of reaction expressions with (n,m) reaction orders: $r=kC_A^nC_B^m$ plays a relevant role. In spite of (n,m) usually differ from (1,1), boundary diagrams have been developed only for the (1,1) case [2]. However, in a recent paper [6] it has been shown that for SBRs operating in the slow reaction regime, using boundary diagrams based on (1,1) reaction orders can lead to both unsafe or not necessary (from a safety point of view) low production operating conditions. Consequently, the main aim of this work is to extend the previous one [6] to fast reaction systems, analyzing in detail the influence of the reaction orders on the shape and location of the boundary diagrams and providing runaway and inherently safe regions for some (n,m) couples. The effect of changing the reaction order, as well as the influence of the reaction regime (i.e. kinetically or diffusion controlled) is discussed, and some rules-of-thumb for both building and using boundary diagrams in the industrial practice are finally provided.

2.2 Mathematical model

Developing a boundary diagram for a generic (n,m) reaction order and discussing the physical meaning of the dimensionless parameters introduced to define the space where runaway or inherently safe regions are identified, requires a preliminary discussion on how the investigated process can be modeled. However, since the main model assumptions, except for those related to the fast reaction regime, are the same discussed in a previous work [6], in the following they are only briefly summarized, focusing on the main topics characteristic of the fast reaction regime.

At time equal to zero the supply of the coreactant A to an indirectly cooled semibatch reactor filled with a given amount of component B is started at a constant rate, until the stoichiometric ratio between the two components has been reached, according to the chemical reaction:

$$\nu_A A + \nu_B B \rightarrow C + \nu_D D \tag{1}$$

taking place in a biphase (liquid-liquid) system. We further assume a microkinetic rate expression for the reaction (1) of the form:

$$r = k_{n,m} C_A^n C_B^m \tag{2}$$

derived for instance from a data fitting of calorimetric experiments carried out in the slow reaction regime, that is in microkinetic or kinetically controlled conditions.

The reactor model can be defined on the basis of a few reasonable assumptions, that is:

1) the reaction mass is perfectly macromixed;
2) the influence of the chemical reaction on the volume of the single phase is negligible;
3) no phase inversions occur;
4) the solubility of the species A and C in the continuous phase, c, and of components B and D in the dispersed phase, d, is small (in other words, species A and C are almost all in phase d, whereas species B and D are present almost only in phase c);
5) the chemical reaction takes place only in one of the two liquid phases: this situation is very common in many industrial processes (such as nitrations and oxidations), in which the catalyst (typically a strong acid) is present only in one phase;
6) the heat effects are associated to the chemical reaction only;
7) at the beginning, the reaction mass is at the mean coolant temperature, T_{cool}, which is assumed to remain constant for the whole duration of the process (that is, the reactor operates under isoperibolic conditions).

The mass balance equation for the component B (initially charged in the reactor) yields:

$$\frac{d\zeta_B}{d\vartheta} = \frac{\nu_B t_D}{n_{B,0}} r^{eff} V_r \tag{3}$$

where the effective reaction rate, r^{eff}, depends in general on the microkinetic rate expression, the phase in which the reaction takes place and the controlling step among the chemical reaction, the interphase mass transfer and the supply of the coreactant.

In this work we assume that the reactor always operates in the fast reaction regime: this physically means that the ratio between the characteristic time of the chemical reaction and that of the *interphase* mass transport of the transferred species is sufficiently low. Moreover, the ratio between the characteristic time of the chemical reaction and that of the *intraphase* mass transport of the not transferred species in the reaction phase is sufficiently high, so that no depletion phenomena of the same component in the film of the reaction phase occur. These conditions correspond to the Hatta number ranges reported in Table 1 [7]. In the fast reaction regime and for a single reaction of (n,m) orders occurring respectively in the continuous and in the dispersed phase, the expressions of the macrokinetic conversion rates are [7]:

$$r_{fast,c}^{eff} = a\left(\frac{2D_{L_c,A}k_{n,m_c}}{n+1}\right)^{1/2} C_{A,I_c}^{\frac{n+1}{2}} C_{B_c}^{\frac{m}{2}} \tag{4}$$

$$r_{fast,d}^{eff} = a\left(\frac{2D_{L_d,B}k_{n,m_d}}{m+1}\right)^{1/2} C_{B,I_d}^{\frac{m+1}{2}} C_{A_d}^{\frac{n}{2}} \tag{5}$$

where $a=6/d_b \cdot \varepsilon\vartheta/(1+\varepsilon\vartheta)$ is the interphase surface per unit liquid volume and $\varepsilon=V_D/V_c$ is the relative volume increase throughout the dosing period. For baffled reactors equipped with turbine type stirrers, the Sauter mean diameter, d_b, of the dispersed phase drops can be estimated through the following equation [8]:

$$d_b = d_{b,0}\left(1+2.5\varepsilon_d\right) \tag{6}$$

where $d_{b,0}$, (namely the mean diameter when the hold-up of the dispersed phase approaches zero) depends on the stirrer type, speed and on the physical properties of the two phases. For instance, for a blade turbine stirrer, it can be estimated through the relation [8]: $d_{b,0}/d_{turbine}=0.047We^{-0.6}$, which involves the Weber number, $We = \hat{\rho}_c N^2 d_{turbine}^3 \big/ \sigma_d$, representing the ratio between the dispersing forces induced by turbulent mixing and the surface tension of the phase to be dispersed.

The mass balance eq. (3) for species B can be rearranged in the form:

$$\frac{d\zeta_B}{d\vartheta} = \nu_A\, Da\, RE_{fast,c/d}\; f_{fast,c/d}\; \kappa_{n,m}^{1/2} \tag{7}$$

where $Da=k_{n,m,R}t_D C_{B,0}^{n+m-1}$ is the Damköhler number for (n,m) order kinetics, which contains the information on the dosing time, and $\kappa_{n,m}=\exp[\gamma(1-1/\tau)]$ is the dimensionless reaction rate constant, that is the ratio of the reaction rate constant to the same quantity evaluated at a reference temperature, T_R. $\gamma=E/(RT_R)$ is then the dimensionless activation energy and $\tau=T/T_R$ is the dimensionless temperature. A comparison of eq. (7) with the correspondent mass balance equation in the slow reaction regime [6] shows that in the fast reaction regime the apparent activation energy is halved with respect to its microkinetic value: this is the reason why a runaway in the fast reaction regime is normally accompanied by a lower thermal exceeding of the target temperature, which in practice means that it usually exerts a more moderate effect [8]. Using now the functional dependences of the concentrations of A in the dispersed phase and of B in the continuous phase on the dimensionless time ϑ and on the molar conversion ζ_B and performing suitable algebraic manipulations of eqs. (3), (4) and (5) along the same lines discussed elsewhere [6], the expressions of the reactivity enhancement factor, RE, and of the function, f, can be derived for the two cases of fast reactions taking place in the dispersed ($RE_{fast,d}$ and $f_{fast,d}$) or in the continuous ($RE_{fast,c}$ and $f_{fast,c}$) phase. These expressions, which are summarized in Table 1, also involve the distribution coefficient, m_i, which is defined as the ratio of the concentration of component i in the phase in which its solubility is small to that in the other phase. As will be discussed in the following section, the dependence of $f_{fast,c/d}$ on the values of n and m reflects on the shape and location of the

boundary diagrams.

The energy balance equation for the reactor can be written in dimensionless form as:

$$\left(1+R_H\varepsilon\vartheta\right)\frac{d\tau}{d\vartheta}=\Delta\tau_{ad,0}\frac{d\zeta_B}{d\vartheta}-\left[U^*Da\left(1+\varepsilon\vartheta\right)+\varepsilon R_H\right]\left(\tau-\tau_{cool}^{eff}\right) \tag{8}$$

where $d\zeta_B/d\vartheta$ is the only factor dependent on the kinetic regime (slow or fast reactions) and $T_{cool}^{eff}=\dfrac{U^*Da\left(1+\varepsilon\vartheta\right)T_{cool}+\varepsilon R_H T_D}{U^*Da\left(1+\varepsilon\vartheta\right)+\varepsilon R_H}$ is an effective cooling temperature which takes into account the effects of both the heat removal by the coolant and the sensible heat of the dosing stream.

The numerical integration (which has been carried out using the MATLAB suite of programs) of eqs. (7) and (8) with the proper initial conditions generates the conversion and temperature time profiles for the reactor. For the sake of example, in Figure 1 the temperature evolutions for single fast reactions of different kinetics occurring in the dispersed phase are shown. As happens in the slow reaction regime, a greater influence of the reaction order of the dosed component, n, than of the reactant initially present in the reactor, m, can be observed. As will be discussed in the following section, for a given set of dimensionless parameters and the same initial conditions, a runaway situation can disappear for increasing values of n but not of m, whereas if such a situation disappears for increasing values of m, certainly the same will happen for increasing n values. The order of reaction of the dosed species has in fact a direct influence on its accumulation also in the fast reaction regime. The higher n is, the higher the macrokinetic conversion rate normally becomes for a given increase of the hold-up of unreacted A in the system. This counteracts the accumulation phenomena and results in a safer operation of the reactor.

2.3 Thermally safe operating conditions

The thermally safe operation of a SBR in which an exothermic liquid-liquid reaction occurs corresponds to conditions in which the overall kinetics of the process is largely determined by the dosing rate of the coreactant, which accumulation in the system remains consequently confined below a critical value. To characterize quantitatively the thermal behaviors of a SBR, a so-called target temperature can be derived from the energy balance eq. (8) by stating that the characteristic time of the chemically enhanced mass transfer between the liquid phases (that is, of the macrokinetic conversion) is much smaller than the characteristic time of the coreactant supply and that the reactor temperature evolution is largely dominated by the heat removal contribution, which allows for a quasi-steady-state assumption on the temperature itself [6]. Such operating conditions lead to the following temperature-time dependence, called “target temperature”:

$$\tau_{ta} = \tau_{cool}^{eff} + 1.05\frac{\Delta\tau_{ad,0}}{U^{*}Da\left(1+\varepsilon\vartheta\right)+\varepsilon R_{H}} \tag{9}$$

The factor "1.05" has been introduced to give a "use oriented" definition of the target temperature itself, because of the unavoidable accumulation which must be expected to occur in every real reactor, due to never infinite conversion rates [9]. In this respect, it should also be mentioned that other definitions of runaway conditions for SBRs have been proposed in the literature, which are based on some mathematical behaviors of the temperature-time profile. These criteria are, in some sense, more intrinsic and do not require the assumption of any arbitrary factor [10]. It is clear that τ_{ta} does not depend on the kinetic regime (slow or fast reactions), as it refers to conditions where the conversion rate is completely determined by the supply rate of the coreactant.

Also in the fast (as in the slow) reaction regime, by comparing the real temperature evolution of a SBR with the corresponding target temperature it is possible to classify the thermal behavior of the system from a safety point of view. The exceeding of the target temperature is regarded as a runaway situation and provides the starting point for building boundary diagrams on a suitable dimensionless space that, as in the slow reaction regime, can be conveniently derived from the energy balance eq. (8). At the right hand side of this equation one can recognize an enthalpic contribution associated to the chemical reaction:

$$\dot{Q}_{r} = \Delta\tau_{ad,0}\frac{d\zeta_{B}}{d\vartheta} \tag{10}$$

and an enthalpic contribution which takes into account the heat removal from the reactor by both the coolant and the dosing stream:

$$\dot{Q}_{cool} = \left[U^{*}Da\left(1+\varepsilon\vartheta\right)+\varepsilon R_{H}\right]\left(\tau-\tau_{cool}^{eff}\right) \tag{11}$$

Following the same procedure discussed elsewhere for the slow reaction regime [6], one can calculate the temperature derivatives of eqs. (10) and (11):

$$\frac{d\dot{Q}_{r}}{d\tau} = \Delta\tau_{ad,0}\,\nu_{A}\,Da\,RE\,f\,\kappa^{1/2}\frac{\gamma}{2\tau^{2}} \tag{12}$$

$$\frac{d\dot{Q}_{cool}}{d\tau} = U^{*}Da\left(1+\varepsilon\vartheta\right)+\varepsilon R_{H} \tag{13}$$

Eqs. (12) and (13) can be rewritten in a more compact form by introducing a reactivity factor, F_R, mainly related to the reaction rate, an exothermicity factor, F_E, mainly related to the adiabatic temperature rise, and a cooling factor, F_{cool}, related to the cooling potential:

$$F_R = \nu_A\, Da\, RE\, \kappa^{1/2} = \frac{1}{f}\frac{d\zeta_B}{d\vartheta} \tag{14}$$

$$F_E = \Delta\tau_{ad,0}\,\frac{\gamma}{2\tau^2} \tag{15}$$

$$F_{cool} = U^* Da\left(1+\varepsilon\vartheta\right) + \varepsilon R_H \tag{16}$$

Eqs. (12) and (13) consequently become:

$$\frac{d\dot{Q}_r}{d\tau} = f F_R F_E \tag{17}$$

$$\frac{d\dot{Q}_{cool}}{d\tau} = F_{cool} \tag{18}$$

As discussed elsewhere for the slow reaction regime [6], different sets of the parameters appearing in the model eqs. (7) and (8) can generate the same instantaneous value of the expression (17), but very different values of F_R and F_E. More precisely, for given instantaneous values of $d\dot{Q}_r/d\tau$ and f, we can identify two asymptotic situations: the first one (referred to as situation a) is characterized by a very high (theoretically infinite) value of F_R and a very low (theoretically approaching zero) value of F_E, whereas the second one (referred to as situation b) is characterized by a very low (theoretically approaching zero) value of F_R and a very high (theoretically infinite) value of F_E. The aforementioned two situations are completely different from a safety point of view. Situation a corresponds to potentially very high macrokinetic conversion rates (which counteract the accumulation of the coreactant in the system) and very low values of the activation energy and/or the adiabatic temperature rise: regardless of the cooling potential this situation is always safe. Situation b implies the opposite and, regardless of the cooling potential, results in a runaway. Intermediate cases, characterized by finite values of F_R and F_E, cannot be classified (in terms of runaway or safe conditions) without relating them to the heat removal contribution from the system, $d\dot{Q}_{cool}/d\tau$. Also in the fast (as in the slow) reaction regime, the ratios of the reactivity and the exothermicity factor to the cooling factor, evaluated at the coolant temperature, can be conveniently chosen to define the space where the boundary diagrams are reported. These two quantities, respectively called reactivity, R_y, and exothermicity, E_x, number, have the following expressions in the fast reaction regime:

$$R_y = \left.\frac{F_R}{F_{cool}}\right|_{\vartheta=0} = \frac{\nu_A\, Da\, RE\, \kappa^{1/2}\left(\tau_{cool}\right)}{U^* Da + \varepsilon R_H} = \frac{\nu_A\, Da\, RE\, \kappa^{1/2}\left(\tau_{cool}\right)}{\varepsilon\left(Co + R_H\right)} \tag{19}$$

$$E_x = \left.\frac{F_E}{F_{cool}}\right|_{\vartheta=0} = \frac{\gamma}{2\tau_{cool}^2}\frac{\Delta\tau_{ad,0}}{U^* Da + \varepsilon R_H} = \frac{\gamma}{2\tau_{cool}^2}\frac{\Delta\tau_{ad,0}}{\varepsilon\left(Co + R_H\right)} \tag{20}$$

where the cooling number $Co=U^*Da/\varepsilon$ has been also introduced. The comparison between the expressions of E_x and R_y in the slow and fast reaction regimes, shows that the two definitions become coincident if they are expressed in terms of an apparent activation energy that, as previously noticed, in the fast reaction regime corresponds to the half of the microkinetic value.

The comparison between the temperature-time profile and the corresponding target temperature line represents a useful way for classifying the thermal behavior of the system [5]. Given a set of values for the parameters appearing in eqs. (7) and (8), and solving such equations for increasingly values of the coolant temperature, it is possible to identify the same typologies of thermal behaviors of the reactor observed in the slow reaction regime: no ignition (characterized by a high but not dangerous accumulation of the coreactant in the system, but also by a low productivity of the reactor), runaway (characterized by a maximum temperature larger than the local target value) and QFS (characterized by a temperature evolution which quickly approaches the target line and remains close to it throughout the dosing period, at the end of which the conversion is almost complete). These regions can be reported on a boundary diagram, where the runaway region is enclosed inside the continuous line and is surrounded by the no ignition region (for low R_y values), the QFS region (for high R_y values) and by an inherently safe region. The latter is characterized by either E_x values lower than the minimum E_x value of the runaway boundary, $E_{x,MIN}$, or by R_y values larger than the maximum R_y value of the runaway boundary, $R_{y,QFS}$. In such diagrams, the aforementioned asymptotic behaviors a and b correspond respectively to the left-upper ($R_y\to\infty$, $E_x\to0$) and right-bottom ($R_y\to0$, $E_x\to\infty$) regions of the diagram itself [6]. The diagrams can be easily used to solve two typologies of problems:

1. for an existing reactor, operating at known values of the fixed parameters Co, R_H, n and m, and in the fast reaction regime, the corresponding boundary diagram can be used to identify thermally safe operating conditions without solving the mathematical model of the reactor;
2. the conclusions drawn for a given reactor from the use of the corresponding boundary diagram can be extended to scaled up systems, provided that both the reactors are characterized by the same Co, R_H, n and m values and operate in the same kinetic regime (in this case, the fast reaction regime).

Each boundary diagram involves a given range of the parameters ν_A Da RE, ε, γ and $\Delta\tau_{ad,0}$, but a fixed value of the parameters Co, R_H, n and m. In particular, both Co and R_H can strongly

influence the shape and location of the boundary diagram also in the fast reaction regime, as shown for the sake of example in Figure 2. However, the same figures also evidences the strong influence of the reaction order on the shape and location of the boundary diagrams. These observations can be quantified through the use of normalized objective sensitivity coefficients of both $E_{x,MIN}$ and $R_{y,QFS}$ with respect to the considered parameters. Such sensitivity coefficients quantify the influence of a small change of one of the involved parameters on the values of either $E_{x,MIN}$ or $R_{y,QFS}$, and can be defined as [10]:

$$S_{i,j} = \frac{\alpha_j}{\beta_i}\frac{\partial \beta_i}{\partial \alpha_j} \approx \frac{\alpha_j}{\beta_i}\frac{\Delta \beta_i}{\Delta \alpha_j} \tag{21}$$

where β_i is either $R_{y,QFS}$ or $E_{x,MIN}$, and α_j can be Co, R_H, n or m, respectively. The values of such sensitivity coefficients, summarized in Table 2, clearly show the influence of the various parameters. From these data we can see that also in the fast reaction regime the influence of the reaction order on the values of both $R_{y,QFS}$ and $E_{x,MIN}$ can be larger than that of both Co and R_H. It follows that the influence of n and m on the shape and location of the boundary diagrams can be disregarded only as a first approximation. However, the available boundary diagrams for fast reaction systems refer only to reaction orders equal to (1,1) [8]. This is obviously a limitation since the microkinetic reaction orders are not always equal to (1,1). The influence of the reaction order values on the shape and location of the boundary diagrams is shown in Figures 3 and 4, referring to reactions in the dispersed and in the continuous phase, respectively. These diagrams are the results of a series of simulations extended to the following ranges of parameters: $0.025<\nu_A$ Da RE<14, $0.3<\varepsilon<0.55$, $32<\gamma<42$, $0.29<\Delta\tau_{ad,0}<0.7$, Co=10, R_H=1. From these data we can observe that, when the order of only one component (that is, either n or m) changes, the use of a boundary diagram obtained for a certain reaction order is safe for reactions of larger order. Moreover, for both the cases (fast reaction taking place in the dispersed or in the continuous phase), variations in the order of the dosed coreactant, n, imply much larger differences in the extension of the correspondent runaway regions than variations of the reaction order of the reactant initially charged in the reactor, m. This is logical because the higher the reaction order of the dosed coreactant is, the faster the macrokinetic reaction rates (4) and (5) become for a given increase (due to accumulation phenomena) of the hold-up of unreacted coreactant in the system: this counteracts directly the accumulation of the coreactant in the reactor and consequently can result in a sensibly narrower runaway region, even for relatively small increases of n. Consequently, if between the microkinetic rate expression to which a boundary diagram refers to and that of the investigated system the order of the dosed component changes, the conclusions drawn from the use of the diagram, even when safe, can be too conservative and hence unrealistic. For these reasons, the use of the correct boundary diagram is always advisable. As previously observed in the analysis of slow reaction

systems [6], the aforementioned conclusions about the safe use of an available boundary diagram for the analysis of a system characterized by a different kinetics hold when only the reaction order of one component (that is, either n or m) changes, as is the case of Figures 3 and 4. If both n and m change, the overall reaction order (that is, n+m) is not a suitable parameter for establishing if the use of the boundary diagram is safe. This comes from the different dependence of the shape and location of a boundary diagram on n and m, respectively, the former being much stronger. For the sake of example, in Figure 5, the boundary diagram for a fast reaction occurring in the dispersed phase with n=0.7 and m=1.4 is compared with that for n=m=1. This figure clearly shows that the runaway region for (0.7,1.4) is larger than that for (1,1) reaction order, even if the overall microkinetic reaction order for the former case is higher (that is, 0.7+1.4=2.1 vs. 1+1=2).

In the fast reaction regime the concentration profiles of the transferred species in the reaction phase are far from being uniform because of the mass transfer limitations. In such a situation the macrokinetic reaction rates (4) and (5) can be conveniently splitted in the product of the microkinetic reaction rate evaluated at the liquid-liquid interface and a utilization factor, which takes into account the concentration drop of the transferred species in the reaction phase itself. The utilization factors for single fast reactions occurring in the continuous or dispersed phase respectively, η_c and η_d, are consequently defined by the relation:

$$J_{A/B}a = \eta_{c/d}\nu_{A/B}r_{I_{c/d}}\left(1-\varepsilon_{d/c}\right) \tag{22}$$

where J is the interphase molar flux of the transferred species and a is the interfacial area per total liquid volume. It can be demonstrated that for (n,m) order reactions the utilization factors have the following expressions:

$$\eta_c = \frac{2}{n+1}\frac{1}{Al_c Ha_c} \tag{23}$$

$$\eta_d = \frac{2}{m+1}\frac{1}{Al_d Ha_d} \tag{24}$$

where Al is the Hinterland ratio and Ha is the Hatta number. Whilst in the slow reaction regime the utilization factors reach values close to one, in the fast reaction regime they are usually lower than one: in particular, as can be easily deduced from eqs. (23) and (24), the higher the reaction orders are, the lower the average utilization degrees of the reaction phase during the supply period normally become. This explains the much weaker dependence of the thermal behavior on the phase in which the reaction takes place that has been found for the fast reaction regime than that evidenced for the slow reaction regime. This especially holds as the reaction orders increase. In the slow reaction regime, where the degree of utilization of the reaction phase is close to one, the

average values of the "$r^{eff}V_r$" terms in the mass balance equations during the supply period are much larger for reactions occurring in the continuous than in the dispersed phase, because the dispersed phase volume increases during the supply period from zero to its final value, whereas the continuous phase volume is constant (and maximum) from the beginning. This leads to a much larger extension of the runaway region for a slow reaction occurring in the dispersed than in the continuous phase, as it is evident from the boundary diagrams reported in Figure 6. On the contrary, in the fast reaction regime the chemical reaction takes place in a region close to the interface because of the mass transfer limitations and hence the dependence of the thermal behavior of the system on the reaction phase becomes less important, as shown for the sake of example in Figure 7, that can be directly compared with Figure 6. The importance of this effect depends also on the reaction orders as summarized in Figure 8, where some couples of boundary diagrams are represented. We can observe for instance that for n=2, using the boundary diagram for the reaction occurring in the dispersed phase to predict the safe operation of a system characterized by the same microkinetic rate expression but in which the reaction takes place in the continuous phase, leads to more realistic results than using the boundary diagram calculated for a (1,1) reaction order in the right reaction phase. As a first approximation, for a given set of Co, R_H, m and for $n \geq 2$ it is possible to use only the boundary diagrams for reactions occurring in the dispersed phase also for systems in which the reaction occurs in the continuous phase. The same conclusions can be drawn also from the data summarized in Table 3, where the differences, $\Delta R_{y,QFS}$, between the $R_{y,QFS}$ values for a fast (n,m) reaction taking place in the continuous and dispersed phase, respectively, are reported, for given values of Co, R_H and m, and for increasing n values. The differences between the correspondent $E_{x,MIN}$ values, $\Delta E_{x,MIN}$, are also reported. It can be observed that whereas the $\Delta E_{x,MIN}$ variations remain in the ±20% range with respect to an average value, the $\Delta R_{y,QFS}$ values become sensibly lower with increasing n, clearly showing that the influence of the phase in which the reaction occurs on the shape and location of the boundary diagrams becomes less important.

It can be concluded that in the fast (as in the slow) reaction regime the use of a boundary diagram built for a given microkinetic reaction order can be unsafe for the analysis of a system characterized by a different kinetics, and the comparison between the overall reaction orders is not a suitable way for establishing that. Besides, even when the use of a boundary diagram for a different kinetics is safe, the conclusions drawn can be too conservative. Moreover, in the fast reaction regime as the reaction orders (in particular n) increase, the boundary diagrams for the reactions taking place in the dispersed and in the continuous phase respectively, calculated for the same Co, R_H, n and m values, become more similar.

For a practical use, boundary diagrams for various n values are reported in Figures 9 to 12. In these figures, the influence of the cooling number and of the heat capacity ratio on the location

and extension of a boundary diagram is shown, for n=0.5 and n=2. Boundary diagrams for the basic case n=m=1 have been already reported elsewhere [8]. As it has been observed for the slow reaction regime [6], the boundary diagrams reported in this work can be used as a first approximation, according to the rules-of-thumb given above and following the procedure discussed in detail elsewhere [2]. On the other hand, there are several systems for which it could be useful to refer to the correct boundary diagram. The procedure for building the boundary diagrams for a single fast reaction of (n,m) orders occurring in the continuous or dispersed phase is the same as described in detail elsewhere [6], provided that the expressions of E_x and R_y for the fast reaction regime given in this work are used. Once built, the boundary diagram can be employed for the a-priori analysis of several changes in operating conditions of an existing reactor and for scale-up purposes, provided that Co and R_H do not change and that the reactor always operates in the fast reaction regime.

Finally, it is interesting to notice that an infinite number of real reactor conditions can correspond to a single set of parameters which must be assigned to solve the dimensionless model eqs. (7) and (8) (or the analogous equations for slow reaction systems). For the sake of example, let us consider several reactors, which only differ in the values of the pre-exponential factor of the kinetic constant (which is involved only in the ν_A Da RE parameter) and of the relevant distribution coefficient (which is involved only in the reactivity enhancement factor, RE), and let's also assume that the product of these two quantities is a constant, so that also the dimensionless group ν_A Da RE in the dimensionless mass and energy balances is constant. It is clear that among this infinite number of reaction systems, the higher the pre-exponential factor is (and consequently the lower the relevant distribution coefficient), the higher the Hatta number becomes, until the system moves from the slow to the fast reaction regime. It follows that when *calculating* a boundary diagram it does not make any sense to check whether we are dealing with a slow or fast reaction system, because when considering the single parameters set we are not dealing with a single but with infinite reactor conditions. However, when *using* a boundary diagram for the analysis of the operating conditions of a real reactor, we must check whether the reactor operates in the slow or fast reaction regime, in order to chose the proper boundary diagram. This check can be performed by evaluating the order of magnitude of two relevant parameters, that is Ha and Al Ha^2 [7].

2.4 Conclusions

The comparison between the target temperature and the real temperature-time profile of a SBR in which a single exothermic liquid-liquid reaction takes place in the fast reaction regime is the starting point for building boundary diagrams in terms of proper exothermicity and reactivity

parameters. The boundary diagrams are a powerful tool to perform simple and fast safety analyses of any change in the operating conditions of a liquid-liquid SBR without solving the correspondent mathematical model, as well as to scale up a process from the laboratory or pilot to the industrial scale.

However, it has been shown that the conclusions drawn from the use of boundary diagrams developed assuming a (1,1) reaction order are not always safe for the analysis of systems characterized by different kinetics. Moreover, the comparison between the overall reaction orders is not a suitable way for establishing whether an available boundary diagram can be safely used when the orders of both the reactants change. Even when the use of a (1,1) boundary diagram is safe, if the order of the dosed coreactant changes, the conclusions drawn can be too conservative. In the paper a number of boundary diagrams are provided for reaction orders different from one, which can be used, according to the rules-of-thumb reported, for better approximating the real conditions. Requirements related to the reaction order of the reactant initially charged in the reactor are less stringent than those related to the order of the dosed coreactant. When only this parameter changes, a boundary diagram obtained for a given reaction order can be used also for the preliminary analysis of higher reaction order systems.

In the fast reaction regime the degree of utilization of the reaction phase can be sensibly lower than 100% (which is the case of slow reaction systems) and its value normally diminishes with increasing the reaction orders (in particular the order respect to the dosed coreactant). The strong dependence observed for the thermal behavior of slow reaction systems on the reaction phase, which comes from the unbalance of the continuous and dispersed phase volumes during the supply period, becomes for this reason much less important in the fast reaction regime. Consequently, as the reaction order respect to the dosed coreactant increases, more realistic results can be obtained by using a boundary diagram for reactions occurring in the dispersed phase also for the analysis of a continuous reaction phase system with the same chemical kinetics, rather than using a boundary diagram relative to reactions occurring in the continuous phase but calculated for an approximated (typically for n=m=1) reaction order. However, the best and more reliable results can be obtained using the proper boundary diagram for the case of interest.

Finally it should be stressed that when *calculating* a boundary diagram, no checks on the kinetic regime (slow or fast reaction) must be performed. However, when *using* a boundary diagram, it is necessary to verify whether the reactor operation is kinetically or diffusion controlled, in order to chose the proper boundary diagram.

Nomenclature

Symbols	
a	interfacial area per unit liquid volume, m^2/m^3
A	heat transfer area of the reactor (associated to the jacket and/or the coil), m^2
Al	$=\left(1-\varepsilon_{c/d}\right)k_{L_{d/c}B/A}\Big/\left(a\,D_{L_{d/c}B/A}\right)$, Hinterland ratio (total volume/film volume of the reaction phase), -
C	molar concentration, $kmol/m^3$
Co	$=U^{*}Da/\varepsilon$, cooling number, -
$\tilde{C}_P$	molar heat capacity, kJ/(kmol·K)
d_b	Sauter mean diameter of the dispersed phase drops, m
$d_{b,0}$	d_b at hold up of the dispersed phase approaching zero, m
D	diffusivity, m^2/s
Da	$=k_{n,m,R}t_D C_{B,0}^{\,n+m-1}$, Damköhler number for (n,m) order reactions, -
E	activation energy, kJ/kmol
E	enhancement factor of the interphase molar flux, -
E_∞	asymptotic value of E for high Hatta numbers, -
E_x	exothermicity number, eq. (20), -
$\Delta E_{x,MIN}$	difference between the $E_{x,MIN}$ values for the reaction occurring in the dispersed and continuous phase (absolute value), -
f	function of the dimensionless time and conversion of B in eq. (7), -
F_E	exothermicity factor, eq. (15), -
F_R	reactivity factor, eq. (14), -
F_{cool}	cooling factor, eq. (16), -
$\Delta\tilde{H}$	reaction enthalpy, kJ/kmol
Ha	Hatta number, -
J	interphase molar flux, $kmol/(m^2\cdot s)$
$k_{n,m}$	reaction rate constant, $m^{3(n+m-1)}/(kmol^{n+m-1}\cdot s)$
k_L	mass transfer coefficient, m/s
m	order of reaction respect to component B, -
m	equilibrium distribution coefficient ($m_A=C_{A,c}/C_{A,d}$; $m_B=C_{B,d}/C_{B,c}$), -
n	order of reaction respect to component A, -
n	number of moles, kmol
N	stirring speed, $rad\cdot s^{-1}$

$\dot{Q}_r$	enthalpic contribution due to the reaction, eq. (10), -
$\dot{Q}_{cool}$	enthalpic contribution due to the heat removal, eq. (11), -
r	reaction rate referred to the total liquid volume, kmol/(m^3·s)
R	gas constant = 8.314, kJ/(kmol·K)
RE	reactivity enhancement factor in eq. (7), -
R_H	$= \tilde{\rho}_d \tilde{C}_{P,d} \big/ \left(\tilde{\rho}_c \tilde{C}_{P,c} \right) \approx \tilde{\rho}_D \tilde{C}_{P,D} \big/ \left(\tilde{\rho}_c \tilde{C}_{P,c} \right)$, heat capacity ratio, -
R_y	reactivity number, eq. (19), -
$\Delta R_{y,QFS}$	difference between the $R_{y,QFS}$ values for the reaction occurring in the dispersed and continuous phase (absolute value), -
S	normalized objective sensitivity coefficient, eq. (21), -
t	time, s
T	temperature, K
$\Delta T_{ad,0}$	$= \left(-\Delta \tilde{H}_r \right) n_{B,0} \big/ \left(\nu_B \tilde{\rho}_c \tilde{C}_{P,c} V_c \right)$, adiabatic temperature rise, K
U	overall heat transfer coefficient, kW/(m^2·K)
U^*Da	$= \left(UA \right)_0 t_D \big/ \left(\tilde{\rho}_c \tilde{C}_{P,c} V_c \right)$, modified Stanton number, -
V	liquid volume, m^3
We	$= \hat{\rho}_c N^2 d_{turbine}^3 \big/ \sigma_d$, Weber number, -

Greek symbols

α, β	generic symbols, eq. (21), -
γ	$=E/(RT_R)$, dimensionless activation energy, -
ε	relative volume increase at the end of the semibatch period, -
ε_c	volume fraction of the continuous phase, -
ε_d	volume fraction of the dispersed phase, -
ζ	molar conversion, -
η	utilization factor of the reaction phase, -
ϑ	$=t/t_D$, dimensionless time, -
κ	$=k/k_R$, dimensionless reaction rate constant, -
ν	stoichiometric coefficient, -
$\tilde{\rho}$	molar density, kmol/m^3
$\hat{\rho}$	mass density, kg/m^3
σ	surface tension, N/m
τ	$=T/T_R$, dimensionless temperature, -

Subscripts and superscripts	
A,B,C,D	components A, B, C and D
ad	adiabatic
b	in the dispersed phase drop diameter d_b
c	continuous phase
cool	coolant
d	dispersed phase
D	dosing stream or dosing time
E	in the cooling factor F_E
eff	effective
fast	fast reaction regime
H	in the heat capacity ratio R_H
I	interface
L	in the liquid phase
m	order of reaction respect to component B
n	order of reaction respect to component A
MIN	in $E_{x,MIN}$
QFS	in $R_{y,QFS}$
r	reaction
R	reference
R	in the reactivity factor F_R
ta	target
x	in the exothermicity number E_x
y	in the reactivity number R_y
0	start of the semibatch period
∞	in the asymptotic value of the enhancement factor E

Literature cited

1. Benuzzi, A., Zaldìvar, J.M. Eds. Safety of Chemical Reactors and Storage Tanks. 1998, *Kluwer Academic Publishers: Dordrecht, The Netherlands*.

2. Westerterp, K.R., Molga, E.J. No more runaways in fine chemical reactors. *Ind. Eng. Chem. Res.* 2004, *43 (16),* 4585-4594.

3. Hugo, P., Steinbach, J. Praxisorientierte Darstellung der thermischen Sicherheitsgrenzen für den indirekt gekühlten Semibatch-Reaktor. *Chem. Ing. Tech.* 1985, *57, Nr. 9,* 780-782.

4. Hugo, P., Steinbach, J. A comparison of the limits of safe operation of a SBR and a CSTR. *Chem. Eng. Sci.* 1986, *41,* 1081-1087.

5. Steensma, M., Westerterp, K.R. Thermally safe operation of a cooled semi-batch reactor. Slow liquid-liquid reactions. *Chem. Eng. Sci.* 1988, *43, Nr.8,* 2125-2132.

6. Maestri, F., Rota, R. Thermally safe operation of liquid-liquid semibatch reactors. Part I: single kinetically controlled reactions with arbitrary reaction order. *Chem. Eng. Sci.* 2005, *60,* 3309-3322.

7. Westerterp, K.R., van Swaaij, W.P.M., Beenackers, A.A.C.M. Chemical reactor design and operation. *2nd ed.* 1984, *John Wiley & Sons, Chichester, U.K.*.

8. Steensma, M., Westerterp, K.R. Thermally safe operation of a semibatch reactor for liquid-liquid reactions. Fast reactions. *Chem. Eng. Technol.* 1991, *14,* 367-375.

9. Steensma, M., Westerterp, K.R. Thermally safe operation of a semibatch reactor for liquid-liquid reactions. Slow reactions. *Ind. Eng. Chem. Res.* 1990, *29,* 1259-1270.

10. Varma, A., Morbidelli, M., Wu, H. Parametric Sensitivity in Chemical Systems. 1999, *Cambridge University Press*.

Table 1 *Expressions of the reactivity enhancement factor, RE, and of the function, f, for fast reactions taking place in the dispersed or continuous phase. Requirements for fast reaction regime are also reported [7].*

	Fast reaction in the *dispersed* phase, d	**Fast reaction in the *continuous* phase, c**
$\mathbf{RE_{fast,c/d}}$	$\frac{6}{d_{b,0}} m_B^{\frac{m+1}{2}} C_{B,0}^{\frac{1-n-m}{2}} \left(\frac{\nu_B}{\nu_A}\right)^{1-\frac{n}{2}} \left[\frac{2D_{L_d,B}}{(m+1)k_{n,m,R_d}}\right]^{\frac{1}{2}}$	$\frac{6}{d_{b,0}} m_A^{\frac{n+1}{2}} C_{B,0}^{\frac{1-n-m}{2}} \left(\frac{\nu_B}{\nu_A}\right)^{\frac{1-n}{2}} \left[\frac{2D_{L_c,A}}{(n+1)k_{n,m,R_c}}\right]^{\frac{1}{2}}$
$\mathbf{f_{fast,c/d}}$	$\frac{(\vartheta-\zeta_B)^{\frac{n}{2}}(1-\zeta_B)^{\frac{m+1}{2}}(\varepsilon\vartheta)^{1-\frac{n}{2}}}{1+2.5\varepsilon\vartheta/(1+\varepsilon\vartheta)}$	$\frac{(\vartheta-\zeta_B)^{\frac{n+1}{2}}(1-\zeta_B)^{\frac{m}{2}}(\varepsilon\vartheta)^{\frac{1-n}{2}}}{1+2.5\varepsilon\vartheta/(1+\varepsilon\vartheta)}$
check for *fast reactions*	$2 < Ha_d << E_{B,\infty} - 1$ $Ha_d = \frac{1}{k_{L_d,B}}\sqrt{\frac{2}{m+1}k_{n,m_d}D_{L_d,B}C_{B,I_d}^{m-1}C_{A,d}^{n}}$ $E_{B,\infty} = 1+\frac{\nu_B}{\nu_A}\frac{D_{L_d,A}C_{A,d}}{D_{L_d,B}m_B C_{B,c}}$	$2 < Ha_c << E_{A,\infty} - 1$ $Ha_c = \frac{1}{k_{L_c,A}}\sqrt{\frac{2}{n+1}k_{n,m_c}D_{L_c,A}C_{A,I_c}^{n-1}C_{B,c}^{m}}$ $E_{A,\infty} = 1+\frac{\nu_A}{\nu_B}\frac{D_{L_c,B}C_{B,c}}{D_{L_c,A}m_A C_{A,d}}$

Table 2 *Normalized sensitivity coefficients of $R_{y,QFS}$ and $E_{x,MIN}$ computed from the data shown in Figure 2.*

	Fast reaction in the *dispersed* phase, d				**Fast reaction in the *continuous* phase, c**			
	Co	$\mathbf{R_H}$	**n**	**m**	**Co**	$\mathbf{R_H}$	**n**	**m**
$\mathbf{R_{y,QFS}}$	0.19	0.14	0.54	0.11	0.06	0.17	0.56	0.12
$\mathbf{E_{x,MIN}}$	0.62	0.04	1.04	0.35	0.19	0.06	0.62	0.22

Table 3 *Displacement of the $E_{x,MIN}$ and $R_{y,QFS}$ values for single fast reactions occurring in the dispersed and continuous phase, respectively, for some couples of boundary diagrams.*

$$\Delta R_{y,QFS} = \left| \left(R_{y,QFS} \right)_d - \left(R_{y,QFS} \right)_c \right|$$
$$\Delta E_{x,MIN} = \left| \left(E_{x,MIN} \right)_d - \left(E_{x,MIN} \right)_c \right|$$

Fast reaction regime with Co=10, m=1, R_H=1.
0.025< ν_A Da RE<14, 0.3<ε<0.55, 32<γ<42, 0.29<$\Delta\tau_{ad,0}$<0.7.

	n=0.5	**n=1**	**n=1.5**	**n=2**	**n=2.5**
$\Delta R_{y,QFS}$	1.61	0.82	0.53	0.39	0.28
$\Delta E_{x,MIN}$	0.82	0.88	0.69	0.88	0.60

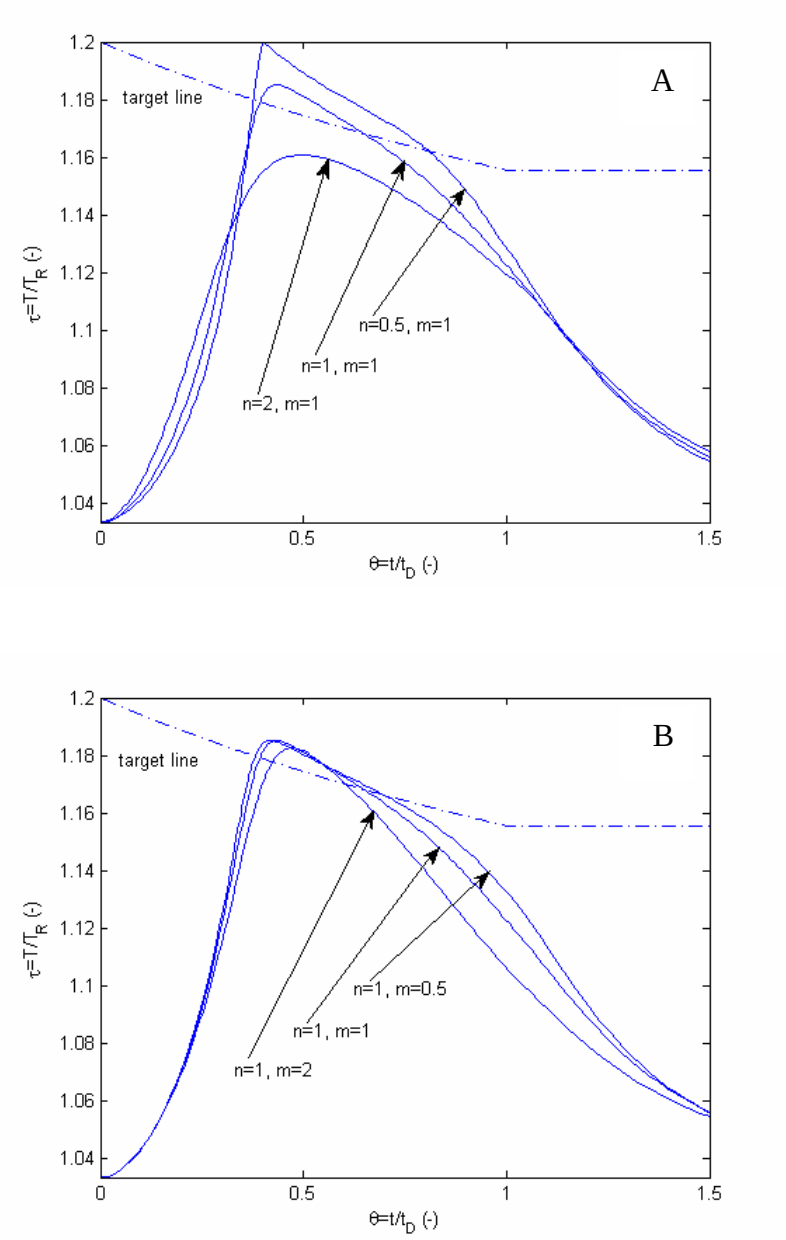

Figure 1 *Temperature-time profiles in a SBR for a fast reaction in the dispersed phase.*

ν_A Da RE=3, ε=0.4, γ=38, R_H=1, $\Delta\tau_{ad,0}$=0.7, Co=10.

Coolant and dosing stream temperature values equal to the initial reactor temperature.

A) influence of the reaction order of the coreactant, n;

B) influence of the reaction order of the reactant initially charged in the reactor, m.

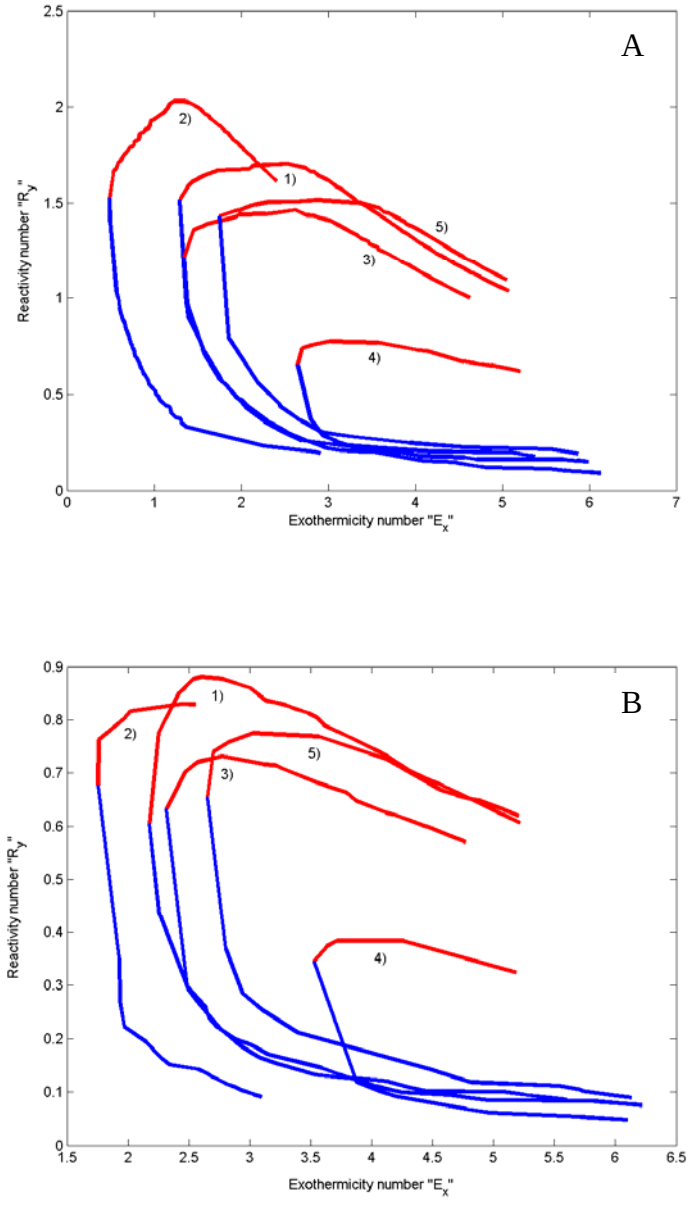

Figure 2 *Sensitivity of the boundary diagrams with respect to the model parameters.*
Fast reaction regime. $0.025 < \nu_A\, Da\, RE < 14$, $0.3 < \varepsilon < 0.55$, $32 < \gamma < 42$, $0.29 < \Delta\tau_{ad,0} < 0.7$.
1) $Co=10$, $R_H=1$, $n=1$, $m=1$; *2)* $Co=20$, $R_H=1$, $n=1$, $m=1$; *3)* $Co=10$, $R_H=2$, $n=1$, $m=1$;
4) $Co=10$, $R_H=1$, $n=2$, $m=1$; *5)* $Co=10$, $R_H=1$, $n=1$, $m=2$.
A) reaction in the dispersed phase; B) reaction in the continuous phase.

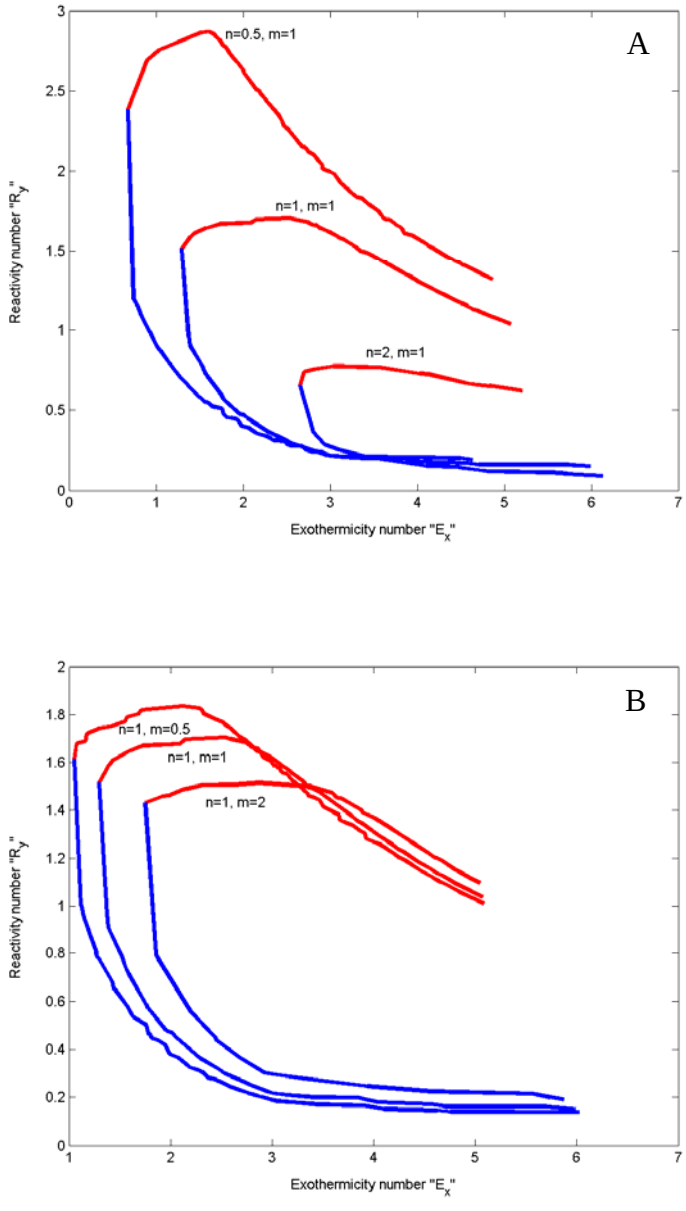

Figure 3 *Boundary diagrams for fast (n,m) order reactions in the dispersed phase.*
$0.025<\nu_A Da\ RE<14$, $0.3<\varepsilon<0.55$, $32<\gamma<42$, $0.29<\Delta\tau_{ad,0}<0.7$, $Co=10$, $R_H=1$.
A) influence of the reaction order of the coreactant, n;
B) influence of the reaction order of the reactant initially charged in the reactor, m.

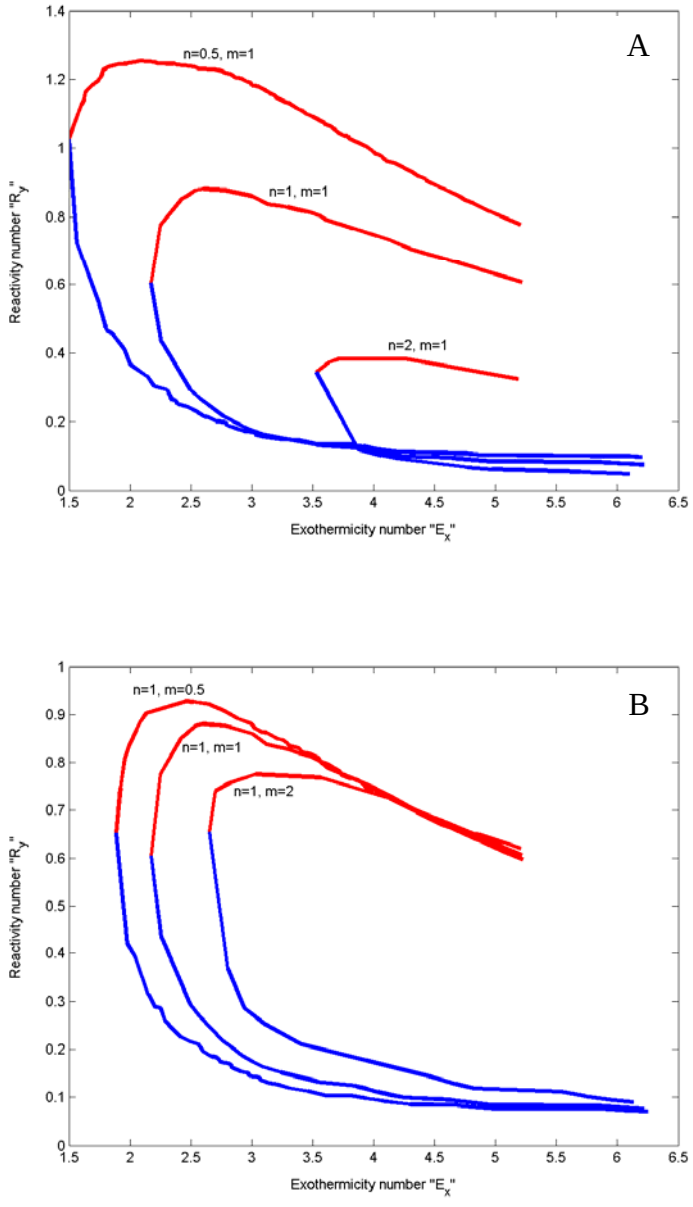

Figure 4 *Boundary diagrams for fast (n,m) order reactions in the continuous phase. Legend and other parameters as in Figure 3.*

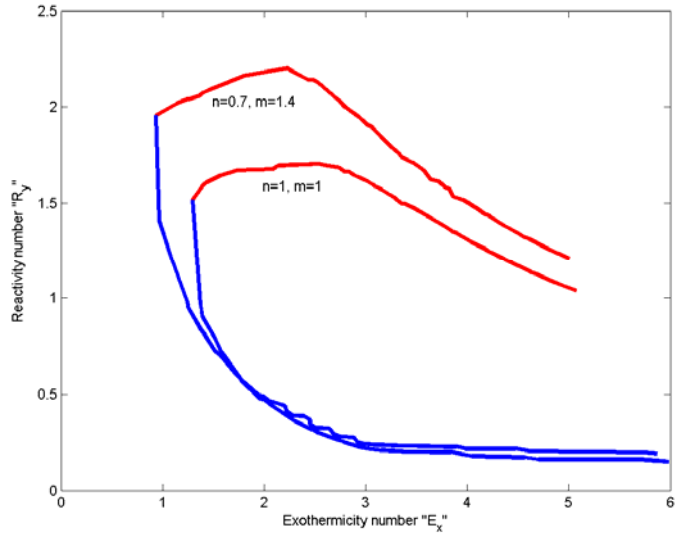

Figure 5 *Boundary diagrams for fast (n,m) order reactions in the dispersed phase. Legend and other parameters as in Figure 3.*

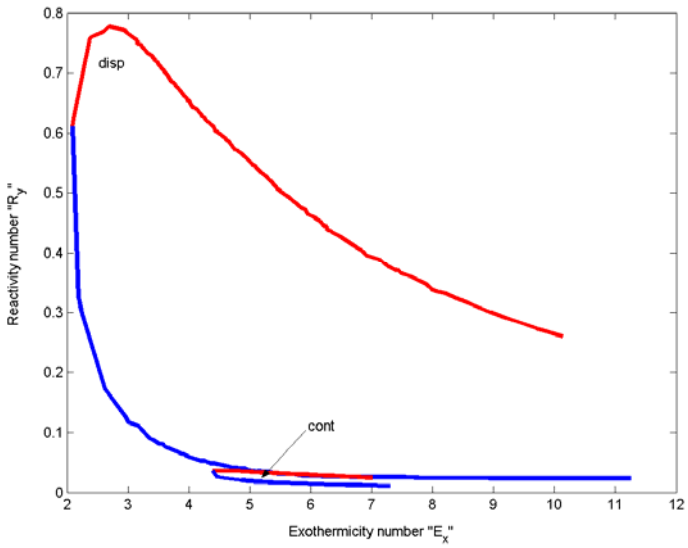

Figure 6 *Comparison between the boundary diagrams for a single reaction in the dispersed and in the continuous phase.*
Slow reaction regime with Co=10, n=1, m=1, R_H=1.
0.025< ν_A Da RE<14, 0.3<ε<0.55, 32<γ<42, 0.29<$\Delta\tau_{ad,0}$<0.7.

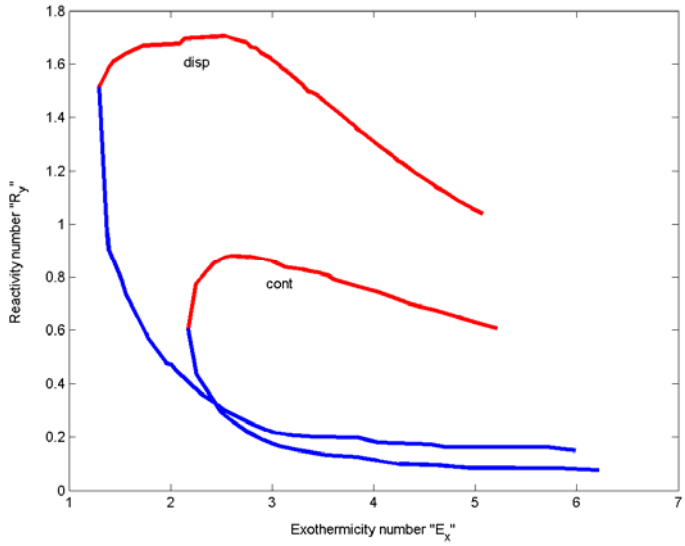

Figure 7 *Comparison between the boundary diagrams for a single reaction in the dispersed and in the continuous phase.*

Fast reaction regime with Co=10, n=1, m=1, R_H=1.

0.025< ν_A Da RE<14, 0.3<ε<0.55, 32<γ<42, 0.29<$\Delta\tau_{ad,0}$<0.7.

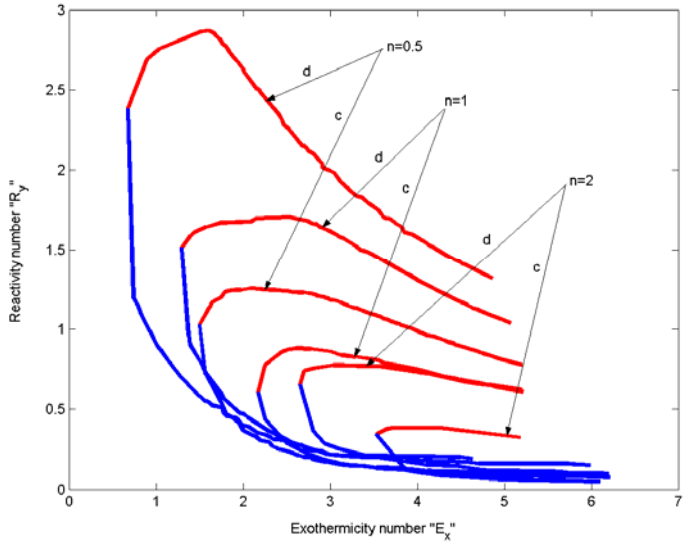

Figure 8 *Comparison between the boundary diagrams for a single reaction in the dispersed and in the continuous phase: influence of the reaction order of the coreactant, n.*

Fast reaction regime with Co=10, m=1, R_H=1.

0.025< ν_A Da RE<14, 0.3<ε<0.55, 32<γ<42, 0.29<$\Delta\tau_{ad,0}$<0.7.

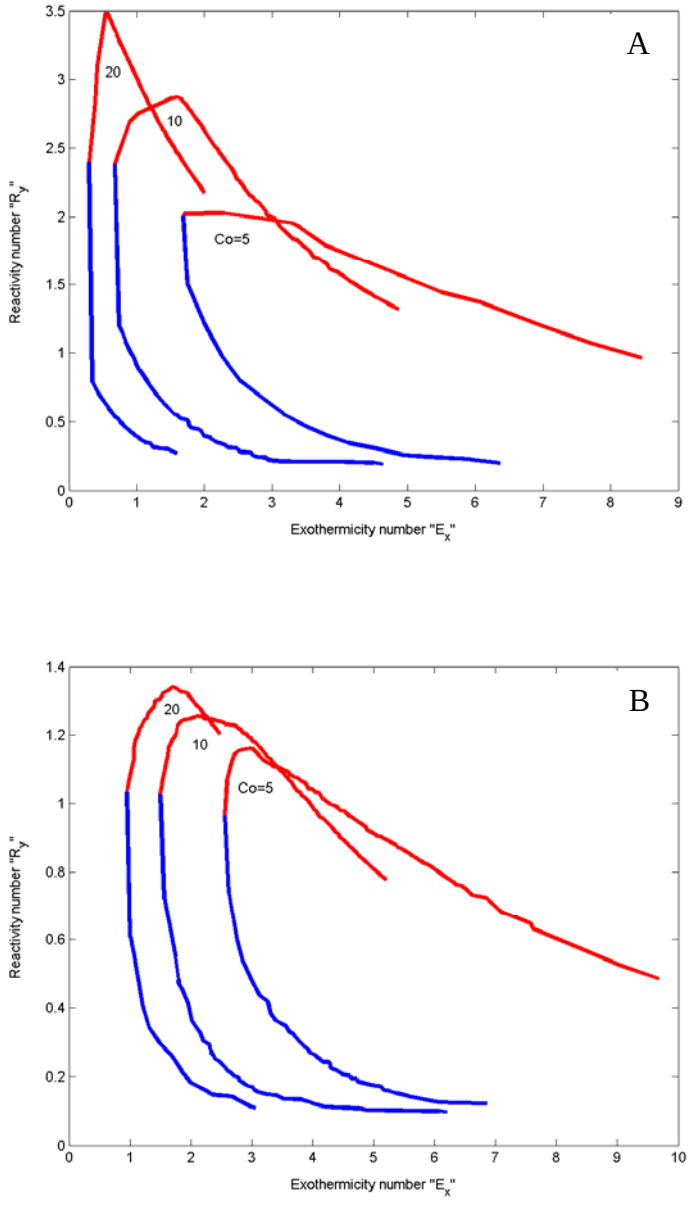

Figure 9 *Influence of the cooling number on the boundary diagrams shape and location.*

Fast reaction regime with n=0.5, m=1, R_H=1.

0.025< ν_A Da RE<14, 0.3<ε<0.55, 32<γ<42, 0.29<$\Delta\tau_{ad,0}$<0.7.

A) reaction in the dispersed phase; B) reaction in the continuous phase.

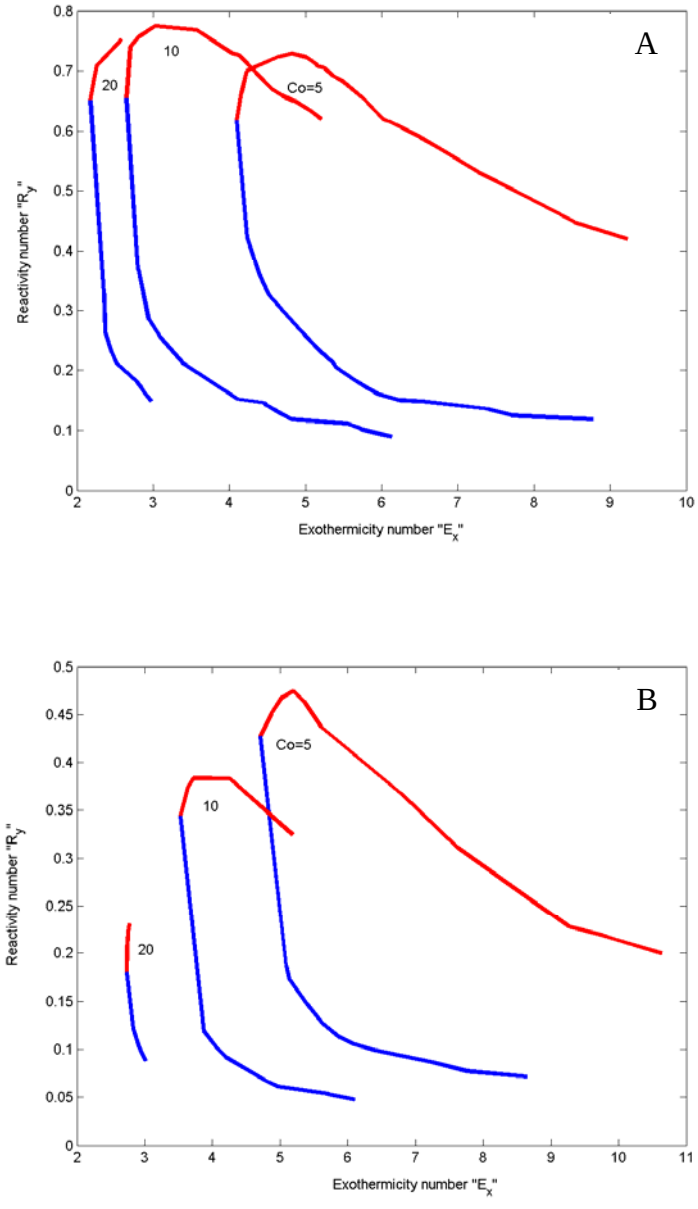

Figure 10 *Influence of the cooling number on the boundary diagrams shape and location.*

Fast reaction regime with n=2, m=1, R_H=1.

Legend and other parameters as in Figure 9.

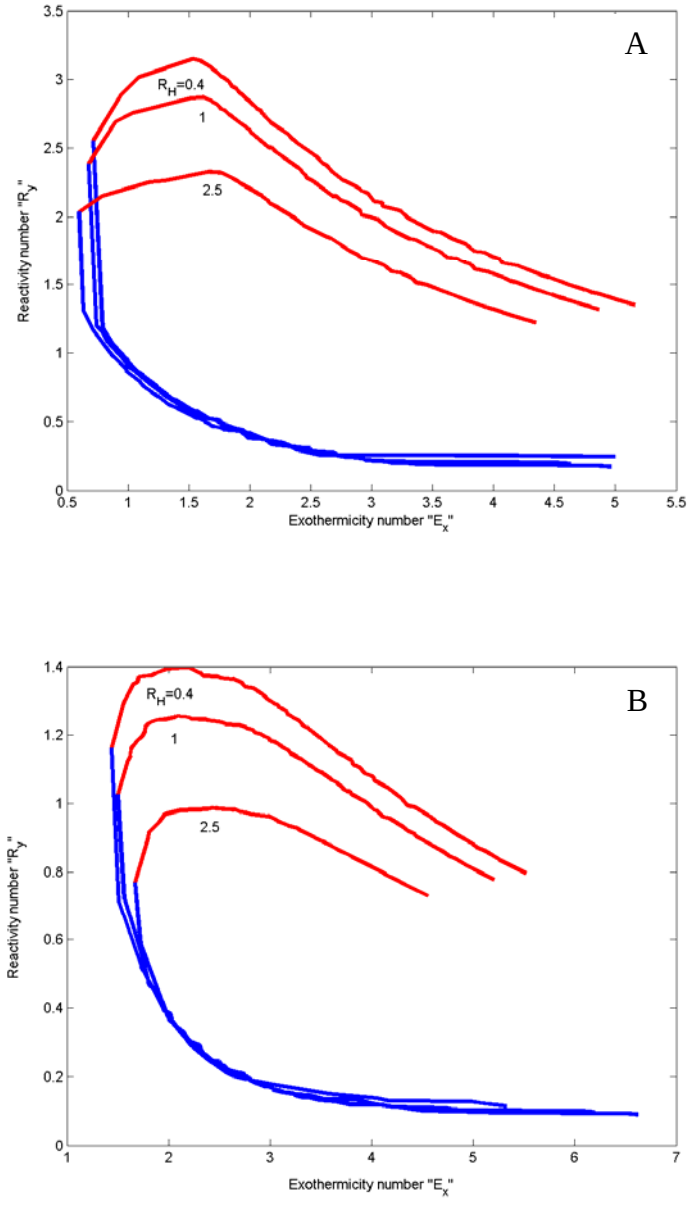

Figure 11 *Influence of the heat capacity ratio on the boundary diagrams shape and location. Fast reaction regime with n=0.5, m=1, Co=10.*

$0.025 < \nu_A\, Da\, RE < 14$, $0.3 < \varepsilon < 0.55$, $32 < \gamma < 42$, $0.29 < \Delta\tau_{ad,0} < 0.7$.

A) reaction in the dispersed phase; B) reaction in the continuous phase.

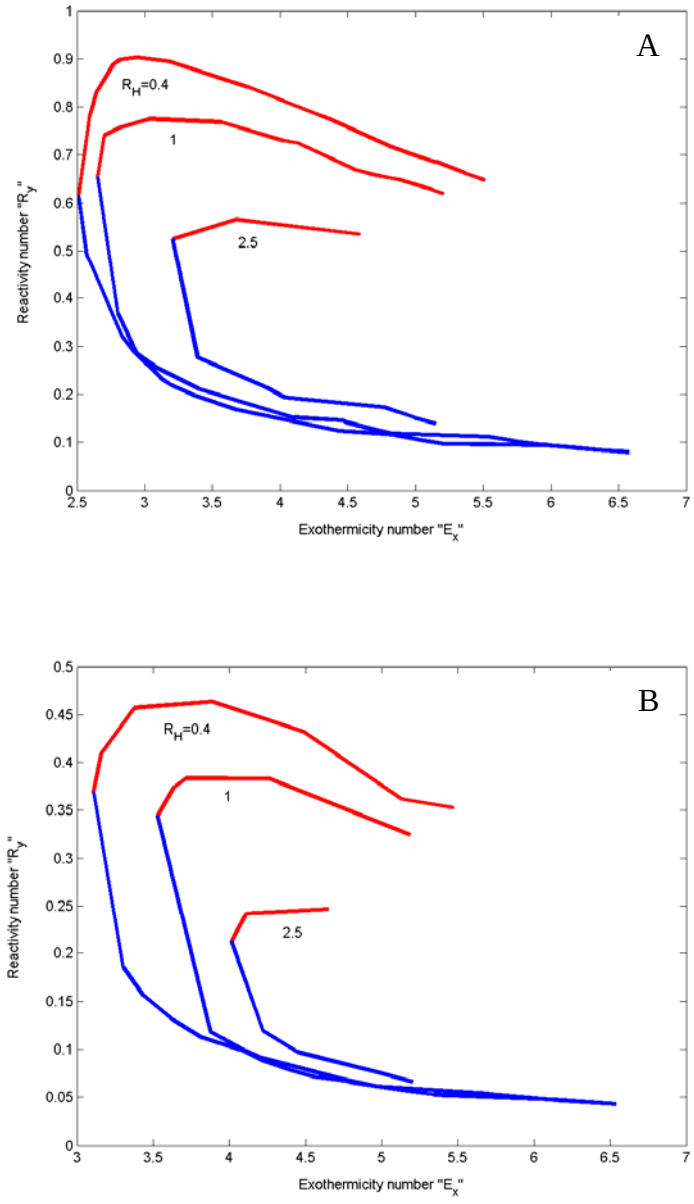

Figure 12 *Influence of the heat capacity ratio on the boundary diagrams shape and location.*

Fast reaction regime with n=2, m=1, Co=10.

Legend and other parameters as in Figure 11.

3. Temperature diagrams for preventing decomposition or side reactions in liquid-liquid semibatch reactors

Francesco Maestri, Renato Rota*

Politecnico di Milano

Dip. di Chimica, Materiali e Ingegneria Chimica "G. Natta"

via Mancinelli 7 - 20131 Milano – Italy

fax: +39 0223993180; e-mail: renato.rota@polimi.it

Abstract

The operation of an indirectly cooled semibatch reactor in which an exothermic reaction occurs is usually considered safe if the characteristic time of the coreactant dosing is much higher than the characteristic times of all the other phenomena involved (chemical reaction and mass transfer), so that the conversion rate is controlled by the coreactant supply itself. Such operating conditions imply a small accumulation of the coreactant in the system and are characterized by a temperature evolution which quickly approaches a target temperature and remains close to it throughout the dosing period, at the end of which the conversion is almost complete.

The so called boundary diagrams are useful means for identifying the previously described operating conditions without solving the mathematical model of the reactor. However, avoiding accumulation phenomena can be not sufficient for classifying a selected set of operating conditions as thermally safe when the maximum temperature reached by the system under normal operation exceeds a maximum allowable temperature (which can be related either to safety problems, when dangerous decomposition reactions can be triggered, or to productivity problems, when side reactions can significantly lower the product yield above a given threshold temperature).

In this work the boundary diagrams for the prevention of excessive accumulation conditions in liquid-liquid semibatch reactors are coupled with new diagrams, called temperature diagrams. These new diagrams, involving the same dimensionless parameters used for the

* to whom correspondence should be addressed

representation of the boundary diagrams, allow to determine -for a given set of operating conditions- the maximum temperature increase with respect to the initial reactor temperature which can be expected to occur during normal operation. This information can be compared with the maximum allowable temperature for the reacting mixture. Then the operating conditions can be verified through the boundary diagrams, in order to reject conditions of excessive coreactant accumulation. Several temperature diagrams are provided for various kinetically or diffusion controlled reactions of general kinetics, and their use together with a general procedure for calculating them is presented.

Keywords:
Semibatch reactors; Temperature diagrams; Boundary diagrams; Runaway; Safety; Scale-up.

3.1 Introduction

Runaway phenomena in chemical reactors have been thoroughly analyzed in the process safety literature of the last thirty years. It is well known that a runaway reaction is a consequence of the thermal loss of control of a reacting system in which an exothermic reaction occurs. This situation, also called thermal explosion, is primarily responsible for an increase of the rate of the desired reaction and can also lead to the triggering of consecutive decomposition reactions of one or more components of the reacting mixture: realistic data and complete information about the reacting system are required to estimate the probability and the consequences of such events. In order to evaluate the consequences of a runaway, the main data required are the rate of heat evolution due to the chemical reactions and the heat transfer efficiency of the reactor. In particular, it is necessary to know the reaction enthalpy and the heat capacity of the reacting mixture, the adiabatic temperature rise under the process conditions, the boiling point of the reacting mixture, the temperature range in which dangerous decomposition reactions can be triggered and their reaction enthalpy, the amount and rate of gas evolution, the effect of operational errors and impurities. Through a combination of this process information, Stoessel [1] divided the exothermic reaction processes into five classes as a function of the relative ranking of the process temperature, the maximum temperature that can be achieved by the synthesis reaction as a consequence of the cooling system failure (MTSR), the boiling point of the solvent and the maximum allowable temperature (MAT) in order to avoid the decomposition reactions to take place. Situations characterized by MTSR values higher than the MAT values must be regarded as critical from a safety point of view: for instance, a less exothermic reaction system with a low decomposition temperature can be much more dangerous than a more exothermic one with a very high decomposition temperature.

It is important to stress that similar conclusions arise also when a product decomposition or a side reaction which is not critical for safety (since it is neither very exothermic nor produces large amounts of gases) can take place above a threshold temperature: such situations are very frequent in the fine chemical and pharmaceutical industries, where several processes involve products which can chemically degrade above an experimentally determined temperature. In this case the MAT value must not be reached, since the plant productivity would be compromised. This means that regardless the typology of problem we are dealing with (safety or productivity), one of the constraints we have to fulfill in the production plant is often summarized through a threshold temperature value that cannot be exceeded neither during the normal reactor operation nor under upset operating conditions, such as those arising from a cooling failure.

As thoroughly discussed in the literature [2], if the coreactant accumulation in a semibatch reactor (SBR) increases above a critical value, a situation can arise in which, as the reaction ignites,

the heat removal rate cannot balance anymore the enthalpic contribution due to the chemical reaction: this results in a temperature jump which, depending on its entity, can exceed the MAT value. The most frequent causes of accumulation phenomena in SBRs are wrong assumptions on the reaction kinetics, which can be also related to the uninvestigated presence of impurities, too high rates of coreactant supply, too low initial reaction temperatures, insufficient mixing or cooling system efficiency.

Among all the causes, we will focus on the too low initial temperatures, which primarily lead to a high coreactant accumulation in the system and, in most cases, to the thermal loss of control of the system itself as the reaction ignites. The resulting temperature jump can then reach the thermal range for the triggering of the undesired decomposition event. For this reason a higher initial temperature is often safer than a lower one, in order to avoid accumulation phenomena and temperature jumps. However, this can be a *necessary* condition to prevent the exceeding of the MAT value (note that avoiding accumulation of the coreactant usually allow to avoid thermal runaways even when the cooling system fails, provided that the coreactant supply is suddenly stopped), but not a *sufficient* condition. If the initial temperature is too high, a situation can arise in which the coreactant accumulation is confined below critical values, but the initial temperature itself is too close to the MAT value for avoiding the overshooting of the aforementioned threshold temperature.

For the identification of low accumulation operating conditions in liquid-liquid SBRs in which exothermic reactions occur, Steensma and Westerterp [3-5] firstly developed the so called boundary diagrams method. Such diagrams, in a suitable dimensionless space defined through an "exothermicity number", E_x, and a "reactivity number", R_y, (see Figure 1B), provide a representation of the regions in which excessive accumulation and inherently safe operating conditions are expected.

Van Woezik and Westerterp [6,7] and Westerterp and Molga [8,9] extended this method to the case of multiple (consecutive) reactions, analyzing both theoretically and experimentally the nitric acid oxidation of 2-octanol to 2-octanone with further oxidation of the reaction products to unwanted carboxylic acids. However, their approach requires the knowledge of the kinetics of both the synthesis and the decomposition (or side) reaction: because of money and time constraints, this information is usually not available, at least for the unwanted reaction and is lumped through a MAT value.

Recently the original works of Steensma and Westereterp on slow liquid-liquid reaction systems were improved by Westerterp and Molga [8,9], who extended the boundary diagrams for slow (1,1) order reactions to the full range of cooling numbers of interest in the industrial practice, providing also some insights on how practically recover the information required by the boundary diagram method.

Moreover, Maestri and Rota [10,11] demonstrated the key role that the reaction kinetics can play in determining the shape and location of the boundary diagrams for both the slow and the fast reaction regime, providing also a general procedure for calculating such diagrams. In other words, for many practical systems the problem of avoiding excessive coreactant accumulation in a semibatch reactor can be easily faced.

However, as previously mentioned, when dealing with an exothermic semibatch reaction system in which an unwanted reaction can be triggered above a threshold temperature, the only use of the boundary diagrams does not in general allow to classify as acceptable a selected set of operating conditions. In fact, even if operating conditions belonging to the excessive accumulation region of the boundary diagram are normally characterized by a higher reaction temperature rise than QFS conditions [4], it must be stressed that for a higher initial temperature even a lower temperature rise can cause the maximum reaction temperature to exceed the MAT value. As a consequence, it would be useful to find a way to integrate the information that can be deduced from the boundary diagrams with another information, that is the maximum temperature value which can be expected under normal operating conditions. Finding such a way, that has to be as simple as the use of the boundary diagrams to be effective, is the main aim of the present work.

It has been found that the *boundary diagrams* for the identification of excessive accumulation and inherently safe operating conditions in liquid-liquid SBRs can be coupled with a new kind of diagrams, which have been called *temperature diagrams*. Such diagrams, involving the same set of dimensionless parameters employed for the representation of the boundary diagrams, provide -for a given set of operating conditions- the highest ratio of the maximum to the initial reactor temperature which can be expected to occur, which was the missed information to be compared with the MAT value.

In the following, the procedure for building the temperature diagrams is discussed and a number of such diagrams for various operating conditions is provided, to allow end users to easily identify operating conditions characterized by both a sufficiently low coreactant accumulation and maximum temperature values under normal operation lower than the MAT.

3.2 Mathematical model

Developing diagrams for the simple and reliable prediction of the maximum temperature attained in a SBR in which an exothermic liquid-liquid reaction of the form:

$$\nu_A A + \nu_B B \rightarrow C + \nu_D D \tag{1}$$

occurs, requires a preliminary discussion on how the process can be modelled, through the statement of a few reasonable assumptions. In the following, we assume that the microkinetic rate of the reaction (1) can be expressed through a power law type functional dependence:

$$r = k_{n,m} C_A^n C_B^m \tag{2}$$

derived form a data fitting of RC1 experiments performed in the kinetically controlled regime.

The following model assumptions can be reasonably stated:

1) the reaction mass is perfectly macromixed;
2) the influence of the chemical reaction on the volume of the single phase is negligible;
3) no phase inversions occur;
4) the solubility of the species A (the dosed coreactant) and C in the continuous phase, c, and of components B (the component initially charged in the reactor) and D in the dispersed phase, d, is small (in other words, species A and C are almost all in phase d, whereas species B and D are present almost only in phase c);
5) the chemical reaction takes place only in one of the two liquid phases: this situation is very common in many industrial processes (such as nitrations and oxidations), in which the catalyst (typically a strong acid) is present only in one phase;
6) the heat effects are associated to the chemical reaction only;
7) at the beginning, the reaction mass is at the mean coolant temperature, T_{cool}, which is assumed to remain constant for the whole duration of the process (that is, the reactor operates under isoperibolic conditions).

The mass balance equation for the component B can be written in dimensionless form as [3]:

$$\frac{d\zeta_B}{d\vartheta} = \frac{\nu_B t_D}{n_{B,0}} r^{eff} V_r \tag{3}$$

where the effective conversion rate, r^{eff} -that depends on the microkinetic rate expression (2) and on the phase in which the reaction occurs- can be in general determined either by the chemical reaction or by the mass transfer phenomena or by the coreactant supply. Depending on the kinetic

regime, eq. (3) can be rearranged in the form:

$$\frac{d\zeta_B}{d\vartheta} = \nu_A \, Da \, RE_{slow,c/d} \; f_{slow,c/d} \; \kappa_{n,m} \tag{4}$$

for the kinetically controlled regime [10] and in the form:

$$\frac{d\zeta_B}{d\vartheta} = \nu_A \, Da \, RE_{fast,c/d} \; f_{fast,c/d} \; \kappa_{n,m}^{\;1/2} \tag{5}$$

for the diffusion controlled regime [11], where $Da=k_{n,m,R}t_D C_{B,0}^{\;n+m-1}$ is the Damköhler number for (n,m) order kinetics, which contains the information about the dosing time, and $\kappa_{n,m}=\exp[\gamma(1-1/\tau)]$ is the dimensionless reaction rate constant, that is the ratio of the reaction rate constant to the same quantity evaluated at a reference temperature, T_R. $\gamma=E/(RT_R)$ is the dimensionless activation energy and $\tau=T/T_R$ is the dimensionless temperature. The expressions for the calculation of the reactivity enhancement factor, RE, and for the function, f, have been derived elsewhere [10,11] and are summarized in Table 1.

The energy balance equation for the reactor yields [3]:

$$\left(1+R_H\varepsilon\vartheta\right)\frac{d\tau}{d\vartheta} = \Delta\tau_{ad,0}\frac{d\zeta_B}{d\vartheta} - \left[U^* Da\left(1+\varepsilon\vartheta\right)+\varepsilon R_H\right]\left(\tau-\tau_{cool}^{eff}\right) \tag{6}$$

where $d\zeta_B/d\vartheta$ is the only factor dependent on the kinetic regime (slow or fast reactions) and $T_{cool}^{eff} = \dfrac{U^* Da\left(1+\varepsilon\vartheta\right)T_{cool}+\varepsilon R_H T_D}{U^* Da\left(1+\varepsilon\vartheta\right)+\varepsilon R_H}$ is an effective cooling temperature which takes into account the effects of both the heat removal by the coolant and the sensible heat of the dosing stream. These equations are valid for $0<\vartheta\leq 1$, that is up to the end of the dosing period. It can be easily demonstrated that the same equations can be extended to $\vartheta>1$ by substituting everywhere the $(\vartheta-\zeta_B)/\vartheta$ or $(\vartheta-\zeta_B)$ terms with $(1-\zeta_B)$, the $\varepsilon\vartheta$ terms with ε and by setting $T_D\equiv T$ in the definition of the effective cooling temperature.

In order to identify an excessive accumulation region, the predictions of this model can be lumped using two dimensionless parameters, called exothermicity, E_x, and reactivity, R_y, number. They are defined as the ratios of the exothermicity and reactivity factor respectively, to a cooling factor, all evaluated at the coolant temperature (the aforementioned factors can be derived from the mass and energy balance equations previously reported) and can be calculated through the following equations [10,11]:

$$E_x = \frac{\gamma}{\tau_{cool}^2}\frac{\Delta\tau_{ad,0}}{U^* Da+\varepsilon R_H} = \frac{\gamma}{\tau_{cool}^2}\frac{\Delta\tau_{ad,0}}{\varepsilon\left(Co+R_H\right)} \tag{7}$$

$$R_y = \frac{\nu_A\, Da\, RE\, \kappa(\tau_{cool})}{U^* Da + \varepsilon R_H} = \frac{\nu_A\, Da\, RE\, \kappa(\tau_{cool})}{\varepsilon(Co + R_H)} \tag{8}$$

for the kinetically controlled (or slow reaction) regime and:

$$E_x = \frac{\gamma}{2\tau_{cool}^2} \frac{\Delta\tau_{ad,0}}{U^* Da + \varepsilon R_H} = \frac{\gamma}{2\tau_{cool}^2} \frac{\Delta\tau_{ad,0}}{\varepsilon(Co + R_H)} \tag{9}$$

$$R_y = \frac{\nu_A\, Da\, RE\, \kappa^{1/2}(\tau_{cool})}{U^* Da + \varepsilon R_H} = \frac{\nu_A\, Da\, RE\, \kappa^{1/2}(\tau_{cool})}{\varepsilon(Co + R_H)} \tag{10}$$

for the diffusion controlled (or fast reaction) regime.

A boundary diagram is shown, for the sake of example, in Figure 1B. The excessive accumulation region (EAR) is bounded by the continuous line and is surrounded by the no ignition region (for low R_y values), the Quick onset-Fair conversion-Smooth temperature profile (QFS) region (for high R_y values) and by an inherently safe region. The latter is characterized either by E_x values lower than the minimum E_x value of the EAR boundary, $E_{x,MIN}$, or by R_y values larger than the maximum R_y value of the EAR boundary, $R_{y,QFS}$. More details on the development and use of the boundary diagrams can be found elsewhere in the literature [9,10].

3.3 Thermally safe operating conditions

Following a procedure similar to that employed for the calculation of the boundary diagrams and using the same dimensionless parameters introduced for their representation (that is, the exothermicity number, E_x, and the reactivity number, R_y), it is possible to build new diagrams that, for every (E_x,R_y) couple, provide the maximum value of the T_{max}/T_0 ratio which can be expected for the chosen set of operating conditions. Such diagrams, an example of which is represented in Figure 1A together with the related boundary diagram, will be referred to in the following as *temperature diagrams*.

Before discussing the development of such diagrams, it is worthwhile illustrating their use. Given a set of operating conditions represented by the point A on the boundary diagram of Figure 1B, we know from such a diagram that no dangerous coreactant accumulation is expected. Moving to the temperature diagram of Figure 1A, the same point can be easily identified through the values of E_x (in this case equal to 4) and R_y (in this case equal to $R_{y,QFS} \cong 0.78$). From the temperature diagram it is easy to read the value of the parameter $\psi = (T_{max}/T_0)_{max} \cong 1.13$. Knowing now the initial reaction temperature T_0, it can be concluded that the maximum temperature under normal operation will not exceed $1.13T_0$: this is the value to be compared with the MAT.

In the following a general procedure for building the temperature diagrams is discussed

and a number of such diagrams is provided for different combinations of the reaction phase, the kinetic regime and the Co, R_H, n and m values.

In the mass and energy balance eqs. (4), (5) and (6) or -analogously- in the expressions (7) to (10) of the exothermicity and reactivity numbers, eight dimensionless parameters appear, that is: ν_A Da RE, ε, γ, R_H, $\Delta\tau_{ad,0}$, Co, n, and m. Assigning a value to each of these parameters in compliance with its accepted range and letting the coolant temperature as a variable parameter, the functional dependence between the exothermicity and reactivity numbers, $R_y=\Phi(E_x)$, is univocally identified. Eqs. (7) and (8) or (9) and (10) are the parametric form of this functional dependence (for the slow and the fast reaction regime, respectively), since they provide, for each value of the coolant temperature, a couple of related values of R_y and E_x, as shown, for the sake of example, in Figure 1B. As discussed elsewhere [10], looking at the eqs. (7) and (8) or (9) and (10) it is evident that the *single* $R_y=\Phi(E_x)$ line (that is, a line representing the functional dependence between R_y and E_x) on the *single* boundary diagram (that is, for Co, R_H, n, m values assigned and constant) is identified through the values of the following three dimensionless groups:

$$\begin{cases} \dfrac{\gamma\Delta\tau_{ad,0}}{\varepsilon\left(Co+R_H\right)} = const \\ \dfrac{\nu_A\, Da\, RE}{\varepsilon\left(Co+R_H\right)} = const \\ \gamma = const \end{cases} \qquad (11)$$

that must be also constant along the single $R_y=\Phi(E_x)$ line. As previously mentioned, the number of parameters that must be assigned to solve the mathematical model of the reactor at the current coolant temperature is equal to eight. Since four of them must be constant when a single boundary diagram is considered, the number of independent parameters is equal to four. These must also fulfill the three constraints (11). It follows that the number of sets of parameters which generate the same $R_y=\Phi(E_x)$ line on a given boundary diagram is equal to ∞^1. These sets of parameters can be generated from each member of the single family if one multiplies by the same factor K the parameters ν_A Da RE, ε, $\Delta\tau_{ad,0}$ and U^*Da, while keeping the remaining four (R_H, γ, n, m) constant. It should be noticed that this allows to keep Co=U^*Da/ε constant as well as to fulfill the constraints (11). Selecting now a value of the coolant temperature, a point on the boundary diagram (that is, a couple of E_x and R_y values) is selected, where it is possible to solve ∞^1 systems of the mass and energy balance eqs. (4) or (5) and (6) with the proper initial conditions, being the factor K the parameter through which the ∞^1 model equations are generated. For each K value (varying accordingly to the fixed ranges of the parameters ν_A Da RE, γ, ε and $\Delta\tau_{ad,0}$), the dimensionless temperature T/T_0 as a function of the dimensionless time ϑ is computed and its maximum value

T_{max}/T_0 can be identified. Scanning locally (that is, at the current values of E_x and R_y) the range of variation of the K parameter, it is possible to compute a set of T_{max}/T_0 values, which maximum value, $\psi=(T_{max}/T_0)_{max,}$ is the maximum expected ratio of the reaction temperature to T_0 at the current E_x and R_y values and on the considered boundary diagram. In other words, the K value is locally selected, that maximizes the ratio of the maximum to the initial reactor temperature. By repeating the same procedure on several $R_y=\Phi(E_x)$ lines at a constant value for R_y, a functional dependence $\psi=\Psi(E_x)$ at the current R_y value can be generated. In Figure 1A such functional dependences for different R_y values are represented, with R_y varying in a range selected on the basis of the extension and location of the related boundary diagram (that is, the boundary diagram calculated for the same reaction phase, kinetic regime and for the same Co, R_H, n, m values).

When a set of operating conditions for a liquid-liquid SBR is selected (from which a value of the E_x and R_y parameters can be computed, according to the relations (7) and (8) or (9) and (10)), the temperature diagrams can be used to check whether:

$$\psi \cdot T_0 < MAT \tag{12}$$

If the check (12) is satisfied, two situations may be possible:

a) the calculated (E_x,R_y) point belongs to the $E_x<E_{x,MIN}$ zone of the temperature diagram (see Figure 1A) or to the $E_x>E_{x,MIN}$ zone with $R_y\geq R_{y,QFS}$. In this case the selected operating conditions can be accepted, since they cannot lead to the triggering of unwanted reactions and they belong to the inherently safe region of the boundary diagram, where no excessive coreactant accumulation can occur;
b) the calculated (E_x,R_y) point belongs to the $E_x>E_{x,MIN}$ zone of the temperature diagram (see Figure 1A) with $R_y<R_{y,QFS}$. In this case, it is necessary to refer to the related boundary diagram, to check whether the aforementioned point belongs to the safe region, to the excessive accumulation region or to the no ignition region. It must in fact be emphasized that even operating conditions which satisfy the check (12) cannot be considered thermally safe if they imply an excessive coreactant accumulation, because such operating conditions are typically characterized by sudden temperature and conversion jumps, that are responsible for a bad control of the reacting system and can become very dangerous in case of cooling system failures. Analogously, no ignition operating conditions must be avoided, since they imply a low reactor productivity.

In Figures 2 to 12 several couples of temperature and boundary diagrams are reported, for different combinations of the reaction phase, the kinetic regime and of the Co, R_H, n and m values. In particular, the case of kinetically controlled reactions taking place in the dispersed phase has

been analyzed, since it corresponds to the most critical typology of liquid-liquid SBR from the safety point of view [9]. These diagrams are useful means in order to perform a simple and fast analysis of the operating conditions of a SBR, from the thermal safety point of view. However, it is worthwhile mentioning that the procedures presented in this work for the temperature diagrams and in Maestri and Rota [10] for the boundary diagrams allow to build the temperature and boundary diagrams for any combination of reaction phase, kinetic regime and Co, R_H, n and m values. The ranges of E_x and R_y numbers to which the single temperature diagram is extended are strictly related to the location and extension of the coupled boundary diagram, so that, for a given reaction phase and kinetic regime, the same sensitivity of the aforementioned ranges with respect to the Co, R_H, n and m parameters can be expected for both boundary and temperature diagrams [10,11].

It is interesting to note that on the single temperature diagram, at R_y values lower than $R_{y,QFS}$, the ψ vs. E_x curves typically exhibit a maximum. Such a behavior is logical since if the ψ vs. E_x curve at $R_y=R_{y,QFS}$ is representative of situations in which the maximum reactor temperature is lower or equal to the local target temperature [3], the same curves at $R_y<R_{y,QFS}$ and in the E_x range corresponding to the excessive accumulation region on the related boundary diagram are representative of situations in which the maximum reactor temperature can be higher than the local target value, the entity of such a temperature exceeding being normally much higher than the variations of the target temperature itself with R_y (and hence with the related initial temperature values).

As it can be observed from the temperature diagrams represented in Figures 2 to 12, at R_y values much lower than $R_{y,QFS}$ such maximum ψ values may be of the order of 1.5; this means that if the initial reaction temperature is 300K, the maximum temperature attained by the reacting mixture can reach 450K, temperature which is well above the normal boiling point of almost all the solvents normally employed in the industrial practice. On the other hand, at R_y values equal or higher than $R_{y,QFS}$, the maximum ψ values corresponding to the explored ranges of the different model parameters involved are of the order of 1.2: this analogously means that, under inherently safe conditions, if the initial reactor temperatures is equal to 300K, the maximum temperature will not be higher than 360K, regardless the value of the E_x parameter. However, much lower values of the temperature increase are expected for lower values of E_x. In particular, for $E_x<E_{x,MIN}$ and always referring to the investigated range of parameters, a maximum value of $\psi\cong1.1$ is expected.

3.4 Conclusions

Semibatch reactors in which exothermic reactions take place should never be operated under conditions of excessive coreactant accumulation because, as the desired reaction ignites, a thermal loss of control of the system may occur, which can cause the temperature to raise so much that decomposition reactions of one or more components of the reacting mixture can be triggered. Such events, that can be detected through calorimetric experiments, are normally accompanied by a much higher exothermicity and by the evolution of gases, which are responsible for an increase of the system pressure at rates that can be dangerous.

However, even when dangerous accumulation is avoided, the maximum temperature reached by the system during normal operation can overcome the Maximum Allowable Temperature (MAT), which can be related either to safety problems (exothermic or gas producing decomposition reactions) or to productivity problems (unwanted side or consecutive reactions). Whilst the boundary diagrams are a powerful tool for identifying excessive accumulation operating conditions in SBRs, they do not provide direct information about the temperature increase that can be expected to occur in the reacting system.

In this work the temperature diagrams have been introduced. Such diagrams, using the same dimensionless parameters involved in the representation of the boundary diagrams, allow to determine the aforementioned maximum temperature increase, without solving the mathematical model of the reactor and providing the possibility to extend the information to scaled-up systems.

The two typologies of diagrams (that is the temperature and boundary diagrams) are strictly related from the point of view of their use: once a set of operating conditions for a liquid-liquid SBR has been selected, the temperature diagrams must be firstly used, in order to check whether the temperature increase can reach the MAT value. Then, for conditions involving $E_x > E_{x,MIN}$ and $R_y < R_{y,QFS}$, the boundary diagrams must be used, in order to reject in any case excessive accumulation or no ignition operating conditions.

Nomenclature

Symbols	
A	heat transfer area of the reactor (associated to the jacket and/or the coil), m^2
C	molar concentration, $kmol/m^3$
Co	$=U^*Da/\varepsilon$, cooling number, -
$\tilde{C}_P$	molar heat capacity, kJ/(kmol·K)
$d_{b,0}$	d_b at hold up of the dispersed phase approaching zero, m
D	diffusivity, m^2/s
Da	$=k_{n,m,R}t_D C_{B,0}^{n+m-1}$, Damköhler number for (n,m) order reactions, -
E	activation energy, kJ/kmol
E_x	exothermicity number, eqs. (7) and (9), -
f	function of the dimensionless time and conversion of B in eqs. (4) and (5), -
$\Delta\tilde{H}$	reaction enthalpy, kJ/kmol
K	multiplying factor of the ν_A Da RE, ε, $\Delta\tau_{ad,0}$ and U^*Da parameters, -
$k_{n,m}$	reaction rate constant, $m^{3(n+m-1)}/(kmol^{n+m-1}\cdot s)$
m	equilibrium distribution coefficient ($m_A=C_{A,c}/C_{A,d}$; $m_B=C_{B,d}/C_{B,c}$), -
MAT	maximum allowable temperature, K
MTSR	maximum temperature reached due to the synthesis reaction, K
n	number of moles, kmol
r	reaction rate referred to the total liquid volume, $kmol/(m^3\cdot s)$
R	gas constant = 8.314, kJ/(kmol·K)
RE	reactivity enhancement factor in eqs. (4) and (5), -
R_H	heat capacity ratio, -
R_y	reactivity number, eqs. (8) and (10), -
t	time, s
T	temperature, K
$\Delta T_{ad,0}$	adiabatic temperature rise, K
U	overall heat transfer coefficient, $kW/(m^2\cdot K)$
U^*Da	$=(UA)_0 t_D/(\tilde{\rho}_c \tilde{C}_{P,c} V_c)$ modified Stanton number, -
V	liquid volume, m^3
Greek symbols	
γ	$=E/(RT_R)$, dimensionless activation energy, -
ε	relative volume increase at the end of the semibatch period, -
ζ	molar conversion, -

ϑ	$=t/t_D$, dimensionless time, -
κ	$=k/k_R$, dimensionless reaction rate constant, -
ν	stoichiometric coefficient, -
$\tilde{\rho}$	molar density, kmol/m^3
τ	$=T/T_R$, dimensionless temperature, -
Φ	functional dependence between R_y and E_x
ψ	$=(T_{max}/T_0)_{max}$, maximum dimensionless temperature rise, -
Ψ	functional dependence between ψ and E_x at assigned R_y

Subscripts and superscripts

A,B,C,D	components A, B, C and D
ad	adiabatic
b	in the dispersed phase drop diameter d_b
c	continuous phase
cool	coolant
d	dispersed phase
D	dosing stream or dosing time
eff	effective
fast	fast reaction regime
H	in the heat capacity ratio R_H
L	in the liquid phase
m	order of reaction respect to component B
max	maximum value of a quantity or at the maximum value of a quantity
n	order of reaction respect to component A
MIN	in $E_{x,MIN}$
QFS	in $R_{y,QFS}$
r	reaction
R	reference
slow	slow reaction regime
x	in the exothermicity number E_x
y	in the reactivity number R_y
0	start of the semibatch period

Literature cited

1. Stoessel, F. *Chem. Eng. Prog.* 1993, 68.

2. Steinbach, J. Safety assessment for chemical processes. 1999, *Wiley-vch, Weinheim*.

3. Steensma, M., Westerterp, K.R. Thermally safe operation of a cooled semi-batch reactor. Slow liquid-liquid reactions. *Chem. Eng. Sci.* 1988, *43, Nr.8,* 2125-2132.

4. Steensma, M., Westerterp, K.R. Thermally safe operation of a semibatch reactor for liquid-liquid reactions. Slow reactions. *Ind. Eng. Chem. Res.* 1990, *29,* 1259-1270.

5. Steensma, M., Westerterp, K.R. Thermally safe operation of a semibatch reactor for liquid-liquid reactions. Fast reactions. *Chem. Eng. Technol.* 1991, *14,* 367-375.

6. van Woezik, B.A.A., Westerterp K.R. The nitric acid oxidation of 2-octanol. A model reaction for multiple heterogeneous liquid-liquid reactions. *Chem. Eng. Process.* 2000, *39,* 521-537.

7. van Woezik, B.A.A., Westerterp K.R. Runaway behaviour and thermally safe operation of multiple liquid-liquid reactions in the semibatch reactor. The nitric acid oxidation of 2-octanol. *Chem. Eng. Process.* 2001, *41,* 59-77.

8. Westerterp, K.R., Molga, E.J. Runaway prevention in liquid-liquid semibatch reactors. *Inzynieria Chemiczna i Procesowa* 2004, *25(3/4),* 2041-2050.

9. Westerterp, K.R., Molga, E.J. No more runaways in fine chemical reactors. *Ind. Eng. Chem. Res.* 2004, *43 (16),* 4585-4594.

10. Maestri, F., Rota, R. Thermally safe operation of liquid-liquid semibatch reactors. Part I: single kinetically controlled reactions with arbitrary reaction order. *Chem. Eng. Sci.* 2005, *60,* 3309-3322.

11. Maestri, F., Rota, R. Thermally safe operation of liquid-liquid semibatch reactors. Part II: single diffusion controlled reactions with arbitrary reaction order. *Chem. Eng. Sci.* 2005, *60,* 5590-5602.

Table 1 *Expressions of the reactivity enhancement factor, RE, and of the function, f, for slow and fast reactions taking place in the dispersed or continuous phase. [10,11].*

	Reaction in the *dispersed* phase, d	**Reaction in the *continuous* phase, c**
$\mathbf{RE_{slow,c/d}}$	$\left(\frac{\nu_B}{\nu_A}\right)^{1-n} m_B^m$	$\left(\frac{\nu_B}{\nu_A}\right)^{1-n} m_A^n$
$\mathbf{RE_{fast,c/d}}$	$\frac{6}{d_{b,0}} m_B^{\frac{m+1}{2}} C_{B,0}^{\frac{1-n-m}{2}} \left(\frac{\nu_B}{\nu_A}\right)^{1-\frac{n}{2}} \left[\frac{2D_{L_d,B}}{(m+1)k_{n,m,R_d}}\right]^{\frac{1}{2}}$	$\frac{6}{d_{b,0}} m_A^{\frac{n+1}{2}} C_{B,0}^{\frac{1-n-m}{2}} \left(\frac{\nu_B}{\nu_A}\right)^{\frac{1-n}{2}} \left[\frac{2D_{L_c,A}}{(n+1)k_{n,m,R_c}}\right]^{\frac{1}{2}}$
$\mathbf{f_{slow,c/d}}$	$\frac{(\vartheta-\zeta_B)^n (1-\zeta_B)^m}{(\varepsilon\vartheta)^{n-1}}$	$\frac{(\vartheta-\zeta_B)^n (1-\zeta_B)^m}{(\varepsilon\vartheta)^n}$
$\mathbf{f_{fast,c/d}}$	$\frac{(\vartheta-\zeta_B)^{\frac{n}{2}} (1-\zeta_B)^{\frac{m+1}{2}} (\varepsilon\vartheta)^{1-\frac{n}{2}}}{1+2.5\varepsilon\vartheta/(1+\varepsilon\vartheta)}$	$\frac{(\vartheta-\zeta_B)^{\frac{n+1}{2}} (1-\zeta_B)^{\frac{m}{2}} (\varepsilon\vartheta)^{\frac{1-n}{2}}}{1+2.5\varepsilon\vartheta/(1+\varepsilon\vartheta)}$

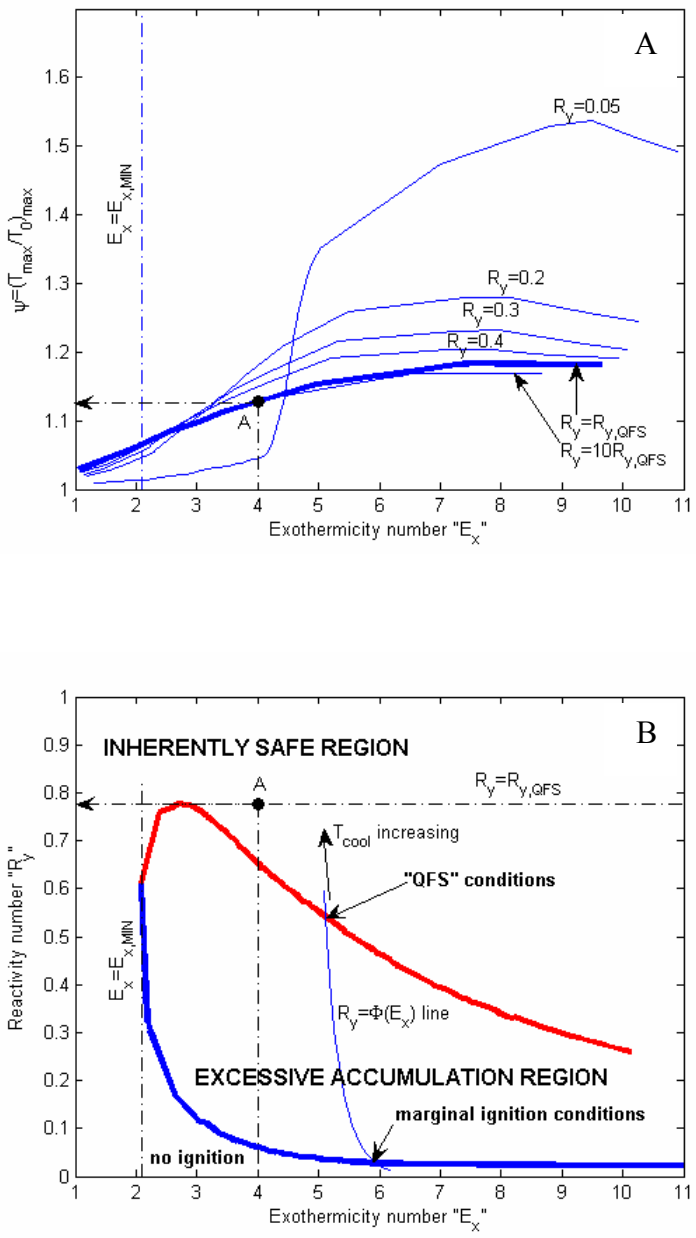

Figure 1 *A) temperature and B) boundary diagram.*

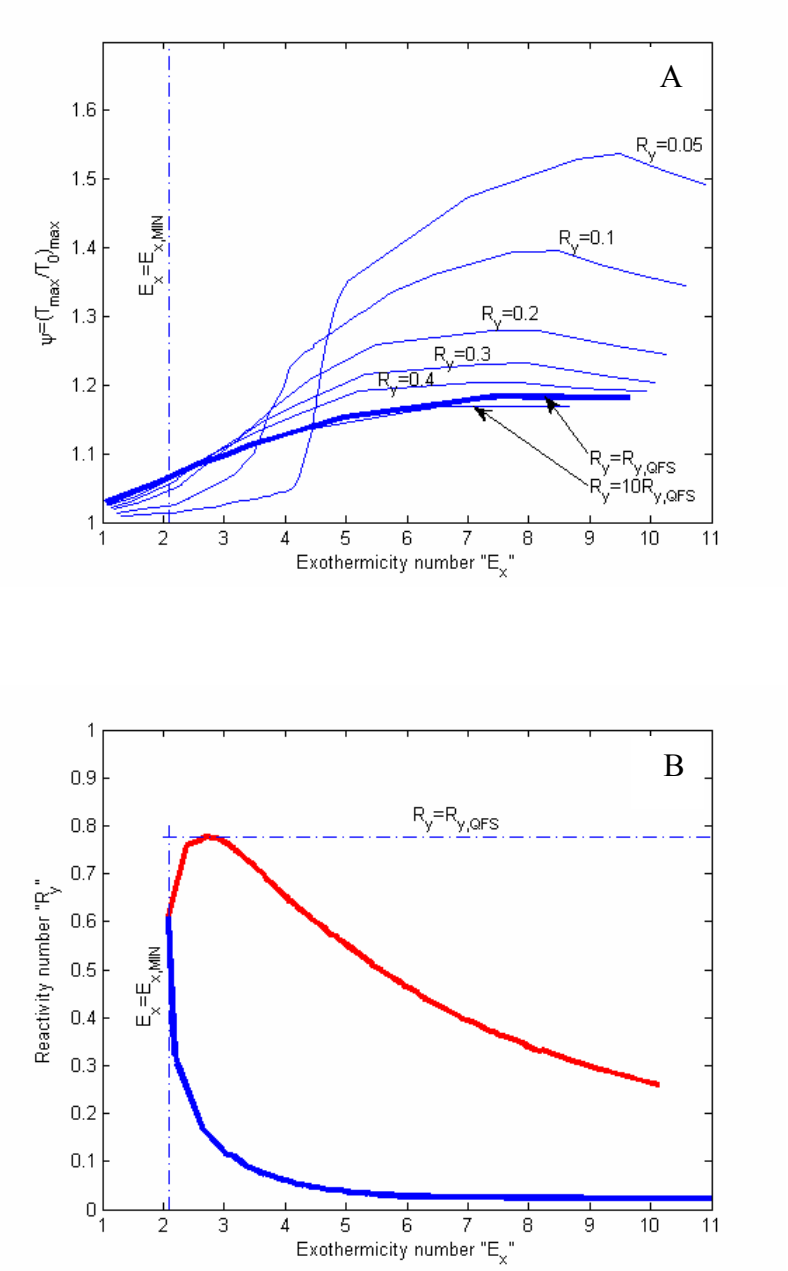

Figure 2 *Slow reaction regime. Reaction in the dispersed phase. Co=10, R_H=1, n=1, m=1. 0.025< ν_A Da RE<14, 0.3<ε<0.55, 32<γ<42, 0.29<$\Delta\tau_{ad,0}$<0.7. A) temperature diagram; B) boundary diagram.*

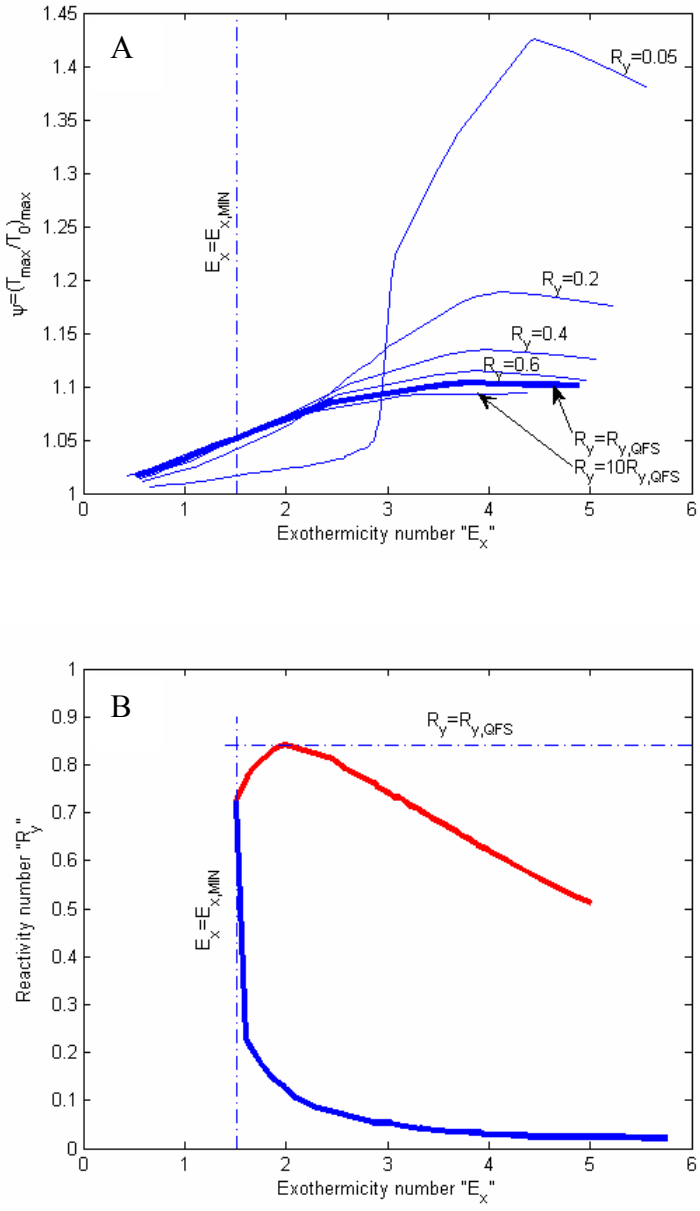

Figure 3 *Slow reaction regime. Reaction in the dispersed phase. Co=20, R_H=1, n=1, m=1. 0.025< ν_A Da RE<14, 0.3<ε<0.55, 32<γ<42, 0.29<$\Delta\tau_{ad,0}$<0.7. A) temperature diagram; B) boundary diagram.*

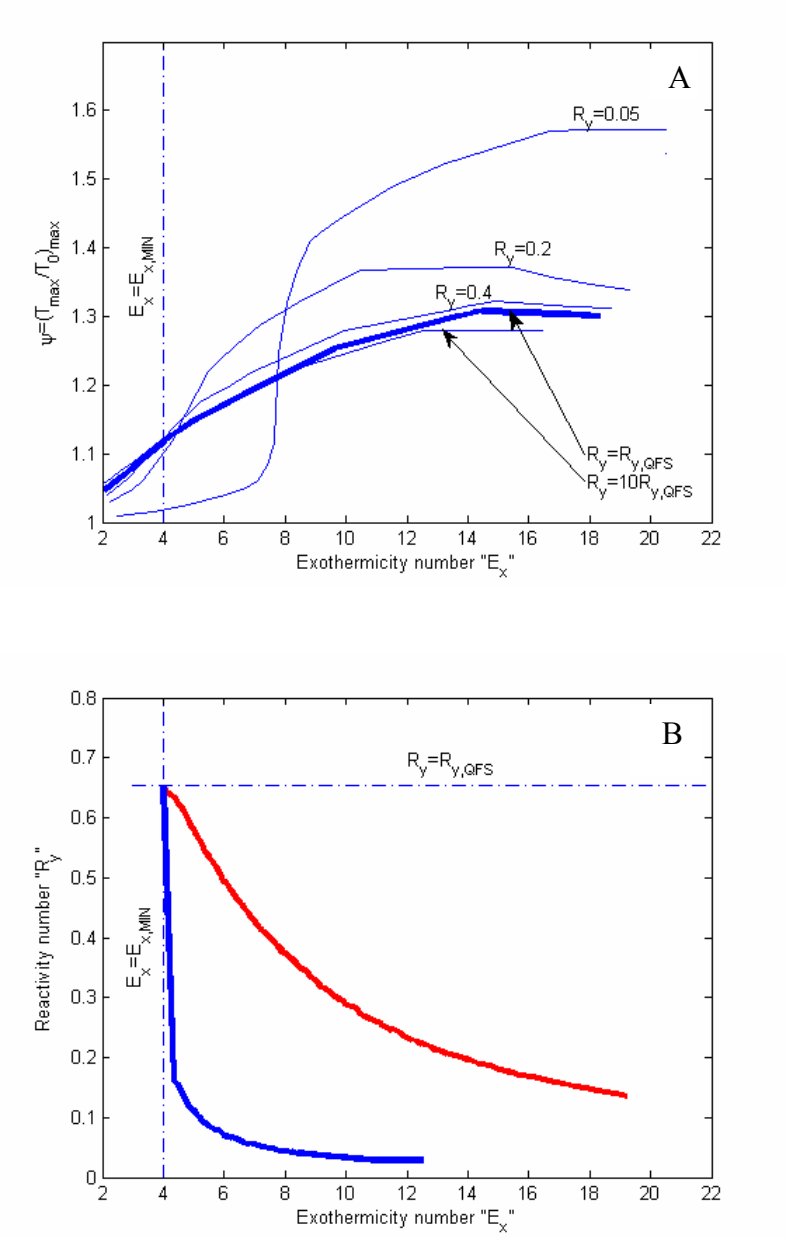

Figure 4 *Slow reaction regime. Reaction in the dispersed phase. Co=5, R_H=1, n=1, m=1. 0.025< ν_A Da RE<14, 0.3<ε<0.55, 32<γ<42, 0.29<$\Delta\tau_{ad,0}$<0.7. A) temperature diagram; B) boundary diagram.*

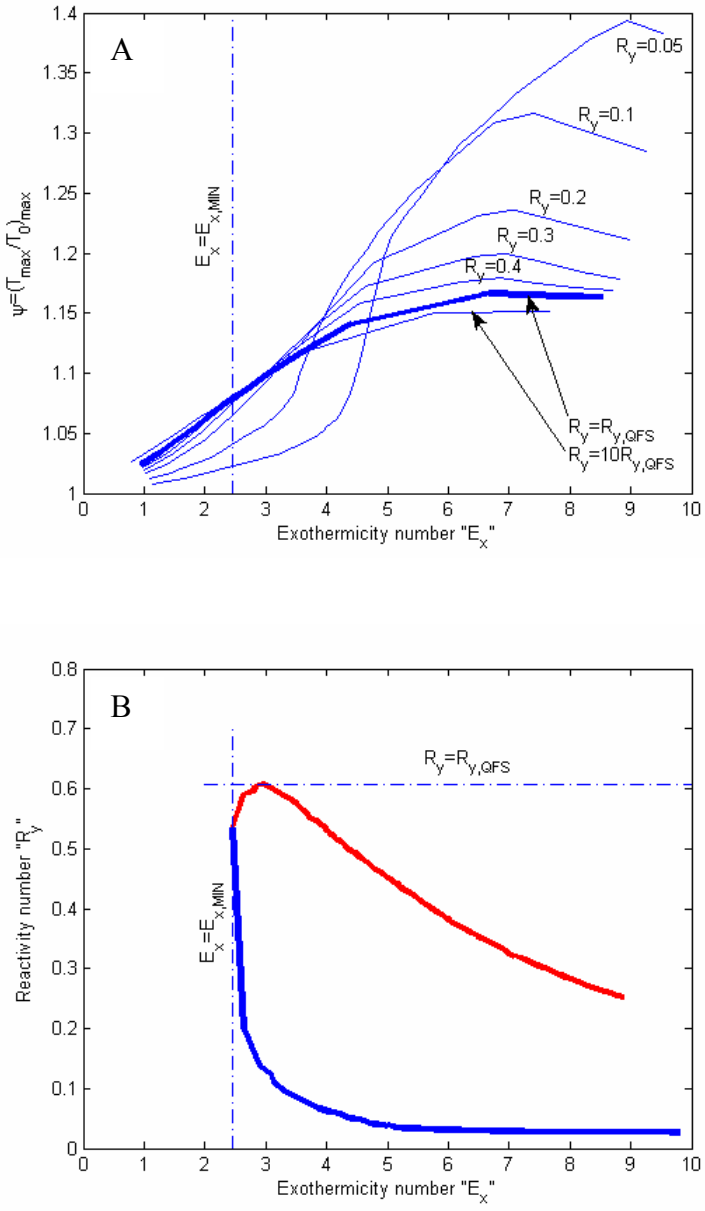

Figure 5 *Slow reaction regime. Reaction in the dispersed phase. Co=10, R_H=2.5, n=1, m=1. 0.025< ν_A Da RE<14, 0.3<ε<0.55, 32<γ<42, 0.29<$\Delta\tau_{ad,0}$<0.7. A) temperature diagram; B) boundary diagram.*

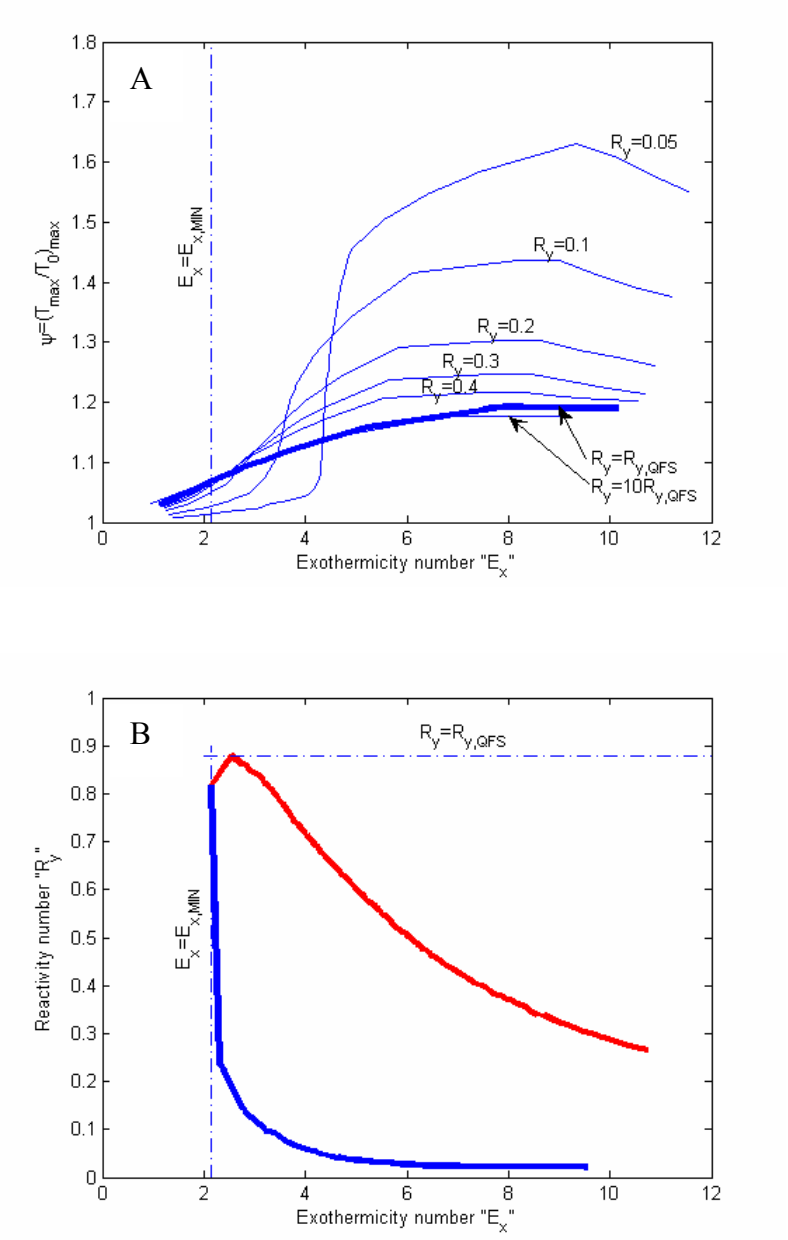

Figure 6 *Slow reaction regime. Reaction in the dispersed phase. Co=10, R_H=0.4, n=1, m=1. 0.025< ν_A Da RE<14, 0.3<ε<0.55, 32<γ<42, 0.29<$\Delta\tau_{ad,0}$<0.7. A) temperature diagram; B) boundary diagram.*

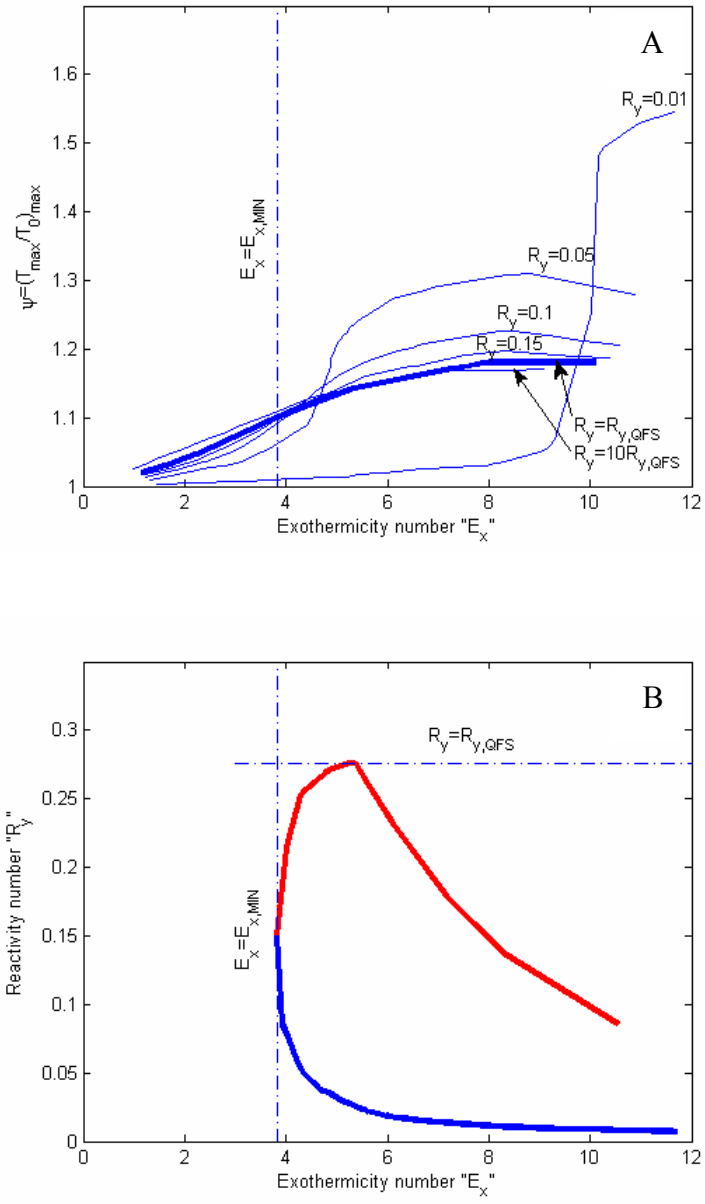

Figure 7 *Slow reaction regime. Reaction in the dispersed phase. Co=10, R_H=1, n=2, m=1. 0.025< ν_A Da RE<14, 0.3<ε<0.55, 32<γ<42, 0.29<$\Delta\tau_{ad,0}$<0.7. A) temperature diagram; B) boundary diagram.*

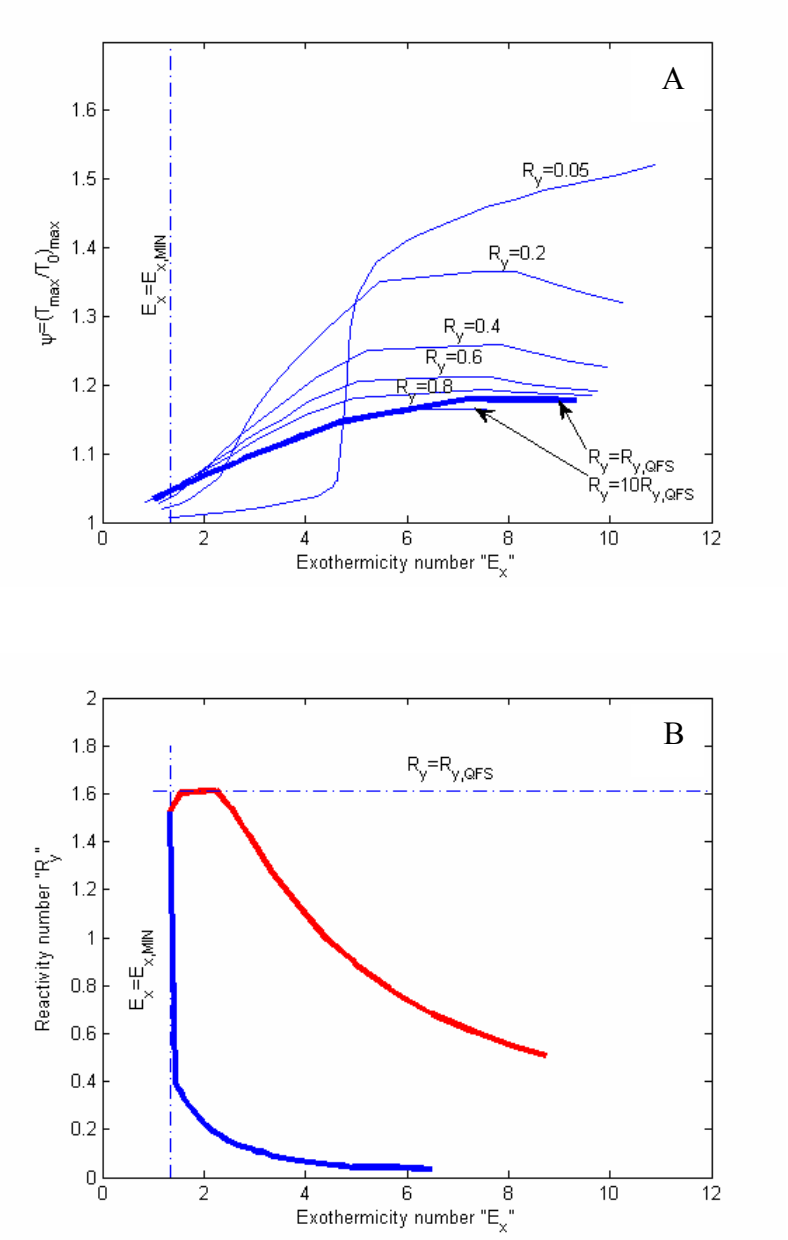

Figure 8 *Slow reaction regime. Reaction in the dispersed phase. Co=10, R_H=1, n=0.5, m=1. 0.025< ν_A Da RE<14, 0.3<ε<0.55, 32<γ<42, 0.29<$\Delta\tau_{ad,0}$<0.7. A) temperature diagram; B) boundary diagram.*

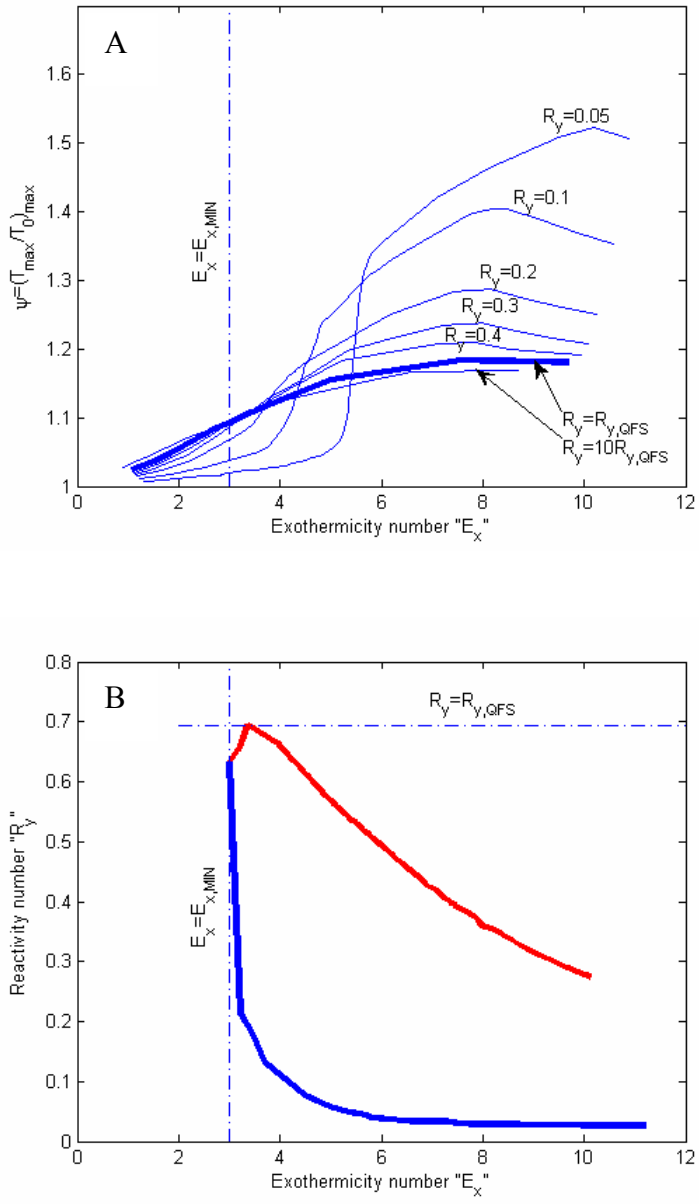

Figure 9 *Slow reaction regime. Reaction in the dispersed phase. Co=10, R_H=1, n=1, m=2. 0.025< ν_A Da RE<14, 0.3<ε<0.55, 32<γ<42, 0.29<$\Delta\tau_{ad,0}$<0.7. A) temperature diagram; B) boundary diagram.*

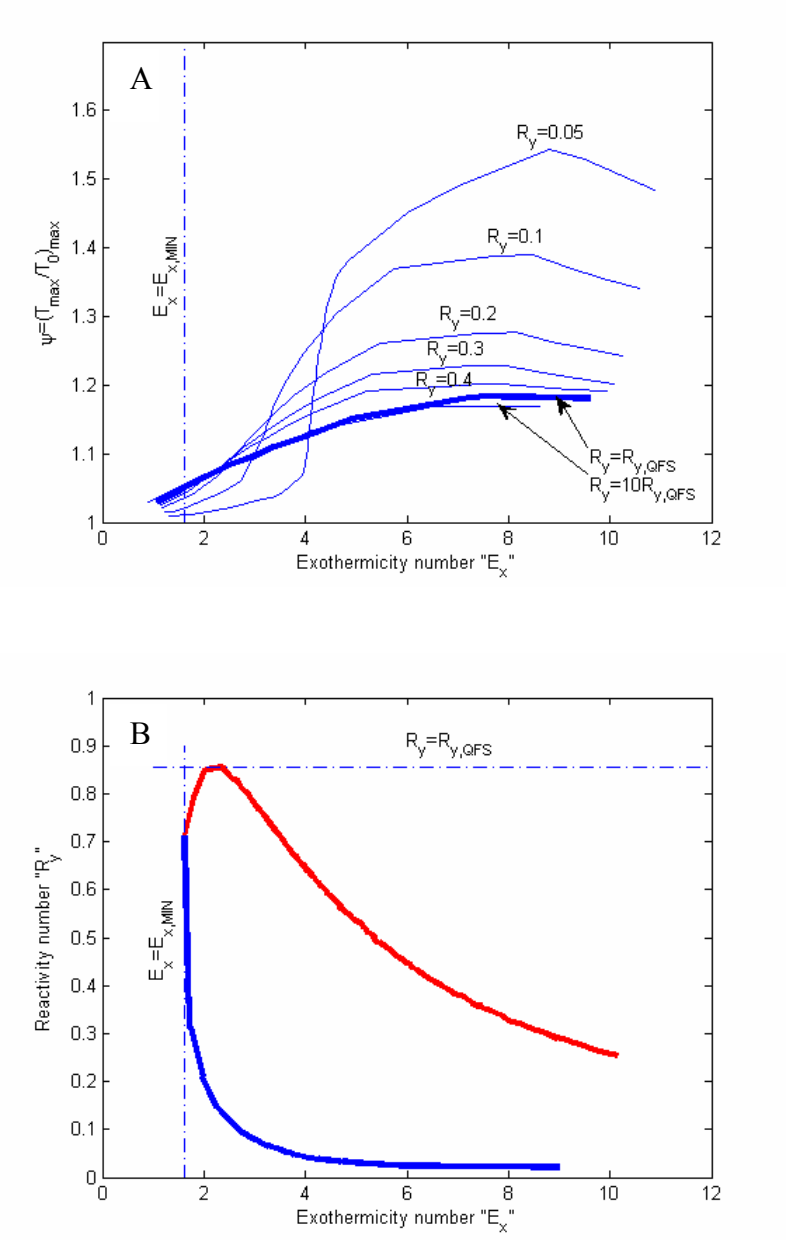

Figure 10 *Slow reaction regime. Reaction in the dispersed phase. Co=10, R_H=1, n=1, m=0.5. 0.025< ν_A Da RE<14, 0.3<ε<0.55, 32<γ<42, 0.29<$\Delta\tau_{ad,0}$<0.7. A) temperature diagram; B) boundary diagram.*

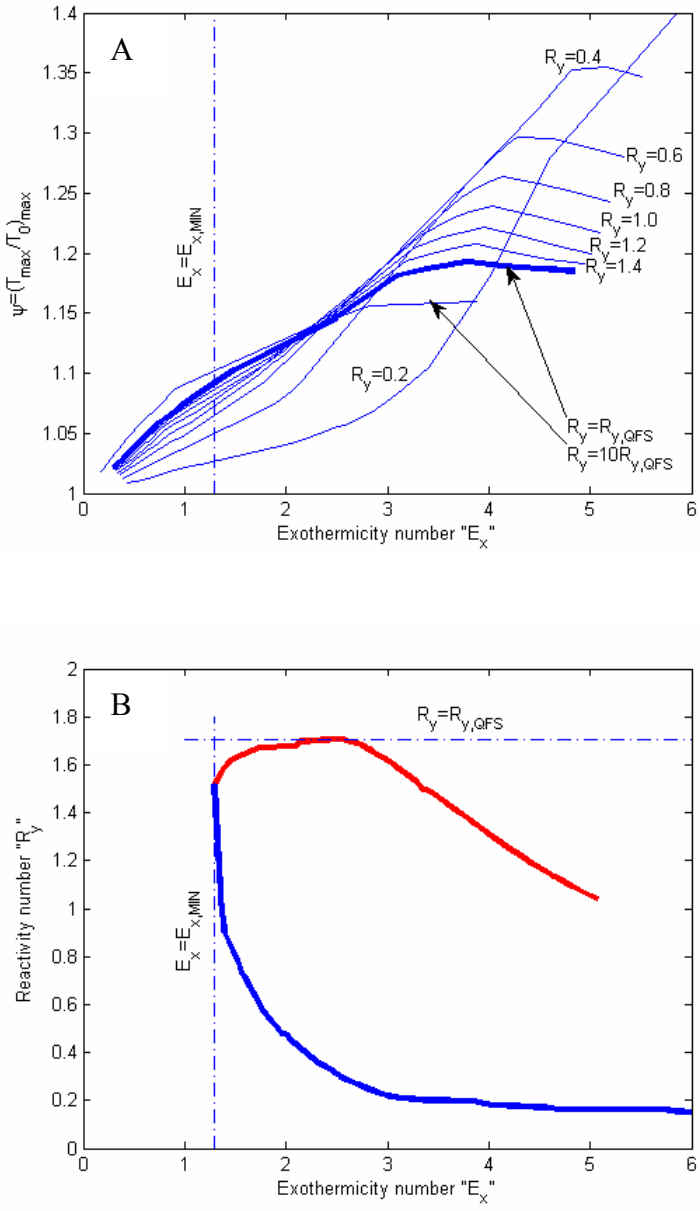

Figure 11 *Fast reaction regime. Reaction in the dispersed phase. Co=10, R_H=1, n=1, m=1. 0.025< ν_A Da RE<14, 0.3<ε<0.55, 32<γ<42, 0.29<$\Delta\tau_{ad,0}$<0.7. A) temperature diagram; B) boundary diagram.*

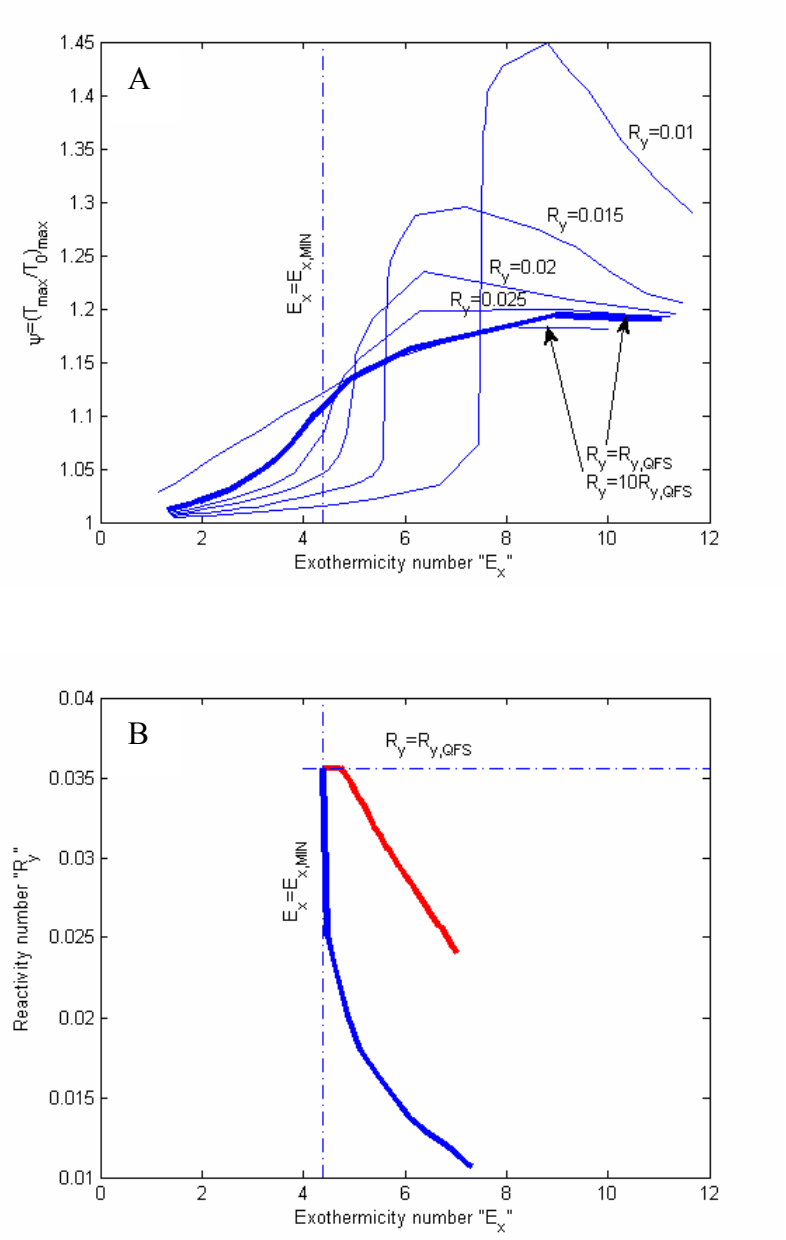

Figure 12 *Slow reaction regime. Reaction in the continuous phase. Co=10, R_H=1, n=1, m=1. 0.025< ν_A Da RE<14, 0.3<ε<0.55, 32<γ<42, 0.29<$\Delta\tau_{ad,0}$<0.7. A) temperature diagram; B) boundary diagram.*

4. Safe and productive operation of homogeneous semibatch reactors with arbitrary reaction kinetics. Part I: development of a procedure

Francesco Maestri, Renato Rota*

Politecnico di Milano

Dip. di Chimica, Materiali e Ingegneria Chimica "G. Natta"

via Mancinelli 7 - 20131 Milano – Italy

fax: +39 0223993180; e-mail: renato.rota@polimi.it

Abstract

The safe operation of an indirectly cooled semibatch reactor in which an exothermic reaction occurs requires that the characteristic time of the coreactant dosing is much higher than the characteristic time of the chemical reaction, which results in a low accumulation of unreacted coreactant in the system. On this basis, it is possible to define a target reaction temperature to which the actual temperature-time profile can be compared, in order to build *boundary diagrams* in a suitable dimensionless space: such diagrams summarize all the possible thermal behaviors of the reactor and can be used for scaling-up the process limiting the coreactant accumulation.

However, when a maximum allowable process temperature must not be exceeded (because of safety or selectivity problems), avoiding accumulation phenomena is just a necessary, not a sufficient condition to classify as acceptable a given set of operating conditions for the reactor. Consequently, the boundary diagrams must be coupled with another typology of diagrams (called *temperature diagrams*), which allow to estimate the maximum temperature increase for a given set of operating conditions.

In this work a procedure based on the use of boundary and temperature diagrams for selecting safe and productive operating conditions of *homogeneous* semibatch reactors is presented and the influence of the reaction kinetics on the shape and extension of such diagrams is discussed.

* to whom correspondence should be addressed

It has been found that using correlations developed for (1,1) reaction order kinetics can lead to both unsafe or not necessary low production operating conditions, especially with reference to the reaction order of the dosed coreactant. Moreover, the dependence of the shape and extension of such diagrams on the chemical kinetics has been found to be completely different when homogeneous or heterogeneous reacting systems are considered. A number of ready-to-use boundary and temperature diagrams is presented, together with some rules of thumb for their use, allowing for easily selecting safe and productive operating conditions for homogeneous semibatch reactors.

Keywords: Semibatch reactors; Boundary diagrams; Temperature diagrams; Runaway; Productivity; Scale-up.

4.1 Introduction

The thermal loss of control of batch and semibatch reactors in which exothermic reactions occur is a very common problem in the chemical industry, that has been thoroughly discussed in the process safety literature from the well known accident of 1976 in Seveso (Italy). Even if only a few runaway phenomena have serious consequences in terms of human lives, the effort that has been made in order to prevent such events, developing procedures for the safe scale up of a process from the laboratory to the industrial scale, is well justified. In order to solve the problem for practice, the aforementioned procedures must be reliable and simple at the same time, taking into account that especially in the fine chemical and pharmaceutical industries, where a wide range of products in a relatively small amount are produced, a detailed mathematical modeling of the single process is usually not justified, due to money and time constraints [1,2].

The operation of an indirectly cooled semibatch reactor (SBR) in which an exothermic reaction takes place is usually considered safe if the characteristic time of the coreactant supply is much higher than the characteristic time of the chemical reaction, so that the accumulation of the coreactant in the system is kept below a critical value and the cooling system can control the heat evolution [3]. On this basis, Hugo et al. [4-6] developed an empirical correlation in order to discriminate between safe and dangerous operating conditions for *homogeneous* SBRs in which an exothermic reaction of (1,1) orders occurs.

The thermally safe operation of *heterogeneous* (liquid-liquid) SBRs has been firstly analyzed along the same line by Steensma and Westerterp [7-9], who introduced the so called *boundary diagrams*, starting from the concept of target temperature. Such diagrams, in a suitable dimensionless space, summarize all the possible thermal behaviours of the reactor, allowing to discriminate between acceptable and excessive accumulation operating conditions, without solving the mathematical model of the reactor.

The boundary diagrams method for heterogeneous (liquid-liquid) reactions has been then extended to the case of multiple heterogeneous reactions by van Woezik and Westerterp [10,11], who analyzed both theoretically and experimentally the nitric acid oxidation of 2-octanol to 2-octanone with further oxidation of the reaction product to unwanted carboxylic acids.

Moreover, Maestri and Rota [12,13] demonstrated the strong influence that the reaction kinetics can have on the shape and location of the boundary diagrams for *heterogeneous* (liquid-liquid) SBRs, operating either in the kinetically or in the diffusion controlled regime. In particular, they showed that the shape and extension of the boundary diagrams is most sensitive with respect to the reaction order of the dosed coreactant, n, and that using a boundary diagram calculated for a higher n value than the real one can lead to strongly unsafe results. This means that the boundary

diagrams method for heterogeneous SBRs requires the knowledge of the reaction kinetics, at least in terms of a lumped expression, that can be deduced from calorimetric experiments.

In the present work, the boundary diagrams method for the identification of low accumulation operating conditions in a SBR is extended to the case of homogeneous reaction systems and the role of the reaction kinetics on the shape and extension of such diagrams is analyzed in detail. It has been found that, as observed for the heterogeneous (liquid-liquid) case, also in the homogeneous case the boundary diagrams are most sensitive with respect to the reaction order of the dosed coreactant. However, as a significant difference with respect to the heterogeneous (liquid-liquid) case, using a boundary diagram calculated for a lower (instead of a higher) n value than the real one can lead to strongly unsafe results.

Moreover, when a maximum allowable process temperature (in the following referred to as MAT) must not be exceeded, limiting accumulation phenomena in a SBR can be not sufficient in order to classify as acceptable a selected set of operating conditions: such a temperature limitation can be related to the triggering of either consecutive decomposition reactions of the reacting mixture, (which can be highly exothermic or produce huge amounts of gases) or side reactions (which can significantly compromise the process yield or the product quality). In the first case the MAT value is related to safety problems, in the second one to productivity problems. However, since both the problems can be lumped in an experimentally determined threshold temperature not to be exceeded, they can be faced as a single problem. To deal effectively with reactive systems presenting a well defined MAT value, Maestri and Rota [14] coupled the boundary diagrams for heterogeneous (liquid-liquid) SBRs with a new typology of diagrams, called temperature diagrams, which involve the same dimensionless parameters and allow to predict the maximum temperature increase for a given set of operating conditions. In this work, the temperature diagrams method is extended to the case of homogeneous semibatch reactions of general kinetics and a number of temperature diagrams is provided to allow end users to easily select operating conditions characterized by both low coreactant accumulation and peak reaction temperatures lower than a threshold value.

4.2 Mathematical model

The development of a criterion for the safe operation of a homogeneous SBR in which an exothermic reaction occurs requires a preliminary discussion on how the reaction system can be modeled. We assume that at time equal to zero the feed of the coreactant A to a SBR filled with a given molar amount, $n_{B,0}$, of component B is started at a constant molar rate, $F_{A,D}$. The coreactant supply is stopped when the stoichiometric molar quantity of A, $n_{A,1}$, has been fed, according to the overall reaction:

$$\nu_A A + \nu_B B \rightarrow C + \nu_D D \tag{1}$$

It follows that: $n_{A,1}=F_{A,D}t_D=(\nu_A/\nu_B)n_{B,0}$, where t_D is the dosing time. We further assume that the rate of reaction (1) can be described through a power law type functional dependence of the form:

$$r = k_{n,m} C_A^n C_B^m \tag{2}$$

The values of the kinetic parameters can be derived from a data fitting of calorimetric (e.g. ARC, Phi-TEC II, RC1) experiments. In order to develop a simple and realistic mathematical model of such reactors, the following assumptions can be stated:

1) the reaction mass is perfectly mixed;
2) the influence of the chemical reaction on the reaction volume is negligible; this means that the reaction volume increases during the supply period only because of the coreactant dosing, whereas the changes in the system density related to the composition evolution can be disregarded;
3) the heat effects are associated with the chemical reaction only;
4) the reactor operates in isoperibolic conditions; in particular, at time equal to zero, the reaction mass temperature is equal to the mean coolant temperature and to the dosing stream temperature, which remain constant for the whole duration of the process.

The mass balance equation for the i-th chemical species is:

$$\frac{dn_i}{dt} = F_{i,D} \pm \nu_i r^{eff} V_r \tag{3}$$

where $F_{i,D}$ is the molar feed rate of the i-th component, which differs from zero for the species A only, ν_i is the absolute value of the stoichiometric coefficient of the i-th species and the +/- signs hold if the i-th component is a product or a reactant, respectively. Moreover, r^{eff} is the effective conversion rate that can be determined either by the chemical reaction or by the coreactant supply rate. The material balance eqs. (3) are coupled with the initial conditions: $n_i(t=0)=n_{i,0}$, where $n_{i,0}$ differs from zero for B only. Performing suitable combinations of the mass balances (3) and integrating the resulting differential equations together with the related initial conditions, the following functional dependences of the concentrations of species A and B on dimensionless time, $\vartheta=t/t_D$, and conversion, $\zeta_B=1-n_B/n_{B,0}$, can be derived:

$$C_A = \frac{\nu_A}{\nu_B} C_{B,0} \frac{\vartheta - \zeta_B}{1 + \varepsilon\vartheta} \tag{4}$$

$$C_B = C_{B,0}\frac{1-\zeta_B}{1+\varepsilon\vartheta} \tag{5}$$

where $\varepsilon=V_D/V_{r,0}$ is the relative volume increase at the end of the dosing period. Moreover, the mass balance equation for component B can be rewritten as:

$$\frac{d\zeta_B}{d\vartheta} = \frac{\nu_B t_D}{n_{B,0}} r^{eff} V_r \tag{6}$$

and finally rearranged in the form:

$$\frac{d\zeta_B}{d\vartheta} = \nu_A Da\, RE\, f\, \kappa \tag{7}$$

where $Da=k_{n,m,R}t_D C_{B,0}^{n+m-1}$ is the Damköhler number for (n,m) order reactions, which contains the physical information about the chemical kinetics and the dosing time, $RE=(\nu_B/\nu_A)^{1-n}$ involves information on the stoichiometry, $f=[(\vartheta-\zeta_B)^n(1-\zeta_B)^m]/(1+\varepsilon\vartheta)^{n+m-1}$ is the only factor containing the functional dependence on ϑ and ζ_B, and $\kappa_{n,m}=\exp[\gamma(1-1/\tau)]$ is a dimensionless reaction rate constant, that is, the ratio of the reaction rate constant evaluated at the actual temperature, T, to that evaluated at a reference temperature, T_R, with $\gamma=E/(RT_R)$ and $\tau=T/T_R$.

The energy balance equation for the reactor states that the reaction temperature variations are the result of three enthalpic contributions, related to the dosing stream, the chemical reaction and the heat removal by the coolant:

$$n\widetilde{C}_{P,m}\frac{dT}{dt} = F_D\widetilde{C}_{P,D}\left(T_D - T\right) + r^{eff}V_r\left(-\Delta\widetilde{H}_r\right) - UA\left(T - T_{cool}\right) \tag{8}$$

Eq. (8) can be conveniently rewritten in the following dimensionless form:

$$\left(1+\varepsilon\vartheta\right)\frac{d\tau}{d\vartheta} = \Delta\tau_{ad,0}\frac{d\zeta_B}{d\vartheta} - \left[U^* Da\left(1+\varepsilon\vartheta\right) + \varepsilon R_H\right]\left(\tau - \tau_{cool}^{eff}\right) \tag{9}$$

where $\Delta\tau_{ad,0}$ is the adiabatic temperature rise, that contains the physical information about the reaction enthalpy, $U^* Da = \left(UA_0\right)t_D \big/ \left(\widetilde{\rho}_m\widetilde{C}_{P,m}V_{r,0}\right)$ is a modified Stanton number accounting for the cooling efficiency and $R_H = \widetilde{\rho}_D\widetilde{C}_{P,D}\big/\widetilde{\rho}_m\widetilde{C}_{P,m}$ is the ratio between the volumetric heat capacities of the dosing stream and the reacting mixture. Moreover, $\tau_{cool}^{eff} = \dfrac{U^* Da\left(1+\varepsilon\vartheta\right)\tau_{cool} + \varepsilon R_H\tau_D}{U^* Da\left(1+\varepsilon\vartheta\right) + \varepsilon R_H}$ is an effective cooling temperature, that summarizes the enthalpic contributions of both the heat removal by the coolant and the dosing stream. The model equations presented above are valid up to the end of the supply period. It can be easily

demonstrated that the same equations can be extended to $\vartheta>1$ by substituting everywhere the $(\vartheta-\zeta_B)/\vartheta$ and $(\vartheta-\zeta_B)$ terms with $(1-\zeta_B)$, the $\varepsilon\vartheta$ terms with ε and by setting $T_D \equiv T$ in the definition of the effective cooling temperature.

The numerical integration of eqs. (7) and (9) with the proper initial conditions results in the temperature and conversion time profiles. For the sake of example, Figure 1 shows the influence of the reaction order of both the reactants, n and m, on the temperature-time profiles. As will be discussed in detail in the following paragraphs, these profiles vary significantly with n, even for $\vartheta<0.5$ as can be observed from Figure 1A. This implies that, as discussed elsewhere for heterogeneous (liquid-liquid) systems [12,13], developing a safety criterion for homogeneous SBRs the role of the reaction kinetics cannot be disregarded.

4.3 Thermally safe operating conditions

As previously mentioned, the operation of a SBR in which an exothermic reaction occurs is usually considered safe if the overall conversion rate is determined by the supply rate of the coreactant, the accumulation of which in the reaction system is kept at sufficiently low values. The procedure for developing boundary diagrams for homogeneous systems follows the same lines as for heterogeneous systems. Since the procedure for heterogeneous systems has been thoroughly discussed elsewhere [7,12], it is only briefly summarized in the following.

In order to develop a quantitative criterion for the identification of low accumulation operating conditions, the mass balance eq. (6) can be conveniently rewritten as:

$$\frac{d\zeta_B}{d\vartheta} = \frac{t_D}{t_P} \tag{10}$$

where $t_P=n_{B,0}/(\nu_B r^{eff} V_r)$ is the instantaneous characteristic time of the process, which is related to the overall conversion rate. If we assume that, after a quick initial onset of the reactor, the overall conversion rate is completely determined by the dosing rate of the coreactant, the characteristic time of the process, t_P, becomes equal to the characteristic time of the coreactant supply, t_D, and the mass balance eq. (10) simplifies to:

$$\frac{d\zeta_B}{d\vartheta} = 1 \tag{11}$$

Along the same line, the energy balance for the reactor can be rewritten as:

$$\frac{d\tau}{d\vartheta} = \Delta\tau_{ad,0}\frac{t_D}{t_P} - \left(\tau - \tau_{cool}^{eff}\right)\frac{t_D}{t_{cool}^{eff}} \tag{12}$$

where $t_{cool}^{eff} = \left(\frac{UA}{n\widetilde{C}_{P,m}} + \frac{n_D \widetilde{C}_{P,D}}{t_D n \widetilde{C}_{P,m}} \right)^{-1}$ is the instantaneous characteristic time for the reaction mass cooling, by both the external coolant and the sensible heat of the dosing stream. If we further assume that the characteristic time of the cooling, t_{cool}^{eff}, is much lower than the characteristic time of the process (and hence of the enthalpic effects associated to the conversion rate), t_P, a situation arises in which the reaction temperature increase due to the heat of reaction is counteracted at a much smaller time scale by the contribution given by the reaction mass cooling. Such a situation allows for the introduction of a pseudo steady state assumption on the temperature-time profile, so that:

$$\frac{d\tau}{d\vartheta} \cong 0 \tag{13}$$

Substituting conditions (11) and (13) into the energy balance for the reactor (9), the following temperature-time functional dependence can be derived:

$$\tau - \tau_{cool}^{eff} = \frac{\Delta\tau_{ad,0}}{U^* Da(1+\varepsilon\vartheta) + \varepsilon R_H} \tag{14}$$

Eq. (14) represents conditions where the overall conversion rate is completely determined by the coreactant supply rate (which implies a negligible coreactant accumulation in the system) and the temperature evolution is completely determined by the cooling power of the system. However, in every real reactor a certain coreactant accumulation cannot be avoided. This is the reason why Steensma and Westerterp [7] introduce a 5% overestimation of the temperature difference (14), obtaining the following definition of the *target temperature*:

$$\tau_{ta} = \tau_{cool}^{eff} + 1.05 \frac{\Delta\tau_{ad,0}}{U^* Da(1+\varepsilon\vartheta) + \varepsilon R_H} \tag{15}$$

to which the actual temperature-time profile of the reactor can be directly compared. In this context it should be mentioned that other criteria for identifying runaway regions have been proposed in the literature, based on some mathematical properties of the mass and energy balance equations, which are free from the aforementioned assumption [15]. Eq. (15) is valid up to ϑ=1; the analogous expression for ϑ>1 can be easily obtained by substituting in the same equation the $\varepsilon\vartheta$ term with ε.

On this basis, the thermal behaviors of SBRs in which an exothermic reaction is performed at increasing coolant temperatures can be classified into the following four categories [7]:

1) for sufficiently low values of the coolant temperature, the peak temperature attained is much lower than the local target value, which means that the reaction is

not ignited. In such a situation the accumulation of the coreactant in the system reaches obviously high values but the reaction is never fast enough to cause the thermal loss of control of the system;

2) as the coolant temperature increases, the peak temperature "pinches" locally the target line: this situation is referred to as a marginal ignition;
3) increasing further the coolant temperature, the reaction rate is at the same time not so high to keep the accumulation of the coreactant sufficiently low and not so low to avoid -as the reaction itself ignites- the thermal loss of control of the system. This situation implies peak reaction temperatures higher than the local target value;
4) as the coolant temperature still increases, the reaction rate becomes fast enough to keep the accumulation of the coreactant in the system sufficiently low, so that the peak reaction temperature never exceeds the target temperature and a high conversion at the end of the dosing period is reached. The minimum coolant temperature for which the exceeding of the local target value by the peak reaction temperature disappears is referred to as a QFS (Quick onset, Fair conversion, Smooth temperature profile) condition.

Situations 1) to 4) can be represented in a suitable dimensionless space through the so called boundary diagrams, an example of which is given in Figure 2. The dimensionless parameters for the representation of the boundary diagrams can be derived from the energy balance of the reactor (9), following the same procedure described in detail in Maestri and Rota [12] for heterogeneous (liquid-liquid) reaction systems. The resulting expressions of the exothermicity and reactivity numbers for homogeneous SBRs are:

$$E_x = \frac{\gamma}{\tau_{cool}^2}\frac{\Delta\tau_{ad,0}}{U^* Da + \varepsilon R_H} = \frac{\gamma}{\tau_{cool}^2}\frac{\Delta\tau_{ad,0}}{\varepsilon\left(Co + R_H\right)} \tag{16}$$

$$R_y = \frac{\nu_A Da\, RE\, \kappa\left(\tau_{cool}\right)}{U^* Da + \varepsilon R_H} = \frac{\nu_A Da\, RE\, \kappa\left(\tau_{cool}\right)}{\varepsilon\left(Co + R_H\right)} \tag{17}$$

where the cooling number, $Co=U^*Da/\varepsilon$, has been also introduced. In this dimensionless space a boundary can be identified separating a region of excessive accumulation, EAR (that must obviously be avoided), from a region of low coreactant accumulation for high enough R_y values or low enough E_x values. An inherently safe region can be also identified for R_y values higher than the maximum value of R_y for which excessive accumulation can occur ($R_{y,QFS}$: in this region no excessive accumulation is possible regardless the value of E_x) or lower than the minimum value of E_x for which excessive accumulation can occur ($E_{x,MIN}$: in this region no excessive accumulation is possible regardless the value of R_y). The boundary diagrams allow end users to identify low

coreactant accumulation operating conditions for an existing homogeneous SBR, operating at given values of the fixed parameters Co, R_H, n and m, without solving the mathematical model of the reactor. This allows also for an easy and fast scale-up from laboratory to real size reactors. It should be stressed that the procedure used for building the boundary diagrams guarantees that operating conditions outside the excessive accumulation region will be safe. Depending on the real values of the dimensionless operating parameters, conditions corresponding to a point inside the EAR are not necessarily unsafe. This is a common (and desired) behavior when safety problems have to be faced: one can reject safe conditions but unsafe conditions must never be accepted. A number of boundary diagrams for different conditions, as discussed in detail in the following, are reported in Figures 3 to 9. We can see that in the case of homogeneous semibatch reaction systems that can be described through a (1,1) reaction order kinetics, the reactor operation can be always considered safe if the condition $R_y>1$ is fulfilled. Taking into account that for homogeneous reaction systems R_H is usually close to one, this condition can be further recast in the following relation:

$$R_y \cong \frac{\nu_A k C_{B,0} t_D}{\frac{V_D}{V_{r,0}}\left(1+\frac{UA_0 t_D}{\widetilde{\rho}_m \widetilde{C}_{P,m} V_D}\right)} > 1 \tag{18}$$

This criterion was firstly introduced by Hugo et al. [5] and is valid for homogeneous SBRs in which an exothermic reaction of (1,1) order occurs. However, each boundary diagram is valid for given values of four model parameters, that is, Co, R_H, n and m. As can be observed from Figure 3, where several boundary diagrams corresponding to different values of Co, R_H, n and m are reported, the parameter with respect to which the EAR extension (and in particular the values of $R_{y,QFS}$ and $E_{x,MIN}$ defining the inherently safe region) is most sensitive is the reaction order of the dosed coreactant, n. This can be more precisely quantified in terms of normalized sensitivity coefficients of $E_{x,MIN}$ and $R_{y,QFS}$ with respect to Co, R_H, n and m. As previously mentioned, $E_{x,MIN}$ and $R_{y,QFS}$ are the limits of the inherently safe region of the single boundary diagram. Such sensitivity coefficients can be defined according to Varma et al. [15] as:

$$S_{i,j} = \frac{\alpha_j}{\beta_i}\frac{\partial \beta_i}{\partial \alpha_j} \approx \frac{\alpha_j}{\beta_i}\frac{\Delta \beta_i}{\Delta \alpha_j} \tag{19}$$

where β_i is either $R_{y,QFS}$ or $E_{x,MIN}$, and α_j is one of the investigated parameters. Taking the (1,1) reaction order kinetics case as a reference case, the computed values of such sensitivity coefficients are summarized in Table 1. From these results, it is evident that, as happens for heterogeneous (liquid-liquid) SBRs [12], also in the homogeneous case the influence of the reaction kinetics (and in particular of the reaction order of the dosed coreactant) on the shape and extension of the

boundary diagrams can be much more important than that of the remaining parameters, that is Co and R_H. This means that using the boundary diagrams method for identifying low accumulation operating conditions of homogeneous SBRs requires the knowledge of the reaction kinetics at least in terms of a lumped expression which describes satisfactorily the experimental data: such an information can be obtained through calorimetric experiments (typically performed in an ARC, Phi-TEC II or RC1 equipment) that are not much more expensive and time consuming than those necessary to estimate the remaining kinetic parameters, that is the pre-exponential factor and the activation energy. However, as a significant difference with respect to the heterogeneous (liquid-liquid) case, in the homogeneous reactions case the extension of the boundary diagrams (and in particular the $R_{y,QFS}$ value) increases with increasing n. This means that when the boundary diagrams method is applied to the analysis of the operating conditions of homogeneous SBRs, the use of a boundary diagram calculated for an approximated reaction kinetics (for example, of (1,1) reaction orders) can lead to unsafe results if the real reaction system involves a higher reaction order of the dosed coreactant, n. Such a behavior is exactly the opposite with respect to that observed in the heterogeneous (liquid-liquid) case [12], so that also the rules of thumb for using an available boundary diagram in the analysis of a reaction system of different kinetics change completely. Such a problem is of particular importance for end users, because whereas the evaluation of the E_x and R_y parameters according to the real reaction kinetics through eqs. (16) and (17) is straightforward, building a dedicated boundary diagram -when not available- is much more complicated and time consuming. Consequently, end users usually employ boundary diagrams built for reaction kinetics close enough to that of interest. For the sake of end users convenience, in Figures 3 to 9 a number of boundary diagrams for homogeneous systems characterized by several values of the operating parameters are reported. However, it should be mentioned that the best choice is always using the proper boundary diagram. A step-by-step procedure for building the boundary diagrams is discussed elsewhere [12]. In any case, providing reliable and simple rules for using approximated boundary diagrams (that is, boundary diagrams calculated for a slightly different kinetic expression than that of the real system) is important for the practical applicability of this method.

To identify the reasons of the aforementioned different behavior between homogeneous and heterogeneous SBRs, it is useful to analyze the time evolution of the coreactant accumulation in the two cases. This can be done using two dimensionless parameters, defined by Steensma and Westerterp [7], as a relative coreactant amount:

$$M_A = \frac{n_A}{n_{A,1}} \tag{20}$$

and a relative coreactant concentration:

$$\Gamma_A = \frac{C_A}{C_{A,D}} \tag{21}$$

For heterogeneous (liquid-liquid) SBRs, operating either in the kinetically or in the diffusion controlled regime, assuming that the solubility of the coreactant, A, in the dispersed phase, d, is much higher than that in the continuous phase, c, the expressions (20) and (21) still hold with $n_A \approx n_{A,d}$ and $C_A \approx C_{A,d}$. Using eqs. (4) and (5) for the homogeneous reaction case and the corresponding equations for the heterogeneous (liquid-liquid) case [12], the functional dependences of M_A and Γ_A on dimensionless time, ϑ, and conversion, ζ_B, can be derived. Such expressions are reported in Table 2. At the beginning of the supply period (that is at $\vartheta \to 0$, where also $d\zeta_B/d\vartheta \to 0$), it is easy to demonstrate that in the homogeneous case $\Gamma_A \to 0$ (which also means that $C_A \to 0$), whereas in the heterogeneous (liquid-liquid) case $\Gamma_A \to 1$ (which also means that $C_A \to C_{A,D}$). Figures 10 and 11 show the time profiles of M_A and Γ_A for homogeneous and heterogeneous (liquid-liquid) SBRs operating in the kinetically controlled regime with the chemical reaction occurring in the dispersed phase. In particular, the variations of such profiles with the reaction order of the dosed coreactant, n, are represented. In the homogeneous case, $C_A \to 0$ as $\vartheta \to 0$. This means that as the reaction order of the dosed coreactant, n, increases, a time interval starting from $\vartheta = 0$ exists in which $\overline{C}_A$ remains close to zero and, consequently, increasing the n value leads to reducing the average reaction rate during this time interval. Therefore, the initial coreactant accumulation becomes higher as n increases, as can be observed from Figure 10A. This is not true for heterogeneous systems, for which at the beginning of the supply period, C_A is not close to zero but to $C_{A,D}$ and, in the explored range of the parameters involved, the initial coreactant accumulation decreases as n increases, as shown in Figure 11A. It should be noticed that the coreactant accumulation has to be considered critical for safety when it occurs at the beginning of the dosing time, when the conversion is still low and the reactant initially loaded in the reactor has not been yet consumed. For this reason one must focus on the coreactant accumulation in the first part of the supply period, whereas the accumulation occurring at high conversion values is less critical for safety. The consequence of such a different behavior between homogeneous and heterogeneous SBRs is that in the homogeneous case, at fixed Co, R_H and m values the extension of the EAR (in particular, the $R_{y,QFS}$ value) increases when n increases, whereas in the heterogeneous (liquid-liquid) case the opposite occurs. This result is of particular importance for end users, who often have to face the problem of using an available boundary diagram or safety criterion (e.g., eq. (18)) obtained for a given reaction kinetics (for instance, for (1,1) reaction order), for the analysis of a reacting system involving a different reaction kinetics. To solve this problem for practice, the following rules of thumb, that arise directly from the results presented above, can be used:

1) when the kinetics related to the available boundary diagram or safety criterion differs from the real kinetics of the reaction system of interest in the reaction order of the dosed coreactant, n, the boundary diagram or safety criterion should not be used, since the conclusions drawn can either be unsafe or compromise the reactor productivity; in particular, they will be unsafe when, dealing with a homogeneous reaction system, the kinetic expression of the boundary diagram or the safety criterion is characterized by a lower n value. The opposite occurs for heterogeneous (liquid-liquid) reaction systems.
2) when the kinetics assumed for the derivation of the available boundary diagram or safety criterion differs from the real kinetics in the reaction order of the reactant initially loaded in the reactor, m, the approximated boundary diagram or safety criterion can in general be used, since the sensitivity of the $E_{x,MIN}$ and $R_{y,QFS}$ values with respect to the parameter m is relatively low (see Table 1);
3) because of the significantly different sensitivities of $E_{x,MIN}$ and $R_{y,QFS}$ to n and m, the global reaction order (n+m) should never be used as a discriminating parameter in order to establish whether a boundary diagram or safety criterion developed for a given reaction kinetics can be used for the safety analysis of a system with a different kinetics. For the sake of example, in Figure 5 the boundary diagram for a homogenous reaction with n=1.25 and m=0.5 is compared with that for n=m=1. It can be easily observed that the runaway region for (1.25,0.5) is larger than that for (1,1) reaction orders, even if the overall reaction order for the former case is lower (that is, 1.25+0.5=1.75 vs. 1+1=2).

When dealing with exothermic semibatch reaction processes which can undergo an undesired event above a threshold temperature (usually referred to as the MAT value), avoiding the coreactant accumulation is a necessary, but not a sufficient condition in order to classify as thermally safe a selected set of operating conditions for the reactor. If the initial reaction temperature is too high, a situation can arise in which the coreactant accumulation is kept below a critical value, but the temperature is so high that even a lower temperature rise (which is the consequence of a limited coreactant accumulation) can cause the peak reaction temperature to exceed the limit for the triggering of the undesired reaction. To identify these situations, the boundary diagrams can be coupled with another typology of diagrams, called temperature diagrams, which involve the same set of dimensionless parameters employed for the representation of the boundary diagrams and provide the highest ratio of the maximum to the initial reaction temperature, ψ, to be expected for a given set of operating conditions. An example of such diagrams is shown in Figure 12. For a given set of operating conditions, the values of E_x and R_y can be easily computed, as for the use of the boundary diagrams. These two values identify a point on

the temperature diagram from which the corresponding value of $\psi=(T_{max}/T_0)_{max}$ can be easily read. Given the initial temperature value, T_0, the maximum reaction temperature that will not be exceeded during normal operation of the SBR is safely estimated as $T_{max}=\psi \cdot T_0$. Such an information can be directly compared with the MAT value. Operating conditions implying peak temperatures higher than MAT must not be adopted since they can lead to the triggering of undesired reactions. A general procedure for building the temperature diagrams is provided elsewhere for heterogeneous systems [14] and it can be easily adapted to homogeneous reaction systems. It should be noticed that, whereas the information provided by the boundary diagrams is affected by a degree of arbitrariness given by the quantitative definition of "excessive coreactant accumulation" and summarized through the 1.05 factor in eq. (15), the conclusions drawn through the temperature diagrams are independent on any degree of arbitrariness, apart from the identification of the $E_{x,MIN}$ and $R_{y,QFS}$ values on the diagram itself. In Figures 13 to 16 a number of temperature diagrams for homogeneous SBRs characterized by several Co, R_H, n and m values (in the range typically encountered in the industrial practice) is provided: such diagrams can be used together with the correspondent boundary diagrams given in Figures 4 to 9, to classify a given set of operating conditions.

In particular, when a set of operating conditions is selected (from which a value of the E_x and R_y parameters can be computed according to the relations (16) and (17)), the temperature diagrams must firstly be used to check whether:

$$\psi \cdot T_0 < MAT \tag{22}$$

If the check (22) is satisfied, two situations may be possible:

a) the calculated (E_x,R_y) point belongs to the $E_x \leq E_{x,MIN}$ zone of the temperature diagram (see Figure 12) or to the $E_x > E_{x,MIN}$ zone with $R_y \geq R_{y,QFS}$. In this case the selected operating conditions can be accepted since they cannot lead to the triggering of unwanted reactions and they belong to the inherently safe region of the boundary diagram, where no excessive coreactant accumulation can occur;
b) the calculated (E_x,R_y) point belongs to the $E_x > E_{x,MIN}$ zone of the temperature diagram (see Figure 12) with $R_y < R_{y,QFS}$. In this case, it is necessary to refer to the related boundary diagram, to check whether the aforementioned point belongs to the safe region, to the excessive accumulation region or to the no ignition region. It must in fact be noticed that even operating conditions which satisfy the check (22) cannot be considered thermally safe if they imply an excessive coreactant accumulation since such operating conditions are typically characterized by sudden temperature and conversion jumps which are responsible for a bad control of the reactor. Moreover, it must be stressed that a given set of operating

conditions must be safe not only during the normal reactor operation, but also during upset conditions, such as those arising from a cooling system failure: in such situations, operating with a minimum coreactant accumulation allows to keep the process safety by stopping immediately the coreactant feed. Finally, no ignition operating conditions must be avoided since they imply a low reactor productivity.

As can be observed from the temperature diagrams presented in Figures 13 to 16, for homogeneous SBRs operating at low R_y values (that is, at R_y values much lower than $R_{y,QFS}$) maximum ψ values as high as 1.8 could occur; this means that if the initial reaction temperature is 300K, the peak temperature could reach 540K, temperature which is well above the normal boiling point of almost all the solvents employed in the industrial practice. On the other hand, operating conditions characterized by R_y values higher than $R_{y,QFS}$ imply much lower ψ values, especially at high cooling numbers. Finally, for poorly exothermic reaction systems, characterized by E_x values lower than $E_{x,MIN}$, ψ values even lower than 1.1 occur.

4.4 Conclusions

The thermally safe operation of homogeneous SBRs in which exothermic reactions of (1,1) orders occur has been thoroughly analyzed in the literature and reliable criteria have been developed in order to easily select inherently safe operating conditions for such reaction systems. The same results can be obtained through the boundary diagrams method. However, the conclusions drawn through such criteria, as well as through boundary diagrams calculated on the basis of a (1,1) order kinetics, are not always safe when dealing with systems characterized by reaction orders of the dosed coreactant different from one. The same results have been obtained elsewhere in the literature for heterogeneous (liquid-liquid) SBRs [12,13]. However, if for heterogeneous reaction systems the use of a boundary diagram calculated on the basis of a higher reaction order of the dosed coreactant leads to unsafe results, the opposite occurs for homogeneous reaction systems. This means that the rules of thumb for using kinetically approximated boundary diagrams or safety criteria are in the two cases completely different.

Moreover, when during the reactor operation a maximum temperature must not be exceeded to prevent the triggering of unwanted reactions (either because of safety or productivity problems), a new typology of diagrams, called temperature diagrams, can be coupled with the boundary diagrams. Such diagrams, on the basis of the same set of dimensionless parameters than that employed for the representation of the boundary diagrams, provide information on the maximum peak temperature to be expected for a selected set of operating conditions. A number of boundary and temperature diagrams for easily identifying inherently safe operating conditions of

homogeneous SBRs have been built and provided, together with some rules of thumb for their safe use.

Nomenclature

Symbols	
A	heat transfer area of the reactor (associated to the jacket and/or the coil), m^2
C	molar concentration, $kmol/m^3$
Co	$=U^*Da/\varepsilon$, cooling number, -
$\tilde{C}_P$	molar heat capacity, kJ/(kmol·K)
Da	$=k_{n,m,R}t_D C_{B,0}^{n+m-1}$, Damköhler number for (n,m) order reactions, -
E	activation energy, kJ/kmol
E_x	exothermicity number, -
f	function of the dimensionless time and conversion of B in eq. (7), -
F	molar feed rate, kmol/s
$\Delta\tilde{H}$	reaction enthalpy, kJ/kmol
$k_{n,m}$	reaction rate constant, $m^{3(n+m-1)}/(kmol^{n+m-1}\cdot s)$
M	$=n_A/n_{A,1}$, relative coreactant amount, -
MAT	maximum allowable temperature, K
n	number of moles, kmol
r	reaction rate, $kmol/(m^3\cdot s)$
R	gas constant = 8.314, kJ/(kmol·K)
RE	reactivity enhancement factor in eq. (7), -
R_H	heat capacity ratio, -
R_y	reactivity number, -
S	normalized objective sensitivity coefficient, -
t	time or characteristic time, s
T	temperature, K
$\Delta T_{ad,0}$	$= \dfrac{\left(-\Delta\tilde{H}_r\right)C_{B,0}}{\nu_B\tilde{\rho}_m\tilde{C}_{P,m}}$, adiabatic temperature rise, K
U	overall heat transfer coefficient, $kW/(m^2\cdot K)$
U^*Da	$=(UA)_0 t_D/\left(\tilde{\rho}_m\tilde{C}_{P,m}V_{r,0}\right)$, modified Stanton number, -
V	liquid volume, m^3
Greek symbols	
α, β	generic symbols, eq. (19), -
γ	$=E/(RT_R)$, dimensionless activation energy, -
Γ	$=C_A/C_{A,D}$, relative coreactant concentration, -

ε	relative volume increase at the end of the semibatch period, -
ζ	molar conversion, -
ϑ	$=t/t_D$, dimensionless time, -
κ	$=k/k_R$, dimensionless reaction rate constant, -
ν	stoichiometric coefficient, -
$\tilde{\rho}$	molar density, $kmol/m^3$
τ	$=T/T_R$, dimensionless temperature, -
ψ	$=(T_{max}/T_0)_{max}$, maximum dimensionless temperature rise, -

Subscripts and superscripts

A,B,C,D	components A, B, C and D
ad	adiabatic
cool	coolant
D	dosing stream or dosing time
eff	effective
H	in the heat capacity ratio R_H
i	"i-th" component
m	order of reaction respect to component B
m	reacting mixture
max	maximum value of a quantity or at the maximum value of a quantity
n	order of reaction respect to component A
P	process
MIN	in $E_{x,MIN}$
QFS	in $R_{y,QFS}$
r	reaction
R	reference
ta	target
x	in the exothermicity number E_x
y	in the reactivity number R_y
0	start of the semibatch period
1	end of the semibatch period

Literature cited

1. Westerterp, K.R.; Molga, E.J. No more runaways in fine chemical reactors. *Ind. Eng. Chem. Res.* 2004, *43 (16),* 4585-4594.

2. Westerterp, K.R.; Molga, E.J. Runaway prevention in liquid-liquid semibatch reactors. *Inzynieria Chemiczna i Procesowa* 2004, *25(3/4)*, 2041-2050.

3. Steinbach, J. Safety assessment for chemical processes. 1999, *Wiley-WCH.*

4. Hugo, P.; Steinbach, J. Praxisorientierte Darstellung der thermischen Sicherheitsgrenzen für den indirekt gekühlten Semibatch-Reaktor. *Chem. Ing. Tech.* 1985, *57, Nr. 9,* 780-782.

5. Hugo, P.; Steinbach, J. A comparison of the limits of safe operation of a SBR and a CSTR. *Chem. Eng. Sci.* 1986, *41*, 1081-1087.

6. Hugo, P.; Steinbach, J.; Stoessel, F. Calculation of the maximum temperature in stirred tank reactors in case of a breakdown of cooling. *Chem. Eng. Sci.* 1988, *43, 8*, 2147-2152.

7. Steensma, M.; Westerterp, K.R. Thermally safe operation of a cooled semi-batch reactor. Slow liquid-liquid reactions. *Chem. Eng. Sci.* 1988, *43, Nr.8,* 2125-2132.

8. Steensma, M.; Westerterp, K.R. Thermally safe operation of a semibatch reactor for liquid-liquid reactions. Slow reactions. *Ind. Eng. Chem. Res.* 1990, *29,* 1259-1270.

9. Steensma, M.; Westerterp, K.R. Thermally safe operation of a semibatch reactor for liquid-liquid reactions. Fast reactions. *Chem. Eng. Technol.* 1991, *14,* 367-375.

10. van Woezik, B.A.A.; Westerterp K.R. The nitric acid oxidation of 2-octanol. A model reaction for multiple heterogeneous liquid-liquid reactions. *Chem. Eng. Process.* 2000, *39,* 521-537.

11. van Woezik, B.A.A.; Westerterp K.R. Runaway behaviour and thermally safe operation of multiple liquid-liquid reactions in the semibatch reactor. The nitric acid oxidation of 2-octanol. *Chem. Eng. Process.* 2001, *41,* 59-77.

12. Maestri, F.; Rota, R. Thermally safe operation of liquid-liquid semibatch reactors. Part I: single kinetically controlled reactions with arbitrary reaction order. *Chem. Eng. Sci.* 2005, *60,* 3309-3322.

13. Maestri, F.; Rota, R. Thermally safe operation of liquid-liquid semibatch reactors. Part II: single diffusion controlled reactions with arbitrary reaction order. *Chem. Eng. Sci.* 2005, *60,* 5590-5602.

14. Maestri, F.; Rota, R. Temperature diagrams for preventing decomposition or side reactions in liquid-liquid semibatch reactors. *Chem. Eng. Sci.* 2006, *61,* 3068-3078.

15. Varma, A.; Morbidelli, M.; Wu, H. Parametric Sensitivity in Chemical Systems. 1999, *Cambridge University Press*.

Table 1 *Normalized sensitivity coefficients of $R_{y,QFS}$ and $E_{x,MIN}$ computed from the data shown in Figure 3.*

	Co	**R_H**	**n**	**m**
$R_{y,QFS}$	0.032	$9.7 \cdot 10^{-4}$	5.376	0.154
$E_{x,MIN}$	0.295	0.075	0.232	0.401

Table 2 *Functional dependences of the relative coreactant amount, M_A, and of the relative coreactant concentration, Γ_A on ϑ and ζ_B. Expressions valid up to $\vartheta=1$. For $\vartheta>1$, the $(\vartheta-\zeta_B)/\vartheta$ and the $(\vartheta-\zeta_B)$ terms must be replaced with $(1-\zeta_B)$, and the $\varepsilon\vartheta$ terms with ε.*

	Heterogeneous (liquid-liquid) SBRs	**Homogeneous SBRs**
M_A	$\vartheta - \zeta_B$	$\vartheta - \zeta_B$
Γ_A	$\dfrac{\vartheta - \zeta_B}{\vartheta}$	$\dfrac{\varepsilon}{1+\varepsilon\vartheta}\left(\vartheta - \zeta_B\right)$

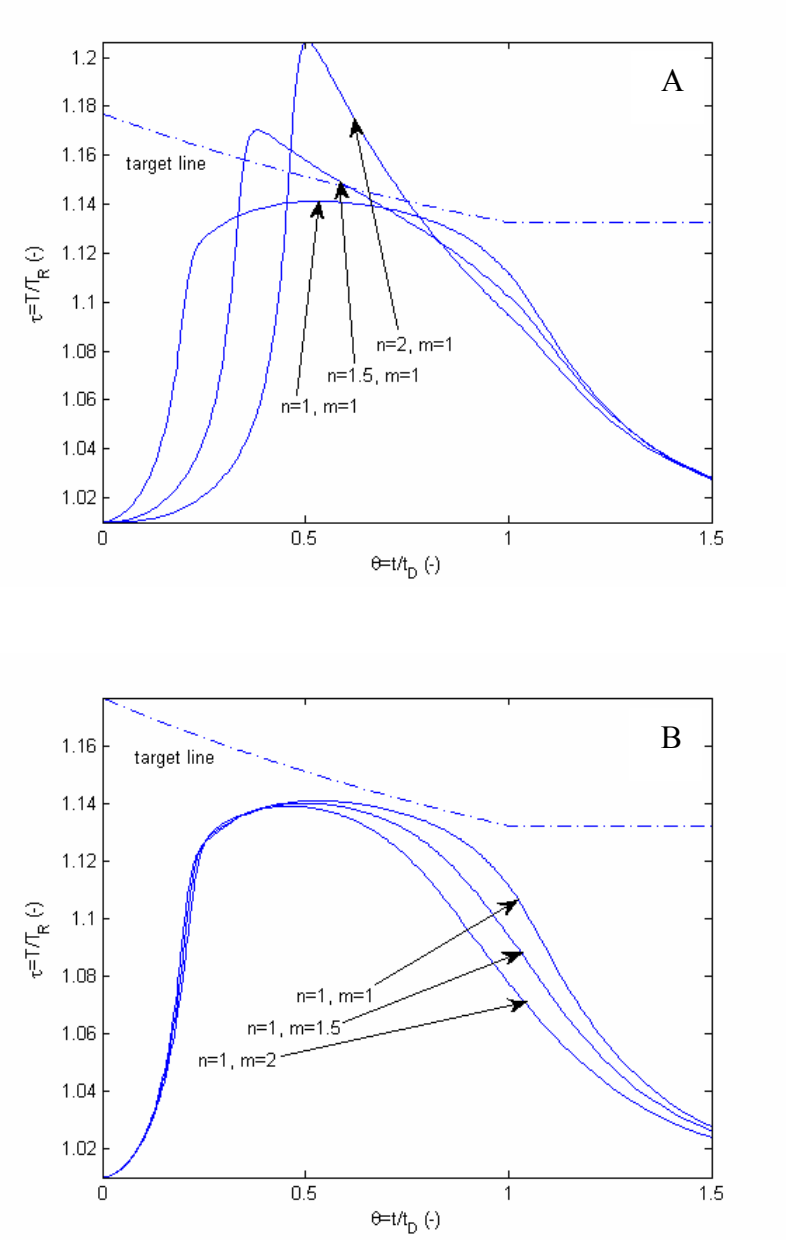

Figure 1 *Temperature-time profiles in a homogeneous SBR.* ν_A *Da RE=3,* ε*=0.4,* γ*=38,* R_H*=1,* $\Delta\tau_{ad,0}$*=0.7, Co=10. Coolant and dosing stream temperatures equal to the initial reactor temperature. A) influence of the reaction order of the coreactant, n; B) influence of the reaction order of the reactant initially charged in the reactor, m.*

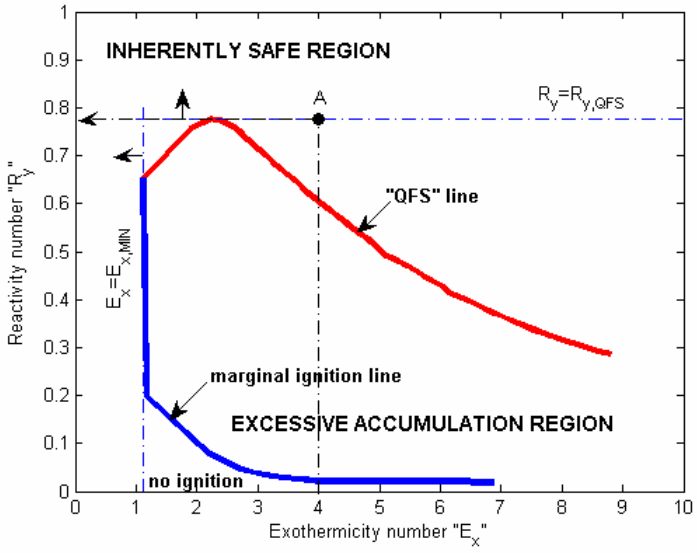

Figure 2 *Boundary diagram for the identification of excessive accumulation operating conditions in a homogeneous SBR.*

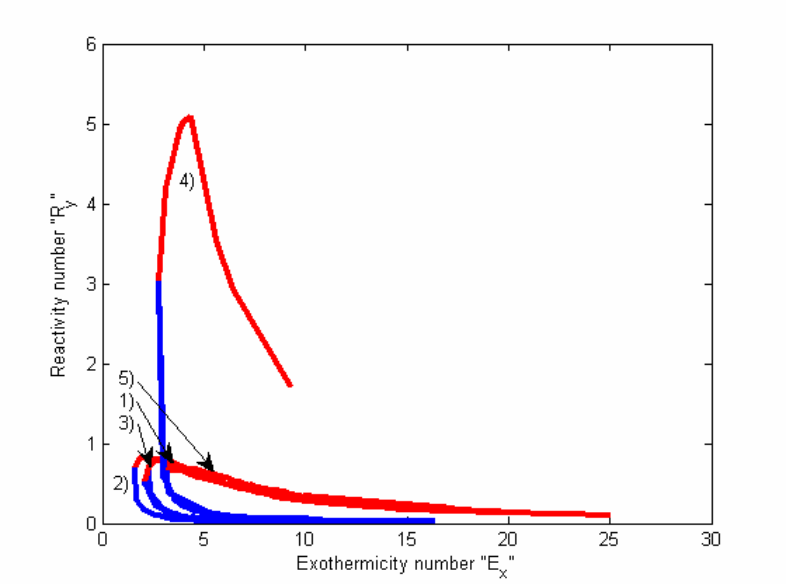

Figure 3 *Sensitivity of the boundary diagrams for homogeneous semibatch reactions with respect to the model parameters. 0.02< ν_A Da RE<20, 0.05<ε<0.6, 30<γ<45, 0.1<$\Delta\tau_{ad,0}$<0.7. 1) Co=10, R_H=1, n=1, m=1; 2) Co=20, R_H=1, n=1, m=1; 3) Co=10, R_H=2, n=1, m=1; 4) Co=10, R_H=1, n=2, m=1; 5) Co=10, R_H=1, n=1, m=2.*

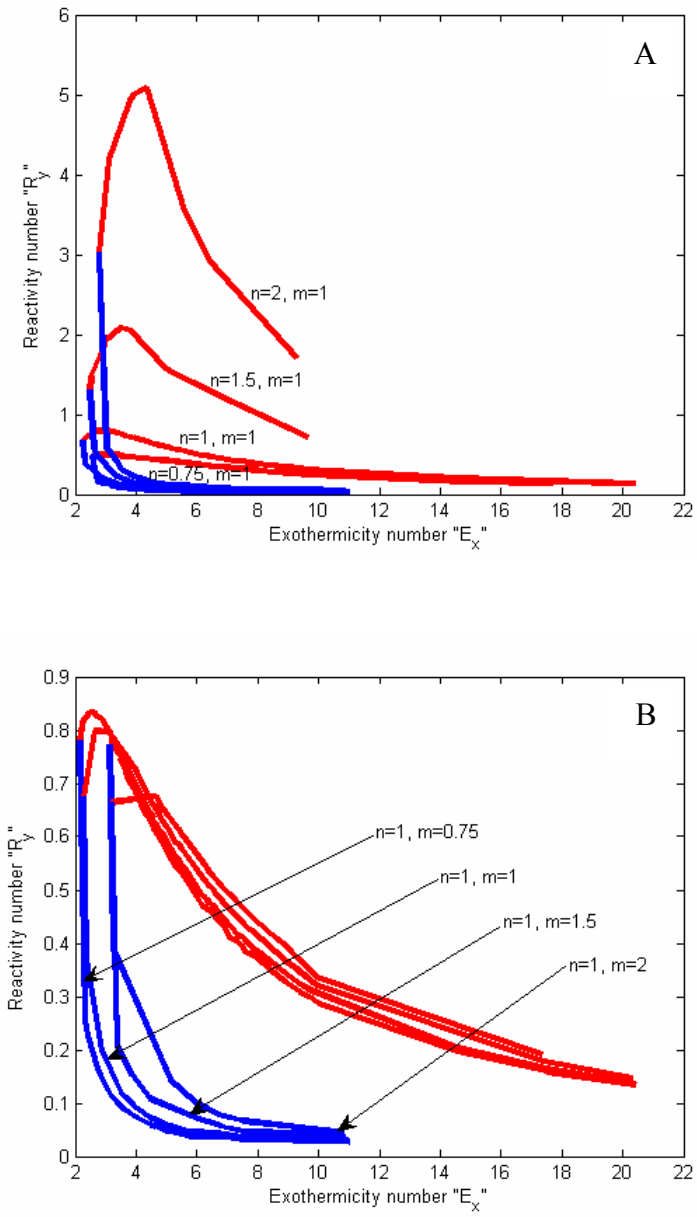

Figure 4 *Boundary diagrams for homogeneous (n,m) order reactions. 0.02< ν_A Da RE<20, 0.05<ε<0.6, 30<γ<45, 0.1<$\Delta\tau_{ad,0}$<0.7, Co=10, R_H=1. A) influence of the reaction order of the coreactant, n; B) influence of the reaction order of the reactant initially charged in the reactor, m.*

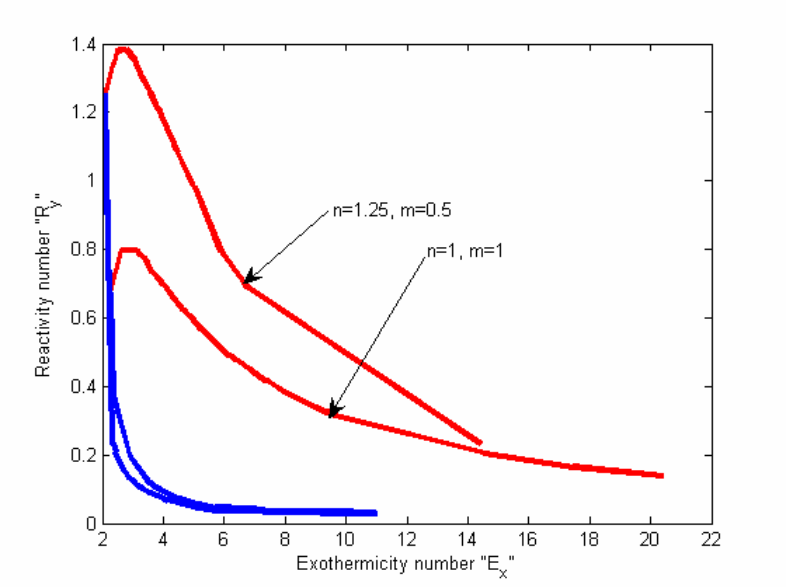

Figure 5 *Boundary diagrams for homogeneous (n,m) order reactions. 0.02< ν_A Da RE<20, 0.05<ε<0.6, 30<γ<45, 0.1<$\Delta\tau_{ad,0}$<0.7, Co=10, R_H=1.*

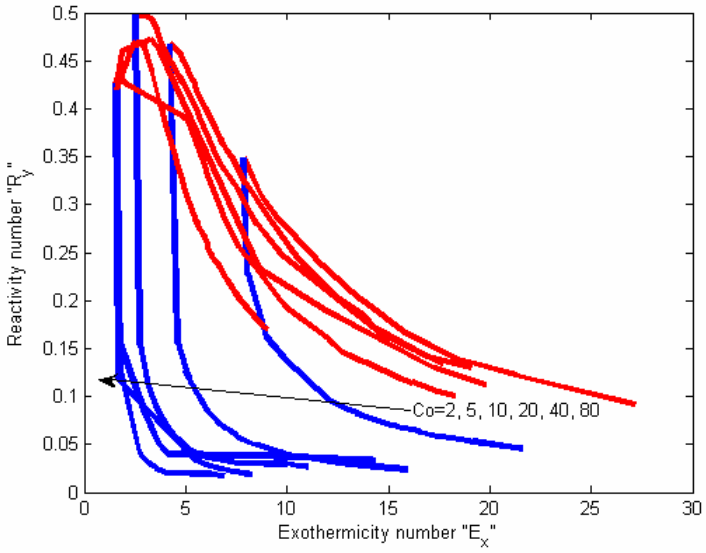

Figure 6 *Influence of the cooling number on the boundary diagrams shape and location. Homogeneous reactions with n=0.75, m=1, R_H=1. 0.02< ν_A Da RE<20, 0.05<ε<0.6, 30<γ<45, 0.1<$\Delta\tau_{ad,0}$<0.7.*

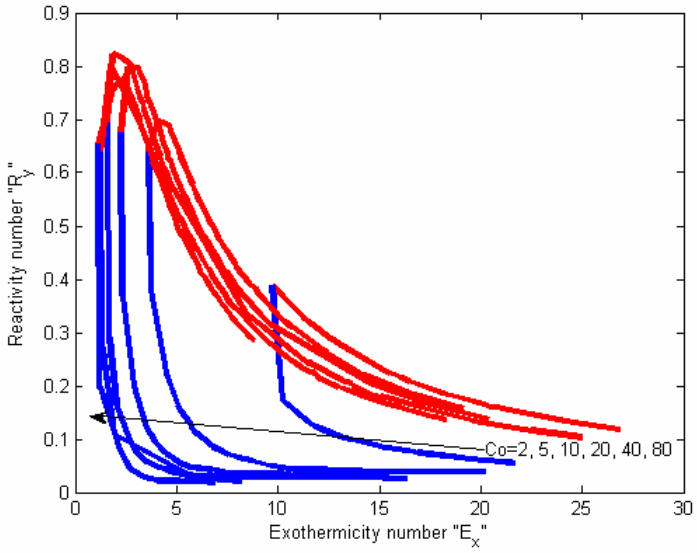

Figure 7 *Influence of the cooling number on the boundary diagrams shape and location. Homogeneous reactions with n=1, m=1, R_H=1. 0.02< ν_A Da RE<20, 0.05<ε<0.6, 30<γ<45, 0.1<$\Delta\tau_{ad,0}$<0.7.*

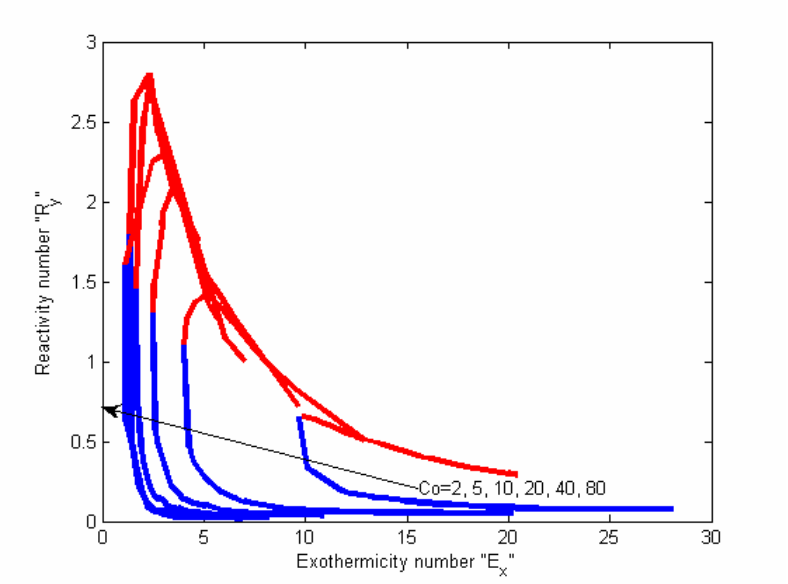

Figure 8 *Influence of the cooling number on the boundary diagrams shape and location. Homogeneous reactions with n=1.5, m=1, R_H=1. 0.02< ν_A Da RE<20, 0.05<ε<0.6, 30<γ<45, 0.1<$\Delta\tau_{ad,0}$<0.7.*

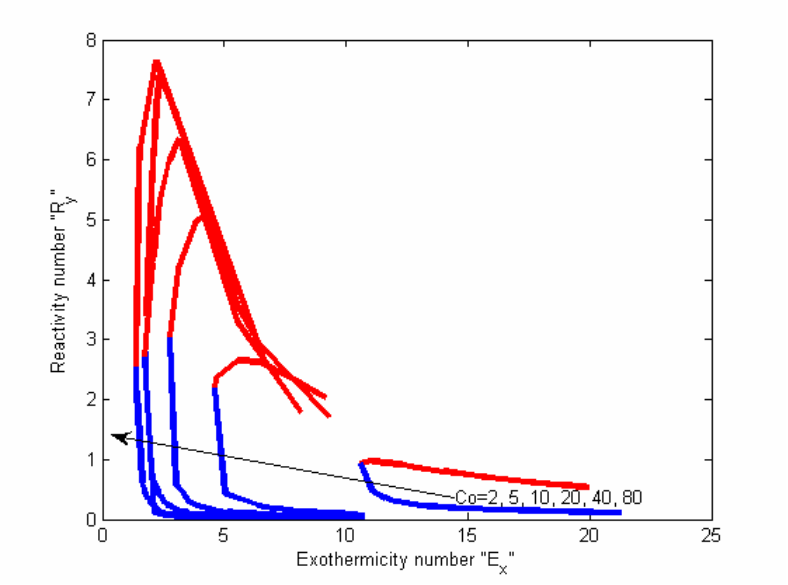

Figure 9 *Influence of the cooling number on the boundary diagrams shape and location. Homogeneous reactions with n=2, m=1, R_H=1. 0.02< ν_A Da RE<20, 0.05<ε<0.6, 30<γ<45, 0.1<$\Delta\tau_{ad,0}$<0.7.*

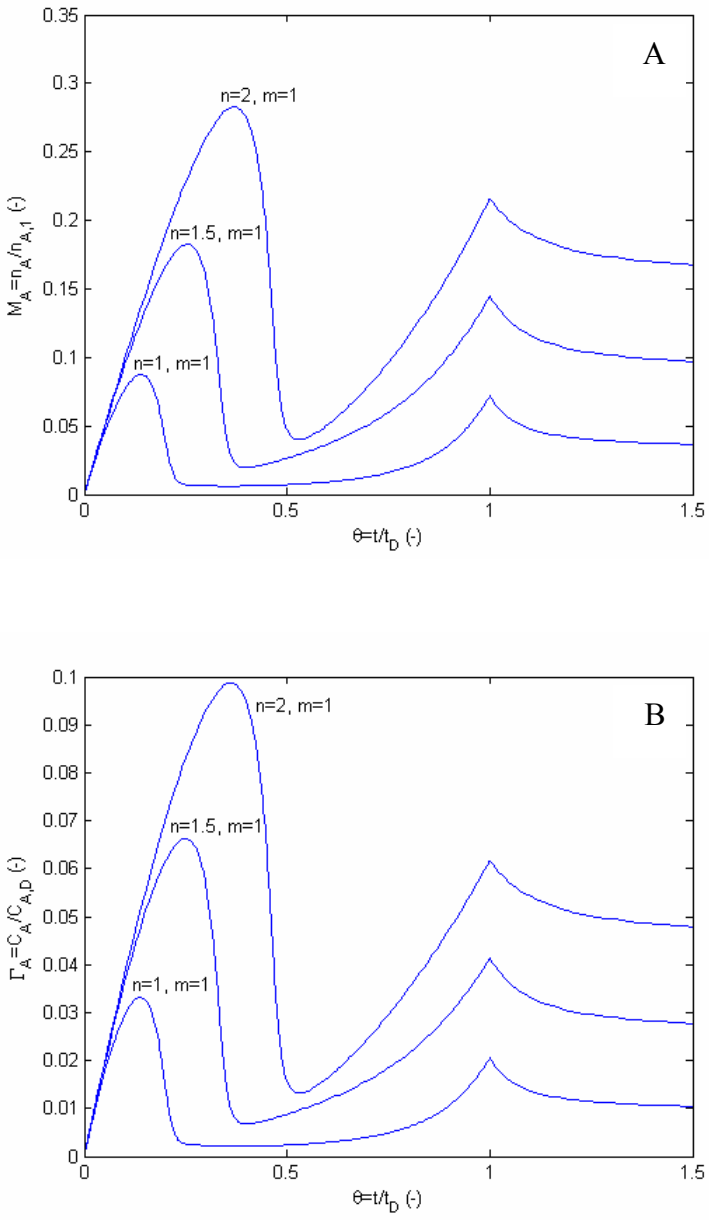

Figure 10 *Coreactant accumulation time-profiles in a homogeneous SBR.* ν_A *Da RE=3,* ε*=0.4,* γ*=38,* R_H*=1,* $\Delta\tau_{ad,0}$*=0.7, Co=10.* T_0*=303K,* T_R*=300K. Coolant and dosing stream temperatures equal to the initial reactor temperature. A) relative coreactant amount; B) relative coreactant concentration.*

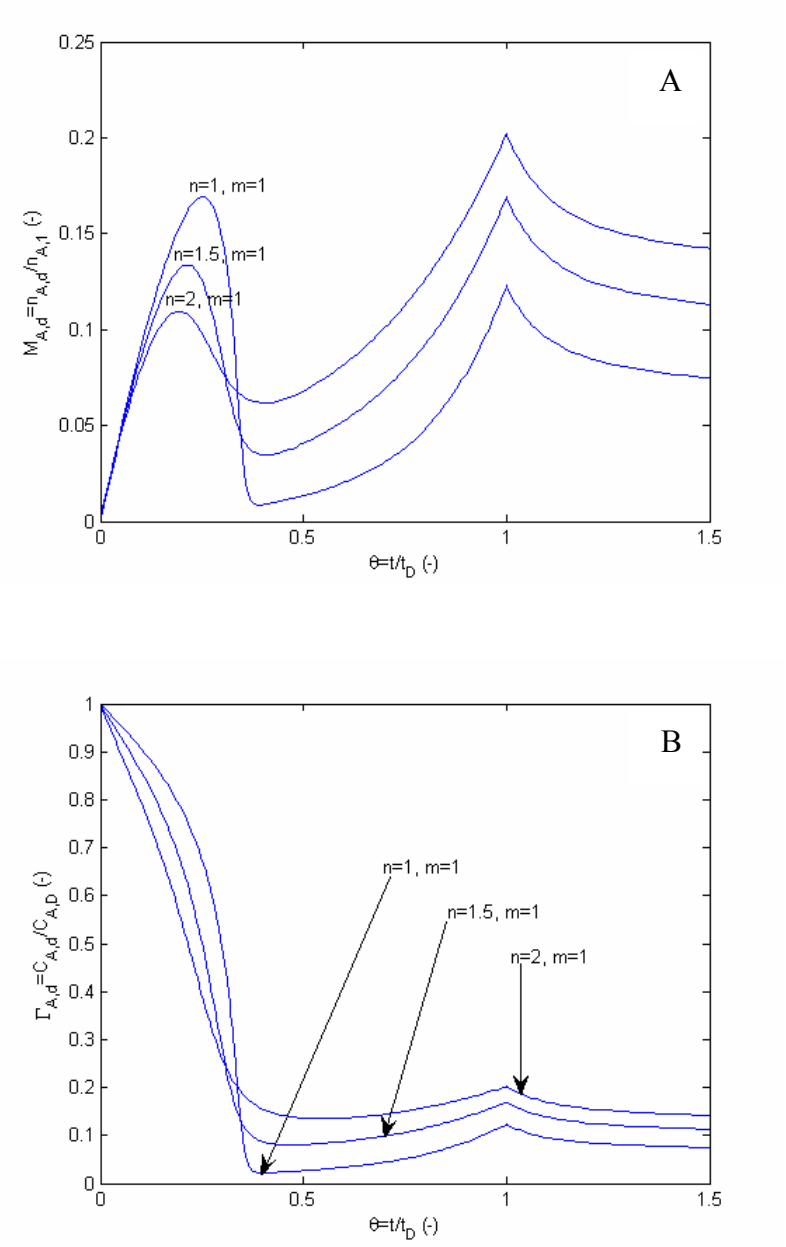

Figure 11 *Coreactant accumulation time-profiles in a heterogeneous (liquid-liquid) SBR. Slow reaction regime. Reaction occurring in the dispersed phase* ν_A *Da RE=1.8,* ε*=0.4,* γ*=38,* R_H*=1,* $\Delta\tau_{ad,0}$*=0.6, Co=10.* T_0*=* T_R*=300K. Coolant and dosing stream temperatures equal to the initial reactor temperature. A) relative coreactant amount; B) relative coreactant concentration.*

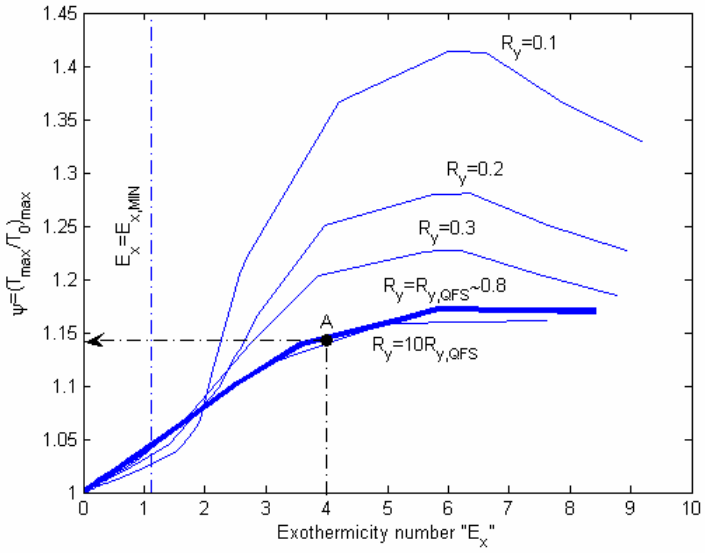

Figure 12 *Temperature diagram for the determination of the peak reaction temperature in a homogeneous SBR.*

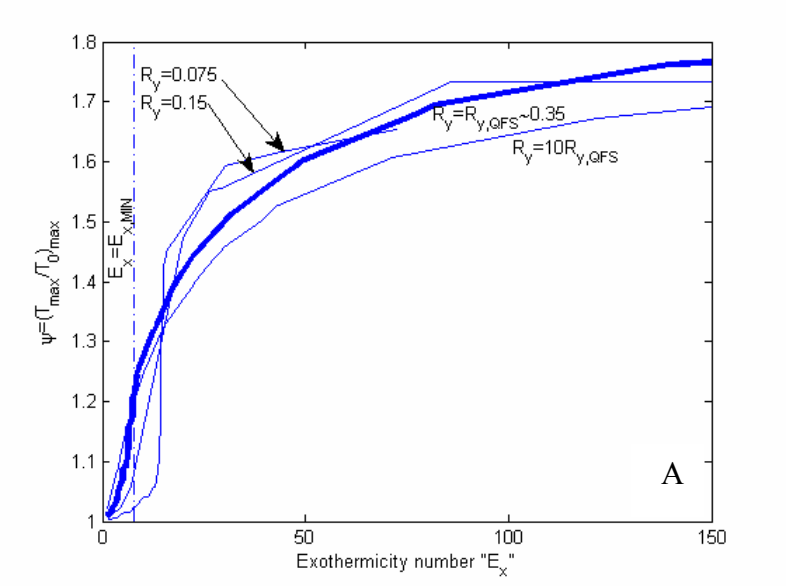
R_y=0.075
R_y=0.15
R_y=$R_{y,QFS}$~0.35
R_y=10$R_{y,QFS}$
E_x=$E_{x,MIN}$
ψ=(T_{max}/T_0)$_{max}$
Exothermicity number "E_x"
A

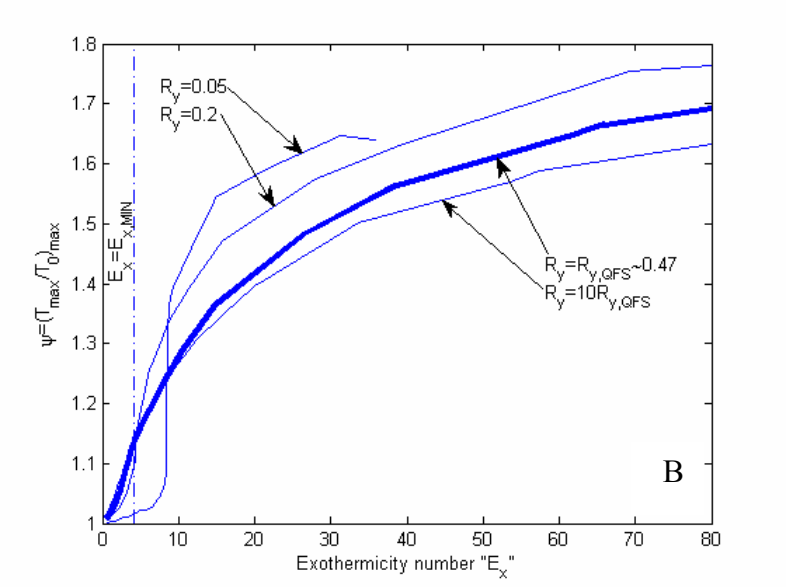
R_y=0.05
R_y=0.2
R_y=$R_{y,QFS}$~0.47
R_y=10$R_{y,QFS}$
E_x=$E_{x,MIN}$
ψ=(T_{max}/T_0)$_{max}$
Exothermicity number "E_x"
B

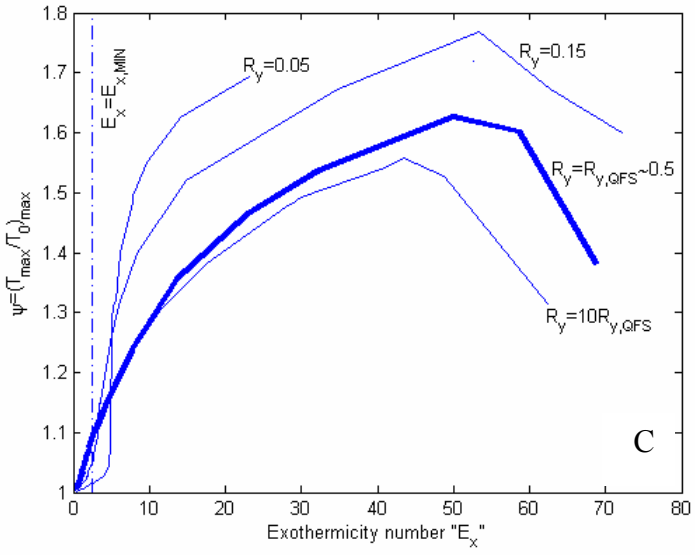
$E_X=E_{X,MIN}$
R_y=0.05
R_y=0.15
$R_y=R_{y,QFS}$~0.5
R_y=10$R_{y,QFS}$
$\psi=(T_{max}-T_0)/T_{0,max}$
Exothermicity number "E_X"
C

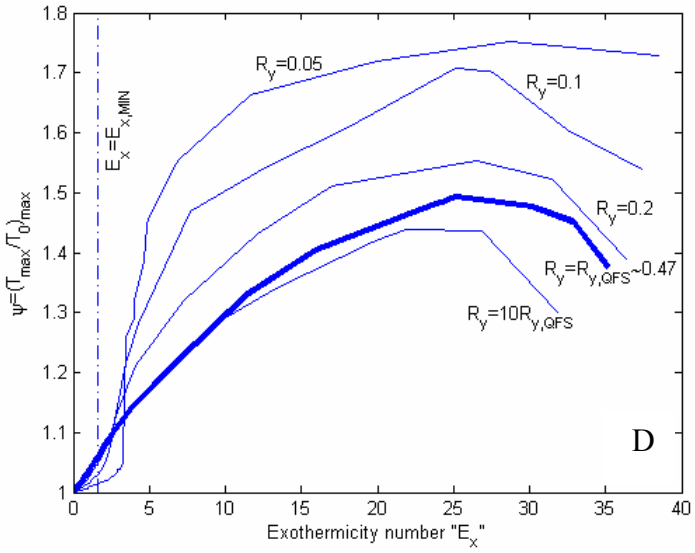
$E_X=E_{X,MIN}$
R_y=0.05
R_y=0.1
R_y=0.2
$R_y=R_{y,QFS}$~0.47
R_y=10$R_{y,QFS}$
$\psi=(T_{max}-T_0)/T_{0,max}$
Exothermicity number "E_X"
D

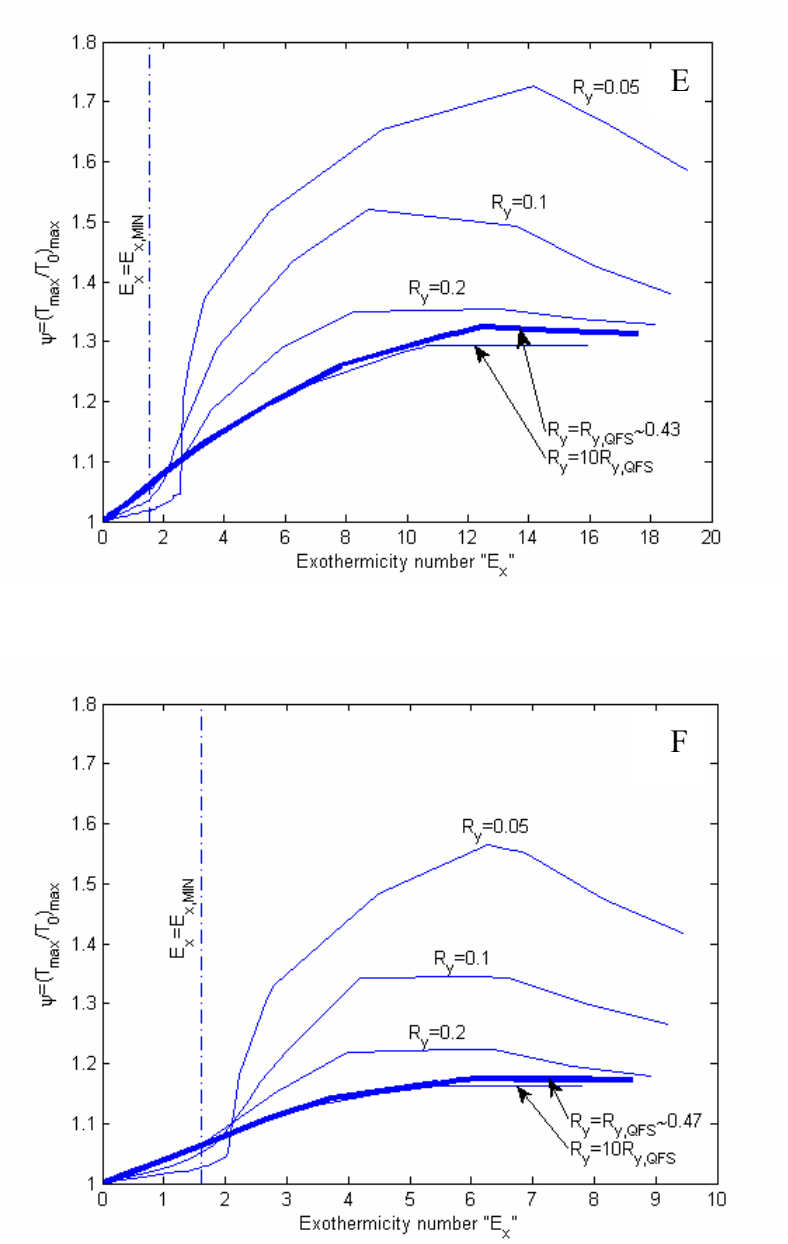

Figure 13 *Influence of the cooling number on the temperature diagrams for homogeneous SBRs with n=0.75, m=1, R_H=1. 0.02< ν_A Da RE<20, 0.05<ε<0.6, 30<γ<45, 0.1<$\Delta\tau_{ad,0}$<0.7. A) Co=2; B) Co=5; C) Co=10; D) Co=20; E) Co=40; F) Co=80.*

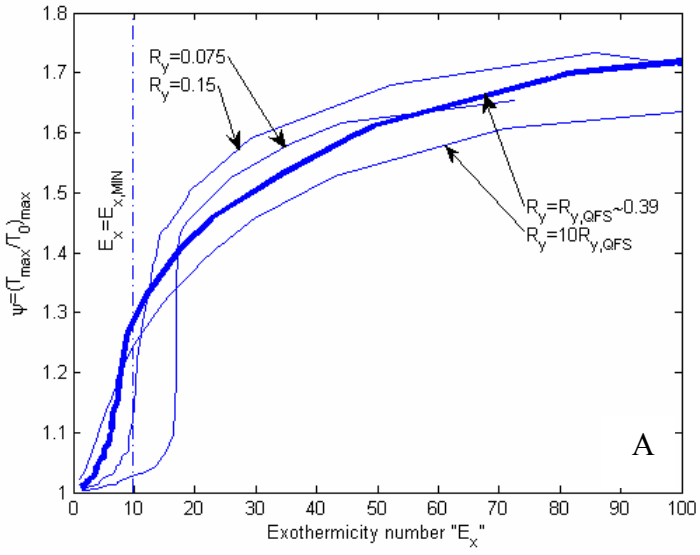
R_y=0.075
R_y=0.15
E_x=E_x,MIN
R_y=R_y,QFS~0.39
R_y=10R_y,QFS
A
ψ=(T_max/T_0)_max
Exothermicity number "E_x"

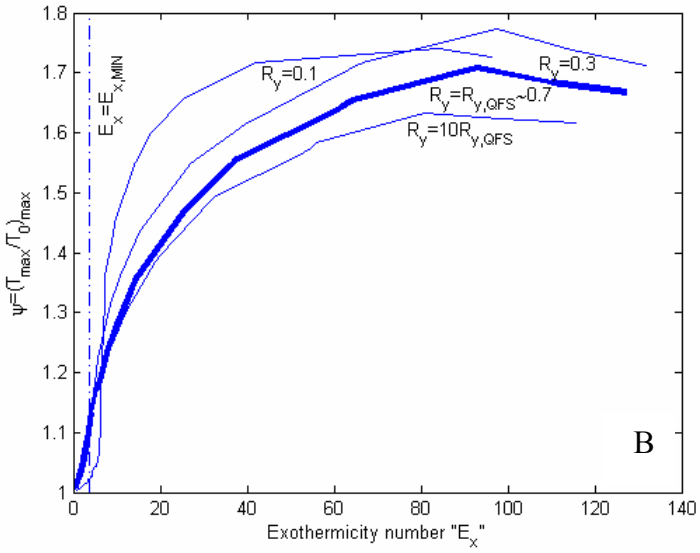
E_x=E_x,MIN
R_y=0.1
R_y=0.3
R_y=R_y,QFS~0.7
R_y=10R_y,QFS
B
ψ=(T_max/T_0)_max
Exothermicity number "E_x"

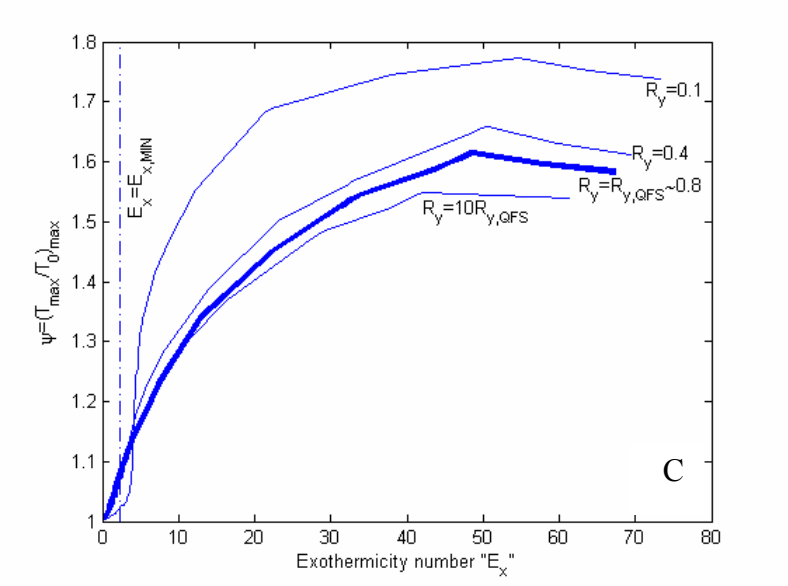
R_y=0.1
R_y=0.4
R_y=$R_{y,QFS}$~0.8
R_y=10$R_{y,QFS}$
E_x=$E_{x,MIN}$
ψ=(T_{max}/T_0)$_{max}$
Exothermicity number "E_x"
C

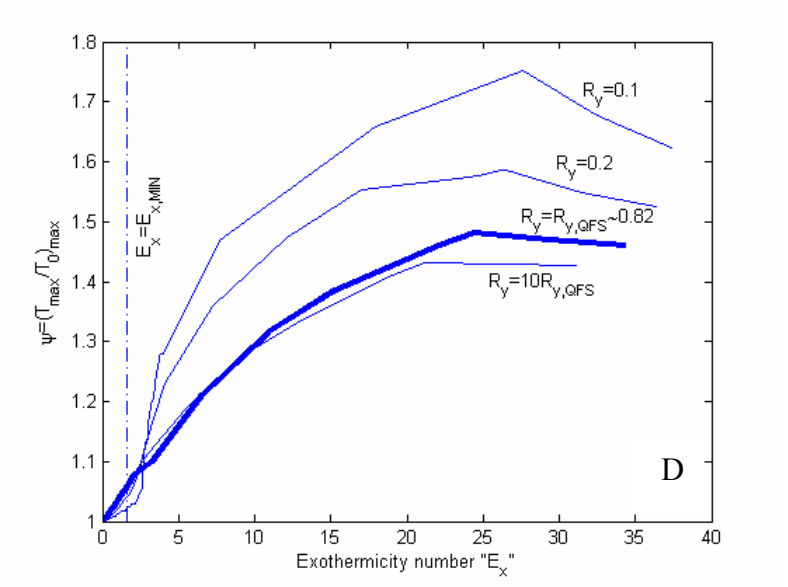
R_y=0.1
R_y=0.2
R_y=$R_{y,QFS}$~0.82
R_y=10$R_{y,QFS}$
E_x=$E_{x,MIN}$
ψ=(T_{max}/T_0)$_{max}$
Exothermicity number "E_x"
D

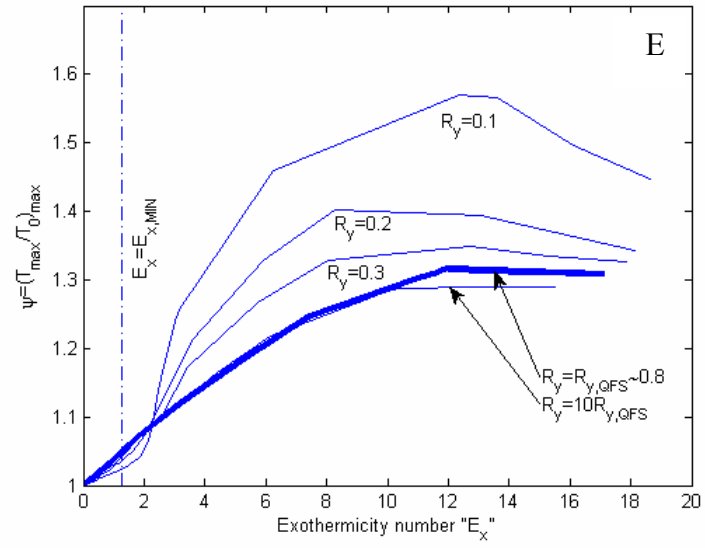

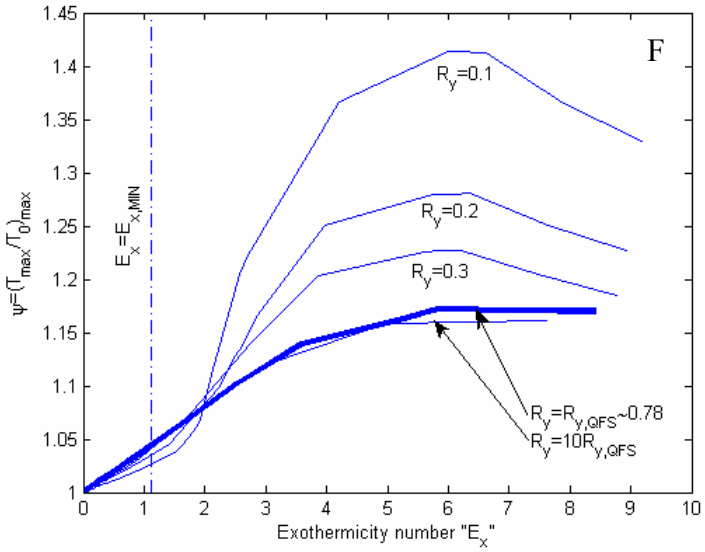

Figure 14 *Influence of the cooling number on the temperature diagrams for homogeneous SBRs with n=1, m=1, R_H=1. 0.02< ν_A Da RE<20, 0.05<ε<0.6, 30<γ<45, 0.1<$\Delta\tau_{ad,0}$<0.7. A) Co=2; B) Co=5; C) Co=10; D) Co=20; E) Co=40; F) Co=80.*

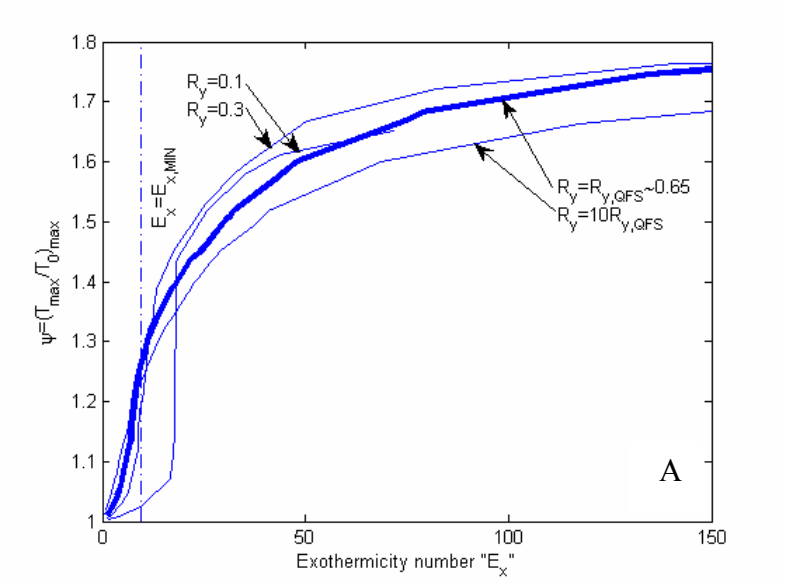
R_y=0.1
R_y=0.3
E_x=$E_{x,MIN}$
R_y=$R_{y,QFS}$~0.65
R_y=10$R_{y,QFS}$
A
ψ=(T_{max}/T_0)$_{max}$
Exothermicity number "E_x"

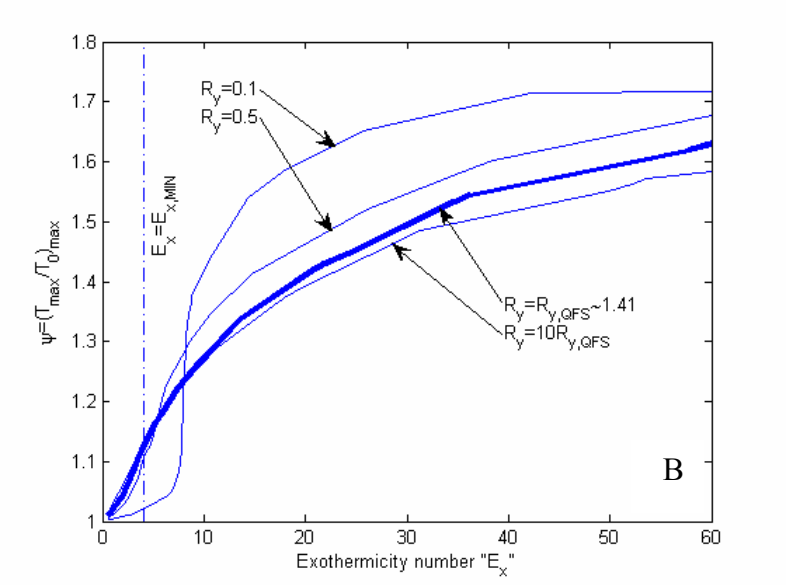
R_y=0.1
R_y=0.5
E_x=$E_{x,MIN}$
R_y=$R_{y,QFS}$~1.41
R_y=10$R_{y,QFS}$
B
ψ=(T_{max}/T_0)$_{max}$
Exothermicity number "E_x"

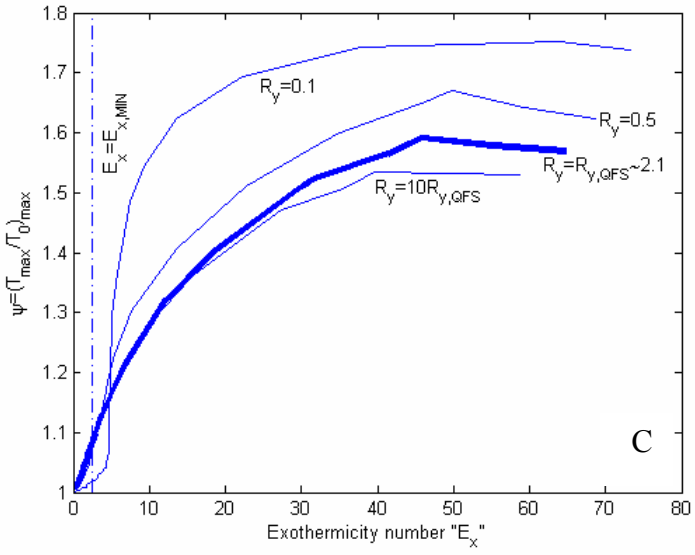
R_y=0.1
R_y=0.5
R_y=$R_{y,QFS}$~2.1
R_y=10$R_{y,QFS}$
E_x=$E_{x,MIN}$
ψ=(T_{max}/T_0)/max
Exothermicity number "E_x"
C

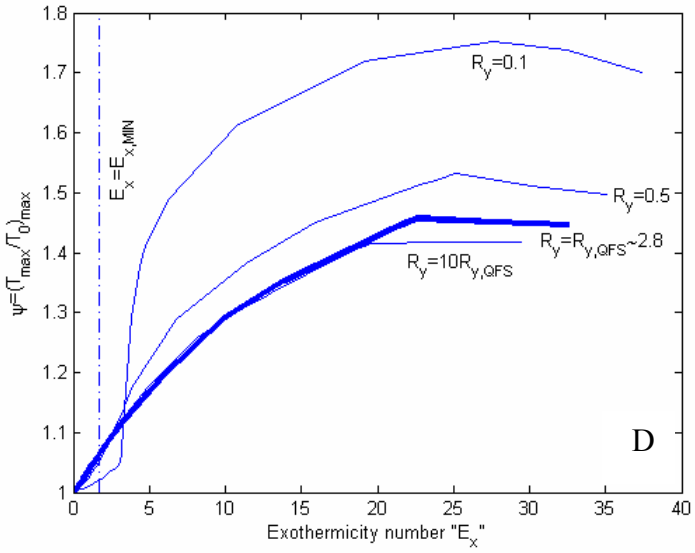
R_y=0.1
R_y=0.5
R_y=$R_{y,QFS}$~2.8
R_y=10$R_{y,QFS}$
E_x=$E_{x,MIN}$
ψ=(T_{max}/T_0)/max
Exothermicity number "E_x"
D

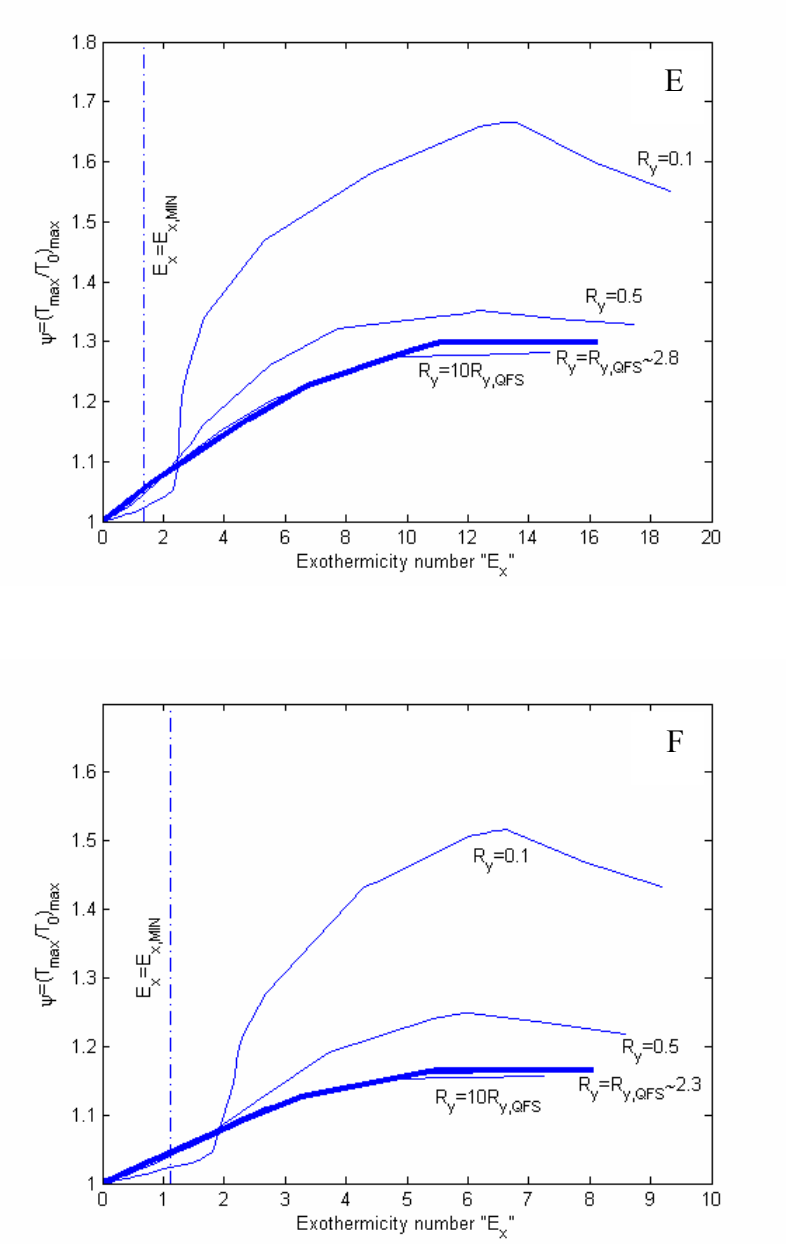

Figure 15 *Influence of the cooling number on the temperature diagrams for homogeneous SBRs with n=1.5, m=1, R_H=1. 0.02< ν_A Da RE<20, 0.05<ε<0.6, 30<γ<45, 0.1<$\Delta\tau_{ad,0}$<0.7. A) Co=2; B) Co=5; C) Co=10; D) Co=20; E) Co=40; F) Co=80.*

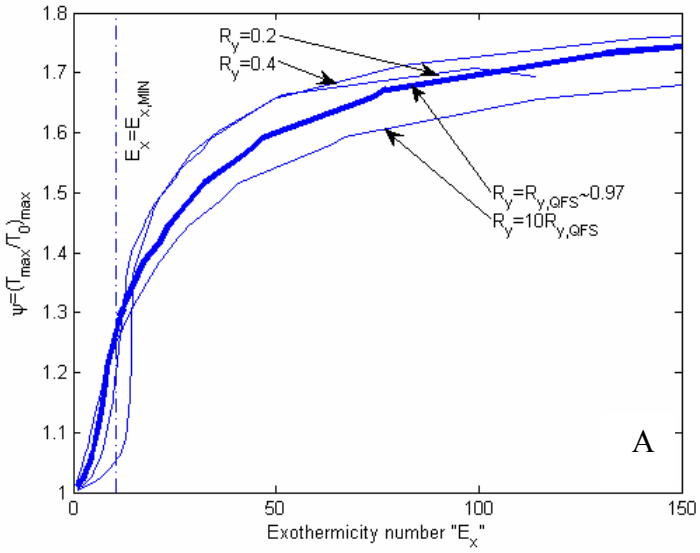
R_y=0.2
R_y=0.4
E_X=E_X,MIN
R_y=R_y,QFS~0.97
R_y=10R_y,QFS
A
ψ=(T_max-T_0)/T_0,max
Exothermicity number "E_X"

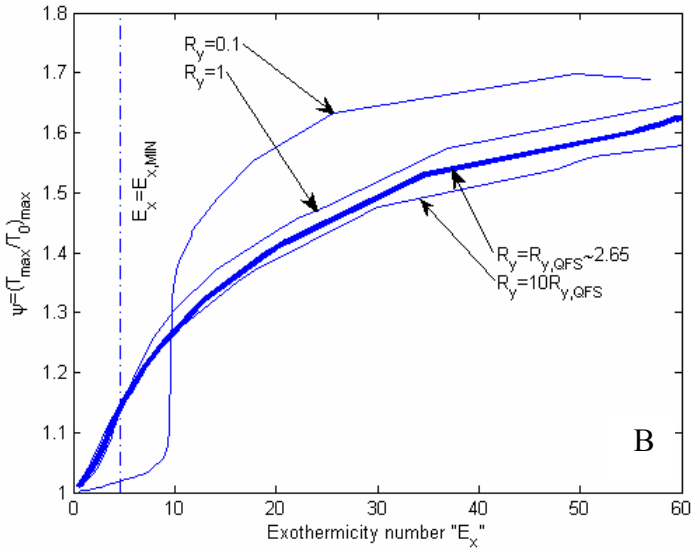
R_y=0.1
R_y=1
E_X=E_X,MIN
R_y=R_y,QFS~2.65
R_y=10R_y,QFS
B
ψ=(T_max-T_0)/T_0,max
Exothermicity number "E_X"

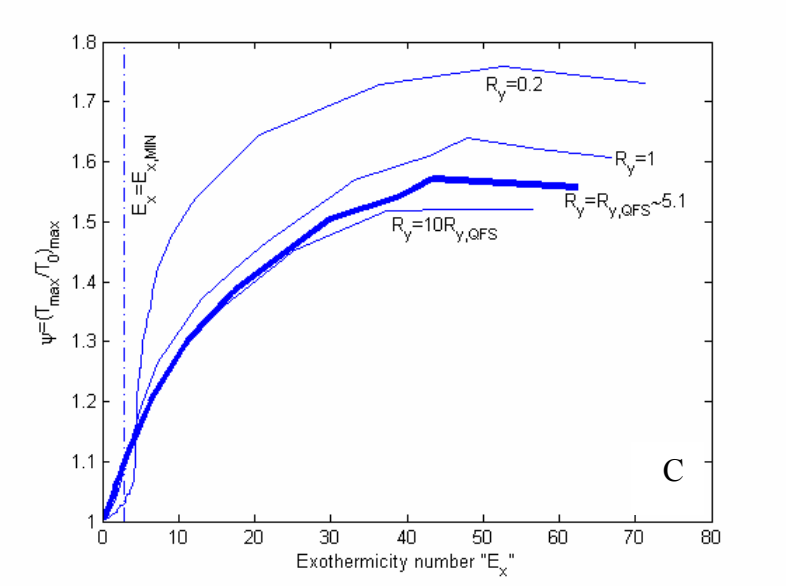
R_y=0.2
R_y=1
R_y=$R_{y,QFS}$~5.1
R_y=10$R_{y,QFS}$
E_x=$E_{x,MIN}$
ψ=(T_{max}/T_0)$_{max}$
Exothermicity number "E_x"
C

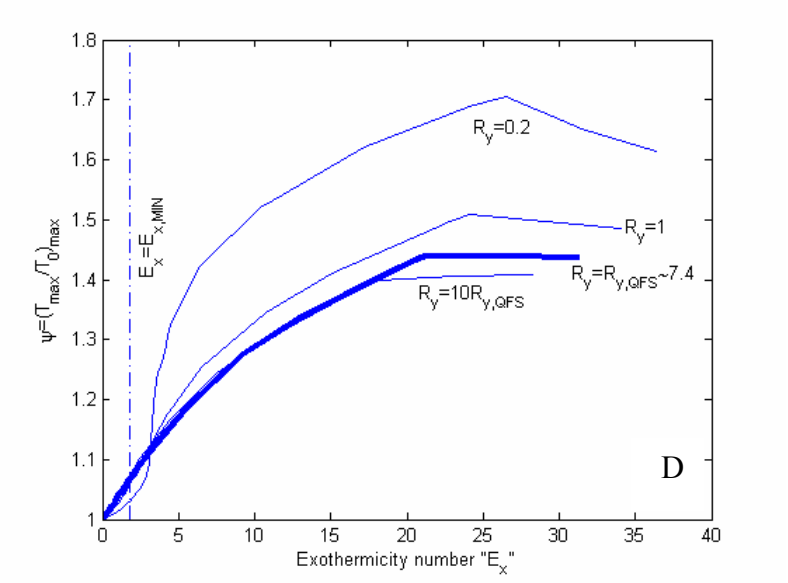
R_y=0.2
R_y=1
R_y=$R_{y,QFS}$~7.4
R_y=10$R_{y,QFS}$
E_x=$E_{x,MIN}$
ψ=(T_{max}/T_0)$_{max}$
Exothermicity number "E_x"
D

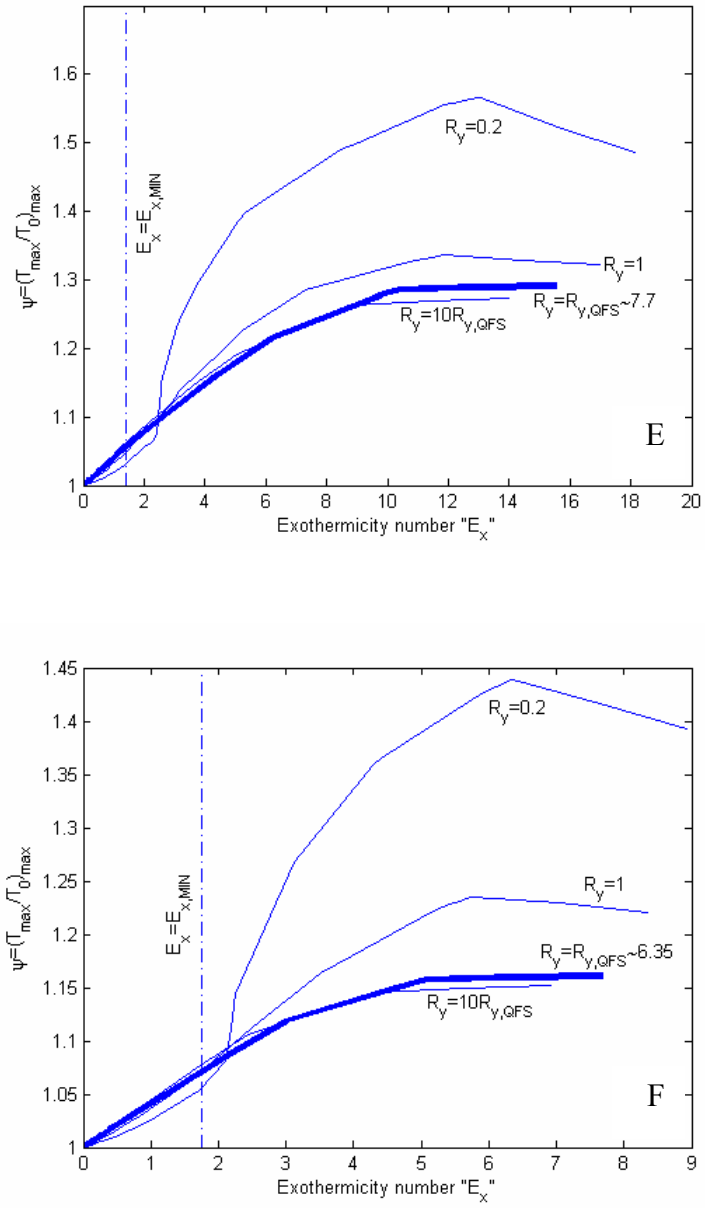

Figure 16 *Influence of the cooling number on the temperature diagrams for homogeneous SBRs with n=2, m=1, R_H=1. 0.02< ν_A Da RE<20, 0.05<ε<0.6, 30<γ<45, 0.1<$\Delta\tau_{ad,0}$<0.7. A) Co=2; B) Co=5; C) Co=10; D) Co=20; E) Co=40; F) Co=80.*

5. Safe and productive operation of homogeneous semibatch reactors with arbitrary reaction kinetics. Part II: the nitration of N-(2-phenoxyphenyl) methane sulphonamide

Francesco Maestri, Leonardo Re Dionigi, Renato Rota*

Politecnico di Milano

Dip. di Chimica, Materiali e Ingegneria Chimica "G. Natta"

via Mancinelli 7 - 20131 Milano - Italy

fax: +39 0223993180; e-mail: renato.rota@polimi.it

Lucia Gigante, Angelo Lunghi, Paolo Cardillo

Stazione Sperimentale per i Combustibili

viale De Gasperi 3 - 20097 San Donato Milanese - Milano - Italy

Abstract

The operation of indirectly cooled semibatch reactors in which nitration reactions are performed is often critical from the safety point of view, since nitric acid, under upset conditions, can oxidize a number of organic compounds, with further decomposition of one or more components of the reacting mixture: such events are typically accompanied by a much higher exothermicity than that of the desired reaction and by the evolution of high amounts of gases, that can lead to a dangerous increase of the reactor pressure. In order to prevent the triggering of such events, the nitric acid accumulation in the system during the normal reactor operation must be kept at sufficiently low values. The boundary and temperature diagrams are a useful tool for easily selecting operating conditions characterized by both a low nitric acid accumulation and peak reaction temperatures lower than a threshold value established for the single process.

* to whom correspondence should be addressed

In this work the method of boundary and temperature diagrams has been applied to the analysis of an industrial nitration process for the production of a pharmaceutical active ingredient, that is the nitration of N-(2-phenoxyphenyl) methane sulphonamide to N-(4-nitro, 2-phenoxyphenyl) methane sulphonamide, carried out in homogeneous phase in an indirectly cooled semibatch reactor, in which nitric acid is dosed over an acetic acid solution of the reactant. It has been verified through calorimetric experiments performed in a RC1 equipment that the boundary and temperature diagrams allow to safely select operating conditions characterized by a rapid nitric acid consumption, which imply a better thermal control of the reactor. Moreover, it has been shown that using the boundary and temperature diagrams method requires the knowledge of the reaction kinetics, at least in terms of a lumped expression corresponding to an optimum fitting of the experimental data. Such an information can be obtained through proper calorimetric experiments (e.g. performed in an adiabatic Phi-TEC II equipment): uncontrolled approximations on the reaction order of the dosed coreactant can lead to unsafe conclusions, whereas the requirements for the reaction order of the reactant initially charged in the reactor are much less stringent.

Keywords: Semibatch reactors; Boundary diagrams; Temperature diagrams; N-(2-phenoxyphenyl) methane sulphonamide; N-(4-nitro, 2-phenoxyphenyl) methane sulphonamide; Productivity; Runaway; Experiments.

5.1 Introduction

The safe operation of an indirectly cooled semibatch reactor (SBR) in which an exothermic reaction is carried out requires the accumulation of the coreactant in the system to be low enough that the cooling system can control the heat evolution. Such operating conditions prevent the thermal loss of control of the system, so that the reaction temperature rise with respect to the initial temperature can be limited below a critical value. This thermal behavior is of particular importance when the reaction mass can undergo decomposition reactions above a threshold temperature, which are normally characterized by a much higher exothermicity than that of the desired reaction and by the evolution of huge gas amounts: this can lead to a dangerous increase of the reactor pressure and -as an extreme consequence- to the explosion of the reactor itself if it is not equipped with a properly sized vent system.

In the last thirty years a huge amount of work has been done in order to develop simple and reliable criteria for selecting low accumulation operating conditions in indirectly cooled SBRs. A method based on the coreactant accumulation in the system has been firstly introduced by Hugo et al. [1-3], who developed a semi-empirical correlation for homogeneous SBRs.

This method has been then extended to heterogeneous (liquid-liquid) SBRs by Steensma and Westerterp [4-6] and Westerterp and Molga [7,8] who provided a more rigorous definition of coreactant accumulation in a SBR introducing the concept of a target temperature time profile, to which the actual reactor temperature evolution can be compared in order to classify the thermal behavior of the reactor itself: such an information has been then summarized in the so called boundary diagrams, which, in a suitable dimensionless space, allow to easily discriminate between safe and excessive accumulation operating conditions without solving the mathematical model of the reactor.

An experimental validation of the boundary diagrams method has been performed by van Woezik and Westerterp [9,10], who analyzed the nitric acid oxidation of 2-octanol to 2-octanone with further oxidation of the reaction product to unwanted carboxylic acids.

Maestri and Rota [11,12] analyzed the influence of the whole set of kinetic parameters on the conclusions drawn through the boundary diagrams, proving that a detailed kinetic investigation (performed through calorimetric techniques) on the system of interest is of crucial importance for a reliable application of the method: such a conclusion holds for both heterogeneous and homogeneous reaction systems.

Moreover, when a threshold temperature (in the following referred to as the Maximum Allowable Temperature, MAT) must not be exceeded neither during normal nor during upset reactor operation, limiting accumulation phenomena can be just a necessary, not a sufficient condition in order to accept a given set of operating conditions: such a temperature limitation can

arise from a number of chemical or plant factors [13]. For these reasons, in the first part of this work [14] a new typology of diagrams (called temperature diagrams) to be coupled with the boundary diagrams has been provided for homogeneous SBRs. These diagrams allow to safely predict the maximum temperature increase with respect to the initial temperature to be expected for a given set of operating conditions.

In this work, the final reaction step for the synthesis of a pharmaceutical active ingredient that is, the nitration of N-(2-phenoxyphenyl) methane sulphonamide (FAM) to N-(4-nitro, 2-phenoxyphenyl) methane sulphonamide (NIM) has been analyzed both theoretically and experimentally. Nitration processes are frequently involved in industrial accidents because nitric acid, under upset reaction conditions, can oxidize a lot of organic compounds with the evolution of huge heat amounts. Moreover, a number of nitro-compounds can undergo strongly exothermic decomposition reactions above a threshold temperature. Such events are mainly favoured by excessive nitric acid accumulations in the system and by the exceeding of a threshold temperature during the reactor operation. For these reasons SBRs in which nitration processes are carried out must be operated under conditions in which the nitric acid consumption occurs at a much smaller time scale than the nitric acid dosing. Once a kinetic investigation on the system of interest has been performed, the boundary and temperature diagrams are a powerful tool to easily select such operating conditions, without solving the mathematical model of the reactor. In the present work, after a preliminary characterization of the thermal stability of the reaction mass carried out through DSC measurements, the reaction calorimeter Phi-TEC II has been used to estimate the thermodynamic parameters for the system of interest and to derive a rate of reaction expression. The boundary and temperature diagrams have been then used to perform an a-priori selection of the operating conditions of an RC1 calorimeter, through which the previously derived kinetic expression has been validated and the selected set of operating conditions experimentally tested. The conclusions drawn through the boundary and temperature diagrams have been found to be consistent with the experimental results, allowing to safely select operating conditions characterized by both a sufficiently low nitric acid accumulation during the supply period and peak reaction temperatures lower than the MAT.

5.2 Reaction system

The nitration of FAM is carried out in indirectly cooled SBRs in which a 65% w/w nitric acid aqueous solution is added to a 17% w/w acetic acid solution of FAM, previously charged in the reactor. The reaction involved, occurring in homogeneous phase, is:

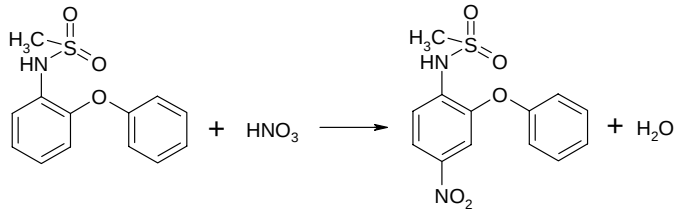

(1)

FAM + HNO_3 → NIM + H_2O

The relevant thermodynamic properties of reaction (1) have been firstly estimated through the Benson contribution groups method, using the software CHETAH of ASTM [15]: a relatively high value of the reaction enthalpy has been calculated (that is, -127.4kJ/mol), which is typical of nitration reactions.

When analyzing an exothermic reaction process from the safety point of view, the thermal stability of each species as well as of the reaction mixture should be previously investigated. Such an information can be as a first approach derived from the chemical structure of each species involved, checking whether functional groups that are typically responsible for the thermodynamic instability of a molecule are present: for the sake of example, a number of nitro-compounds are thermodynamically unstable, since they incorporate in their chemical structure both the oxidizing agent and the substrate to be oxidized. Through the aforementioned software CHETAH of ASTM it is possible to estimate an energy release potential (ERP) of a chemical species, arising from the combination of a number of criteria [15], involving the heat of decomposition, the heat of combustion and an oxygen stoichiometric balance for the molecule: the lower the ERP value is, the higher the thermal instability of the substance is. In Figure 1 the ERP values of the reaction mass as a function of the conversion of FAM are plotted. It can be noticed that:

- the ERP value decreases as the FAM conversion increases. This means that the concentration of the reaction product (NIM) is the factor influencing the thermal stability of the reaction mass. In particular, the most critical situation occurs as the reaction extent reaches 100%;
- the ERP value of NIM is lower than that of the initial reaction mass but much higher than that of the final reaction mass. This means that the thermal stability of the product is greatly lowered by the other components of the final reaction mixture.

These conclusions have been then verified through DSC experiments. In Figure 2 the DSC thermal characterizations of FAM and NIM in static air and static nitrogen respectively are reported. For both the products an endothermic effect associated to the solid-liquid transition can be observed. Moreover, for the measurements carried out in static air an exothermic effect related to the product oxidation has been detected at higher temperatures. In Figure 2 the same

characterization for the final reaction mass in static air is also reported. It can be observed that the final reaction mixture undergoes a strongly exothermic decomposition event at 210°C, not detected for the pure species (FAM and NIM): this proves that the thermal instability of the reaction product is enhanced by the other components of the final reaction mixture.

The set of kinetic parameters for the system of interest as well as the relevant thermodynamic properties of reaction (1) have been estimated through adiabatic experiments performed in a Phi-TEC II calorimeter equipped with a 120cm^3 cell, dosing 2.17g of a 65% w/w nitric acid aqueous solution over 31.9g of a 17% w/w acetic acid solution of FAM at 85°C: such an initial temperature has been selected taking into account that at 65°C the product crystallizes from the reaction mixture and that the solvent boiling point is equal to 120°C. An observed temperature rise equal to 13°C has been measured, which, accounting for the thermal inertia of the calorimeter, corresponds to an effective temperature rise equal to 32.5°C. Moreover, a reaction enthalpy equal to -110kJ/mol has been estimated, which is in good agreement with the value previously calculated through the CHETAH software of ASTM. The experimental data (temperature vs. time) have been then fitted through a power law type expression, using the MATLAB suite of programs. The rate of reaction expression corresponding to the best fit of the aforementioned data is:

$$r = k_{n=2,\, m=0.2} \cdot C_{HNO_3}^{2} C_{FAM}^{0.2} \tag{2}$$

where $k_{n=2,\, m=0.2} = 6.44 \cdot 10^{15} \exp\left(-1.127 \cdot 10^{5} / RT\right)$ and the units are kJ, kmol, K, m^3, s. The parity plot of this fitting is represented in Figure 3. The value of the mean squared relative error:

$$\sigma = 100 \cdot \sum_{j=1}^{n_{data}} \left(\frac{T_{j,e} - T_{j,c}}{T_{j,e}} \right)^2 \tag{3}$$

is equal to 0.1%, where $T_{j,e}$ and $T_{j,c}$ are the measured and computed values of the reaction temperature at time t_j.

5.3 Mathematical model

As previously mentioned, the nitration of FAM is carried out in indirectly cooled SBRs filled with a 17% w/w acetic acid solution of the reactant. At time equal to zero the feed of a 65% w/w nitric acid aqueous solution is started at a constant rate, until the stoichiometric quantity of nitric acid has been fed. The following model assumptions can be reasonably stated:

1) the reaction mass is perfectly mixed;
2) the influence of the chemical reaction on the reaction volume is negligible; this means that the reaction volume increases during the supply period only because of the nitric acid

dosing, whereas the changes in the system density related to the composition evolution can be disregarded;

3) the heat effects are associated with the chemical reaction only;
4) the reactor operates in isoperibolic conditions; in particular, at time equal to zero, the reaction mass temperature is equal to the mean coolant temperature and to the dosing stream temperature, which remain constant for the whole duration of the process.

The concentrations of nitric acid and FAM as a function of the dimensionless time $\vartheta=t/t_D$ and of the conversion $\zeta_{FAM}=1-n_{FAM}/n_{FAM,0}$ can be evaluated through the following expressions [14]:

$$C_{HNO_3} = C_{FAM,0}\,\frac{\vartheta-\zeta_{FAM}}{1+\varepsilon\vartheta} \tag{4}$$

$$C_{FAM} = C_{FAM,0}\,\frac{1-\zeta_{FAM}}{1+\varepsilon\vartheta} \tag{5}$$

where $\varepsilon=V_D/V_{r,0}$ is the relative volume increase at the end of the supply period.

The mass balance equation for FAM can be written as:

$$\frac{d\zeta_{FAM}}{d\vartheta} = k_{n=2,\,m=0.2}\cdot t_D\cdot C_{FAM,0}^{1.2}\cdot f \tag{6}$$

where $f=[(\vartheta-\zeta_{FAM})^2(1-\zeta_{FAM})^{0.2}]/(1+\varepsilon\vartheta)^{1.2}$ is the only factor containing the functional dependence on ϑ and ζ_{FAM}; the units employed in eq. (6) are kJ, kmol, K, m^3, s.

The energy balance for the reactor yields:

$$(1+\varepsilon\vartheta)\frac{dT}{d\vartheta} = \Delta T_{ad,0}\,\frac{d\zeta_{FAM}}{d\vartheta} - \varepsilon\left[Co(1+\varepsilon\vartheta)+R_H\right](T-T_{cool}) \tag{7}$$

where $\Delta T_{ad,0}$ is the adiabatic temperature rise, containing the physical information about the reaction enthalpy, $Co=(UA)_0\,t_D\big/\left(\tilde{\rho}_m\tilde{C}_{P,m}V_D\right)$ is the cooling number, which is related to the heat transfer efficiency and to the volumetric feed rate and $R_H=\left(\tilde{\rho}\tilde{C}_P\right)_D\big/\left(\tilde{\rho}\tilde{C}_P\right)_m$ is the average ratio between the volumetric heat capacities of the dosing stream and the reaction mixture. The model eqs. (4) to (7), that are valid during the supply period, can be easily extended to $\vartheta>1$ by substituting everywhere the $\vartheta-\zeta_{FAM}$ terms with $1-\zeta_{FAM}$ and the $\varepsilon\vartheta$ terms with ε.

The numerical integration of eqs. (6) and (7) with the related initial conditions (that is: $\zeta_{FAM}=0$ and $T=T_0$ at $\vartheta=0$) results in the conversion and temperature time profiles according to the model stated, that will be compared in the following with the corresponding experimental profiles.

5.4 Development of the safety criterion

In order to prevent excessive nitric acid accumulation in the system, operating conditions must be selected that imply maximum reaction temperatures lower than a local target value, defined as [14]:

$$T_{ta,\max} = T_{cool} + 1.05\frac{\Delta T_{ad,0}}{\varepsilon\left[Co\left(1+\varepsilon\vartheta_{\max}\right)+R_H\right]} \tag{8}$$

where ϑ_{max} is the dimensionless time at which the peak reaction temperature occurs and the $\varepsilon\vartheta_{max}$ term must be replaced with ε if $\vartheta_{max}>1$.

In order to perform an easy a-priori selection of the aforementioned operating conditions, boundary and temperature diagrams can be calculated and used. The dimensionless space in which such diagrams are represented consists of two parameters, that is an exothermicity number, E_x, related to the reaction enthalpy and a reactivity number, R_y, related to the initial dependence of the conversion rate on temperature. For this reaction system, the expressions for evaluating such parameters become [14]:

$$E_x = \frac{E}{RT_{cool}^2}\frac{\Delta T_{ad,0}}{\varepsilon\left(Co+R_H\right)} \tag{9}$$

$$R_y = \frac{k_{n=2,\,m=0.2}\left(T_{cool}\right)\cdot t_D \cdot C_{FAM,0}^{1.2}}{\varepsilon\left(Co+R_H\right)} \tag{10}$$

Operating conditions implying a couple of (E_x,R_y) values belonging to the inherently safe region of the related boundary diagram correspond to a situation of ignited reaction in which the peak reaction temperature cannot exceed the local target value (8). On the contrary, operating conditions located inside the excessive accumulation region correspond to situations in which the peak reaction temperature can exceed the local target value.

However, even operating conditions implying a low coreactant accumulation can be characterized by too high values of the initial reaction temperature, leading to a maximum temperature during normal reactor operation higher than the MAT. This is the case of the nitration process in question, for which such a temperature limitation can arise either from the solvent boiling point, that occurs at 120°C, or from the possible triggering of a dangerous decomposition event of the final reacting mixture, that occurs at 210°C. Since solvent boiling should be prevented in the reactor selected for the industrial production, the former value defines the maximum allowable temperature (MAT) for the process. The fulfilment of this constraint can be analyzed through the so called temperature diagrams [14]. Such diagrams, through the same set of dimensionless parameters used for the representation of the boundary diagrams, provide the

maximum temperature increase with respect to the initial temperature that can be expected to occur for a given set of operating conditions: this is the information to be compared with the previously defined MAT.

5.5 Experimental set-up and procedure

The reaction calorimeter RC1 has been used both to validate the kinetic expression previously derived from the data fitting of adiabatic Phi-TEC II experiments and to identify operating conditions characterized by both a low nitric acid accumulation and peak reaction temperatures lower than the MAT. The equipment consists of a stirred 2.5 lt glass reaction vessel with a jacket in which a diathermic fluid circulates. An external cryostat removes the reaction heat. The calorimeter is equipped with a PID temperature control system that can operate in the three following modes:

- in the T_{jacket} mode isoperibolic experiments can be performed, the controlled variable being the mean coolant temperature between the inlet and the outlet sections of the jacket;
- in the $T_{reactor}$ mode isothermal experiments can be performed, the controlled variable being the reaction mass temperature;
- in the adiabatic mode the controlled variable is the temperature difference between the jacket and the reactor, which is set to zero.

Calibration tests carried out with the initial and final reaction mixtures, led to average values of the overall heat transfer coefficient and of the heat capacity of the reaction mixture equal to 160W/(m^2 K) and 2kJ/(kg K), respectively. The other relevant process and equipment parameters are summarized in Table 1: the experiments have been carried out dosing 43.4g of a 65% w/w nitric acid aqueous solution over 639.2g of a 17% w/w acetic acid solution of FAM.

In order to identify operating conditions (in terms of initial reaction temperature and dosing time) characterized by both a low nitric acid accumulation and a peak reaction temperature lower than the MAT value, the number of RC1 experiments has been minimized performing an a-priori screening of the aforementioned operating conditions through the boundary and temperature diagrams. For homogeneous reaction systems, such diagrams are identified through a set of the Co, R_H, n and m values, the only parameter depending on the selected operating conditions (and in particular on the volumetric feed rate, $Q_D=V_D/t_D$) being the cooling number, Co. Assuming nitric acid dosing times equal to 3, 5, 7 and 12 minutes, the resulting cooling numbers vary approximately between 10 and 50. For each dosing time three initial reaction temperatures have been selected, namely 68, 78 and 88°C, according to the previously mentioned constraints on the

reaction temperature itself. These operating conditions have been labelled through a number, representing the dosing time in minutes, and a letter, related to the initial reaction temperature, that is a, b and c for T_0=68, 78 and 88°C, respectively. In Figures 4 to 7 four couples of related boundary and temperature diagrams are reported, corresponding to the four selected values of the dosing time, t_D (and hence of the cooling number, Co). For each selected dosing time the effect of initial reaction temperature variations can be then observed from the single couple of related boundary and temperature diagrams. In Table 2 the calculated values of the E_x and R_y parameters for each scheduled experiment have been summarized and the corresponding (E_x,R_y) points have been then plotted in Figures 4 to 7. Moreover, the same table also reports the expected maximum peak temperatures for each experiment as deduced from the temperature diagrams. Obviously, values higher than 120°C are meaningless since the model does not account for solvent evaporation; they simply indicate that the MAT is exceeded. From these data operating conditions 3b, 3c, 5c and 7c must be rejected since they can lead to peak reaction temperatures higher than the MAT. Analogously, the operating conditions 5a, 7a and 12a cannot be adopted since they can imply an excessive nitric acid accumulation, as it is evident from the boundary diagrams. These conditions cannot be accepted even if the maximum temperature value is lower than the MAT since a selected set of operating conditions must be safe not only during normal reactor operation but also during upset conditions, as those arising from a cooling system failure: in such cases, operating with a limited coreactant accumulation allow to keep the process safe by immediately stopping the coreactant supply. All the remaining operating conditions are inherently safe and they are consequently characterized by comparably high values of the FAM conversion at the end of the supply period. Consequently, we finally select the operating conditions 5b as the optimum ones, since they minimize the dosing time and hence maximize the reactor productivity.

The conclusions drawn from the use of boundary and temperature diagrams have been then experimentally validated through RC1 experiments carried out for each of the aforementioned operating conditions. The results of these experiments can be used as a first task to validate the kinetic expression derived from independent adiabatic Phi-TEC II experiments. The value of the mean squared relative error according to eq. (3) averaged over all the experiments is equal to 0.3%. This value, which is of the same order of magnitude of that found in the fitting procedure, strongly confirms that the kinetic expression (2) describes with sufficient accuracy the system behaviour. For the sake of example, a typical comparison between experimental data and predicted values is shown in Figure 8 for the selected operating conditions 5b. The predictions of the temperature diagrams have been validated comparing the maximum temperature values predicted by the diagrams (as reported in Table 2) with the corresponding experimental values. As it is evident from Figure 9, where the experimental data are compared with the predicted ones, the temperature diagrams always overestimate the maximum temperature. This is not only a welcome feature since

it provides conservative estimations (allowing for safely scaling up the process through the temperature diagrams) but it follows from the procedure used to build the diagrams. As discussed in detail in the first part of this work [14], for a given couple of E_x and R_y values, the temperature diagrams provide the maximum achievable value of the peak temperature among all the possible combinations of the dimensionless parameters characterizing the SBR dynamics. This means that the particular combination of such parameters representing the system under examination can be the one providing the maximum peak temperature, but most probably it is not. In this case, the experimental temperature will be lower than that predicted through the temperature diagrams. In any case, the experimental maximum temperature can never be higher than the value predicted through the temperature diagrams, coherently with the findings summarized in Figure 9. Moreover, it should be noticed that predicted temperature values higher than the reaction mixture boiling point means only that the MAT is exceeded, since the mathematical model does not account for solvent evaporation. However, this is not a problem since disregarding solvent evaporation leads to conservative results in terms of maximum achievable temperature. We can also note from Figure 9 that all the main experimental trends are correctly predicted by the temperature diagrams. For instance, the values of the maximum temperature for the experiments performed at the same initial temperature decrease with increasing the dosing time (runs 3→5→7→12 with the same letter in Figure 9) as well as it decreases by decreasing the initial temperature at the same dosing time (runs c→b→a with the same number in Figure 9). The predictions of the boundary diagrams have been analogously validated with respect to the experimental values of the relative coreactant amount at the end of the dosing time. This is defined as [14]:

$$M_{HNO_3} = \frac{n_{HNO_3}}{n_{HNO_3}\big|_1} = \vartheta - \zeta_{FAM} \tag{11}$$

This is a meaningful parameter since we expect that operating conditions characterized by (E_x,R_y) values located inside the excessive accumulation region imply higher values of the quantity (11). Coherently, we can see from Figure 10 that all the experimental runs belonging to the inherently safe region imply values of the relative coreactant amount in the range 10÷15%, whereas the three runs characterized by operating parameters located inside the excessive accumulation region imply relative coreactant amounts close to 25%.

The conclusions presented above have been drawn using boundary and temperature diagrams calculated for the current cooling number, Co, and for the estimated values of the R_H, n and m parameters (that is, for R_H=1.4, n=2 and m=0.2). As thoroughly discussed in the first part of this work [14], similar conclusions could have been obtained using diagrams calculated for approximated values of the R_H and m parameters (e.g. R_H=1 and m=1), because of the relatively low sensitivity of the location and extension of the diagrams themselves on the R_H and m values.

However, uncontrolled approximations on the reaction order of the dosed coreactant can lead to unreliable conclusions. This can be easily demonstrated by forcing n=m=1 in the fitting procedure of the Phi-TEC II data. The kinetic expression which minimizes the deviation between the model and the experimental data becomes:

$$r = k_{n=1,\,m=1} \cdot C_{HNO_3} C_{FAM} \tag{12}$$

where $k_{n=1,\,m=1} = 9.922 \cdot 10^{14} \exp\left(-1.0713 \cdot 10^{5} / RT\right)$ with units kJ, kmol, K, m^3, s. The E_x and R_y values computed according to the rate of reaction expression (12) for all the operating conditions tested are reported in Table 3, while in Figures 11 to 13 the (E_x,R_y) points for the experiments performed at T_0=68°C have been represented together with the related boundary diagrams. As can be observed, these points belong now to the inherently safe region of the diagrams and should therefore represent operating conditions characterized by a low nitric acid accumulation in the system. The same results can also be obtained through the safety criterion of Hugo et al. [1-3] for homogeneous (1,1) order reactions, according to which operating conditions implying R_y values higher than one can be considered safe. However, such conclusions do not agree with the experimental results previously discussed, thus confirming that when using boundary and temperature diagrams uncontrolled approximations on the reaction order of the dosed coreactant can lead to unsafe conclusions. From this point of view, it is useful to notice that the difference between the R_y values calculated according to the two sets of reaction orders (that is n=2, m=0.2 and n=m=1 respectively) is much lower than the corresponding difference between the $R_{y,QFS}$ values: in particular, for the experiments performed at 68°C R_y varies approximately between 6 (for n=2, m=0.2) and 7 (for n=m=1), whereas $R_{y,QFS}$ undergoes an order of magnitude variation, ranging from 9 (for n=2, m=0.2) to 0.9 (for n=m=1). In other words, a-priori constraints on the reaction orders followed by a correspondent adjustment of the remaining kinetic parameters (that is the pre-exponential factor and the activation energy) in order to fit the experimental data, typically lead to minor changes in the R_y values, but to significant variations in the $R_{y,QFS}$ values: however, since the classification of a given set of operating conditions from the safety point of view arises from a comparison between the R_y and $R_{y,QFS}$ values, it is clear that the aforementioned assumptions can lead to unreliable results.

Once a set of operating conditions has been selected through the boundary and temperature diagrams and they have been experimentally tested through proper calorimetric experiments, it can be finally scaled up to the industrial plant selecting a set of process parameters (in terms of dosing time, initial reaction temperature, initial and dosed volumes) that implies values of the cooling number, Co, and of the exothermicity and reactivity parameters (E_x and R_y) both belonging to the inherently safe region of the related temperature diagrams and fulfilling the constraint $\psi \cdot T_0$<MAT.

5.6 Conclusions

The nitration of N-(2-phenoxyphenyl) methane sulphonamide (FAM) to N-(4-nitro, 2-phenoxyphenyl) methane sulphonamide (NIM) in an indirectly cooled SBR has been analyzed experimentally through calorimetric techniques and theoretically through the temperature and boundary diagrams.

A preliminary characterization of the thermal stability of the species involved as well as of the reaction mixture has been performed through DSC experiments, finding that the most critical situation is reached at the end of the reaction, when the mixture can undergo a decomposition event, that has not been detected for the pure reaction product.

The relevant thermodynamic and kinetic parameters of the process reaction have been derived from adiabatic experiments performed in a Phi-TEC II equipment. A relatively high value of the reaction enthalpy has been estimated, which is a typical characteristic of many nitration processes. Moreover, reaction orders equal to 2 for nitric acid and to 0.2 for FAM have been estimated.

In order to select a set of SBR operating conditions characterized by both a low nitric acid accumulation and peak reaction temperatures lower than a threshold value, the boundary and temperature diagrams method has been used. The predictions of this method have been experimentally validated through calorimetric experiments performed in a RC1 equipment. It has been found that the temperature and boundary diagrams method allows to easily identify safe and productive operating conditions, therefore drastically reducing the experimental effort, with a significant saving of time and money.

It has been finally experimentally verified that when using the boundary and temperature diagrams method, no arbitrary assumptions on the reaction order of the dosed coreactant can be accepted, since they can lead to unsafe conclusions.

Nomenclature

Symbols	
A	heat transfer area of the reactor (associated to the jacket and/or the coil), m^2
C	molar concentration, $kmol/m^3$
Co	$=U^{*}Da/\varepsilon$, cooling number, -
$\tilde{C}_P$	molar heat capacity, kJ/(kmol·K)
Da	$=k_{n,m,R}t_D C_{FAM,0}^{\,n+m-1}$, Damköhler number for (n,m) order reactions, -
E	activation energy, kJ/kmol
ERP	energy release potential, -
E_x	exothermicity number, -
f	function of the dimensionless time and conversion of FAM in eq. (6), -
$\Delta\tilde{H}$	reaction enthalpy, kJ/kmol
$k_{n,m}$	reaction rate constant, $m^{3(n+m-1)}/(kmol^{n+m-1}\cdot s)$
m	mass, kg
M	$= n_{HNO_3} \Big/ n_{HNO_3}\Big\vert_1$, relative nitric acid amount, -
MAT	maximum allowable temperature, K
n	number of moles, kmol
Q	volumetric feed rate, m^3/s
r	reaction rate, $kmol/(m^3\cdot s)$
R	gas constant = 8.314, kJ/(kmol·K)
R_H	heat capacity ratio, -
R_y	reactivity number, -
t	time or characteristic time, s
T	temperature, K
$\Delta T_{ad,0}$	$= \dfrac{\left(-\Delta\tilde{H}_r\right)C_{FAM,0}}{\tilde{\rho}_m\tilde{C}_{P,m}}$, adiabatic temperature rise, K
U	overall heat transfer coefficient, $kW/(m^2\cdot K)$
$U^{*}Da$	$= (UA)_0 t_D \Big/ \left(\tilde{\rho}_m\tilde{C}_{P,m}V_{r,0}\right)$, modified Stanton number, -
V	liquid volume, m^3
Greek symbols	
γ	$=E/(RT_R)$, dimensionless activation energy, -
ε	relative volume increase at the end of the semibatch period, -
ζ	molar conversion, -

ϑ	$=t/t_D$, dimensionless time, -
$\tilde{\rho}$	molar density, kmol/m^3
σ	mean squared relative error, -
τ	$=T/T_R$, dimensionless temperature, -
ψ	$=(T_{max}/T_0)_{max}$, maximum dimensionless temperature rise, -

Subscripts and superscripts

ad	adiabatic
c	calculated
cool	coolant
D	dosing stream or dosing time
e	experimental
FAM	N-(2-phenoxyphenyl) methane sulphonamide
H	in the heat capacity ratio R_H
HNO_3	nitric acid
j	j-th time
m	order of reaction respect to FAM
m	reacting mixture
max	maximum value of a quantity or at the maximum value of a quantity
n	order of reaction respect to nitric acid
MIN	in $E_{x,MIN}$
NIM	N-(4-nitro, 2-phenoxyphenyl) methane sulphonamide
QFS	in $R_{y,QFS}$
r	reaction
R	reference
ta	target
x	in the exothermicity number E_x
y	in the reactivity number R_y
0	start of the semibatch period
1	end of the semibatch period

Literature cited

1. Hugo, P.; Steinbach, J. Praxisorientierte Darstellung der thermischen Sicherheitsgrenzen für den indirekt gekühlten Semibatch-Reaktor. *Chem. Ing. Tech.* 1985, *57, Nr. 9,* 780-782.

2. Hugo, P.; Steinbach, J. A comparison of the limits of safe operation of a SBR and a CSTR. *Chem. Eng. Sci.* 1986, *41,* 1081-1087.

3. Hugo, P.; Steinbach, J.; Stoessel, F. Calculation of the maximum temperature in stirred tank reactors in case of a breakdown of cooling. *Chem. Eng. Sci.* 1988, *43, 8,* 2147-2152.

4. Steensma, M.; Westerterp, K.R. Thermally safe operation of a cooled semi-batch reactor. Slow liquid-liquid reactions. *Chem. Eng. Sci.* 1988, *43, Nr.8,* 2125-2132.

5. Steensma, M.; Westerterp, K.R. Thermally safe operation of a semibatch reactor for liquid-liquid reactions. Slow reactions. *Ind. Eng. Chem. Res.* 1990, *29,* 1259-1270.

6. Steensma, M.; Westerterp, K.R. Thermally safe operation of a semibatch reactor for liquid-liquid reactions. Fast reactions. *Chem. Eng. Technol.* 1991, *14,* 367-375.

7. Westerterp, K.R.; Molga, E.J. No more runaways in fine chemical reactors. *Ind. Eng. Chem. Res.* 2004, *43 (16),* 4585-4594.

8. Westerterp, K.R.; Molga, E.J. Runaway prevention in liquid-liquid semibatch reactors. *Inzynieria Chemiczna i Procesowa* 2004, *25(3/4),* 2041-2050.

9. van Woezik, B.A.A.; Westerterp K.R. The nitric acid oxidation of 2-octanol. A model reaction for multiple heterogeneous liquid-liquid reactions. *Chem. Eng. Process.* 2000, *39,* 521-537.

10. van Woezik, B.A.A.; Westerterp K.R. Runaway behaviour and thermally safe operation of multiple liquid-liquid reactions in the semibatch reactor. The nitric acid oxidation of 2-octanol. *Chem. Eng. Process.* 2001, *41,* 59-77.

11. Maestri, F.; Rota, R. Thermally safe operation of liquid-liquid semibatch reactors. Part I: single kinetically controlled reactions with arbitrary reaction order. *Chem. Eng. Sci.* 2005,

60, 3309-3322.

12. Maestri, F.; Rota, R. Thermally safe operation of liquid-liquid semibatch reactors. Part II: single diffusion controlled reactions with arbitrary reaction order. *Chem. Eng. Sci.* 2005, *60*, 5590-5602.

13. Maestri, F.; Rota, R. Temperature diagrams for preventing decomposition or side reactions in liquid-liquid semibatch reactors. *Chem. Eng. Sci.* 2006, *61*, 3068-3078.

14. Maestri, F.; Rota, R. Safe and productive operation of homogeneous semibatch reactors with arbitrary reaction kinetics. Part I: development of a procedure. *Ind. Eng. Chem. Res.* 2006, *submitted for publication.*

15. Seaton, W.H.; Freedman, E.; Treweek, D.N. CHETAH – The ASTM Chemical Thermodynamics and Energy Release Potential Evaluation Program, 1974, ASTM DS 51, Philadelphia.

Table 1 *Process and equipment parameters for reaction (1) carried out in a 2.5 lt RC1 calorimeter.*

$V_{r,0} \quad \left(m^3\right)$	$5.58 \cdot 10^{-4}$
$V_D \quad \left(m^3\right)$	$3 \cdot 10^{-5}$
$C_{FAM,0} \quad \left(kmol/m^3\right)$	0.75
$\tilde{\rho}_m \quad \left(kmol/m^3\right)$	16.378
$\tilde{C}_{P,m} \quad \left(kJ/kmol\,K\right)$	138.4
$\tilde{\rho}_D \quad \left(kmol/m^3\right)$	36.385
$\tilde{C}_{P,D} \quad \left(kJ/kmol\,K\right)$	87.3
$\left(UA\right)_0 \quad \left(kW/K\right)$	$4.76 \cdot 10^{-3}$
$\Delta\tilde{H}_r \quad \left(kJ/mol\right)$	-110
$\Delta T_{ad,0} \quad \left(K\right)$	36.4

Table 2 *Exothermicity and reactivity parameters for the operating conditions tested, according to the kinetic expression (2) and estimated values of the peak reaction temperature according to the temperature diagrams.*

		t_D=3' (Co≅12)	**t_D=5' (Co≅21)**	**t_D=7' (Co≅29)**	**t_D=12' (Co≅50)**
T_0=68°C	**E_x**	-	3.5	2.6	1.5
(a)	**R_y**	-	6.3	6.4	6.5
	T_{max}	-	109°C	102°C	88°C
T_0=78°C	**E_x**	5.3	3.3	2.4	1.4
(b)	**R_y**	18.7	19.5	19.9	20.2
	T_{max}	141°C	120°C	113°C	99°C
T_0=88°C	**E_x**	5.0	3.1	2.3	1.4
(c)	**R_y**	54.5	56.8	57.8	58.9
	T_{max}	153°C	131°C	124°C	110°C

Table 3 *Exothermicity and reactivity parameters for the operating conditions tested, according to the kinetic expression (12).*

		t_D=3' (Co≅12)	t_D=5' (Co≅21)	t_D=7' (Co≅29)	t_D=12' (Co≅50)
T_0=68°C	**E_x**	-	3.3	2.4	1.4
(a)	**R_y**	-	7.3	7.5	7.6
T_0=78°C	**E_x**	5.0	3.1	2.3	1.3
(b)	**R_y**	20.6	21.4	21.8	22.2
T_0=88°C	**E_x**	4.7	3.0	2.1	1.3
(c)	**R_y**	56.9	59.2	60.3	61.5

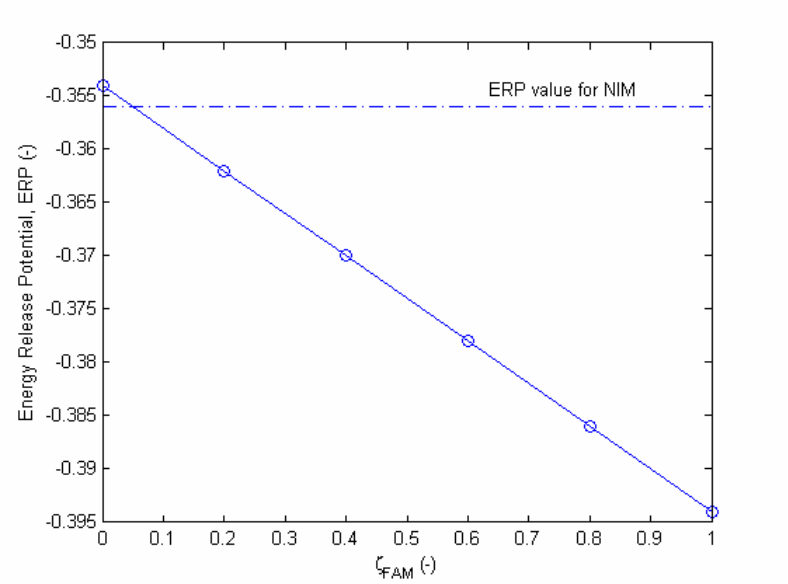

Figure 1 *Nitration of N-(2-phenoxyphenyl) methane sulphonamide (FAM) in acetic acid as a solvent: ERP values for the reacting mixture as a function of the FAM conversion.*

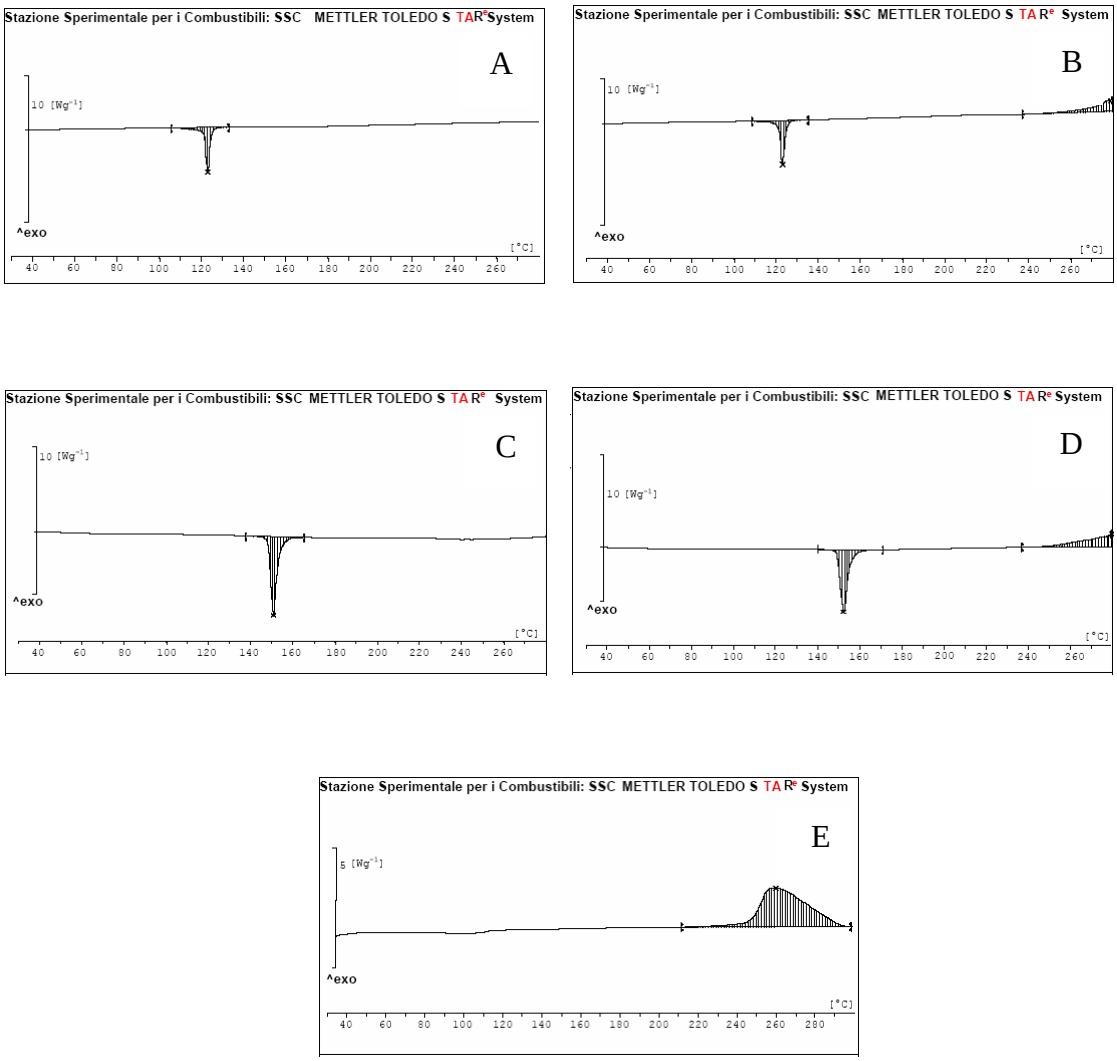

Figure 2 *A) DSC thermal characterization of N-(2-phenoxyphenyl) methane sulphonamide (FAM) in static nitrogen. Sample amount: 6.04mg; heating rate: 5°C/min; temperature range: 30-280°C.*
B) DSC thermal characterization of N-(2-phenoxyphenyl) methane sulphonamide (FAM) in static air. Sample amount: 3.55mg; heating rate: 5°C/min; temperature range: 30-280°C.
C) DSC thermal characterization of N-(4-nitro, 2-phenoxyphenyl) methane sulphonamide (NIM) in static nitrogen. Sample amount: 5.03mg; heating rate: 10°C/min; temperature range: 30-280°C.
D) DSC thermal characterization of N-(4-nitro, 2-phenoxyphenyl) methane sulphonamide (NIM) in static air. Sample amount: 5.14mg; heating rate: 10°C/min; temperature range: 30-280°C.
E) DSC thermal characterization of the final reaction mixture in static air. Sample amount: 6.17mg; heating rate: 5°C/min; temperature range: 30-300°C.

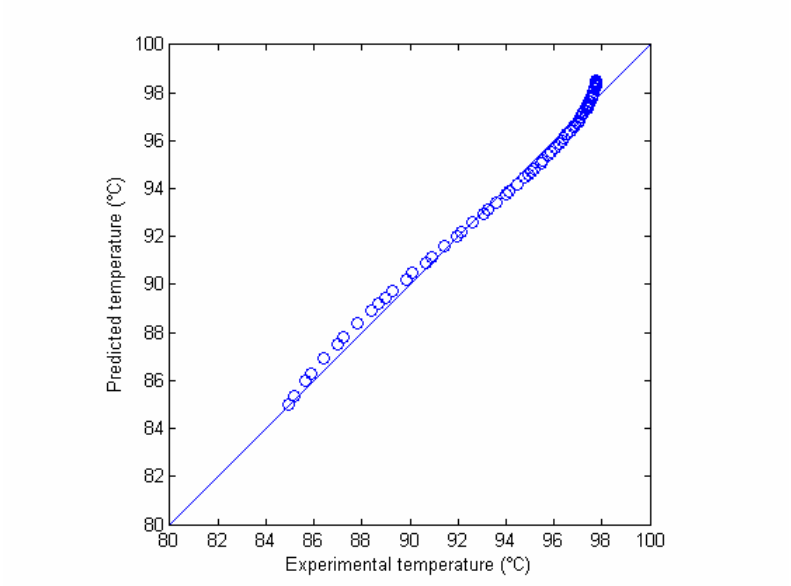

Figure 3 *Adiabatic (Phi-TEC II) experiments: parity plot according to the rate of reaction expression (2).*

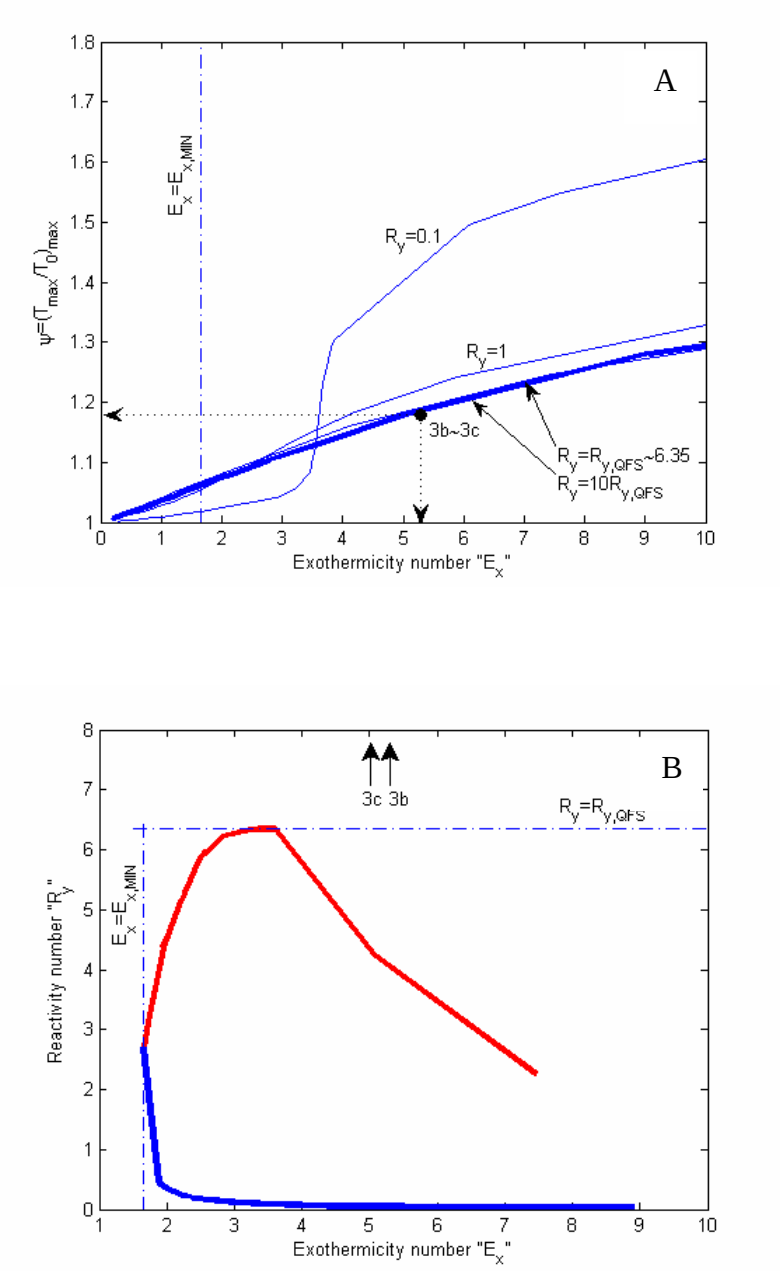

Figure 4 *Safety characterization of the operating conditions with t_D=3min through the temperature A) and boundary B) diagrams. Co=12, R_H=1.4, n=2, m=0.2. 0.02<Da<20, 0.05<ε<0.6, 30<γ<45, 0.1<$\Delta\tau_{ad,0}$<0.7 (T_R=303K).*

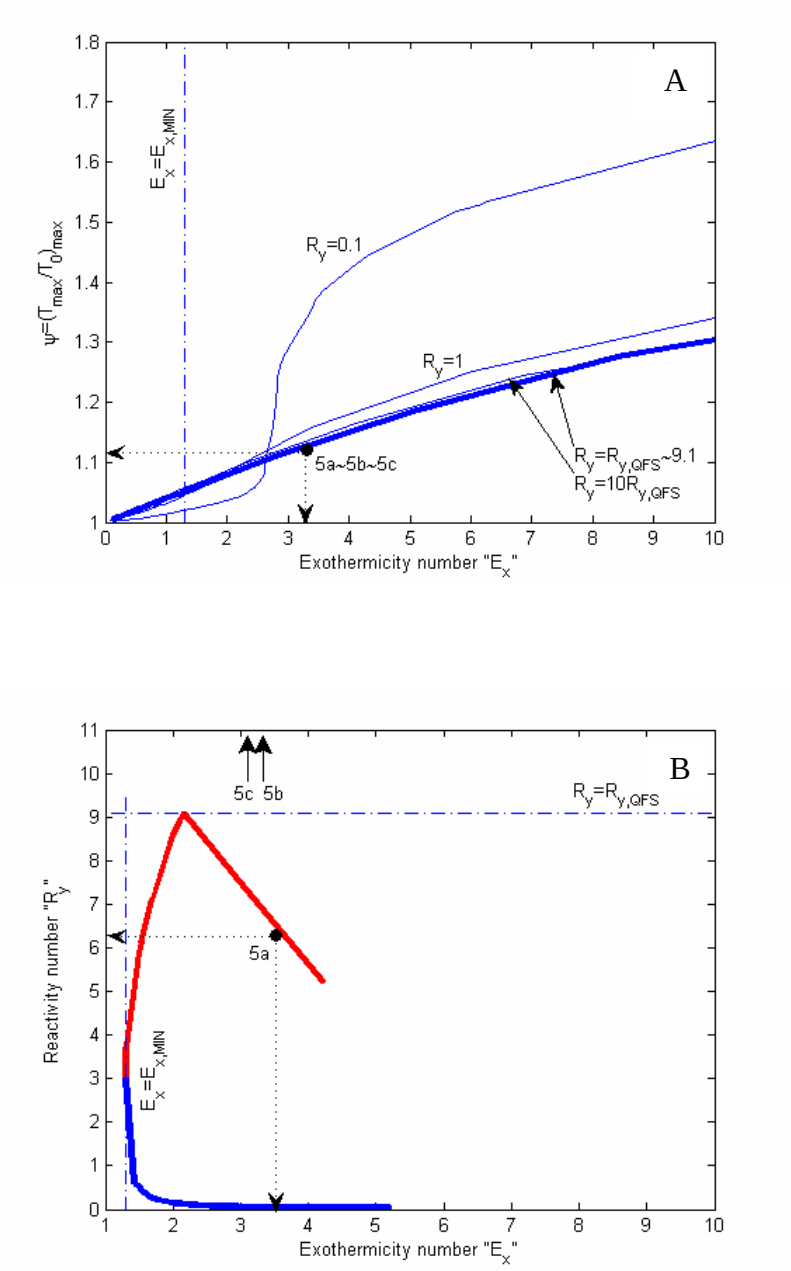

Figure 5 *Safety characterization of the operating conditions with t_D=5min through the temperature A) and boundary B) diagrams. Co=21, R_H=1.4, n=2, m=0.2. 0.02<Da<20, 0.05<ε<0.6, 30<γ<45, 0.1<$\Delta\tau_{ad,0}$<0.7 (T_R=303K).*

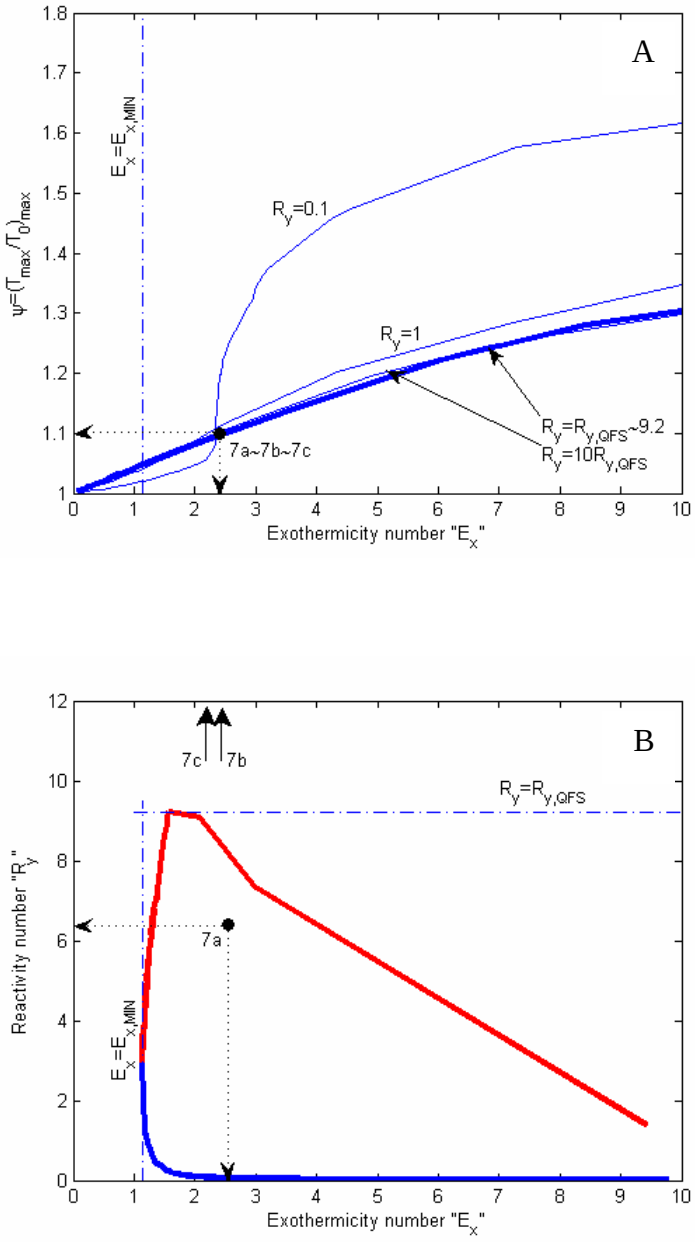

Figure 6 *Safety characterization of the operating conditions with t_D=7min through the temperature A) and boundary B) diagrams. Co=29, R_H=1.4, n=2, m=0.2. 0.02<Da<20, 0.05<ε<0.6, 30<γ<45, 0.1<$\Delta\tau_{ad,0}$<0.7 (T_R=303K).*

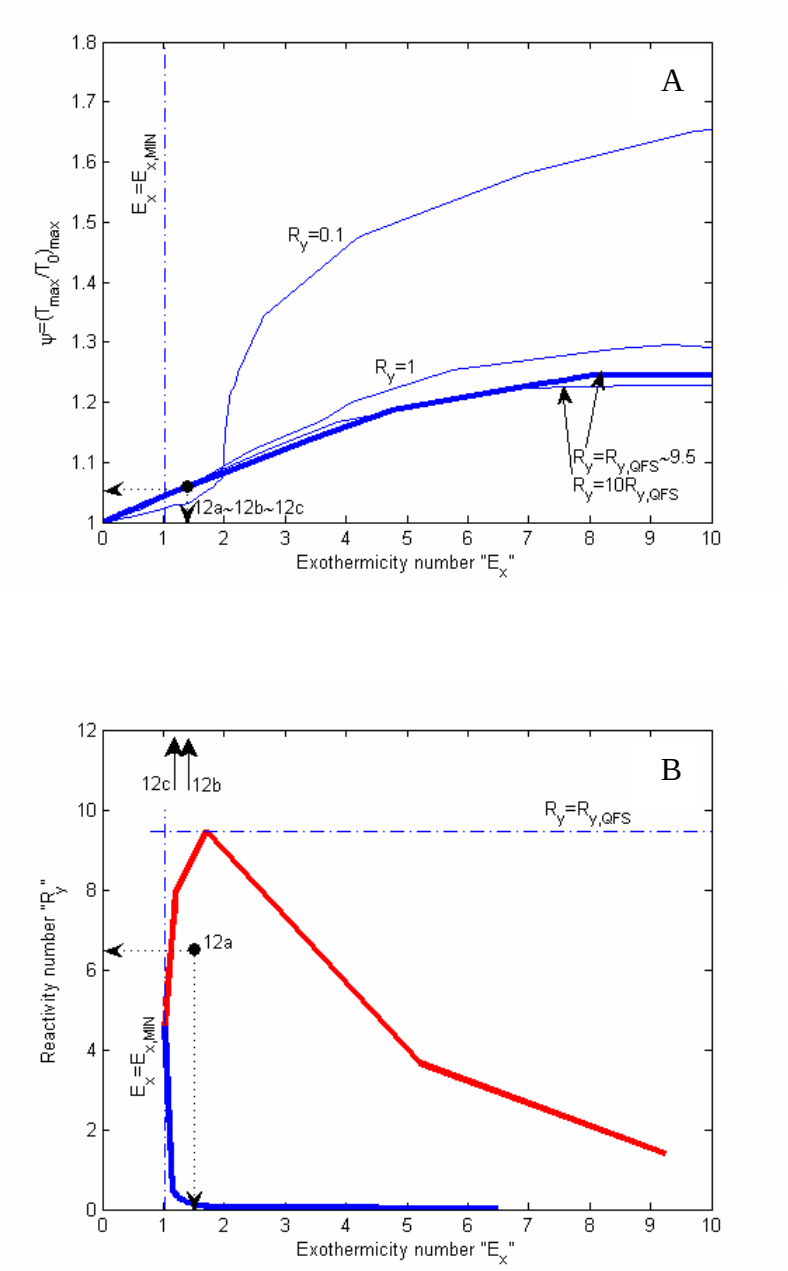

Figure 7 *Safety characterization of the operating conditions with* t_D*=12min through the temperature A) and boundary B) diagrams. Co=50,* R_H*=1.4, n=2, m=0.2. 0.02<Da<20, 0.05<*ε*<0.6, 30<*γ*<45, 0.1<*$\Delta\tau_{ad,0}$*<0.7 (*T_R*=303K).*

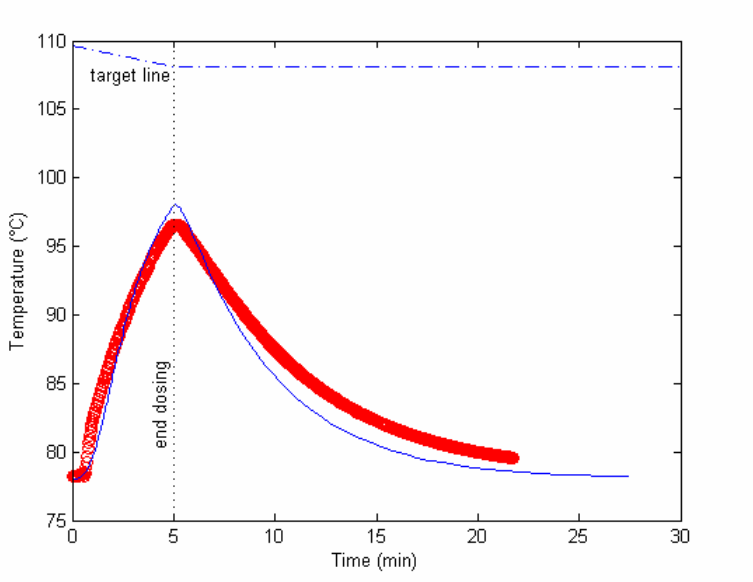

Figure 8 *Experimental (symbols) and predicted (continuous line) temperature-time profiles for the operating conditions 5b:* t_D*=5min,* T_0*=78°C.*

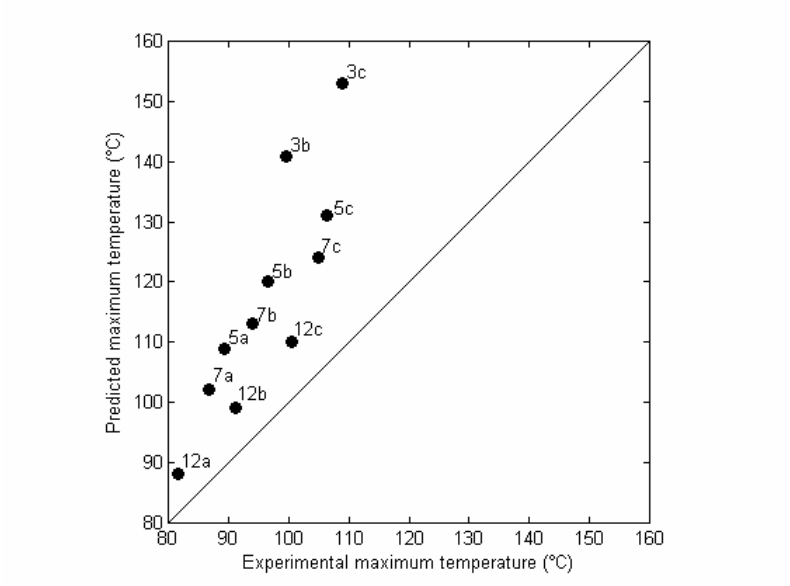

Figure 9 *Parity plot for experimental and predicted (through the temperature diagrams, see Table 2) maximum temperature values for the experimental runs tested.*

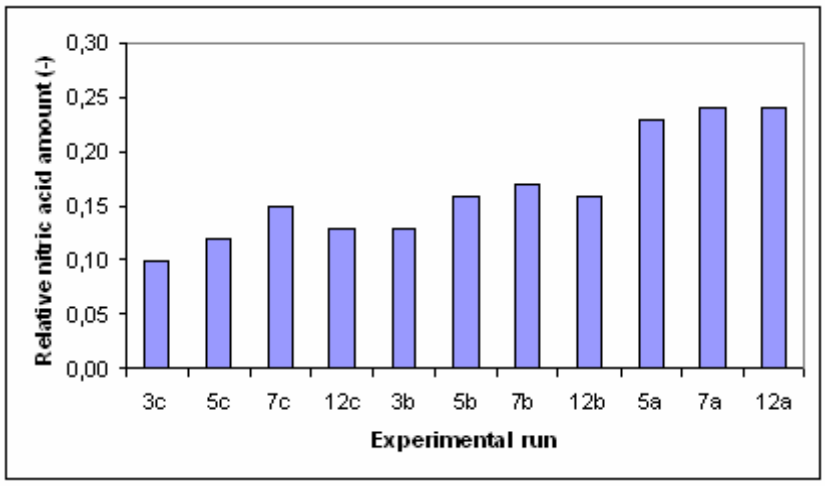

Figure 10 *Experimental values of the relative coreactant amount at the end of the dosing period.*

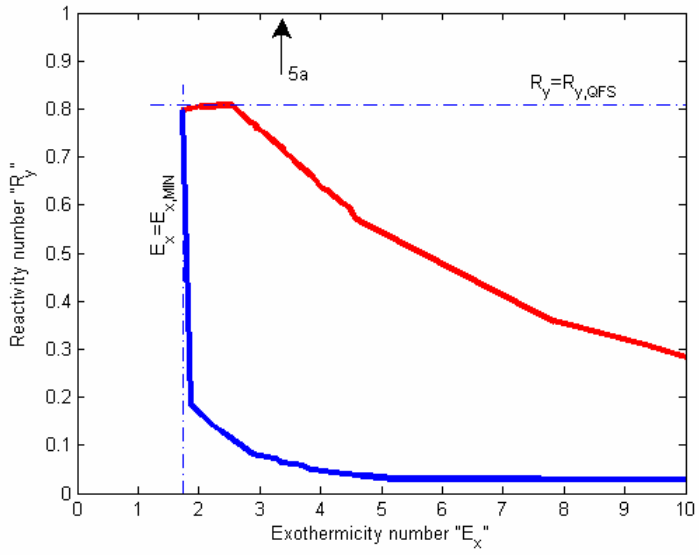

Figure 11 *Safety characterization of the operating conditions with t_D=5min and T_0=68°C through the boundary diagrams. Co=21, R_H=1.4, n=1, m=1. 0.02<Da<20, 0.05<ε<0.6, 30<γ<45, 0.1<$\Delta\tau_{ad,0}$<0.7 (T_R=303K).*

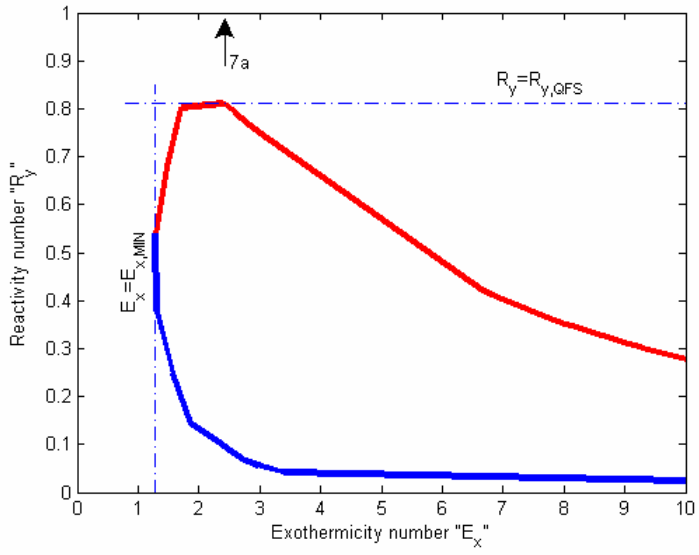

Figure 12 *Safety characterization of the operating conditions with t_D=7min and T_0=68°C through the boundary diagrams. Co=29, R_H=1.4, n=1, m=1. 0.02<Da<20, 0.05<ε<0.6, 30<γ<45, 0.1<$\Delta\tau_{ad,0}$<0.7 (T_R=303K).*

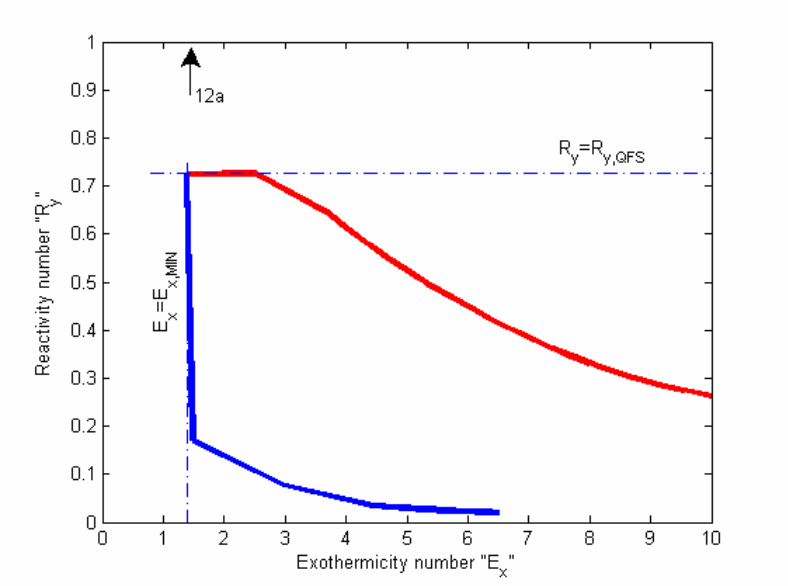

Figure 13 *Safety characterization of the operating conditions with t_D=12min and T_0=68°C through the boundary diagrams. Co=50, R_H=1.4, n=1, m=1. 0.02<Da<20, 0.05<ε<0.6, 30<γ<45, 0.1<$\Delta\tau_{ad,0}$<0.7 (T_R=303K).*